Removal of heavy metals from aqueous solutions by novel melamine-formaldehyde-polyaminopolycarboxylic acid chelating adsorbents

By

Ahmad Baraka

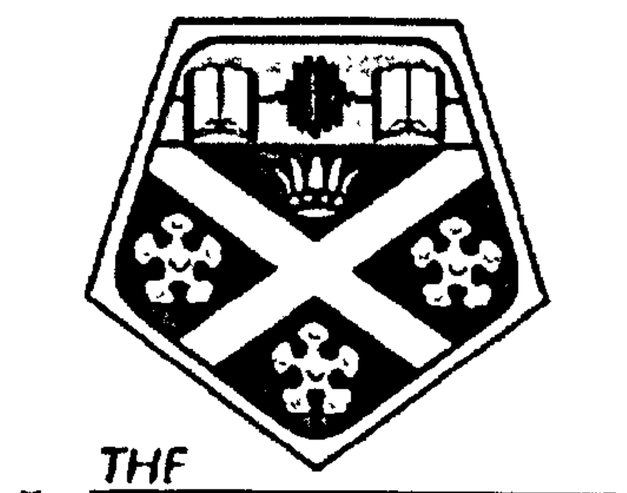

A thesis submitted to the Department of Chemical and Process Engineering, University of Strathclyde, in part fulfilment of the regulations for the Degree of Doctor of Philosophy

(2006)

Page Numbering as Bound

Copyright

Acknowledgements

I am most grateful to my supervisor Prof. ***P.J.Hall*** for his guidance, valuable comments and constant support. My special thanks to my supervisor Dr. ***M.J.Heslop*** for his continuous support and advice through the period of this study.

I would like to thank Mr. **Stuart Adams** and Mr. ***Ian Airdrie*** for continuous help in the laboratory. I wish to express my sincere gratitude to Mr. ***Gerry Dougan*** (Mechanical Engineering Department) for his help to use atomic absorption, without his help this study would not have been completed.

I am thankful and grateful to ***Egyptian Government*** for granting me in this study.

Last but not the least I present my warm thanks to my **parents, wife** and all members of the family for their support at all time during my study. Without the tremendous assistance and support of a great many other people, this research could not have been done. I offer sincere thanks to them all.

Abstract

The contamination of water recourses by heavy metals is a serious worldwide environmental problem. Industrial activities, mining and coal combustion are typical contamination sources. Removal of these metals from wastewater effluents is crucial as this contamination is non-biodegradable and highly toxic.

Extensive research has been carried out to introduce new materials which alleviate these metals from wastewater effluents before their discharge into water bodies such as rivers and lakes. Conventional methods to remove heavy metals from wastewater include chemical precipitation, ion-exchange and chelation-adsorption.

Adsorption is an important and developing research area because of the new material types available according to the application. Furthermore, it is standard process to place the adsorbent in a column and pump the wastewater through in a continuous system. It is also a cost-effective process. Chelating adsorbents are typically characterised by functional groups containing O, N, S, and P donor atoms which coordinate to different heavy metal ions. It is necessary that the adsorbent has a high capacity and that the kinetics of adsorption is sufficiently fast.

Polyaminepolycarboxylic (PAPC) acids are strong chelating agents and form stable chelates with different types of metals: transition, lanthanides and actinides. In spite of its exceptional chelating power, many of the PAPC compounds – such as DTPA (8-coordinations), CDTA (6-coordinations) and NTA (4-coordinations) – have not been thoroughly studied for use as active sites in adsorbent materials for heavy metal remediation from contaminated water effluents. Furthermore, the effect of the number of coordination groups on the adsorption behaviour has not been investigated. Use of these strong chelating agents (PAPC) for heavy metal removal by a polymeric adsorbent is presented in this study, with discussion of the chelation mechanism and affinity. The PAPC chelating agents were anchored on melamine-formaldehyde (MF) gel.

Although MF gel has suitable chemical and physical properties allowing the production of an adsorbent for heavy metal removal, it has not been studied. MF gel is porous and its matrix has a suitable platform to functionalize with some chelating compounds. PAPC-modified melamine-formaldehyde matrix is easy to produce compared to conventional chelating resins based on styrene/divinylbenzene.

In this work, melamine-formaldehyde-polyaminepolycarboxylic acid (MF-PAPC) chelating adsorbents were synthesised by anchoring polyaminepolycarboxylic acids (PAPC) to melamine by the reaction of the carboxylic group of PAPC with a primary amine group of melamine forming a covalent amide bond during MF matrix formation. A series of samples of these adsorbents were prepared by varying water content, acidity of water and temperature as parameters to control the properties of the product.

Samples of MF-DTPA, MF-NTA and MF-CDTA were chemically characterized using IR, elemental analysis, TPD-MS, ^{13}C-NMR and ^{15}N-NMR. Physical characterisation was carried out using BET, FE–SEM, and XRD techniques. Elemental analysis and BET results were used to select optimum samples for adsorption experiments.

Selected MF-PAPC adsorbent samples are hydrophilic, amorphous and rigid. The content of PAPC in the dry adsorbent samples ranges from 1.08 to 2.28 mmole g^{-1}. The MF-PAPC adsorbents have reasonable surface areas (ranges from 159 to 179 m^2 g^{-1}) and a mesoporous structure (average pore diameter: 19 – 130 Å).

The adsorption performance of MF-PAPC adsorbents was investigated against environmentally problematic divalent metal ions, namely, Cu(II), Co(II), Cd(II) and Zn(II). The adsorption behaviour of these adsorbents was characterised using mixture solutions of these four ions.

The effects of different controlling parameters (solution initial pH, temperature, metal ions initial concentration and contact time) on adsorption were considered. Experimental data was fitted to the selected kinetic and isotherm models to suggest the best models to represent the adsorption process on MF-PAPC adsorbents. The thermodynamic parameters (adsorption free energy, enthalpy and entropy) were also calculated and a mechanism of adsorption is suggested according to the evaluation of the results.

It was found that MF-PAPC adsorbents follow reversible first order and pseudo second order models to represent the adsorption kinetics. The Langmuir isotherm model gives the best representation of the adsorption processes. These findings indicate the chemical and reversible nature of the adsorption process.

Thermodynamically, the adsorption was found to be spontaneous and exothermic. The entropy change shows that adsorption is not favourable. The results indicate that chelation and ion exchange are the mechanisms of adsorption with chelation the dominant type especially at lower temperatures and higher initial pH values. The PAPC type controls the affinity order of the four heavy metals.

MF-PAPC adsorbents are distinguished by chelation-adsorption. The adsorption can be universal, or selective according to the PAPC type. Moreover, the selectivity order is different and depends on the PAPC type. MF-PAPC adsorbents can be used for metal-separation applications due to the higher affinity towards transition elements, lanthanides and actinides with respect to alkali and alkaline earth metals. The elution of the adsorbed metal ions was successfully accomplished using a solution of EDTA due to its high chelation power.

The MF-DTPA adsorbent was used in a packed column for removal of the Cu(II) ion in a continuous up-flow system. The parameters of the study were: Bed height, flow rate and initial concentration. The Thomas model was used to fit the kinetic data. The BDST model was used to examine the possibility of scaling-up the laboratory set-up to industrial scale.

The capacity of adsorption was found to be sensitive to bed height (positive: due to mass transfer), initial concentration (positive: due to concentration driving force) and flow rate (negative: due to contact time). It was found that the adsorption zone moves up the column at a constant speed for different bed heights. Hence, the process can be scaled-up for practical use using a BDST model.

List of Figures

Appendix figures:

List of Tables

Chapter 1

Wastewater and contamination by heavy metals

1.1 Water contamination by heavy metals

The total amount of water present on the earth has been estimated to be 10^9 km^3, of which 97% is oceanic and 3% is fresh water. About 75% of this fresh water is locked up as ice in the polar regions and about 14% as deep ground-water. About 0.06 % of the fresh water is readily available as lakes and rivers. These water resources receive the majority of the wastes in the form of sewage, trade and industrial effluents [1].

Water is an essential reactant in biological systems and necessary for metabolism. It carries and distributes nutrients and other important chemicals in the living bodies. Furthermore, water is the natural habitat of many forms of life. Mankind's need for water is crucial and therefore it is of paramount importance to guarantee supplies of pure water [2].

Many water resources are polluted to different extents due to one or more of the many polluting activities. The definition of water pollution is relative, but generally water is considered polluted if it is no longer suitable for the purpose to which it is needed. Some important manufacturing processes (e.g. medicine and electronic chips) require water of high purity, where the need for the removal of minute traces of organic and inorganic materials is essential [2].

Pollution can be classified by eight attributes: colour, turbidity, temperature, suspended solids, floating materials, biological effects, organic materials and inorganic substances [1].

Metals are inorganic substances that occur naturally in geological formation. Trace amounts of metals are common in water, and these are normally not harmful to health. In fact, some metals such as calcium, magnesium, potassium, and sodium are essential to sustain life and must be present for normal biological functions.

Although considered toxic, low levels of cobalt, copper, iron, manganese, molybdenum, selenium, and zinc are needed as well as catalysts for enzyme activities but water containing high levels of these essential metals – or highly toxic

metals such as aluminium, arsenic, barium, cadmium, chromium, lead, mercury, selenium, and silver – may be hazardous to health [3].

As heavy metals are natural constituents of the earth's crust and are present in varying concentrations in all ecosystems, trace amounts of metals naturally enter water sources as rain percolates through rock and soil material dissolving minute quantities. These amounts are natural and useful to the system and do not cause pollution. The pollution originates from extra amounts entering the system due to mankind activities. The major contributors to water pollution are industrial sectors (paint, electroplating, textile, coal combustion, battery, fertilizer and tanneries, etc.) mining and agriculture [4]. Another source of water contamination by metals is corrosion of pipes and leakage from waste disposal sites [5].

Although heavy metals are conventionally known as water pollutants, they are transported from place to place through the air as species adsorbed on suspended particulate matter [5].

The most important characteristic of these metals is that they are non-degradable and therefore persistent in water [6]. If the wastewater is discharged directly into natural water bodies, it will constitute a great risk to aquatic ecosystems and public heath. Alternatively, if directly discharged into the sewerage system, it may have an adverse affect on the biological treatment process [7].

This study is concerned with the removal of well known toxic metals – cadmium (II), cobalt(II), zinc(II) and copper(II) – by new synthesised polymeric adsorbent, melamine-formaldehyde-polyaminecarboxylic acids (MF-PAPC). Cadmium(II) is one of the most toxic metals. It can be introduced to the environment by the wastewaters of the following sectors: mining, metallurgy, cadmium electroplating, phosphate fertilizers, Cd–Ni batteries, stabilizers, alloys, pigments and ceramics [8,9]. Contamination by zinc(II) arises from many industries such as acrylic fibre, rayon, cellophane and special synthetic rubber [9]. The presence of copper(II) ions in water originates from several industrial activities such as dyeing, paper,

copper/brass-plating and copper/ammonium rayon. The Cu(II) ion concentration typically approaches 100–120 mg l^{-1} in the wastewater effluents of copper-cleaning, copper plating and metal-processing industries and this concentration should ideally be reduced to a value of 1.0–1.5 mg l^{-1} [10]. Cobalt(II) and its salts are used in different industries and applications: nuclear medicine, enamels and semiconductors, grinding wheels, painting on glass and porcelain, hygrometers and electroplating, as a foam stabilizer in beer, manufacture of vitamin B12, as a drier for lacquers, varnishes and paints and as a catalyst for organic chemical reactions. The permissible limits of cobalt in irrigation water and livestock watering are 0.05 and 1.0 mg l^{-1} [11].

The destinations of most contaminated waters are large water bodies (rivers, lakes, seas and oceans) which are used as drinking (and irrigation) water sources. Heavy metals are highly soluble in aquatic systems and can be absorbed by living organisms before entering the human food chain. Ingestion of these toxic metals beyond threshold concentration can cause serious health problems [12]. Mammals, as well as humans, are subjected to these metals either by drinking contaminated water or through the food chain [3].

Because of their undesired effects on human physiological systems, heavy metals should be removed from the wastewater effluents prior to discharge. In the treatment of industrial wastewaters, copper, silver, zinc, cadmium, mercury, lead, chromium, cobalt, aluminium, iron and nickel are of particular concern. Most heavy metals present in wastewater are in the inorganic form but in some industries, for example dyeing and textile, heavy metals are present in the effluent wastewater in the organic form (complexes and/or organometallic compounds) [13].

Toxic metals may exist in high concentrations in wastewater (even up to 500 mg l^{-1}) and if discharged into a water body, this will be a major threat to aquatic life [7].

The contamination of the aquatic environment by these toxic metals is a major worldwide problem and developing countries, specifically, face the problem of trying to afford high-cost remediation technologies [14].

1.2 Health Effects

Entrance of heavy metal ions into human beings causes various diseases due to binding with vital cellular components of living organisms like proteins, enzymes and nucleic acids. For example, the toxicity of many heavy metals is because of the binding with sulfhydryl (–SH) groups on proteins. This binding alters the functions of these components and gives rise to toxicity.

The syndromes of toxicity are observed when the amount (or concentration) of the heavy metal ion(s) exceeds a certain threshold value. Toxicity can occur, as well, by consuming low-level contaminated water over longer periods of time.

Also, the inorganic form of heavy metals can bio-accumulate in specific tissues [15] and this accumulation can lead to organ failure. Research is still being conducted on the toxicity of many elements. The Environmental Protection Agencies (EPA) has set a maximum contaminant level (MCL) for each metal which means that public water supplies must be monitored for these metals on a regular basis (for example MCL values for cadmium, copper and zinc are 0.01, 1.0 and 5.0 mg l^{-1} respectively [16]).

Chapter 2

Methods of Removal heavy metals from wastewater

Increasingly stringent regulations on effluent discharge mandate efficient heavy metal removal techniques from wastewater. The commonly used techniques for removing metal ions (heavy metals) from aqueous effluents include chemical precipitation, metal ion reduction, ion exchange, reverse osmosis, solvent extraction and adsorption [17]. Other techniques which incorporate electrochemical aspects (based on electric current-driving force) used for wastewater treatment are electrodialysis (ED), electrochemical ion exchange (EIX) and electrowinning [18,19]. The use of a certain technique is dictated by several factors: waste type, other constituents, concentration, level of clean-up required and cost-effectiveness [19].

Chapter 2 gives a brief presentation of the theory of each method, its advantages, applications and limitations.

2.1 Chemical precipitation

Precipitation of metals has been the primary method for wastewater treatment. It is used primarily to remove or reduce the hardness in water caused by excessive salts of calcium and magnesium and this process is called softening [20]. Subsequently, the produced precipitates can be removed from treated water by physical methods which include settling, filtration (mechanical separation of two phases), coagulation (agglomeration of the primary particles into particles up to 1 mm in size), and flocculation (fine particles to form stable aggregates of interconnected agglomerates up to 1 cm in size) [20,21].

Precipitation of soluble metals has traditionally been achieved by the addition of hydroxide to form the corresponding insoluble metal hydroxide sludge. The most conventional widely used chemical precipitants are hydroxides, sulphides, carbonates, phosphate and thiocarbamates [21]. Theoretically, this technique can be used for heavy metal removal which depends on concentration level. If the concentration is sufficiently high, the process is performed.

2.1.1 Hydroxide precipitation

In hydroxide precipitation, the metal ion forms an insoluble metal-hydroxide precipitate. The agents belonging to this category are caustic soda [NaOH], lime [CaO], hydrated lime [$Ca(OH)_2$] and magnesium hydroxide [$Mg(OH)_2$] [22]. Generally, the process is simple and consists of the addition and mixing of precipitant with wastewater. The precipitation reaction is as follows [23]:

$$M^{2+} + 2NaOH \quad \leftrightarrows \quad M(OH)_{2\,(S)} + 2\,Na^{+}$$

This process is usually used for wastewater of high concentration. There are some drawbacks when using this technique:

1. The precipitation of mixed metal systems does not permit the efficient removal of all metals due to minimum solubility of individual metal hydroxides occurring at different pH values [22].
2. The precipitation reaction is of an equilibrium type, i.e. some of the formed metal hydroxide will disassociate resulting in metal ions going back into solution.
3. The increasing use of chelating agents in industry, such as EDTA, citrates, etc. (e.g. in electro-plating processes) poses significant or often impossible precipitation using pH adjustment techniques due to formation of stable soluble metal complexes.
4. Metal-hydroxide sludge is inherently susceptible to leaching by acid which in turn can result in metal transport into ground water when sludge is disposed of in landfills.
5. Metal-hydroxide sludge is heavily hydrated. This characteristic transfers to costly sludge disposal.

2.1.2 Sulphide precipitation

Sulphide precipitation has been the most widely used method after hydroxide precipitation. Soluble metals can be removed by precipitating them as metal sulphides by the addition of sodium sulphide to the waste solution which have very low solubility values throughout the pH range [22]. This method yields more

complete metal removal than hydroxide precipitation. However, it is not as widely used as hydroxide precipitation because of residues of toxic sulphides in solution [22].

2.1.3 Carbonate precipitation

Precipitation of dissolved heavy metals from wastewaters can be achieved by using a carbonate precipitating agent, such as soda ash [Na_2CO_3], sodium bicarbonate [$NaHCO_3$], or calcium carbonate [$CaCO_3$]. In some particular cases metal carbonates are less soluble than their corresponding hydroxides, hence carbonate precipitation is an effective treatment alternative to hydroxide precipitation. Some metals precipitation using calcium carbonate, e.g. lead and nickel, gives lower final residual metals concentrations than those of hydroxide. Generally, the solubility values of metal-carbonates are intermediate between those of metal-hydroxide and metal-sulphide. The solubility values of metal-carbonates depend on the specific metal ion precipitated and the pH of the wastewater.

The main advantage of using carbonate precipitation is that it can operate at a low pH range, typically between 7 and 9. Carbonate precipitation is price-competitive in relation to hydroxide precipitation. The produced metal-carbonate sludges generally have better dewatering characteristics than corresponding hydroxide sludges. However, there are a few disadvantages:

1. The treatment chemicals tend to be abrasive to feed equipment.
2. Slower reacting carbonate-based chemistry causes longer retention times.
3. The sludge produced in this process is gelatinous and difficult to settle.

2.1.4 Phosphate precipitation

Toxic metals have low solubility values in the form of phosphate salts. Hence, heavy metal can be precipitated and removed by reaction with a phosphatic agent [22]. The removal of heavy metals benefiting from this precipitation reaction is now advanced by using phosphatic sorbent where heavy metal ions are phosphate-micro-

precipitated in this sorbent. These sorbents are mainly clays which include phosphate in their structure.

2.1.5 Precipitation by thiocarbamates

The solubility of metal-thiocarbamate is not dependent on pH as with metal-hydroxide. For this reason, metals can be precipitated in acidic or caustic media. For mixtures of metal ions, the use of hydroxide precipitation may not achieve residual metal levels for some of these ions that meet discharge limits. In this case, thiocarbamates precipitation could be used as a subsequent step to precipitate the remaining soluble metal to meet discharge limits.

Thiocarbamates are ligands and can precipitate metals when treated water contains chelated metals. This is the case for some textile industry and electroplating process. The metal-thiocarbamate precipitates are stable to leaching under acidic conditions. The metal-thiocarbamate precipitate results in an anhydrous form and this allows for more efficient disposal (less weight and volume leads to lesser transport costs).

An example of its use: soluble zinc, copper and iron traces can be removed from nickel-plating effluent by mixing with nickel dimethyldithiocarbamate, dibutyldithiocarbamate or diethyldithiocarbamate. These compounds form very low soluble complexes with soluble metallic traces in the acidic nickel-plating solution. The insoluble metal-complexes then are removed by filtration [24]. However, thiocarbamates are toxic to water organisms and fish. Hence, its practical use is limited.

2.2 Metal ions reduction

There are several reducing agents which have been used in heavy metal remediation according to pH range and degree of reduction (i.e. to the elemental state).

2.2.1 Sodium Borohydride ($NaBH_4$)

Sodium borohydride is an extremely strong reducing agent and can reduce both chelated and non chelated metals. In wastewater treatment, the main application is the recovery of valuable metals [25].

This process has the advantage of producing the least amount of sludge of any process but it has a number of disadvantages that almost always preclude its use in an efficient and cost effective system. A major disadvantage is that unless the liquid is removed from the sludge immediately, metals tend to go back into solution with the water. Another problem is that pH control is critical. Explosive hydrogen gas is evolved at acidic pH values. High cost of this reagent has also been a problem, and as a result, it has been very difficult to justify its use [22].

2.2.2 Ferrous sulphate

This reducing agent is widely used for wastewater containing Cr^{6+} ion. The main advantages are: safe to use, inexpensive and additional co-precipitation of toxic metal ions [22]. Another significant advantage is that reduction can be achieved under acidic conditions [25].

2.2.3 Hydrazine (N_2H_4)

Hydrazine can be used for the removal of heavy metals from wastewater due to its powerful reducing properties [25]. Hydrazine can reduce nickel, cobalt, iron and chromium to the elemental state [22]. The drawbacks are: (1) the residue of hydrazine is polluting (carcinogenic) and (2) explosion under certain conditions is probable [22,25].

2.3 Ion Exchange

In the ion exchange process, toxic cations or anions in the treated water are exchanged with equivalent quantities (charges) of other, non harmful, cations or

anions on a solid insoluble sorbent and charge neutrality is maintained in the system (the liquid and the solid). The process is reversible which allows extended use of the sorbent material before replacement and discharge [2,21]. The well known application is water softening in which calcium and magnesium ions are removed and replaced by sodium ions. This process is ideal when the total dissolved solids (TDS) value of the influent wastewater is less than 700 ppm [2].

Many inorganic and organic materials have ion-exchange properties. Synthetic organic ion-exchange resins, natural and synthetic zeolites, silica gels, soils, clays, ash and metal oxides are some examples.

Synthetic organic resins are of great importance for removal purposes due to possibility for production according to certain application (introducing specific active groups) and controllable chemical and physical characteristics. In 1944, d'Alelio invented polystyrene sulphonic acid cation exchange resin by the copolymerization of styrene and divinylbenzene, suspended as liquid droplets in water, to form spherical beads. The produced beads were sulphonated giving a cation exchange of great physical and chemical stability which possessed reasonably high exchange capacity [2].

Before sulphonation, the produced beads were ion-exchange inert and hydrophobic. After sulphonation, the material is hydrophilic and water permeable including some of 50% by weight of water (even if apparently dry). The fixed sulphonic groups are immovable; each group carries a negative charge, while the associated hydrogen ion is completely mobile moving freely throughout the embedded water. Another important step was achieved during the years 1945–1950, when weakly acidic resins were prepared containing phenolic and carboxylic groups [2].

Generally, synthetic organic ion exchange resins are *polymeric* structures containing active groups fixed within the polymer matrix. Many different synthetic organic ion exchange resins are now available such as phenolic, acrylic and styrenic types in the form of beads, membranes, papers, fibres, foams and liquid extractants. For beads, a

particle size range of 0.3 – 1.2 mm in diameter provides a compromise between acceptable kinetics and pressure drop [21].

Practically, synthetic ion exchange resin are used repeatedly in a cyclic manner (adsorption/desorption or removal/regeneration) over many years. The deterioration of physical and chemical properties can be anticipated. Studying these properties (particle size and shape, density, selectivity, kinetics, water content, swelling and shrinking and hydraulic effects) is helpful to learn more about the adsorbent nature and to understand the main cause of deterioration [21].

Inorganic ion exchange materials (e.g. zeolites, etc.) are being used in a number of areas where synthetic organic ion exchange resins are difficult to apply (chemical or radiation degradation, decomposition, heat, etc.) [21].

However, the ion exchange mechanism is not effective for heavy metal removal in some situations. For example, Fernández et al [26] examined: four *cationic* exchange resins (Amberlite 200, 252-C, IR-120 and Duolite C-464), one *chelating* resin (Amberlite IRC 718) and one *adsorbent* resin for the removal of Cd and Zn present in the leachate from an inorganic industrial waste landfill. The results indicated that cationic resins achieve removal percentages of only 5–7% for Cd and 7–20% for Zn. The adsorbent resin achieves removal percentage of only <5% for Cd and 13% for Zn. Significantly, chelating resin shows removal of 50% for Cd and 93% for Zn. This distinguishable behaviour of chelating resin (Amberlite IRC 718) originates from the higher selectivity of chelating iminodiacetate towards heavy metals such as Cd and Zn versus sodium, calcium and magnesium ions which is not the case for other types of resins studied.

Kocaoba and Akcin [27] used Amberlite IR 120 (strong cation exchange resin) for the removal of toxic chromium and cadmium present in wastewaters. Sodium and hydrogen forms of the resin were used in this study. The results showed that the resin performed well for the removal and recovery of chromium and cadmium. However, the removal is pH dependent (optimum value is 5.5) which is not expected as the

resin is of the strong acid type. The study did not cover the presence of alkali, alkaline earth ions and/or complexing agents in wastewater which are common characteristics of many effluents of certain activities mentioned in study: electroplating, textile printing, chemical industries, leather tanning.

For inorganic adsorbent, Erdem et al [28] used clinoptilolite for the removal of Co^{2+}, Cu^{2+}, Zn^{2+} and Mn^{2+} in order to consider its application to purify metal finishing wastewaters. These results showed that this natural zeolite has great potential to remove cationic heavy metal species from industrial wastewater. However, adsorption capacity (according to Langmuir equation) is limited: 0.24, 0.14, 0.13 and 0.08 mmole/g for Co^{2+}, Cu^{2+}, Zn^{2+} and Mn^{2+} respectively. Zeolites are in general, weakly acidic and the sodium form favours hydrogen which can cause an increase of pH value when treated with dilute electrolyte solution. This makes metal hydroxide precipitation feasible.

Generally, to apply the ion exchange mechanism for heavy metal removal, it is important to consider the probable competitiveness of alkali and alkaline earth ions for adsorption. Optimum pH value has to be determined. The increase of heavy metal solubility in water solution, due to the presence of complexing agents in many of wastewater effluents, suppresses adsorption.

2.4 Reverse Osmosis

Reverse osmosis is a physical process where the targeted dissolved species can be separated (filtered) from the solvent with the assistance of a semi-permeable membrane. The process involves the selective movement of solvent (water) from the concentrated side of a membrane to the other side. To make the process work, pressure is applied to the contaminated solution forcing water through the membrane. This process will allow the removal of particles as small as ions from a solution.

Reverse osmosis (RO) is used to purify water (seawater, wastewater treatment, brackish well water and city water) and remove other impurities in order to improve

the colour, taste or properties of water. Reverse osmosis is suitable for the treatment of wastewater of TDS $\geq$700 ppm [2]. Polymers such as cellulose acetate and cellulose triacetate, linear and crosslinked aromatic polyamide and aryl-alkyl polyetherurea are widely used as membranes [21].

Unlike chemical precipitation, instead of pH, pressure is the major parameter that affects the extent of metal removal by RO. In general, reverse osmosis (RO) is effective for heavy metal removal from inorganic solution and depends on the material, porosity, hydrophilicity, thickness, roughness and charge of the membrane. The advantages of using RO include a high water flux rate, resistance to biological attack, mechanical strength, chemical stability and the ability to withstand high temperatures.

Several industries produce wastewater which contains copper and cadmium. Hany and Hassan [29] prepared synthetic wastewater samples containing Cu^{2+} and Cd^{2+} ions at various concentrations and samples were subjected to treatment by RO in the laboratory. The membrane used is polyamide type with surface area of 2.5 m^2. The results showed that the initial concentration of 500 ppm was reduced to 3 ppm (99.4% removal).

RO enables industrial users to comply with environmental legislation and the reuse of water from industrial process can be achieved. However, RO has some limitations: (1) membrane performance decreases over time, resulting in the decreasing permeate flow rate, (2) higher metal removal efficiencies needs higher pressure, i.e. higher *energy* consumption [23]. Besides, use of RO is recommended for concentrated aqueous solutions from an energy consumption point of view.

2.5 Solvent Extraction

The solvent extraction system composes of two immiscible phases: the metal-contaminated water and the extractant organic solvent [19]. A large number of organic compounds form complexes with metal ions. Many of these complexes are

more soluble in organic solvents hence are extractable from water. The metal is extracted by adding an aqueous solution of the reagent to an aqueous solution of the sample and extracting the metal complex with an organic solvent. The distribution ratio for this type of complex is usually very large, so only one or two extractions with fresh solvents are needed [30].

Surfactants may be used as well as extractants for metal ions. These compounds form reverse micelles in the organic phase. By shaking with metal ions-bearing solution, the metal ions can be encapsulated in the hydrophilic inner region of the micelle. However, selectivity is difficult to achieve. Carbon dioxide is also used for extraction of heavy metals from contaminated water [19].

The major application of solvent extraction technique is the removal of radioactive metals from nuclear waste materials such as removal of uranium and plutonium from fission products (PUREX process) using tributyl phosphate as the organic phase [19].

Investigation of solvent extraction applicability for the removal of a heavy metal as a contaminant element was carried out which indicate the feasibility of this technique for heavy metal removal. During the production of industrial wet process phosphoric acid (WPA), cadmium enters the WPA. It can be found in trace quantities, <100 ppm. Since WPA is used in phosphate fertilizers, the toxic cadmium has to be removed. Nazari et al [31] used tertiary amine extractant (Alamine 336) to remove Cd by solvent extraction in batch experiments. The organic phase constituted from: 1% Alamine 336 and 1.5% iso-dodecanol in B-65 kerosene. The Cd extraction from WPA under optimal conditions was calculated as 74 ± 2.54%. The average Cd extraction, with 20 recyclings of organic phase to the solvent extraction circuit was calculated as 68.57%. It was concluded that this organic phase is efficient for Cd removal from WPA.

The main limitations of the solvent extraction method for wastewater treatment are (1) long process includes mixing two phases, decantation, separation of phases and

separation of heavy metal from organic phase for solvent-recycling and (2) the use of organic solvent which is a contaminant itself.

2.6 Electrochemical Methods

Separation of metals from water making use of electric potential between two electrodes can be classified as electrochemical methods. Electrodialysis (ED) is a membrane process as reverse osmosis but uses electric potential as the driving force rather than pressure. Electrochemical ion exchange (EIX) is an ion exchange process under electric potential conditions. Electrowinning is an electrodeposition (reduction) of metallic ion on the cathode.

2.6.1 Electrodialysis (ED)

Electrodialysis (ED) is an electrochemical separation process in which ionic species are transported through ion selective membranes from one solution into another under the driving force of a direct current (DC) electrical potential [2,24,32].

The process uses ion selective membranes which are essentially ion exchange resin cast in thin sheet form with a network of molecular-size pores too small to allow a significant flow of water through them [2]. Ion exchange membranes are often based on a grid of cross-linked polystyrene which is reinforced with inert woven fabric backing such as dynel or polypropylene to impart physical strength and rigidity.

There are two types of membranes: 1) ion exchange membranes which allow flow of positively charged ions are called cation membranes and 2) ion exchange membranes that allow flow of negatively charged ions are called anion membranes. Cation membranes contain negatively charged groups such as sulfonate which are chemically bonded to the polystyrene base. This produces a negatively charged grid which attracts positively charged cations and repels negatively charged anions. Anion membranes contain positively charged bonded groups such as a quaternary

ammonium compound. The resulting positively charged grid attracts anions and repels cations.

To demineralise a solution using ED, cation and anion membranes are arranged alternately in a stacked configuration with a positive electrode (anode) at one end and a negative electrode (cathode) at the other. When a DC voltage is applied, the electrical potential created becomes the driving force to move ions, with the membranes forming barriers to ions of opposite charge. Therefore, anions attempting to migrate to the anode will pass through the adjacent anion membrane but will be stopped by the first cation membrane they encounter. Cations trying to migrate to the cathode will pass through the cation membrane but will be stopped by the anion membrane. Hence, the membranes form ion diluting compartments and ion concentrating compartments. When two solutions are pumped through these respective compartments, one is demineralised by transfer of ions through the membranes; the other becomes concentrated with those ions [32].

The main use of electrodialysis is the desalination of thin brackish water to produce drinking water and the pre-treatment of high TDS feed-water for ion exchange plant. Electrodialysis can be considered for brackish water of up to 12000 ppm to achieve drinking water with a TDS of 200 ppm [2].

For the removal of heavy metals, Mohammadi et al [33] used the ED technique to remove the Pb^{2+} from wastewater produced in the battery industry. The effects of flow rate, temperature and voltage at different concentrations using two types of commercial membranes were considered. It was found that increasing voltage and temperature improved cell performance; however, the separation percentage decreased with an increasing flow rate. Using membranes with higher ion-exchange capacity resulted in better cell performance. Concentrated solution has been used (1000 ppm) and removal was about 94% whereas dilute solution (100 ppm) shows removal of 72%. This indicates that the ED method is preferred for higher concentration which is not the case for many wastewater effluents.

2.6.2 Electrochemical ion exchange (EIX)

EIX is an advanced ion-exchange process and is becoming an increasingly important method of removing toxic heavy metal ions. It is an alternative to electrodialysis (ED).

Typically for this technique, an ion exchange media (microporous layer over which the wastewater to be treated flows) is physically incorporated into an electrode structure using a binder. An electric potential (driving force) is used to accelerate removal.

Through the choice of adsorption media and the applied potential, EIX systems have shown to adsorb cations of IA, IIA, transition and post-transition metals as well as anions. After complete loading of the ion exchange, reversing polarity can elute the ions, without the use of chemicals, back into a small-volume solution (volume reduction factors of > 1000) [34]. Selectivity is difficult to assign. It is dependent on control of solution speciation (pH adjustment) and select of appropriate adsorbent [34].

2.6.3 Electrowinning

The reaction chamber of an electrowinning unit houses anodes and cathodes. In the simplest design, a set of cathodes and anodes is set in the reaction chamber containing the electrolyte. When the unit is energized, metal ions are reduced onto the cathode. The rate at which metal can be recovered (i.e., plated onto the cathode) from solution depends on several factors, including the concentration of metal in the electrolyte, the size of the unit in terms of current and cathode area, and the species of metal being recovered.

Although electrowinning has traditionally been used only for metal recovery, the use for wastewater treatment was conducted. Elsherief [35] studied the removal of cadmium from simulated wastewaters by electrodeposition on a spiral wound steel electrode by electrowinning of cadmium from dilute sulphate solutions. This reaction

system was found to be effective in reducing metal concentrations to the permissible range. This process can be used for solutions containing single ions for its removal or recovery. For multi-element solutions, separation is not possible.

For electrochemical methods (ED, EIX, Electrowinning), incorporation of electricity part causes some complexation of the system (sophisticated) which make it difficult for wide application especially in developing countries.

2.7 Adsorption

The phenomenon of adsorption is the accumulation of adsorbate at the surface of a porous solid. The binding of a adsorbate is typically physical or chemical. Adsorption of heavy metal is a very well known wastewater treatment method. The binding in this case is chemisorption and ion exchange is the common mechanism for adsorption. Surface micro-precipitation and coordination (complex formation) mechanisms are sometimes observed for some adsorbent as well [36].

Ion exchange was discussed briefly **(section 2.3)** from the mechanism point of view. In this section, the type of material is of interest regardless of the mechanism of removal. The contribution of more than one binding mechanism for adsorption is highly probable for some adsorbents. There are several types of materials used for adsorption. Natural and synthetic zeolites, synthetic organic resins, carbon materials, treated and non-treated residuals of bio-natural materials and hybrid systems of the previous ones are under consideration for metal removal from wastewater streams.

2.7.1 Zeolites and similar materials

Zeolites are hydrated aluminosilicates of alkali and alkaline earth elements with crystal structures consisting of a three-dimensional framework of tetrahedral SiO_4 and AlO_4 linked with each other by shared oxygen atoms. The aluminium ion is small enough to occupy the position in the centre of the tetrahedron of four oxygen atoms, and the isomorphous replacement of Si^{4+} by Al^{3+} produces a negative charge

in the lattice. The net negative charge is balanced by the cation (sodium, potassium, or calcium). These cations are exchangeable with cations in solutions and so zeolites are suitable adsorbents for heavy metal removal as they have a large cation exchange capacity and an affinity for heavy metals [28,37,38]. Many zeolites occur naturally as minerals and others are synthetic which are produced commercially for specific uses. Their framework structure can contain cages, cavities or channels [19].

Clinoptilolite and chabazite are well known zeolites. Clinoptilolite is the most abundant in nature and readily available from more than 40 natural zeolites species. Among the most frequently studied natural zeolites, clinoptilolite was shown to have high selectivity for certain heavy metal ions such as Pb^{2+}, Cd^{2+}, Zn^{2+}, and Cu^{2+} [39]. Clinoptilolites (SIR-600) can be used for selective removal of cesium(I) [19].

Mabel et al [40] investigated the competing interactions of Pb(II), Cd(II), and Cr(VI) for ion-exchange sites in clinoptilolite. Pb(II) and Cd(II) were effectively removed in batch reactors, with high removal (>95%) in the acidic pH range. However, the presence of Cr(VI) significantly diminished the removal of Pb(II) and Cd(II) due to the formation of their anionic complexes in solution. Also, effective removal occurred within long time, 18 hours.

Myroslav et al [41] carried out a study on the adsorption of Pb^{2+}, Cu^{2+}, Ni^{2+}, and Cd^{2+} by raw and pre-treated clinoptilolite. The maximum removal value of Cd^{2+} is 4.2 mg g^{-1} at initial concentration of 80 mg l^{-1} and towards Pb^{2+}, Cu^{2+} and Ni^{2+} was 27.7, 25.8 and 13 mg g^{-1} at initial concentrations of 800 mg l^{-1}. These capacities are very limited with respect to initial concentration used and may be related to the small surface area of raw and treated clinoptilolite: 13.2 and 78.9 m^2 g^{-1} respectively.

Pitcher et al [42] conducted an interesting study for the removal of Zn, Cu, Pb and Cd from synthetic solution and motorway stormwater by mordenite. It was found that removal effectiveness decreased from synthetic water (42–89%) to motorway stormwater (6–44%). This decrease was assigned to the presence of other dissolved contaminants in motorway stormwater.

Zeolites, in general, have smaller surface areas when compared to synthetic organic resins. Hence the capacity is limited. Also, to attain the equilibrium state, a longer period of time is needed. The main mechanism of removal by zeolites is ion exchange.

Fly ash (also called coal combustion product) is a mineral material. It is produced as a finally divided residue resulting from the combustion of coal. Flay ash composes of inorganic matters present in the coal that have been fused during combustion into amorphous-glassy structure. Fly ash particles are generally spherical in shape and their size ranges from 0.5 to 100 μm. The main composition materials are aluminium oxide (Al_2O_3), silicon oxide (SiO_2) and iron oxide (Fe_2O_3) beside varying amounts of carbon, calcium, magnesium and sulphur [43].

Fly ash can remove heavy metals and several adsorption mechanisms have been recognised such as electrostatic attraction, surface complex formation, cation exchange and precipitation [43,44]. Fly ash is a strong alkali material that exhibits pH of 10–13 when added to water and its surface is negatively charged at high pH values. Hence, it can be expected that metal ions can be removed from aqueous solutions by precipitation or electrostatic adsorption [44,45].

Erol et al [45] have examined six fly ashes with different compositions for the removal of Cu^{2+} and Pb^{2+} ions by precipitation from aqueous solutions. The principal oxide constituents of coal ash are acidic (SiO_2, Al_2O_3 and TiO_2) and basic (Fe_2O_3, MgO, CaO, Na_2O and K_2O). The chemical compositions of the fly ashes are different and the final pH values of the solutions of the fly ash samples with the same concentration are significantly different. Final pH > 6 of the fly ash-copper solution mixture caused a sharp decrease in the Cu^{2+} concentration and at pH = 8–9, the Cu^{2+} removal approached 100%. Similar results were reported for Pb^{2+}. It was noticed that the Pb^{2+} and Cu^{2+} removal capacities of the fly ash samples are directly proportional to their CaO contents (basic). Precipitation is the main mechanism of removal in this study. Collective removal of heavy metals from waste effluent contains different

elements by these fly ashes is not expected to be successful as metal hydroxides are of different solubility values.

Clay material is generally a small aggregate of hydrous silicate particles. It is rich in silicon and aluminum oxides and hydroxides with variable amounts of structural water. It possesses a negative surface charge in solution. As pH changes, surface charge also changes, and the adsorption of charged species is affected (attraction between the positively charged metal ion and the negatively charged clay surface) [46].

Ömer et al [47] has used raw kaolinite for the removal of some heavy metals such as Mn(II), Co(II), Ni(II), and Cu(II) from aqueous solution. The sorption capacity of these metals on kaolinite was found as 0.446 mg g^{-1} (Mn), 0.919 mg g^{-1} (Co), 1.669 mg g^{-1} (Ni), 10.787 mg g^{-1} and (Cu) at 25°C. It is suggested that the negative surface (SiO^-) is responsible for attraction and binding metal ion. The adsorption capacity is small compared to many other adsorbents.

2.7.2 Carbon materials

Carbon materials have strong adsorptive properties and have been conventionally used for the removal of colours, tastes and odours from water. Activated carbon is used widely in industrial applications such as solvent recovery, hydrogen purification, decolourising sugar solutions and water treatment. It is formed from carbon micro-crystallites positioned in a random orientation. Traditionally, it is prepared by the thermal decomposition of raw carbonaceous materials (such as woods, rice hulls, peat, lignin, coals, coal tars, pitches and nutshells) followed by an activation process [48].

Polymers and organic resins can be considered as raw material for active carbon. Activation of carbon materials can be carried out through two methods:

1. Steam activation: is the heating of the starting material in the absence of air (400–500°C) to force out the volatile materials and to initiate small pores. The material is then subjected to steam (800–1000°C).
2. Chemical activation: acids and zinc oxide are mixed with the source carbon material in order to produce microporosity (this technique can be problematic because, for example, zinc trace residues may remain in the end product).

Although carbon materials are mainly used for the adsorption of organic matter, many articles showed its versatility for heavy metal removal. But its use for heavy metal removal is limited due to expensive carbon-activation process [17].

Sergei et al [49] prepared activated carbons from co-mingled natural organic wastes. It has been used for adsorption of chromium(III). Total chromium uptake was found to be 1.09 mmole g^{-1} at 30°C. The results suggest that adsorption of Cr(III) was either a physical adsorption or a simple ion-exchange process. Saturation occurred within 4–5 hours.

Youssef et al [50] prepared chemically-activated carbons by reacting corn-stalks with concentrated sulphuric acid at 180–220°C and by activation with zinc chloride at 600°C. Presence of light metals ions such as Na^+ in solution decreased the Cd(II) ion adsorption onto activated carbons and high concentration of Na^+ may stop adsorption of Cd(II). The adsorption of Cd(II) onto chemically-activated carbons takes place via ion exchange mechanism.

Dinesh et al [51] has used low-cost activated carbon (derived from bagass, an agricultural waste material) for the removal of heavy metals from wastewater. The study did not mention the adsorption mechanism, but the type of adsorbent and positive adsorption-enthalpy suggests ion exchange mechanism. Saturation occurred within 8–9 hours.

Kadirvelu et al [52] prepared activated carbon from coir-pith by a chemical activation method and used it for the adsorption of toxic heavy metals, Hg(II), Pb(II),

Cd(II), Ni(II) and Cu(II) from industrial wastewater solutions. The adsorption is pH dependent in the acidic range. The mechanism of adsorption was suggested to be ion exchange.

Kobya et al [53] prepared active carbon from apricot stones by carbonisation followed by activation by sulphuric acid at 200°C for 24 h. The ability of the activated carbon to remove Ni(II), Co(II), Cd(II), Cu(II), Pb(II), Cr(III) and Cr(VI) ions from aqueous solutions by adsorption was investigated. Batch adsorption was dependent on the pH of solution. Highest adsorption occurred at 1–2 for Cr(VI) and 3–6 for the rest of the metal ions. This may make it difficult for universal removal at certain pH. Ion exchange is considered to be the adsorption mechanism.

Carbon aerogels are adsorbent materials composed of covalently bonded nanometer-sized graphite crystals that are arranged in a three-dimensional network and have high porosity and high surface area [54]. Thus, they can be produced in monoliths, powder and sheet forms and provide excellent treatment efficiency in a cost effective manner for the purification of effluents/wastewaters. Stock aerogels are derived from the sol–gel polymerisation of selected resorcinol formaldehyde monomers in solution. The sol–gel solution is cast into the desired shape after the formation of a highly cross-linked gel, and the solvent is removed from the pores of the gel. Resorcinol formaldehyde aerogels are carbonized to form *pure* carbon aerogels. They are mainly prepared by pyrolysis of RF aerogels in an inert atmosphere.

Ajay et al [54] used carbon aerogel for the removal of Cd(II), Pb(II), Hg(II), Cu(II), Ni(II), Mn(II) and Zn(II) from aqueous solutions by batch method. It was found that adsorption is spontaneous and endothermic. The rate of adsorption ranged from 0.03 to 0.2 h^{-1} (according to ion). The capacity ranged from 0.75 for Pb(II) to 562 mg g^{-1} for Cu(II) which is considerably high. The mechanisms suggested to involve in adsorption are surface complexation and ion exchange. However, nearly 100% removal of heavy metal ions (under optimised conditions) occurs within 48 hours.

It is observed that heavy metal removal by carbonaceous adsorbents follows, mostly, the ion exchange mechanism. Adsorption saturation state is generally reached after several hours and sometimes needs more than 24 hours. This characteristic may limit the use of these adsorbents for practical removal of heavy metals especially when the continuous method is applied.

2.7.3 Bio-materials

Recently, researches show that the use of biomaterials is competitive with conventional materials for the removal of heavy metals from contaminated wastewater due to its significant adsorptive structure and low cost.

The cell wall of micro-organisms consists of polysaccharides, proteins and lipids offering many functional groups (such as carboxyl, hydroxyl, thiol, sulphonate, phosphate, amino and imidazole groups) that can bind (coordinate) metal ions. Many micro-organisms (including bacteria, yeasts, fungi and algae) can be used as biomaterials for heavy metal adsorption from wastewater [55]. Also, by-product wastes of agricultural and its related-processes have potential adsorption properties. The cation exchange properties of these residues may be attributed to the presence of carboxylic and phenolic functional groups, which exist either in the cellulosic matrix or in the materials associated with cellulose such as hemicellulose and lignin [56].

Olive stone [57], coconut shell-powder [58], papaya wood [59], chaff [60], green alga (*Spirogyra* species) [61], coir [62], dried marine green macroalga (Caulerpa lentillifera) [63], grape stalk waste [64], rice husk (an agricultural by-product) [65], tea waste [66] and dried *Pseudomonas putida* [67] are examples of bio-materials which have been studied for removal of heavy metals. Some of these materials are of low capacity [57, 62], pH dependent of removal [63–66], removal-affected by presence of alkali metals [64] and all show ion exchange mechanism to be the sole or the main mechanism of adsorption (some time complexation and electrostatic attraction participate in the process)

Bio-materials are extensively studied as they are available and cheap. Also, the ease of use (raw and modified) attracts more researchers to engineer for practical application especially in developing countries. Different mechanisms contribute to adsorption. The adsorption capacity for these materials is, generally, lower than that of other adsorbent types.

2.7.4 Synthetic organic resins

For adsorption applications, resins with sufficient porosity and active surface (suitable functionality) can be viewed under this category regardless of removal mechanism. Synthetic organic resins are the most important type. There have been many investigations of these adsorbents because of variety of starting compound, different preparation methods, porosity and surface morphology controllability. Also, ease of control of the nature of active sites gives the researcher the freedom to engineer materials for specific applications. However, most organic resins follow an ion exchange mechanism for the removal of targeted ionic contaminants.

The traditional synthesis of ion exchange resins begins with the polymerization of monomers to form a solid matrix that is insoluble in both water and solvents. The copolymer matrix then is functionalized with designated groups. The chemistry of the resin matrix, degree of porosity and particle size is controlled during the previous steps. For styrenic resins (widely used commercially), pre-determined amounts of styrene (90–95 wt %) and divinylbenzene (cross-linker: 5–10 wt %) are mixed in the organic phase tank. The produced copolymer is ion exchange-inert itself and the functionalisation step is essential to activate the resin network with adsorbing sites. Functionalisation is carried out chemically by bonding acidic or basic functional groups (according to the final application) to the aromatic rings of styrenic part [21,68].

The type of the group attached to the resin matrix contributes largely to the behaviour of the resin. The total number of active groups per unit weight of the resin determines the exchange capacity. The nature of the group affects both the ion

selectivity and ion exchange equilibrium. Cation exchangers (resins having exchangeable cations) contain functional acid groups such as sulfonic ($R–SO_3H$), phenolic (R–OH), carboxylic (R–COOH) and phosphonic ($R–PO_3H_2$) [32]. Chelating resins are another type where a chelating compound is chemically bonded to the matrix. Commercially available ion exchangers have trade names such as Amberlite, Duolite, Dowex, Ionac and Purolite [69].

Claudia et al [70] reported the use of Dowex M-4195 (chelating resin) to remove copper, nickel, cobalt, iron, manganese and lead from a highly acidic manganese chloride solution (Battery industry). The removal occurred by binding these metal ions to the bis(2-pyridylmethyl) amine functional group on Dowex M-4195. Chelation was the mechanism of adsorption and effective M(II)-elution was carried out by two steps.

Prasun et al [71] synthesised a new chelating resin by incorporation of dithiocarbamate groups to styrene/divinylbenzene copolymer. The total sorption capacity of the resin was 37 mg g^{-1} for Ni(II), 35 mg g^{-1} for Cu(II), 29 mg g^{-1} for Fe(III), 23 mg g^{-1} for Pb(II) and almost nil for As(III). The kinetics study showed a rapid sorption indicating a better accessibility of the chelating sites (loading half time < 12 minutes). However, dithiocabamate sites did not chelate arsenic ion which is against the fact that dithicabamate is well known complexing agent for colourimetric determination of arsenic. This observation indicates that another mechanism, other than chelation, contributes strongly in adsorption.

Bahire et al [72] synthesised terpolymer beads possessing diethylene triamine tetra acetic acid (DTTA) functions. DTTA has EDTA-like chelating units. The terpolymer was able to absorb heavy metal ions such as Fe (III), Zn (II), Cd (II) and Pb (II) ions. However, 1) the DTTA-functionalized terpolymer was prepared through several long steps 2) although chelation was the mechanism of adsorption, the high affinity of DTTA towards Ca(II) and Mg(II) can interfere with heavy metal removal.

Stella et al [73] studied a special class of grafted textiles for the removal of heavy metals from industrial wastewaters. Three cation-exchanger textiles (CET) were tested in a batch reactor, each carrying carboxylate($R–COO^-,Na^+$), sulfonate ($R–SO_3^-$, Na^+) or phosphate ($R–O–PO_3^{2-}$, $2Na^+$) functional groups. Generally, these textiles showed successful adsorption towards Cu(II) and Cd(II) by the ion exchange mechanism. The presence of divalent cations such as Ca(II) and complexing agent such as EDTA (common situation for many industrial wastewater) adversely affect the adsorption process.

Kais and Suhaila [74] synthesised a chelating ion-exchange [poly(salicylaldoxime 3,5-diylmethylene)]. The sorption selectivity towards various divalent ions was: $Cu^{2+} > Cd^{2+} > Zn^{2+} > Ni^{2+} > Ca^{2+} > Mg^{2+}$. It is clear that chelation favours heavy metal ions over alkaline earth ions.

Korngold et al [75] reported the selective removal of heavy metals (Cu, Ni, Co, Mn, Cd, and Pb) from tap water that contains relatively high concentrations of calcium and magnesium by a resin possessing a chelating iminodiacetic acid group (Lewatit TP-207). When the concentration of each of these metals in tap water was of the order of a few ppm, their leakage fell below the permitted level in drinking water. Elution of the heavy metals from the resin was successfully performed with 3 M HCI or HNO_3. Although the adsorption follows the chelation mechanism, the study did not discuss the effect of this mechanism on adsorption selectivity and affinity.

Chuh-Yean et al [76] synthesised magnetic Fe_3O_4–glycidyl methacrylate–iminodiacetic acid–styrene–divinyl benzene resin (MPGI) by the polymerisation of glycidyl methacrylate–iminodiacetic acid (GMA–IDA), divinyl benzene and styrene in the presence of magnetic Fe_3O_4. The MPGI resin was used for the removal of Cu(II), Cd(II) and Pb(II) from aqueous solutions. Although chelation is the mechanism, increasing the concentration (0–0.3 M) of KCl, NaCl, $MgCl_2$ and $CaCl_2$ in Cu(II) or Pb(II) solution slightly affected the adsorption behaviour.

Ramazan et al [77] prepared a fibrous adsorbent by graft copolymerization of methacrylic acid (MAA)/acrylamine (AAm) monomer mixture onto poly(ethylene terephthalate) (PET) fibres. The adsorbent was used for the removal of Cu(II), Ni(II) and Co(II) metal ions from aqueous solution using a batch method. The adsorption is sensitive to solution pH. In fibre structure, groups containing O and N atoms may suggest chelation to contribute in adsorption. However the endothermic nature of the process indicates ion exchange as another important mechanism.

Adil et al [78] synthesised N-methacryloyl-(l)-glutamic acid (MAGA) as a metal complexing ligand and/or co-monomer. Spherical beads were obtained by suspension polymerisation of MAGA and 2-hydroxyethyl methacrylate (HEMA) performed in an aqueous dispersion medium. Poly(HEMA-MAGA) beads were used in the removal studies of Pb^{2+} ions and adsorption equilibrium was achieved in about 60 minutes. The removal occurred by MAGA coordinating Pb^{2+} by two carboxylic groups. The adsorption is highly sensitive to solution pH which suggests contribution of the ion exchange mechanism. The study did not consider the effect of other type of contaminants on adsorption.

Essawy and Ibrahim [79] prepared different compositions of poly(vinylpyrrolidone-co-methylacrylate) hydrogel, [poly(VP-co-MA)]. The tendency of this copolymer gel to extract Cu^{2+}, Cd^{2+} and Ni^{2+} from synthetic wastewater was examined under various conditions such as pH and contact time. Removal for Cu^{2+} was noticed to increase in the pH range of 6.5–8 suggesting binding to ligands containing N and O atoms, but neglecting the effect of precipitation which may occur in this pH range.

Poly(ethylene glycol dimethacrylate-*n*-vinyl imidazole) [poly(EGDMA–VIM)] hydrogel was prepared in the form of beads by copolymerising ethylene glycol dimethacrylate (EGDMA) with *n*-vinyl imidazole (VIM) by Ali et al [80]. The hydrogel was used for the removal of selected heavy metal [Cd(II), Hg(II) and Pb(II)]. pH significantly affected the removal capacity.

Grag et al [81] reported many of chelating resins which are being used for separation and/or preconcentration of heavy metals. These chelating resins are based on: poly(acryloamidoxime)-divinylbenzene copolymer, poly(acrylonitrile)-divinylbenzene copolymer, epithiopropylmethacrylate-divinylbenzene copolymer, Amberlite XAD-2 (polystyrene type), Amberlite XAD-4 (polystyrene-divinylbenzene copolymer type), Amberlite XAD-7 (acrylic ester type), Amberlite XAD-16, cellulose, carbon fiber, activated alumina and silica gel. These resins can be used as well for heavy metal removal from wastewater. Each of these resins has target heavy metal(s) to act upon.

From the previous literature survey [70–81], it can be noticed that chelation is the main mechanism for the removal of heavy metals when using synthetic organic resins [70–72,74–76,78,80] whereas the ion exchange mechanism has some contribution in adsorption for some resins [73,77].

Although chelation is effective for removal, previously studied adsorbents showed some problems when removing heavy metals: sensitivity to solution pH (i.e. considerable difference in removal percentage as solution-pH changes) and suppression of removal by other type of contaminants. This suggests that ion exchange may contribute in the adsorption process and/or the small number of coordinations to M(II) make chelation less stable. The chelation mostly occur by 2–4 coordinations, some of which do not belong to the same chelating site [26,71,75]. The number of coordinating groups present in a chelating site is an important factor for chelation; however no relation with adsorption has been stated. Also, there was no discussion about the role of chelation on the affinity.

It is worth commenting that a considerable number of these adsorbents are based on styrene/divinylbenzene as the matrix on which active sites were grafted and that means several steps of preparation to achieve final-adsorbent product [81]. Other types, not using this matrix [72,74,77–81], also show several steps for synthesis. The need for a simple adsorbent preparation method is recommended, especially in developing countries.

2.7.5 Hybrid adsorbents

Hybrid (or composite) adsorbents are considered a new promising type of adsorbent that started to appear few years ago. The idea behind them is to get the advantages from each component of the composite to enhance the adsorption behaviour (kinetics, capacity, regeneration, stability, etc.). For example, composite materials formed by the combination of inorganic ion exchangers of multivalent metal acid salts and organic conducting polymers (polyaniline, polypyrrole, polythiophene, etc.), provide a new class of organic–inorganic hybrid ion exchangers with better mechanical and granulometric properties, good ion-exchange capacity, higher stability, reproducibility and selectivity for heavy metals [82]. Examples of these systems are alginate–chitosan hybrid gel beads [83] and alumina/chitosan composite membrane [84]. However, composites or hybrid materials have not yet shown suitable behaviour for heavy metal removal.

2.7.6 Adsorption by ion exchange and chelation mechanisms

According to the literature survey the removal of heavy metals by carbon materials, zeolites, fly ash and clays follows ion exchange. With bio-materials, ion exchange, complex formation, physical and electrostatic attraction are the adsorption mechanisms. For synthetic organic resins, chelation is the main adsorption mechanism for many resin types besides traditional resins that follow cationic exchange.

There are some aspects concerning the removal of heavy metals by the ion exchange mechanism which is not shown by the chelating mechanism:

1. Simultaneous removal of several heavy metals is difficult to achieve.
2. Ion exchange mechanism is not highly selective towards heavy metal against alkali and alkaline earth ions which are usually present in many wastewater effluents. Removal is highly probable to decrease or even stop due to the presence of alkali and alkaline earth metal.

3. Presence of complexing agent(s) in treated aqueous solution, which is a common situation for many industries, may suppress heavy metal removal due to a high M(II)-complex agent formation stability constant.
4. The adsorption is sensitive to solution initial pH. The solution pH has to be adjusted at a certain value or in narrow range to have a successful process.
5. Ion exchange mechanism is an endothermic process which is not favourable from enthalpy point of view.
6. Elution is always carried out using mineral acids.

Hence, chelation is a competitive alternative mechanism and seems to be more versatile [26]. It is suggested that using adsorbents having chelating sites (that is having several coordinating groups) is highly probable to be effective for heavy metal removal due to multi-coordinate bonds that can be formed (high formation stability constant). In general, chelation is selective against alkali and alkaline earth ions, successful in the presence of complexing agent in solution as heavy metal-accompanying contaminant, favourable from an enthalpy point of view (exothermic) and less sensitive to solution pH. The adsorption through chelation mechanism is worth studying comprehensively (effect of pH, thermodynamic, kinetics, isotherm and detailed mechanism concerning number of coordinating groups and M(II)-complex formation) to evaluate its potential for heavy metal removal from wastewater and to identify its universal or separation behaviour.

Successful binding of a multi-dentate chelating agent to a porous material can produce a useful adsorbent. The regeneration of this type of resin can be carried out using a solution (of suitable concentration) of the same or another chelating agent rather than conventional mineral acids.

In spite of its exceptionally chelating power, many polyaminepolycarboxylic acids (PAPC) – such as DTPA (8-coordinations), CDTA (6-coordinations), NTA (4-coordinations), etc. – have not been thoroughly studied for their use as active sites in adsorbent material for heavy metal remediation from contaminated water effluents. The effect of the number of coordination groups was not studied as well. Using these

strong chelating agents (PAPC) for heavy metal removal by a polymeric adsorbent is presented in this study discussing the chelation mechanism and affinity. The matrix on which PAPC agents were anchored is melamine-formaldehyde resin. PAPC-modified melamine-formaldehyde matrix is easier to produce compared to conventional activated-styrene/divinylbenzene.

Chapter 3

Modification of melamine formaldehyde resin

3.1 Melamine-formaldehyde resin

The easy-to-produce MF was characterized as tough and chemically resistant. With an associated very low formaldehyde emission, MF is used for a variety of products that have direct contact with human beings such as Formica and melamine dinnerware. Also, it has many important applications such as fabric impregnation, paints, electrical moulding, glass-reinforced substrates, adhesives and engineered wood products [85]. These applications depend on the dense form of MF. The melamine-formaldehyde (MF) condensate resin was first synthesised in the 1930s [93].

By the early 1990s, Pekala et al managed to synthesise different organic monolithic aerogels (resorcinol-formaldehyde and melamine-formaldehyde) from which carbon aerogels (a monolithic three-dimensional network of carbon nanoparticles) were produced. Carbon aerogel has many different uses including electronic applications. Carbon aerogels have high electrical conductance and large surface areas per unit volume and can be exploited in super-capacitors, electrodes for electrochemical applications and electro-sorptive processes [86–88].

The porosity of the starting organic aerogel (resorcinol-formaldehyde and melamine-formaldehyde) is the origin for porosity of the corresponding carbon aerogel. For the melamine-formaldehyde system, different monolithic gels were prepared and the effect of different synthesis conditions on the porosity was studied [89,90].

Porous organic resins are widely used as adsorbents due to their functionalities, high surface area and stability over a wide pH range [91]. As the MF gel is porous, it can be considered as a material that has a potential as an adsorbent. Furthermore, MF organic gel can be functionalized with suitable binding active sites to serve as a metal-adsorbent. This work aims to produce a new synthetic porous organic chelating adsorbent based on MF resin capable of adsorption of heavy metals from water effluents.

3.2 MF-polyaminepolycarboxylic acids (MF-PAPC) adsorbent preparation

Chitosan modified by the chelating agents ethylene diamine tetraacetic acid (EDTA) and diethylene triamine pentaacetic acid (DTPA) were prepared by anchoring these agents to the chitosan structure by the amide bond. Chitosan is a good metal adsorbent, and this modification enhances the adsorption. It was observed that the adsorption order of metal ions by modified chitosan is nearly in agreement with the corresponding formation stability constants of metal-chelates. This suggests that the chelating behaviour is still maintained after anchoring these agents onto the chitosan matrix [92]. However, chitosan includes hydroxyl groups which may give rise to ion exchange in the adsorption process, or alter the chelation behaviour.

The suggested structure of these chelating adsorbents **(Figure 3.1)** shows that each chelating agent is anchored to chitosan by only one amide bond whereas the other carboxylic groups are still free from reaction with chitosan which may explain why chelating agents retain their chelation affinity towards various metal ions. An important drawback of this adsorbent is the partial solubility of chitosan which causes a significant deterioration.

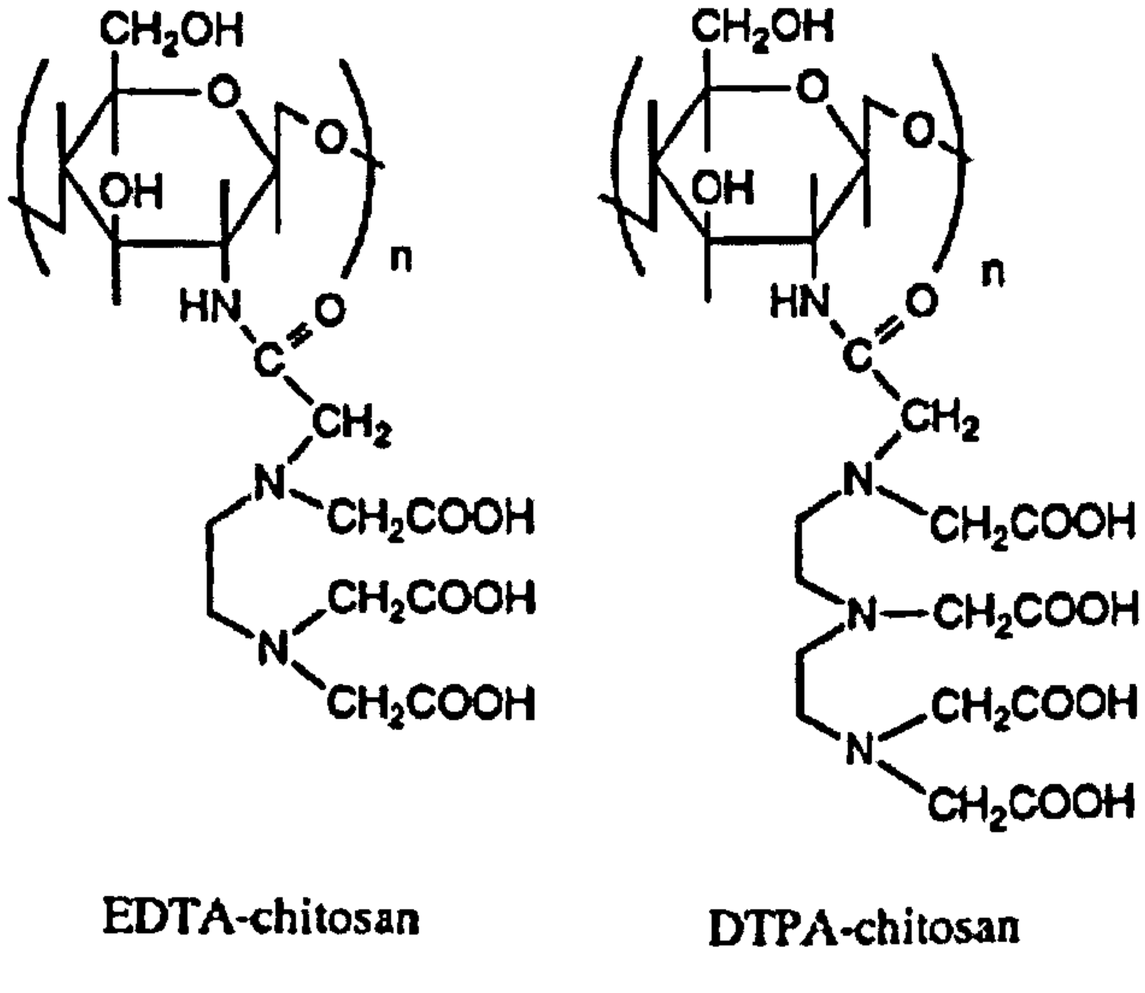

Figure 3.1: Chitosan modified by EDTA and DTPA.

An essential preliminary study was conducted regarding the preparation of melamine-formaldehyde-NTA chelating adsorbent and its use for the removal of Cu(II) ions from synthetic wastewater [94]. The preparation process included a

mixture of guaiacol and acetone as porogens. Guaiacol could react and incorporate itself in the matrix which introduces hydroxyl groups. The presence of –OH groups may contribute to adsorption through ion exchange/coordination as well as chelation by NTA. This study showed that NTA (nitrilotriacetic acid) was anchored to the MF matrix forming MF-NTA chelating adsorbent which is hydrophilic and has a surface area of 163 $m^2 g^{-1}$. Experiments indicated fast removal of Cu(II) ions with promising capacity of 23.1 mg g^{-1} [94]. This study suggested that polyaminepolycarboxylic acid-modified MF is a promising material as an adsorbent for the removal of heavy metals from wastewater [94].

In the present work, melamine-formaldehyde-polyaminepolycarboxylic acid adsorbents (MF-PAPC) were synthesised under acidic conditions at elevated temperature. The normal melamine-formaldehyde resin (MF) synthesis procedure starts with the methylolation of melamine which can be catalyzed by base or acid, where $-NH_2$ groups of melamine react with formaldehyde to produce *methylol* ($-NH-CH_2OH$) groups. Melamine can react to give up to six methylol groups per molecule [95]. Subsequently, these methylol groups condense upon further heating and/or acidification to form two types of bridge. Condensation can occur in two ways: reaction of the methylol group with unreacted amine, to give the methylene bridge ($-CH_2-$) with water loss and condensation of two methylol groups with each other to give an ether bridge ($-CH_2-O-CH_2-$) with the loss of a water molecule [95–99]. Also, there is the possibility of bridging two melamine molecules via their primary amine by two formaldehyde molecules with no loss of water thus conserving two hydroxyl groups in a bridge [93]. Furthermore, formaldehyde can react with $-NH_2$ groups of melamine to form imine groups (>C=N–) accompanied by water production [100]. During bridge formation (matrix construction), carboxylic groups of PAPC acid react with a number of $-NH_2$ melamine groups to form amide covalent bonds, that is anchoring chelating moieties to the MF matrix [94,100,101]. There is a possibility for one PAPC acid molecule to anchor to more than one melamine molecule which acts as a bridge in this case. The suggested mechanism and final adsorbent formula – using DTPA as a representative of PAPC acids – is shown in **Figure 3.2**.

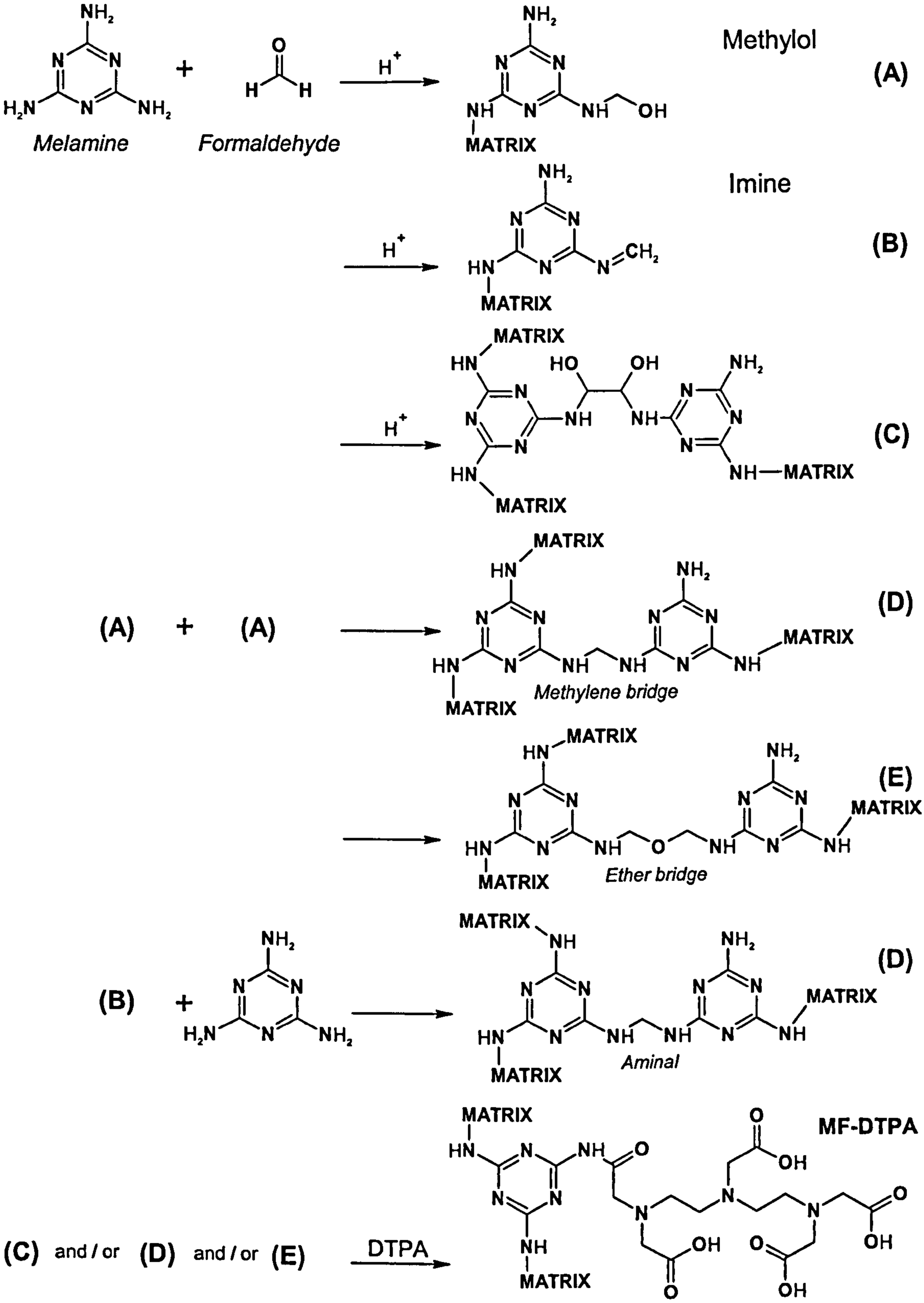

Figure 3.2: Suggested formation mechanism of MF-DTPA adsorbent from melamine, formaldehyde and DTPA precursors under acidic condition.

The MF-PAPC material is produced in monolithic hard form. Hence, it can be used in the form of the monolith, granules or powder which gives the applicator the freedom to select according to the practical application. The monolith form is very promising if it shows good kinetics, as it will have the advantage of being able to withstand hydraulic pressure and undergo less deterioration due to erosion. However, this needs more investigation as the mesoporous structure of the produced material makes it difficult for aqueous flow.

3.3 MF-PAPC acid adsorbent interaction with heavy metals

The produced chelating adsorbents (MF-PAPC) can be used for the removal of heavy metals (transition, lanthanides and actinides metals) from waters because of the active chelating sites pendent from the adsorbent matrix. Transition metals (*d* block elements) are typically characterized by incomplete *d* orbital(s) with some exceptions (zinc group). Transition elements readily form complexes (chelates) as they are characterised by small, highly charged ions and vacant low energy levels which are able to accommodate lone pairs of electrons donated by ligands of PAPC.

The chelating compounds used in this study are diethylene triamine pentaacetic acid (DTPA), cyclohexane diamine tetraacetic acid (CDTA) and nitrilotriacetic acid (NTA). They are known to strongly chelate these metals in aqueous solution. The chelation process depends on the type of metal, pH and the presence of competitive species in solution. The chelation behaviour originates from constitution of these compounds of the donor atoms (nitrogen and oxygen). DTPA has eight coordination groups, CDTA has six coordination groups and NTA has four coordination groups.

According to valence bond theory, upon mixing these adsorbents with a solution containing heavy metal ions, the coordination atoms donate (accommodate) their lone pairs to the vacant orbitals of heavy metals ions. PAPC acids have many coordination sites, and chelates are readily formed as the ring structure is stable and the greater the number of rings formed, the more stable the chelate. This stability is useful in the removal of heavy metals from solutions as it guarantees less elution

during adsorption process. In the case of a mixture of heavy metal ions in solution, the chelating agent shows different affinities towards the metal ions which depend on complex formation constants.

For this type of adsorbent, removal of heavy metals from aqueous solution by chelation is more likely than ion exchange, which is possible because of the carboxylate groups present. This is because the coordination groups are very close to each other – they belong to same molecule – which encourages chelate formation. This synthesised adsorbent type is promising for the removal of heavy metals from aqueous media with pH values varying from weakly acidic to neutral [102]. In this study, Co(II), Cd(II), Zn(II) and Cu(II) were considered as heavy metal contaminants in water and their removal was investigated simultaneously. The way by which the complexes can form by these metal ions is an important consideration as this may play an effective role for their adsorption especially when present as a mixture in the same solution. Most adsorption studies are conducted using aqueous solutions with a single metal. However, the treatment of multi-ion aqueous solutions has many practical applications [103]. In addition, this type of study would give meaningful results concerning the relative affinity of adsorbents towards a variety of heavy metals.

The Co(II) ion complexes are present in tetrahedral (four coordinations) and octahedral (six coordinations) forms since the difference in stability between these two forms is small. Both forms can exist in equilibrium. Also, the Co(II) ion forms more types of tetrahedral complexes than any other transition metal ion. Most Co(II) complexes are high-spin which correspond to the outer orbital form and this form is less stable than the inner orbital form. The Cu(II) ion readily forms distorted octahedral complexes due to the presence of two long trans bonds to each other and four short bonds. In aqueous solution, the Cu(II) ion forms tetrahedral complexes with amines and the two trans positions retain water molecules. The Zn(II) and Cd(II) ions form complexes with compounds which have O donor ligands and also with N and S donor ligands. Both form mainly tetrahedral complexes. Octahedral complexes may form in few situations [104].

Chapter 4

Methods of adsorbent characterization

Physical and chemical properties of an adsorbent have to be determined to understand its adsorption behaviour and to know the cause of its deterioration due to repeated use.

4.1 Adsorbent physical characterizations

4.1.1 Hydrophilic character (Water regain)

Water regain factor ($W\%$) represents the percentage of water intrinsically held by the adsorbent. This factor reflects the hydrophilic character of the adsorbent and hence gives an idea about the ease of aqueous-solution flow through the adsorbent matrix. An increase of regain factor means that water molecules are highly dispersed in the adsorbent. Hence, the metal ions solution can reach almost all parts of the adsorbent matrix which gives high probability for metal ions to react with active chelating sites.

The adsorbent is thoroughly washed with water upon preparation. Excess water is removed by vacuum filtration or centrifugation. Always a significant amount of water is retained in the adsorbent texture associated with the functional groups. Usually no effort is made to remove this adhering water since the adsorbent is used in aqueous medium.

Each adsorbent has its own characteristic water content depending on its texture, chemical structure and density of functional groups and the ionic form of these groups [21]. The more ionic form of adsorbent groups, the more water molecules would be attracted to the matrix. To calculate this factor, the following equation is employed [105]:

$$W\% = \frac{W_w - W_d}{W_w} \times 100$$

Where W_w and W_d are weight of the wet and dried adsorbent-sample respectively.

4.1.2 Adsorbent texture

The study of the internal texture and geometrical structure of the adsorbent material in the micro-scale is important. Factors like cells or pores shape and size and whether the pores are closed or opened are essential data. An adsorbent matrix with open connected cells (pores) allows capability of easy-flow of fluids to diffuse throughout the matrix.

Macroreticular adsorbents are characterized by pores of several hundred Angstroms and are known to be rigid. Their physical picture is an agglomerate of randomly packed microspheres and they have high surface areas. Because of their high porosity and large pore diameter, these adsorbents exhibit less fouling when employed in water and wastewater treatment. This type of adsorbent withstands aggressive operations [68]. They are usually based on co-polymerisation of styrene/divinyl benzene and acrylic acid esters/ divinyl benzene and commercially available in bead form [48].

A broad range of adsorbents can be pictured as a polymeric structure whose active sites are restricted in motion by attachment to the adsorbent-matrix. The active sites are free to rotate about their position of attachment but their translational motion is restricted. Investigating the adsorbent using BET analysis, Scanning Electron Microscopy (SEM) and X-ray Diffraction (XRD) gives data about its morphology.

4.1.2.1 Porosity characteristics (BET)

Adsorbents are either microporous or macroporous (macroreticular). Macroporous types have a measurable porosity which does not close on drying [21]. Porosity measurements are important to get information about surface area, pore volume and average pore diameter and the morphological structure of an adsorbent. According to the IUPAC classification of pores, the size ranges are micropores (< 20 Å), mesopores (20–500 Å) and macropores (> 500 Å).

The surface area, pore volume and average pore diameter of an adsorbent material are usually obtained from nitrogen adsorption measurements carried out at liquid nitrogen temperature (77 K) where adsorption on the surface and capillary condensation of nitrogen in the pores takes place. The thickness of the adsorbed layer on the surface and the size of the pore where condensation happens depend on the partial pressure of the nitrogen. Thus an adsorption isotherm can be converted to the pore size distribution by proper relation between both thickness of adsorbed layer on the surface and the size of the pore with the partial pressure [106].

Internal surface area of the adsorbent can be measured by applying the BET adsorption isotherm, where the amount adsorbed by monomolecular coverage gives the specific surface area by assuming the molecular sectional area of nitrogen to be 16.2 $Å^2$/molecule, which corresponds to 9.76×10^4 m^2/mole [106]. The adsorption data are then interpreted using the BET isotherm which is extensively applied to the determination of the surface area of porous materials. The main assumptions in BET theory are: 1) no interaction between neighbouring adsorbed molecules and 2) the heat evolved during the filling of second and subsequent layers of molecules equals the heat of liquefaction.

The BET measurement gives an adsorption-desorption hysteresis loop as well which is helpful to understand the pore-geometric shape [48].

4.1.2.2 Scanning Electron Microscope (SEM):

SEM gives an image of the material under study in the nanometre scale which helps to understand its texture. Typically in the SEM instrument, beams of electrons are emitted from a tungsten or lanthanum hexaboride (LaB_6) cathode filament towards an anode in a vacuum. The electron beam (having an energy ranging from a few to 50 keV) is collimated by two successive electromagnetic condensing lenses, focussed by an objective lens into a beam with a very fine spot size (~ 5 nm). The beam scans across the surface of the sample by electromagnetic deflection coils. Secondary electrons are emitted from the sample upon collision with the incident beam. The

sample image is produced by collecting secondary electrons that are released by the sample. The secondary electrons are detected by a scintillation material that produces flashes of light. The flashes are then detected and amplified by a photomultiplier tube. By correlating the sample scan position with the resulting signal, an image can be formed that is similar to what would be seen through an optical microscope.

4.1.2.3 X-ray Diffraction (XRD)

Materials can be classified as crystalline, semicrystalline or amorphous. XRD is useful for the qualitative and quantitative identification of the molecules of solid crystalline or semicrystalline materials and can provide the exact crystal structure of a pure single crystal material. Qualitatively, it can specify the type of the material (crystalline, semicrystalline or amorphous). Many inorganic and organic compounds, minerals, metals, alloys and some types of polymers form crystals and can be analyzed by XRD [107].

If the spacing between the planes is about the same dimension as the wavelength of the incident X-ray beam, the reflected beam will be parallel and coherent (instructive or in phase) and a signal will be recorded. If the waves are completely out of phase (destructive), their amplitude cancels each other and no beam emerges, i.e. no signal [107]. The XRD-pattern produced by the diffraction of X-ray through the material under test is recorded and then analyzed to determine the nature of the material. The spacing in the crystal lattice can be determined using Bragg's law.

The observed diffraction pattern of a material indicates whether the material units (atoms, ions or molecules) are arranged in an ordered pattern or not. The crystalline material diffractogram always shows a number of peaks for different incident X-ray angles which indicate several plane spacings. Poor diffractograms (few or no signals) are recorded for amorphous materials which indicate the material units are not arranged in a repeated pattern [107].

It is possible to determine the degree of crystallinity of polymers. XRD is occasionally used to help determine the structure of polymeric materials. The noncrystalline (amorphous) portion simply scatters the X-ray beam to give a continuous background, whereas the crystalline portion gives diffraction signals [107].

A schematic layout of X-ray diffractometer is shown in **Figure 4.1**. The instrument constitutes an X-ray tube, a sample specimen and a rotating detector. Typically, powder is placed in the sample specimen holder. The machine emits a beam of X-rays bombarding the sample and the X-rays are diffracted by their interaction with the electrons in the sample. The X-ray tube consists of an evacuated glass tube containing a wire filament cathode (normally tungsten) and a pure metal anode (commonly copper whose characteristic wavelength for the K radiation is =1.5418Å). The wire is heated electrically giving off electrons which are accelerated towards the anode. Upon striking it, energy is released as radiation of very short wavelength (0.1–100 Å). The produced beam is filtered to produce monochromatic radiation. When this incident beam strikes a powder sample, diffraction occurs in every possible orientation of 2θ. The diffracted beam is detected by using a moveable detector such as a Geiger counter, which is connected to a chart recorder or computing system. In normal use, the counter is set to scan over a range of 2θ values at a constant angular velocity.

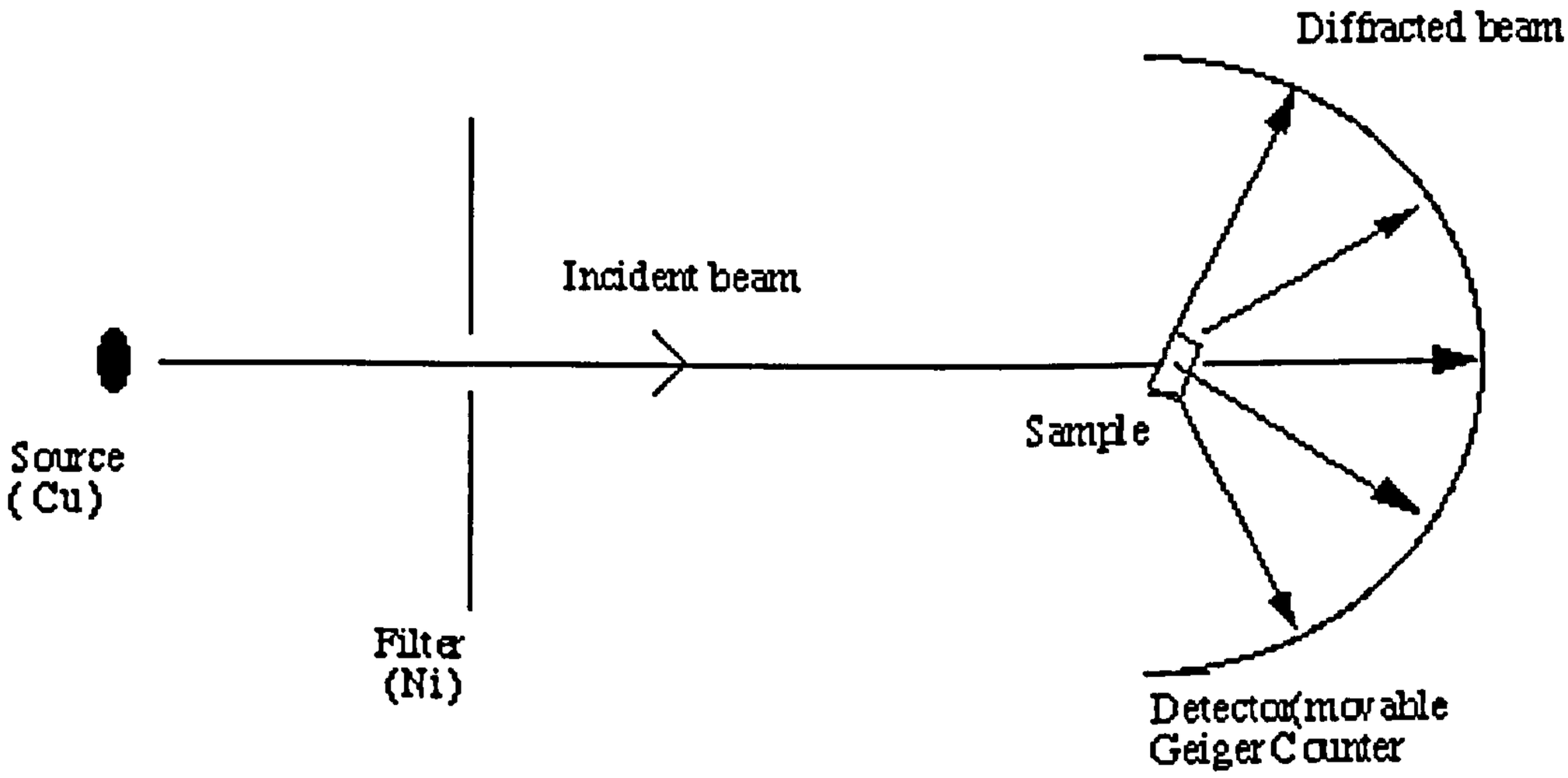

Figure 4.1: Schematic layout of an X-ray powder diffractometer.

4.2 Adsorbent chemical characterization

Investigating chemical structure gives essential data about groups and bonding types present in the adsorbent and reflects the success of preparation techniques to produce the intended product. Infra-red spectroscopy (IR), CHNO elemental analysis, nuclear magnetic resonance (NMR), and temperature programmed decomposition/mass spectrometry (TPD-MS) can give valuable information about chemical structure.

4.2.1 Infra-Red spectroscopy (IR)

IR radiation region includes wavelengths between 14000 and 20 cm^{-1}. The IR radiation part of interest falls between 4000 and 400 cm^{-1} which known as mid-infrared region. Molecules with covalent bonds can absorb IR radiation. The absorption is quantized, i.e. only certain frequencies of IR radiation can be absorbed. The energy associated with IR radiation is sufficient to cause molecule-groups to rotate and vibrate not to excite electrons to higher electronic state. Molecules absorb radiation when a bond in the molecule vibrates at the same frequency as the incident radiation. The frequency absorbed depends mainly on the masses of the atoms forming the bond and the geometry of the molecule. A change in the dipole moment of the absorbing bond is necessary in order to absorb IR radiation [107].

The common bond vibrations that are sensitive to IR radiation are stretching (change in bond length: symmetrical and asymmetrical) and bending (change in bond angle or respective position of a group to molecule: scissoring, rocking, wagging and twisting) vibrations [107].

Powdered potassium promide (KBr) can serve as a holder for the sample in the form of solid thin disc. A radiation source for IR spectroscopy has to fulfil continuity over wavelength range used, cover a wide wavelength range and be constant over long periods of time.

IR spectroscopy is a good qualitative and quantitative technique to analyse organic compounds. Functional groups (amines, ether, carboxyl, hydroxyl, thio, etc.) act

almost as separate groups (stable identity) and have characteristic absorption frequencies relatively independent of the rest of the molecule they belong to. This provides the basis for qualitative structural identification by IR spectroscopy. By examining the absorption spectra of an unknown sample and comparing the bands recorded with the characteristic absorption frequencies of known functional groups, it is possible to identify its functional groups and classify the sample [107].

Qualitative analysis is carried out by matching the wavelengths of the absorption bands in the spectrum of the sample with the wavelength of functional groups listed in tables. Tables of absorption bands and peaks are available for most organic groups which may show slight shift due change in chemical structure from one compound to another.

IR can investigate the energy-absorption by the adsorbent in the range of infrared radiation region. The practical region ranges approximately from 4000 to 400 cm^{-1}. Absorption of radiation energy in this region by an organic molecule causes excitation of vibrational, rotational and bending modes of the adsorbent molecule, while the molecule itself remains in its electronic ground state. IR spectra can give chemical structure information due to absence of peak(s) or band(s), in much the same way, as in the case of presence of a particular peak(s) or band(s). Chemical modification of an adsorbent by certain compound will alter its IR spectrum due to presence of new bonds which can be detected by IR.

Typically, a source for IR emits continuous radiation. This radiation covers a wide frequency range. However, the sample absorbs at certain frequencies. The IR spectrum is recorded by moving a grating so that different frequencies pass through the exit slit towards the sample then detector. This mechanism is applied for FTIR instrumentation [107].

4.2.2 CHNO elemental analysis

Elemental analysis is a process to determine the chemical formula for a chemical compound. The technique of analysis involves transformation of the compound elements into simple gaseous products. For reliable analysis, it is crucial to achieve a complete decomposition of the sample followed by quantitative collection of the decomposition products to be measured accurately by a suitable means. Every new organic material has to be confirmed by elemental analysis [108].

In the CHN analyzer, the organic material is oxidized at high temperature to yield carbon dioxide, water and nitrogen oxides:

$$\text{Organic material} \xrightarrow{O_2\ (1000^\circ C)} CO_2 + H_2O + NO_x$$

The nitrogen oxides are then converted to nitrogen gas in the presence of metallic copper (reduction):

$$NO_x \xrightarrow{Cu\ (600^\circ C)} N_2$$

Subsequently, CO_2, H_2O and N_2 are separated quantitatively and measured individually.

In the Perkin-Elmer elemental analyzer model 2400, the produced gases are separated using high sensitive chromatography technique. The CO_2, H_2O and N_2 gases are then measured in a thermal conductivity cell. According to the previous known weight of the sample, the percentages of carbon, hydrogen, and nitrogen are calculated. For a compound containing oxygen, like samples under study in this work, its percentage is calculated by subtraction.

4.2.3 Temperature-programmed decomposition/mass spectrometry (TPD-MS)

Mass spectrometry (MS) is a powerful analytical tool for many materials: organic, inorganic, polymer, medicine, etc. A mass spectrometer measures the ionised

gaseous-molecules according to their mass-to-charge ratio. The sample is being bombarded by a stream of electrons. The electrons must have sufficient kinetic energy to break covalent bonds forming ionic fragments. The mass spectrometer is provided with an electrostatic field capable of accelerating charged fragments. The charged fragments are separated in a magnetic field [108].

In Temperature-Programmed Decomposition / Mass Spectrometry (TPD-MS), TPD is carried out before mass spectra recording in which the material under study is placed in decomposition glass-tube (TPD cell) and heated at a programmed linear rate in an inert atmosphere flow. The heat causes degradation of the material and degradation-products are drawn continually to the mass spectrometer where ionic fragments are produced. Hence, the given chart is a temperature profile of the fragments' masses. **Figure 4-2** shows the schematic diagram of the instrument.

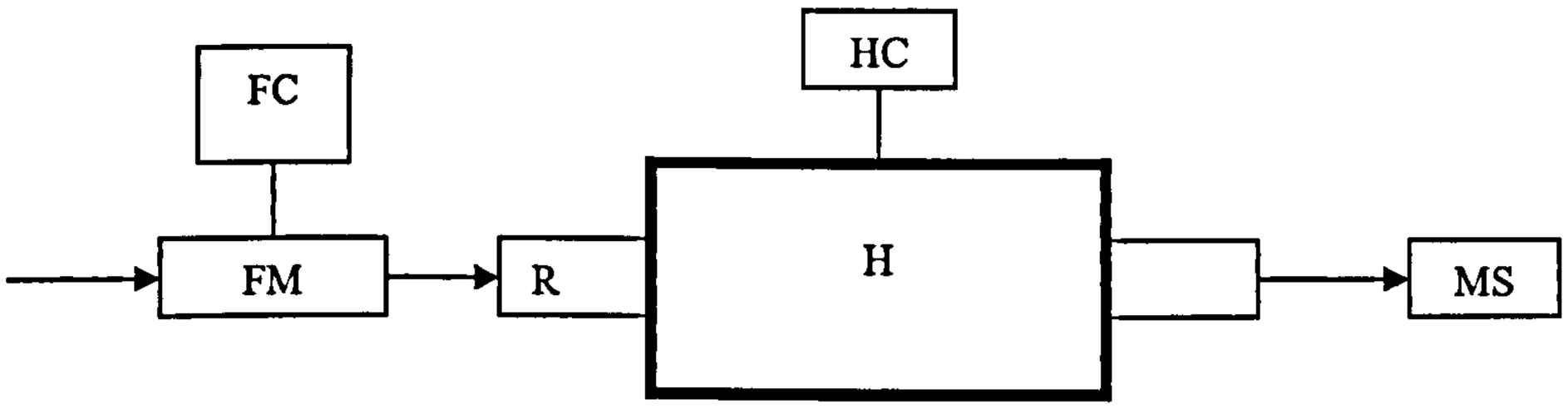

Figure 4.2: TPD-MS set-up: flow meter (FM), flow controller (FC), heater controller (HC), heater (H), TPD cell (R), mass spectrometer (MS).

4.2.4 Nuclear Magnetic Resonance (NMR) spectroscopy

Nuclear magnetic resonance (NMR) spectroscopy is a technique used to obtain chemical structural information about a molecule. NMR is a physical phenomenon related to the magnetic property of atomic nuclei. NMR involves the absorption of radiowaves (low energy electromagnetic radiation) by the nuclei of some atoms in a molecule that is located in a magnetic field. The radiowaves to be absorbed have frequencies of the order of 10^7 Hz. The energy involved in RF is too small to excite an atom or molecule and even cannot cause vibration or rotation of bonds. However, it is sufficiently strong enough to affect the nucleon spin. Nucleons have an intrinsic

spin property. Nuclei that contain odd numbers of nucleons (and some nuclei that contain even numbers of nucleons) have an intrinsic magnetic moment. As a result, spinning nuclei of some atoms in a molecule subjected to a magnetic field can absorb RF radiation and consequently change the direction of the spinning axis [107].

The nuclei of ^{1}H, ^{13}C, ^{15}N, ^{19}F and ^{31}P atoms possess magnetic moments. Hence their use for analyzing organic compounds is very important. An organic compound mainly constitutes carbon and hydrogen. Also, many organic compounds contain oxygen and nitrogen and to a lesser extent phosphor and fluorine.

For organic structure determination, the most important types of NMR spectra are the proton, carbon and nitrogen spectra. They give information about the numbers of hydrogen, carbon and nitrogen atoms in a molecule and how they are connected together (structure) as well as information about functional groups.

The most often-used nuclei are ^{1}H and ^{13}C, although certain isotopes of many other elements nuclei can also be observed.

The NMR-active nuclei exist in discrete nuclear spin states when the nuclei reside in an external magnetic field. The NMR measurement includes absorption of RF radiation by a nucleus while applying a strong magnetic field. Absorption of the RF radiation causes the nuclear spin to flip in the higher-energy direction. After absorbing energy, the flipped nuclei will re-emit RF radiation (relax) to return to the lower-energy state. NMR spectroscopy observes transitions between these spin states. The energy of an NMR transition depends on the magnetic-field strength. But, the local environment around a given nucleus in a molecule will slightly perturb the local magnetic field exerted on that nucleus and affect its exact transition energy. This dependence of the transition energy on the position of a particular atom in a molecule makes NMR spectroscopy extremely useful for determining the structure of molecules.

In the presence of an applied external magnetic field, ^{1}H and ^{13}C (also ^{15}N, ^{19}F and ^{31}P) nuclei exist in two nuclear spin states of different energy. Slightly more than half of the nuclei exist in the lower energy state called alpha (α) than in the higher energy state called beta (β). The external magnetic field B_o is created with a large magnet, commonly a super-conducting solenoid. The energy difference ΔE between the two spin states is proportional to the strength of B_o. The NMR spectroscopy records transitions between these spin states induced by a radio frequency electromagnetic field, B_1.

Consider ^{13}C as an example: If ^{13}C nuclei absorbed energy at exactly the same RF, NMR spectroscopy would not be useful for determination of organic structures. However, different ^{13}C nuclei absorb at slightly different frequencies. This difference results from differences in the small internal magnetic field B_e for each ^{13}C nucleus (The B_e field results from the circulation of electrons of the molecule). The different ^{13}C nuclei have different electron densities surrounding them and consequently, are shielded from the applied field B_o by B_e fields of different magnitude. The differences in (B_o-B_e) translate into differences in the RF needed to cause the nuclear spin transitions.

The NMR measurement complements and confirms the IR results to determine the structure of organic compounds.

The previous instrumental techniques and tests are essential for characterization of a new material (adsorbent). However, further analyses have to be carried out (future work) to comprehensively characterize the adsorbent for enhancement and practical use. The characteristics to detect are density, swelling and shrinking, hydraulic properties, fouling, thermal stability and physical stability.

Chapter 5

Models describing adsorption process of heavy metals

5.1 General

The practical application of adsorption for the removal of contaminates from wastewater is accomplished by contacting the adsorbent with the aqueous solution either in a batch or continuous flow system.

In a batch system, a pre-determined amount of adsorbent is mixed with the wastewater for a given contact period and subsequently is separated (by sedimentation or filtration). For large scale applications, wastewater flows continuously through a column packed with adsorbent where dynamic adsorption of the contaminant occurs. The most common type of bed is where the adsorbent remains fixed (stationary) during the process. The wastewater is pumped through the bed until either a specified (maximum) concentration is achieved or until the bed becomes completely exhausted.

5.2 Metal ions adsorption characterization

A batch arrangement is essential to evaluate the adsorption characteristics of a particular adsorbent–adsorbate system. The adsorption behaviour of an adsorbent towards metal ions in solution can be specified by the kinetics, thermodynamics, isotherm and affinity. For consistency, essential factors have to be specified: initial metal ions concentration, initial pH, temperature, and time of contact. Other parameters (adsorbent dose, grain size, shaking speed and solution volume) can be considered constant for all experiments. For all adsorption experiments, determination of the residual concentration of the metal ions is essential for data analysis and calculations. This concentration measurement is commonly carried out using atomic absorption spectroscopy (AAS).

Atomic absorption spectroscopy (AAS):

AAS is based on the absorption of radiation energy by free gaseous atoms. Atom absorbs energy to excite electron(s) from a lower-energy state to a higher-energy state. As a result, atomic absorption spectra consist of narrow absorption line(s). Each element has a specific number of electrons located in orbitals that is unique to

each element. The lowest energy electronic configuration of an atom is called the ground state which is the most stable electronic state. If exactly the amount of energy is supplied to the atom, the energy will be absorbed to promote the specific electron to a higher electronic position (orbital).

The number of energy levels in an atom is known and the energy differences of these levels are known and tabulated. For practical purposes, all absorption in AAS is by atoms in the ground state. This greatly restricts the number of absorption lines that can be recorded and used for measurement in atomic absorption [107]. A schematic layout of AAS instrumentation is shown in **Figure 5.1.**

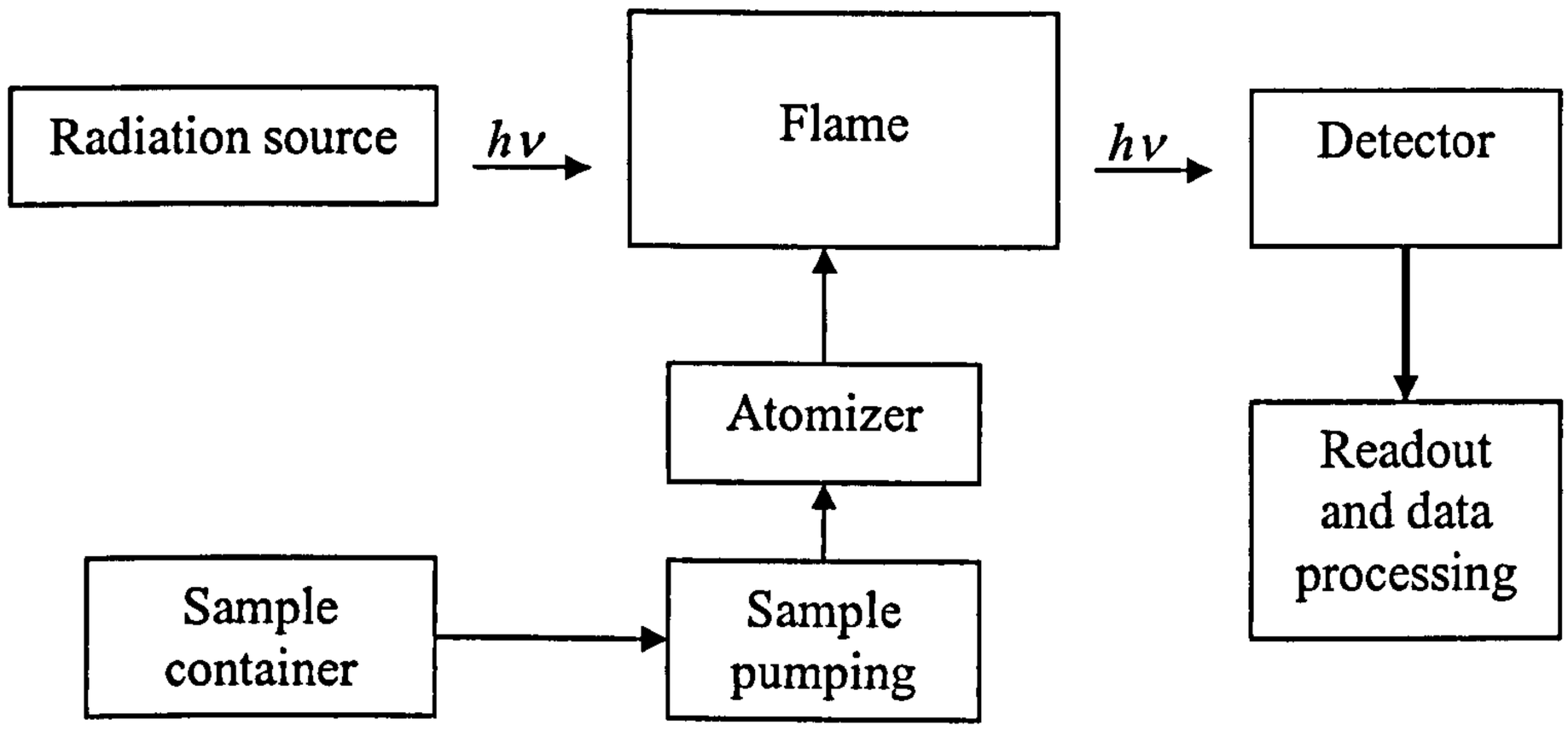

Figure 5.1: A schematic layout of AAS instrumentation.

For a typical measurement process, an amount of solution is pumped from sample-container to the atomizer where ion is converted to atomic state. This is achieved using thermal energy. Light of specific wavelength from the radiation source is directed to the detector through the flame volume which contains the analyte atom. The detector measures how much light is absorbed by the sample. Normally, a calibration curve can be constructed by using standards of various concentrations through the AAS and observing the absorbances. A computer data system converts this change in intensity into an absorbance [107].

5.2.1 Adsorption mechanism and kinetics

The study of adsorption kinetics describes the solute removal rate which controls the contact time of adsorbent with contaminated solution. Furthermore, it gives valuable information about the adsorption mechanism. There are several parameters that determine the adsorption rate, some of which are based on the adsorbent (adsorbent-matrix structure, grain size, surface area, average pore diameter and functional groups on the surface) and others on the solution (initial concentration of metal ions, ionic radius, solution pH, temperature and the presence of foreign species). The adsorption process on a porous material can be divided into four stages: (1) bulk diffusion, (2) film diffusion, (3) pore diffusion and finally (4) the residence (physical or chemical binding) of the solute on the adsorbent surface (**Figure 5.2)**. The overall adsorption kinetics depends on at least one of the previous steps [109,110].

Bulk diffusion controls the adsorption process for systems which have low concentrations of solute, small adsorbent particle size, poor mixing and a high affinity of the adsorbent for the solute. The intraparticle diffusion will control the sorption process for a system with a high concentration of solute, large adsorbent particle size, good mixing and a low affinity of adsorbent for the solute. The bulk diffusion and binding steps are always assumed to be rapid and may be not act as rate determining steps. However, solute transfer within adsorbent particles and inside the pores should be given proper consideration [110].

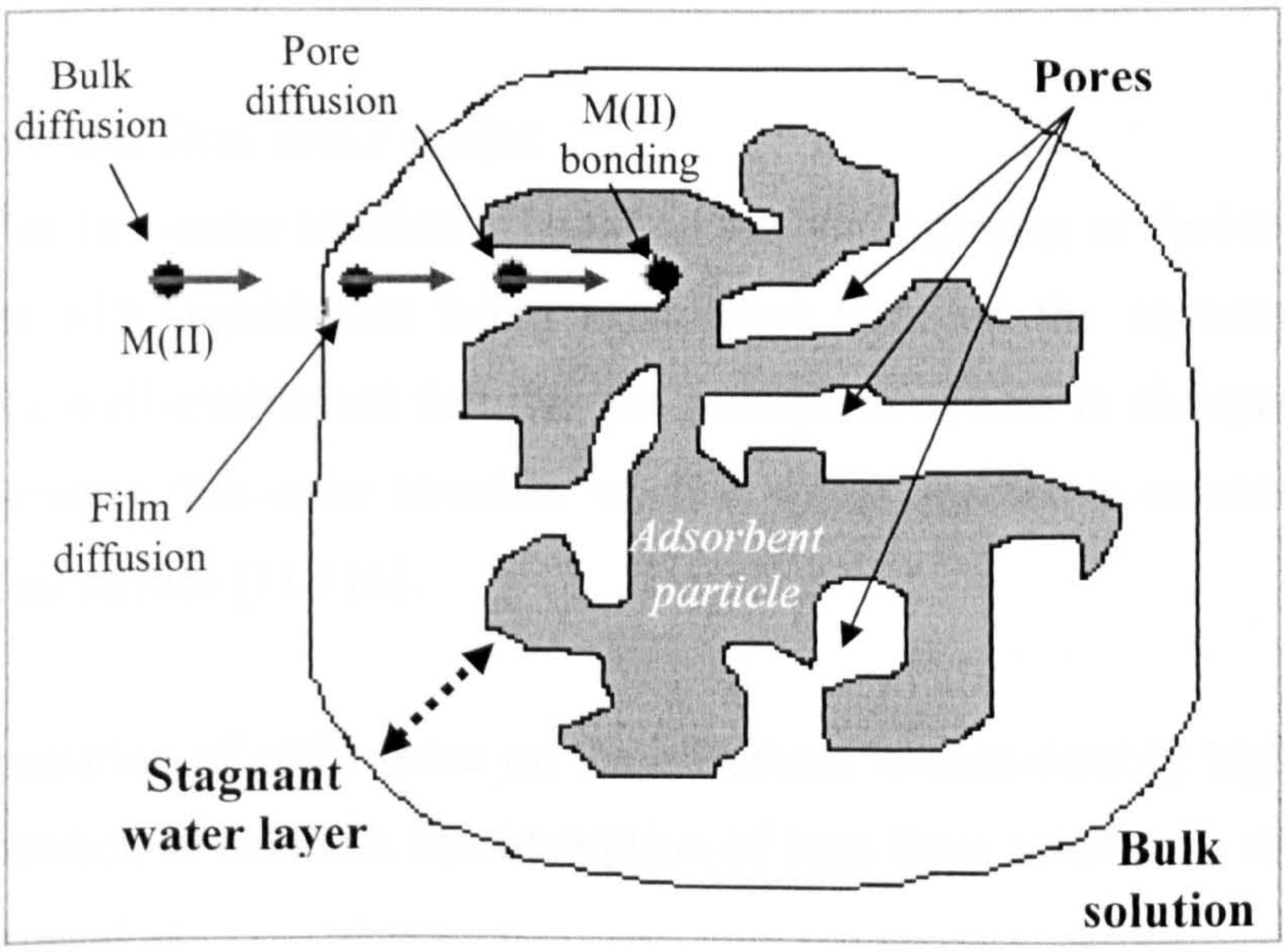

Figure 5.2: A scheme representing M(II) ion adsorption.

To clarify the adsorption mechanism, different kinetic models have to be examined with the experimental data. The extent to which these models fit the experimental data gives indication about the mechanism of adsorption.

It is often incorrect to apply simple kinetic models – such as first or second order rate equations – to adsorption onto solid surfaces which are rarely homogeneous. Moreover, mass transfer and chemical reaction have to be considered together [111].

In this study, four standard kinetic models are used to study the adsorption of metal ions from solution: reversible first-order [111,112], pseudo first-order (Lagergren) [7,9,112–115], pseudo second-order [7,9,112,113] and Elovich [114,115]. The first three models are based on the chemical reaction between adsorbate and adsorbent surface. The first model gives adsorption and desorption rate constants. The second and third models give the adsorption rate constant and adsorption equilibrium capacity. The last model gives an indication about the rate of initial stages of adsorption which is important for design purposes.

The fitting of a model to the experimental results was determined using the correlation factor R^2. A model successfully describes the kinetics of the adsorption process when R^2 is close to one [110].

5.2.1.1 Reversible first-order model

The reversible first-order reaction is based on the concentration of the ion transferred to adsorbent with equilibrium being established between the aqueous and solid phases. It is a well-established fact that the adsorption of ions in an aqueous system follows reversible first-order kinetics, when a single species is considered with a heterogeneous surface [11,116].

If the concentration of active sites on the adsorbent is considerably higher than the ions concentration in solution, the adsorption of ions from solution to the adsorbent may be expressed as:

$$M \underset{k_2}{\overset{k_1}{\longleftrightarrow}} MA$$

where:

M: stands for metal ion in solution.

MA: stands for adsorbed metal ions.

k_1: is the forward rate constant (adsorption rate).

k_2: is the backward rate constant (desorption rate).

If C_i is the initial concentration of the metal ion and C_r is the concentration transferred from solution to adsorbent at any time t, then the reaction rate can be expressed as [11]:

$$\frac{dC_r}{dt} = \frac{-d(C_i - C_r)}{dt} = k_R (C_i - C_r) \quad (1)$$

Hence by integration:

$$k_R = -\frac{1}{t} \ln\left(\frac{C_i}{C_i - C_r}\right) \quad (2)$$

where

k_R: is the overall reaction rate constant.

Since k_1 and k_2 are the rate constants for the forward and reverse process, the rate can be expressed as:

$$\frac{dC_r}{dt} = k_1(C_i - C_r) - k_2 C_r \quad (3)$$

If C_{re} represents the concentration adsorbed at equilibrium, then at equilibrium

$$\frac{dC_r}{dt} = 0 \qquad \text{hence,} \qquad k_1(C_i - C_{re}) - k_2 C_{re} = 0$$

and by rearranging the equation, $$K_C = \frac{C_{re}}{C_i - C_{re}} = \frac{k_1}{k_2} \quad (4)$$

where

K_C: is the dynamic equilibrium constant.

Under equilibrium conditions, the rate becomes [11,112]:

$$\frac{dC_r}{dt} = [k_1(C_i - C_r) - k_2 C_r] - [k_1(C_i - C_{re}) - k_2 C_{re}]$$

or $$\frac{dC_r}{dt} = (k_1 + k_2)(C_{re} - C_r) \quad (5)$$

by integration, $$k_1 + k_2 = -\frac{1}{t}\ln\left(\frac{C_{re}}{C_{re} - C_r}\right) \quad (6)$$

and by re-arranging equation (6)

$$\ln(1 - U_r) = -(k_1 + k_2)t = -k_R t \quad (7)$$

where

$U_r = C_r / C_{re}$.

Further, at equilibrium equations (2) and (6) are similar,

$$k_R = k_1 + k_2 = k_1 + \frac{k_1}{K_C} = k_1\left(1 + \frac{1}{K_C}\right) \quad (8)$$

5.2.1.2 Pseudo first-order model (Lagergren)

In 1898, Lagergren presented the first order rate equation for the adsorption of ocalic acid and malonic acid onto charcoal. The Lagergren kinetics equation has been most widely used for the adsorption of an adsorbate from an aqueous solution. In order to distinguish a kinetics equation based on the adsorption capacity of the solid from the concentration of solution, Lagergren first-order rate equation has been called pseudo-first order since 1998 [117].

The pseudo first-order model (Lagergren) suggests a dependency of the adsorption process on adsorbent capacity. The rate law according to the pseudo first-order equation is expressed as follows [117,118]:

$$\left(\frac{\mathrm{d}q_t}{\mathrm{d}t}\right) = k_L(q_e - q_t) \tag{9}$$

where

q_t: is the adsorbed amount of ion at time t (mg g^{-1}).

q_e: is the adsorbed amount of ion at equilibrium (mg g^{-1}).

k_L: is the rate constant of the pseudo first-order model (min^{-1}).

The integrated linear form of the Lagergren pseudo first-order model has the following expression [117]:

$$\log(q_e - q_t) = \log q_e - \frac{k_L}{2.303}t \tag{10}$$

A plot of $\log(q_e - q_t)$ against time would yield a straight line if the experimental data gives a good fit to the model. The values of q_e and k_L can be determined from the intercept and slope of the plot.

5.2.1.3 Pseudo-second-order model

The second-order kinetic expression for adsorption systems of divalent metal ions using sphagnum moss peat has been reported by Ho *et al* [119]. To distinguish a kinetic equation based on solid phase adsorption from one based on the concentration of the ions in solution, Ho's second-order rate equation has been termed pseudo-second order [119]. The pseudo-second order rate expression has been applied to the adsorption of metal ions, dyes, organic substances and oil from aqueous solutions. The pseudo second-order model is based on adsorption capacity and this capacity is proportional to the number of active sites occupied on the sorbent. It is also based on considering chemical reaction [111]. The pseudo-second-order model is given as [119]:

$$\frac{dq_t}{dt} = k_H (q_e - q_t)^2 \tag{11}$$

where

k_H: is the rate constant of pseudo second-order model (g mg^{-1} min^{-1}).

The parameters q_e and q_t (mg g^{-1}) have the same definitions as for the pseudo first-order model. The integrated linear form of the pseudo second-order model has the following expression [119]:

$$\frac{t}{q_t} = \frac{1}{k_H q_e^2} + \frac{1}{q_e} t \tag{12}$$

If the adsorption data obey this model, then a plot of (t/q_t) against time should give a straight line from which q_e and k_H (g mg^{-1} min^{-1}) can be determined from the slope and intercept of the plot.The initial adsorption rate (h (mg g^{-1} min^{-1})) – as time $t \rightarrow 0$ – can be determined as follows [119]:

$$h = k_H q_e^{\ 2} \tag{13}$$

5.2.1.4 The Elovich model

The Elovich equation is of general application to chemisorption kinetics [120,121]. The equation has been applied satisfactorily to some chemisorption processes and has been found to cover a wide range of slow adsorption rates. It is often valid for systems in which the adsorbing surface is heterogeneous [121,122].The Elovich model is a popular and successful model to describe the kinetics of chemisorption of gases on porous solids [114]. However, it does not predict any definite mechanism [122]. The Elovich model equation is expressed as [120,123]:

$$\frac{dq_t}{dt} = \alpha \exp(-\beta q_t) \tag{14}$$

where:

α: is the initial adsorption rate (mg g^{-1} min^{-1}).

β: is the desorption constant (g mg^{-1}).

Integration of Elovich equation by assuming $\alpha\beta t >> 1$ and applying the boundary conditions yields the following linear form [123]:

$$q_t = \frac{1}{\beta}\ln(\alpha\beta) + \frac{1}{\beta}\ln t \tag{15}$$

5.2.1.5 Experimental capacity (q_{exp})

The following mass balance equation was used to calculate the *experimental* amount of metal ion removed at equilibrium [80,124]:

$$q_{exp} = \frac{V(C_i - C_e)}{m} \tag{16}$$

where:

V: is the volume of the treated solution (l).

m: is the amount of dry adsorbent (g).

C_i: is the initial concentration of the metal ion (mg l^{-1}).

C_e: is the equilibrium concentration of the metal ion (mg l^{-1}).

The experimental capacity is then compared to the capacity derived from pseudo first and second-order models to make a judgment on the suitability of the models to represent the adsorption.

The variation of rate constant with temperature is common in adsorption systems. The value of activation energy of adsorption (E_a (kJ mol^{-1})) can give some information about the mechanism of adsorption and the relative affinity of MF-PAPC to M(II) under investigation. Generally, low activation energies (5–40 kJ/mol) are characteristic of physisorption, while higher energies are conventionally related to chemisorption [125]. The Arrhenius equation provides the relationship between rate constant and temperature as follows:

$$k_1 = Ae^{-E_a/RT} \tag{17}$$

where k_1, A and R are the adsorption (forward) rate constant for the reversible first order model, the frequency factor and the universal gas constant (8.314 J K^{-1} mol^{-1}) respectively. The choice of reversible first order model adsorption rate constant (k_1) to be used for the E_a calculation is based on the reversible adsorption nature of the process and the agreement of rate constant values to M(II)-affinity order.

5.2.1.6 Diffusion mechanism

The kinetic characteristics of a chelating adsorbent depend not only on the presence of chelating sites but also on the accessibility of M(II) ions to these sites. This accessibility is mainly dependent on the matrix texture and its hydrophilic character [126].

The kinetic models mentioned above could not give a complete identification of the adsorption mechanism as it describes the overall process [127]. Diffusion is of great importance in studying adsorption as this phenomenon can be the rate-determining step for liquid adsorption systems [128]. The bulk diffusion has less contribution due to using agitation for the experiments [129]. Two types of diffusion can be considered in this study: film and pore diffusion. Film diffusion concerns the transfer of solute from the liquid boundary towards the adsorbent surface and pore diffusion concerns the transfer inside the adsorbent pores. The following models can be applied for diffusion study [128–130]:

$$\frac{q_t}{q_e} = 6\left(\frac{D_1}{\pi r^2}\right)^{1/2} t^{1/2} \qquad (t << t_{equilibrium}) \qquad (18)$$

and

$$\ln\left(1 - \frac{q_t}{q_e}\right) = \ln\frac{6}{\pi^2} - \left(\frac{D_2 \pi^2}{r^2}\right) t \qquad (t \rightarrow t_{equilibrium}) \qquad (19)$$

Equation (18) represents film diffusion in the early stages of adsorption. Equation (19) represents the process in the latter stage of adsorption (pore diffusion). The parameters D_1 and D_2 ($cm^2\ s^{-1}$) are film and pore diffusion coefficients respectively. The parameter r (cm) is the radius of the adsorbent particle considering a spherical shape. For this study, it is suggested that the diffusion coefficients D_1 and D_2 can be determined by applying adsorption data in the time range 0–30 minutes for equation (18) and 30–60 minutes for equation (19).

5.2.2 Adsorption thermodynamics

The thermodynamic parameters of adsorption are important considerations in subsequent engineering design for the removal process [4]. The thermodynamic study of the adsorption process investigates its spontaneity, type of enthalpy change and type of entropy change which provide understanding of the adsorption

mechanism. The enthalpy change (ΔH) measures the amount and direction of the heat flow. If heat is given off during a transformation from one state to another, then the final state will have lower heat content than the initial state. The enthalpy change (ΔH) will be negative and the process is said to be exothermic. If heat is absorbed during the transformation, then the final state will have higher heat content. The enthalpy change will be positive and the process is said to be endothermic.

The type of enthalpy change for a given transformation may be used to determine the degree of favourability. An exothermic reaction involves a loss of heat and a consequent lower final energy state and thus tends to be favourable, while an endothermic reaction tends to be unfavourable because it involves an increase in energy. Also, the magnitude of this change can help to predict the type of the mechanism of reaction. However, the entropy change (ΔS) must also be taken into account in determining whether or not a given process can occur. The change in entropy (ΔS) represents the change of disorder (randomness) of the system. For the adsorption process:

$$\Delta G^{ads} = \Delta H^{ads} - T\Delta S^{ads} \tag{20}$$

where:

ΔG^{ads} is the Gibbs free energy change of the adsorption process.

ΔH^{ads} is the enthalpy change of the adsorption process.

ΔS^{ads} is the entropy change of the adsorption process.

According to the previous equation, ΔG^{ads} is negative for any transformation for which ΔH^{ads} is negative and ΔS^{ads} is positive, that is ΔG^{ads} is negative for any transformation favoured by both enthalpy and entropy.

The thermodynamic parameter ΔG^{ads} can be calculated using van't Hoff Equation:

$$\Delta G^{ads} = -RT \ln K_c \tag{21}$$

The dynamic equilibrium constant (K_C) derived from the reversible first-order equation was considered to be used as a parameter in van't Hoff equation. The parameters ΔH^{ads} and ΔS^{ads} can be calculated from the following equation:

$$\ln K_C = \frac{\Delta S^{ads}}{R} - \frac{\Delta H^{ads}}{RT} \tag{22}$$

The slope and intercept of the plot of $\ln K_C$ versus $1/T$ give ΔH^{ads} and ΔS^{ads} respectively.

5.2.3 Adsorption isotherm

Adsorption in a solid-aqueous system is the transfer of solute from solution and the accumulation on the surface of the solid. This process goes on for such a time when the concentration of solute remaining in solution is in dynamic equilibrium with that on the surface. For this point of equilibrium, there is a defined distribution ratio of the solute between the aqueous and solid phases. This ratio measures the equilibrium which is a function of solute-concentration. The nature of solid phase, nature of solution and presence of any competitive solutes may affect this point of equilibrium.

The conventional way to determine solute distribution is to measure the specific quantity of solute adsorbed as a function of initial concentration at a fixed temperature. By investigating the adsorption isotherm, the adsorbent maximum capacity can be determined and we can get some idea about the type of interaction between the solute and the adsorbent which depends on the chemical structure and the type of adsorbate. In this investigation, two standard adsorption isotherm models were applied: Freundlich and Langmuir. It is important to determine which of these models provides the better representation to the experimental data.

5.2.3.1. The Freundlich model

This model is one of the earliest *empirical* equations used to describe adsorption equilibrium states and the most widely used for adsorption in aqueous systems. The Freundlich model assumes a heterogeneous surface where the adsorption sites have a range of adsorption-energies. The Freundlich equation is expressed as follows [122,131,132]:

$$q_e = K_F C_e^{\frac{1}{n}} \tag{23}$$

and the linear equation has the following form [122]:

$$\log q_e = \log K_F + \frac{1}{n}\log C_e \tag{24}$$

where,

q_e: is the adsorbed amount at equilibrium.

C_e: is the concentration at equilibrium.

The Freundlich parameters K_F ((mg g^{-1})(mg l^{-1})^n) and n are related to adsorption capacity and adsorption intensity respectively.

5.2.3.2 The Langmuir model

This model was the first to propose a complete theory describing adsorption based on kinetic considerations. The Langmuir model assumes: monolayer adsorption on homogenous surface (adsorption energy is constant over all sites), localised adsorption (adsorbed species are adsorbed at definite sites) and each active site is able to accommodate only one adsorbate species. The theory also considers the dynamic equilibrium between the adsorbed and free solute due to reversibility of adsorption (adsorption/desorption process). The Langmuir isotherm model is

applicable to a homogenous surface with negligible interactions between adsorbate species [4].

The kinetic approach assumes that at equilibrium there is a continuous transfer between the bulk and adsorbed phases with no accumulation at the surface. The Langmuir equation can be derived from the kinetics of adsorption process [133].

If A stands for the total number of unoccupied sites at any instant, then the rate of adsorption (r_a) can be written as follows:

$$r_a = k_a C A(1-\theta) \tag{25}$$

where

C: solute concentration

K_a: adsorption rate constant

θ: fraction of occupied sites

The rate of desorption, r_d, can be written as follows:

$$r_d = k_d A\theta \tag{26}$$

where

k_d: is the adsorption rate constant.

At equilibrium, the two rates are equal:

$$\theta = \frac{q_e}{Q_o} = \frac{k_a C_e}{k_d + k_a C_e} \tag{27}$$

where

q_e: equilibrium capacity.

Q_o: saturation capacity.

Assign b as the equilibrium constant:

$$b = \frac{k_a}{k_d} \tag{28}$$

For adsorption from solution by solid adsorbents, the Langmuir model has the following form [122,134,135]:

$$q_e = \frac{Q_o b C_e}{1 + b C_e} \tag{29}$$

The linear equation has the following known form [122]:

$$\frac{1}{q_e} = \frac{1}{Q_o} + \frac{1}{b Q_o C_e} \tag{30}$$

where, q_e and C_e have the same meaning as the Freundlich model. The parameters Q_o and b are the Langmuir model parameters. The parameter Q_o is the adsorption capacity (mg g^{-1}) of the sorbent and parameter b (l mg^{-1}) is the Langmuir constant and called the affinity constant. The affinity constant is a measure of how strong adsorbate is attached onto the adsorbent surface and is related to the energy of sorption.

A related dimensionless factor R_L is helpful to indicate the type of adsorption: favourable ($0 < R_L < 1$), unfavourable ($R_L > 1$), linear ($R_L = 1$) and irreversible ($R_L = 0$) [128]. The R_L factor is calculated according to the following equation [122,136]:

$$R_L = \frac{1}{1 + b C_i} \tag{31}$$

The parameter C_i is the initial M(II) ion concentration.

The agreement between the experimental data and the models applied (for kinetics and isotherm) is expressed by the correlation coefficient (R^2). The higher the value of R^2 for a model, the better is the agreement with the experimental data [18,137].

5.2.4 Adsorption distribution ratio

The distribution ratio, D (ml/g), provides important information about the affinity of the adsorbent towards a respective metal ion. It is the ratio of amount of metal ion present in the adsorbent to that present in the aqueous phase. It has the following numerical equation:

$$D = \frac{Q_{\text{adsorbent}}}{Q_{\text{solution}}} \tag{32}$$

where $Q_{\text{adsorbent}}$ is mass (mg) of metal ion adsorbed by 1 g of the adsorbent and Q_{solution} is the mass (mg) of metal present in 1 ml of solution.

5.2.5 Continuous-adsorption system

Since practical applications of adsorption for separation and purification are most commonly carried out in fixed beds, it is important to extend the work to include continuous experiments. A key aspect of a dynamic study is the record of effluent concentration with time. This is commonly referred to the breakthrough curve. In practical applications, the flow is stopped when the concentration exceeds a specified maximum value.

In an up-flow fixed bed column, the influent (feed) enters through the bottom and the treated effluent is drawn off at the top. Adsorption within a packed bed column is a continuous process where mass transfer of the solute [Cu(II)] occurs from the mobile phase [Cu(II) solution] to the solid phase (the adsorbent bed). The experimental capacity q_m is the mass of Cu(II) ion (mg) adsorbed by one gram of the adsorbent, and can be calculated using the following equation [138]:

$$q_m = q_{ma} + q_{mb} \tag{33}$$

where the term q_{ma} is the capacity (mg g^{-1}) for the time period where concentration of effluent is zero (**Figure 5.2**) and can be calculated using equation [138]:

$$q_{ma} = \frac{V_{eff} C_o}{1000m} \tag{34}$$

where

V_{eff}: is the effluent volume (ml).

C_o: is the influent metal ion concentration (mg l^{-1})

m: is the mass of adsorbent in the column (g).

The term q_{mb} is the capacity (mg g^{-1}) in the time period where the concentration rises above zero to complete saturation and can be calculated by calculating the area above the breakthrough curve (**Figure 5.2**) [138].

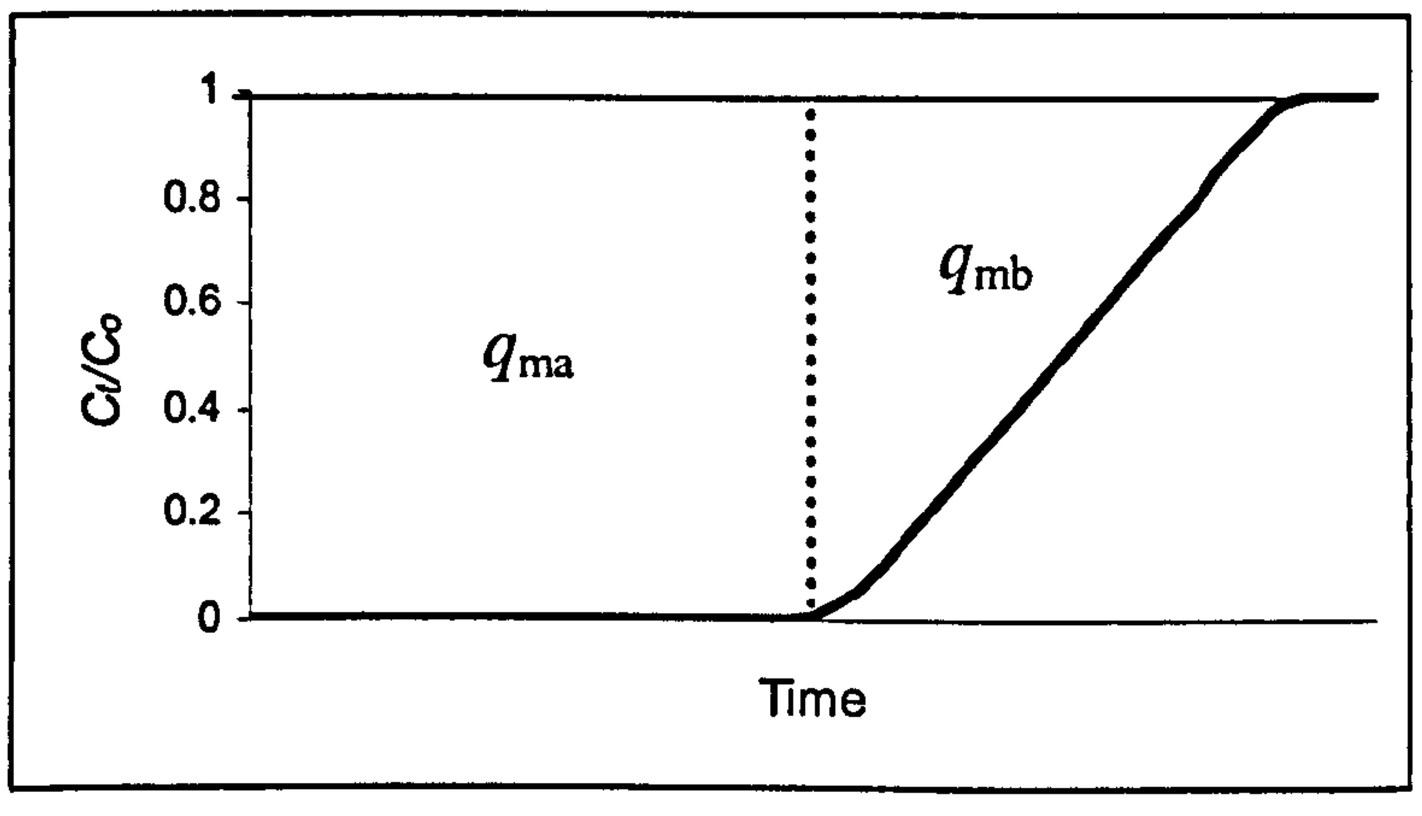

Figure 5.3: Areas to calculate q_{ma} and q_{mb} for the breakthrough curve

5.2.5.1 Adsorption kinetics under continuous condition (Thomas Model)

For a successful column design, a good prediction of the concentration–time profile (breakthrough curve) is required. Various mathematical models can be used to

describe fixed-bed adsorption including the Thomas model (1948). This model is simple to use in the design of a fixed-bed adsorption column and one of the most general and widely used methods in column performance theory. Therefore, the breakthrough data obtained from the experimental column studies were examined using this kinetic model. The Thomas model assumes Langmuir kinetics of adsorption/desorption [139]. It is stated that a weakness of the Thomas model is that its derivation is based on second-order reaction kinetics, whereas adsorption is usually not limited by chemical reaction kinetics but also controlled by mass transfer and this discrepancy can lead to error for certain adsorption systems [140].

The Thomas model has the following expression [60,141]:

$$\ln\left(\frac{C_o}{C_t}-1\right)=\frac{1000k_{Th}Qm}{\upsilon}-\frac{k_{Th}C_oV_{eff}}{\upsilon} \qquad (35)$$

where

C_o: is the influent metal ion concentration (mg l^{-1}).

C_t: is the effluent metal ion concentration (mg l^{-1}) at time t (minute).

k_{Th}: is the Thomas rate constant (l mg^{-1} min^{-1}),

Q: is the capacity of the adsorbent (mg g^{-1}).

m: is the mass of adsorbent in the column (g),

V_{eff}: the effluent volume (ml)

υ: is the flow rate (ml min^{-1}).

The model parameters, Q and k_{Th}, can be determined from the plot of the logarithmic term against time t ($t = V_{eff}/\upsilon$) according to equation (35).

5.2.5.2 The bed depth-service time relation (BDST model)

An important aim for an investigation of column studies is to be able to predict the service time before the column effluent exceeds a pre-defined solute concentration. The practical scaled-up adsorption column can then be designed based on results

obtained from the laboratory-scale adsorption column assuming an appropriate mathematical model.

Bohart and Adams [142] proposed a relationship between the bed depth and the time taken for breakthrough to occur. It assumes that the adsorption rate is proportional to both the residual capacity of the adsorbent and the remaining concentration of the adsorbate [16,48]. It is considered as the simplest and quickest approach to describe column adsorption. The model gives a relation between the column service time (T_s (min.)) and bed depth (Z (cm)). The equation considers characteristic parameters such as the maximum dynamic adsorption capacity (N_o) and the kinetic constant (k_B). This model ignores the intra-particle mass transfer and external film resistances. The service time is related to the various process conditions and operating parameters by [16]:

$$T_s = \frac{N_o Z}{C_o v} - \frac{1}{k_B C_o} \ln\left(\frac{C_o}{C_b} - 1\right) \tag{36}$$

Hence, this equation can be used to calculate the adsorption service time (T_s) for a column of bed height (Z) given the parameters N_o, and k_B which must be pre-determined from laboratory experiments. Performing three experiments for three bed heights at the same flow rate and influent concentration is sufficient to determine the model parameters: N_o, and k_B. The parameter that is likely to change with bed height is the maximum dynamic adsorption capacity (N_o) due to the increase of residence time of the solution inside the column as bed height increase. However, for some adsorption systems, the dynamic adsorption capacity (N_o) can be considered constant.

The dynamic bed capacity (N_o (mg l^{-1})) and the rate constant (k_B (l mg^{-1} min^{-1})) can be evaluated from the slope and intercept of the plot of T_s versus Z. The slope and intercept of equation (36) are as follows:

$$\text{slope} = S = \frac{N_o}{C_o v} \tag{37}$$

$$\text{intercept} = I = \frac{1}{k_B C_o} \ln\left(\frac{C_o}{C_b} - 1\right) \tag{38}$$

where

C_o: is solute initial concentration (mg g^{-1}).

v: is the linear velocity of solution through the bed (cm min^{-1})

C_b: is the pre-specified break through concentration (mg g^{-1}).

The slope of the BDST curves (S) represents the time required for the adsorption zone (Z_o) to travel a unit length through the adsorbent under the given experimental conditions. This can be used to predict the performance of the bed, when there is a change in the initial solute concentration (C_o) to a new value of solute concentration.

Three bed heights at the same flow rate and influent concentration are sufficient to be experimentally carried out to apply the BDST to a particular adsorption system [143,144].

Setting $T_s = 0$ and solving equation (37) for Z gives [16]:

$$Z_o = \frac{v}{N_o k_B} \ln\left(\frac{C_o}{C_b} - 1\right) \tag{39}$$

where Z_o is the minimum column height (adsorption zone) necessary to give the effluent of concentration C_b.

The BDST equation developed from column experiments at one flow rate can be modified to determine service time (T_s) for other flow rates by multiplying the original slope (S) by the ratio of the original and new flow rates [16,145,146]:

$$S' = S\frac{\nu}{\nu'} \tag{40}$$

where S' and ν' are the new slope and new flow rate respectively.

The intercept part of equation (36) does not need to be modified as k_B is assumed to be independent of flow rate. Using this procedure, scale up for other flow rates can be achieved without any extra experiments [16].

Furthermore, prediction of the service time (T_s) for different influent concentrations (C_o) can be achieved by modifying the slope and intercept according to the following respective equations [16,145,146]:

$$S' = S\frac{C_o}{C_o'} \tag{41}$$

$$I' = I\left(\frac{C_o}{C_o'}\right)\frac{\ln\left(\frac{C_o'}{C_b}-1\right)}{\ln\left(\frac{C_o}{C_b}-1\right)} \tag{42}$$

where C_o' and I' are the new influent concentration and new intercept respectively.

Chapter 6

Experimental methods

This chapter describes the preparation method of MF-PAPC acid adsorbents and experimental methods used for characterization of these adsorbents. Also it gives the experimental adsorption procedures concerning the removal of Cu(II) Co(II) Cd(II) and Zn(II) from synthetic wastewater using a batch technique. The last part covers the experiments which have been used for the removal of Cu(II) ions using the column technique.

6.1 Materials and instruments

6.1.1 Chemicals

Analytical grade chemicals were used in this research and chloride salt was used for all metal ions;

$CuCl_2.2H_2O$	(MAY & BAKER LTD),
$CoCl_2.6H_2O$	(BDH), $NiCl_2.6H_2O$ (SIGMA),
$ZnCl_2.2H_2O$	(Fisher Scientific),
$CdCl_2.2.5H_2O$	(SIGMA-ALDRICH),
NaCl	(SIGMA)
Concentrated HCl, 36%	(ALDRICH)
Melamine 99%	(ALDRICH),
Formaldehyde 38%	(BDH)
DTPA	(SIGMA).
CDTA	(SIGMA).
NTA	(SIGMA).
EDTA	(SIGMA)

For all solution preparation, deionised water was used.

6.1.2 Instruments

Different instrumental techniques were used to characterize the blank adsorbent samples and in some cases metal ion-loaded adsorbent samples:

1. A Perkin-Elmer, Spectrum One FT-IR spectrometer was used for IR spectra recording using KBr discs.
2. A Perkin-Elmer Series II CHNS/O Analyser model 2400 was used for elemental analysis of adsorbents.
3. Accelerated Surface Area and Porosimetry Analyzer (ASAP) 2010) was used to examine porosity parameters applying the BET analysis method.
4. CP-MAS NMR spectrometry was used to characterize the samples (^{13}C and ^{15}N solid-state NMR)
5. Field Emission-scanning Electron Microscope (FE-SEM) was employed for imaging the surface of a freeze dried grain of a selected adsorbent samples to elucidate the morphology and porosity (magnification 50000× and accelerating voltage of 1.00 ke V).
6. X-ray powder diffraction patterns were obtained by using a Siemens D500 diffractometer applying CuK_{α} radiation (40 kV, 20 mA).

For adsorption measurements the following instrument were used:

1. Lab-Line, thermostatic Incubator-Shaker was used for the washing process and for batch adsorption experiments.
2. Hanna Instrument pH model H18519 was used for all solution pH adjustments (accuracy ±0.02).
3. A Perkin-Elmer atomic absorption spectrometer 3100 with multi-element hollow cathode lamps and an air-acetylene burner was used for determining the residual metal ion concentrations. The wavelengths, in nm, applied were those recommended by the manufacturer and were as follows: Co (240.7), Cu (324.8), Cd (228.8) and Zn (307.6). The characteristic wavelengths are element specific and accurate to 0.01–0.1nm. The accuracy of measurement of concentrations (ppm) is in the range: 1–3 %.

6.2 Preparation of MF-PAPC adsorbents (conditions optimization)

Three types of melamine-formaldehyde-polyaminopolycarboxylic acids chelating adsorbents (MF-PAPC) were prepared. They are based on the melamine-formaldehyde gel matrix as a platform to anchor polyaminopolycarboxylic acids as chelating active sites. Namely, DTPA, NTA and CDTA (polyaminopolycarboxylic acids) were chosen for this study. They are different in the number of amine and carboxylic groups present in each one and also for one having an aromatic part. For each type, some primary preparation experiments were performed to find out the most suitable range of pH and most suitable water contents. Twelve samples for MF-DTPA, twelve for MF-NTA and eight for MF-CDTA were prepared at different temperatures, water contents and pH. These samples were made for preparation condition optimization, i.e. to get best conditions for preparation. The three chelating adsorbents have the same reactant amounts of melamine and formaldehyde – 0.01 mole melamine (1.26 g) and 2 ml formaldehyde. The amounts of polyaminopolycarboxylic acid chelating agents are presented in **Table 6.1** which correspond to 0.003 M.

Table 6.1: Preparation conditions of MF-PAPC adsorbents.

T(°C)	Water content (ml)	DTPA (1.31g) pH	NTA (0.64g) pH	CDTA (1.15g) pH	Sample No.
90	5	1.5	1.5	Not prepared	1
		1.3	1.3		2
	10	1.5	1.5		3
		1.3	1.3		4
120	5	1.5	1.5	1.5	5
		1.3	1.3	1.3	6
	10	1.5	1.5	1.5	7
		1.3	1.3	1.3	8
150	5	1.5	1.5	1.5	9
		1.3	1.3	1.3	10
	10	1.5	1.5	1.5	11
		1.3	1.3	1.3	12

For each sample, the following procedures were followed. Melamine was added to chelating agent in a vial containing water previously pH adjusted using concentrated and diluted HCl solutions. Finally, formaldehyde was added and the whole mixture

was agitated by electronic agitator to ensure homogenous slurry formation. The tightly closed vial then was put in preheated oven (Memmert oven model 854) at a pre-defined temperature.

The gelation time (solidification of the sample) was recorded for each sample and the formed solid adsorbent was left for an extra 30 minutes at the same preparation temperature for further curing. The vial then was removed and left overnight. The sample then was removed from the vial and left at ambient conditions for four hours. The sample then was ground and sieved. The grains of dimension $710 > f > 355$ μm were collected and washed in 100 ml of deionised water for at least five times at ambient temperature using a shaker at 200 rpm, each wash lasting 30 minutes. These washing processes were for removing extra acidity, any other non-reacted initial materials (melamine, chelating agent and formaldehyde), and any soluble side-products. After the last washing step, the pH value had to be near or equal to that of deionised water used for washing. If not, another one or two washing steps are conducted. The washed sample was then placed in a new clean vial, tightly closed until characterization.

6.3 Preparation of melamine-formaldehyde sample (MF)

A melamine-formaldehyde resin sample (MF) was prepared for the comparison purposes with the MF-PAPC samples. For MF sample preparation: melamine (1.26 g) was added to 5 ml of HCl-acidified water (pH 1.3) and then formaldehyde (2 ml) was added and the whole mixture was agitated by electronic agitator to ensure homogenous slurry formation. The tightly closed vial then was put in preheated oven at 150°C. This condition of preparation was chosen to produce hard monolithic sample and not fluffy product.

6.4 Adsorbent characterization

6.4.1 Water regain determination and rigidity

Water regain was determined for the three MF-PAPC adsorbents. The adsorbent sample was soaked in deionised water for 48 h to ensure uptake equilibrium. The adsorbent sample then was centrifuged for three hours at 1000 rpm to remove excess water and then weighed. The sample was then dried at 50–60°C until complete dryness then weighed again. The water regain equation (chapter 4) was then used to determine the water regain factor.

The rigidity of prepared MF-PAPC samples was determined by observing the resistance of synthesis-produced monolithic form during grinding and by visual observation of tiny particle production due to erosion during adsorption experiments.

6.4.2 Porosity (BET measurements)

Porosity parameters were measured for the three MF-PAPC adsorbents using the Micromeritics accelerated surface area and porosimetry analyzer (ASAP 2010). Prior to analysis, the sample was freeze dried to remove water without destroying the texture of the matrix. The freeze drying process was carried out by freezing the samples at –80°C then evaporating (i.e. sublimating) the water under low pressure (0.06 atm.). The samples were then heated to 50 °C for 2 hours to ensure complete water removal. Porosity analysis comprises adsorption and desorption of nitrogen at 77 K into the sample pores and the working range was p/p_o= 0 to 1.

The partial pressure of nitrogen increases (adsorption direction) or decreases (desorption direction) in steps controlled by the instrument. When equilibrium was attained at each step, the amount (volume) of nitrogen adsorbed is recorded. The porosity parameters of the sample (surface area, micropore surface area and pore volume and pore diameter) were calculated.

6.4.3 Scanning Electron Microscopy (FE-SEM)

This measurement was applied for all MF-PAPC adsorbent types (selected samples). The freeze dried samples of adsorbents were used for this technique. A SEM image was recorded using FE-SEM with an accelerating voltage of 1.00 keV (magnification of 50000×).

6.4.4 Infrared and CHNO elemental analysis

This measurement was used for all MF-PAPC adsorbents and some Cu(II)-loaded MF-DTPA and MF-CDTA samples. The washed samples were dried in an oven at 50–60°C (at atmospheric pressure) for 3–5 hours before IR and CHNO analysis to guarantee complete removal of water. For IR analysis, sample-KBr discs were prepared and scanning for IR transmittance in the range of 4000 to 400 cm^{-1} was recorded. Also, a spectrum for the reference sample – melamine-formaldehyde (MF) – was recorded for comparison. For CHNO elemental analysis, about 30–50 mg of a sample was analysed and result data was recorded using a Perkin-Elmer Series II CHNS/O Analyser model 2400.

6.4.5 Temperature programmed desorption/Mass spectrometry (TPD-MS)

TPD-MS experiments were carried out in an online device with a VG Sensorlab quadrupole mass spectrometer. A fixed bed quartz reactor coupled with an on-line mass spectrometer was used for TPD of the samples. In the experiment, MF-DTPA freeze dried sample was used and its weight was approximately 0.5 g. A sample was placed in the reactor (quartz tube with inner diameter of 4 mm) and heated up to 500°C at a heating rate of 10°C min^{-1} under a helium flow of 120 ml min^{-1}. The generated decomposition products were introduced to the MS (Balzers QMG422 quadrupole mass spectrometer) through a heated capillary. The MS was operated at an inlet pressure of 3×10^{-7} Pa, electron energy of 70 eV, and a scan rate of 1 scan min^{-1}. The mass spectrometer was adjusted to detect *m/z* of 42, 43, 45, 56, 57, 59, and 73. These masses were chosen regarding the DTPA part and amide bond of the adsorbent.

6.4.6 Nuclear Magnetic Resonance (NMR)

This measurement was applied for the MF, MF-DTPA, MF-CDTA and MF-CDTA-Cu(II) adsorbent samples. Dry samples, each of 400 mg, were sent to University of Durham (EPSRC Service) for solid state CP-MAS-NMR (cross polarization-magic angle spinning-NMR) analysis. A Varian unity inova spectrometer and 7.5 mm (rotor o.d.) MAS probe was used. The spectral referencing is with respect to tetramethylsaline (TMS). Cross-polarisation with magic-angle spinning was used to obtain the spectra.

6.4.7 X-ray powder diffraction

This measurement was used for MF, MF-CDTA and Cu(II)-loaded MF-CDTA wet samples. Measurement was performed at a scan rate of 0.2° min^{-1} with a step size of 0.1° (2θ = 5 to 90).

6.5 Heavy Metals adsorption experiments

Standard stock solutions, 1000 ppm, for all metal ions under study were prepared by dissolving corresponding ion chloride salt in 1000 ml deionised water. Fresh working solutions were prepared from these stock solutions by appropriate dilution. Standard diluents were pH-adjusted using concentrated and diluted HCl and NaOH. The dilution process was carried out using a micropipette (range: 1–5 ml, accuracy: ±25.0 µl corresponds to ±0.5 %).

The selective-behaviour of an adsorbent towards several ions is based on comparing the results from single-ion solutions which may not be valid for the practical case of solutions of mixed ions [7]. In this study the removal behaviour of MF-PAPC sorbents towards selected heavy metals were carried out under ions-simultaneous adsorption process.

6.5.1 Batch adsorption experiments

The batch adsorption technique was conducted for determinating the adsorption behaviour. Experimental variables include initial pH (3, 4, 5 and 6), temperature (15, 20, 25, 30 and 35°C) for MF-DTPA and MF-NTA adsorbents and (15, 25 and 35°C) for MF-CDTA adsorbent, contact time (10, 20, 30, 40, 50 and 60 minutes) and metal-ions initial concentrations (20, 30, 40, 50, 60 and 70 mg l^{-1}). Buffering of solutions was avoided due to unknown effects of buffer compounds on adsorption [6] and change of pH values due to adsorption gives information about the mechanism [146]. It is important to note that initial concentrations of these metals are different on a molar basis. Other parameters were set constant, shaking speed (200 rpm), grain size (355–710 μm), solution volume (50 ml) and wet adsorbent dose (MF-DTPA: 0.5 g, MF-NTA: 0.3 g and MF-CDTA: 0.25 g). Also, in all experiments (except isotherm measurement) for MF-DTPA and MF-CDTA adsorbents, 20 mg l^{-1} of competitive Na(I) ion was present representing the salt matrix effect. All batch experiments were carried out using clean 150 ml Elmer conical flasks. The cleaning process was conducted by washing the flasks with 50 ml deionised water (4-5 times) followed by drying at 60°C.

For initial pH studies, pH values above 6 were avoided because of probable metal hydroxide formation which may give spurious adsorption results, e.g. copper hydroxide precipitation occurs above pH 6.5 and cobalt start to significantly precipitate as hydroxide at a pH value around 8 [6,59,147,148]. Besides, most metal-laden wastewater effluents occur at acidic pH values [149]. **Figure 6.1** shows speciation percentage of Cu(II) and Cd(II) as an example. It is noticed that M^{2+} is the dominant form for both ions at pH ≤6.

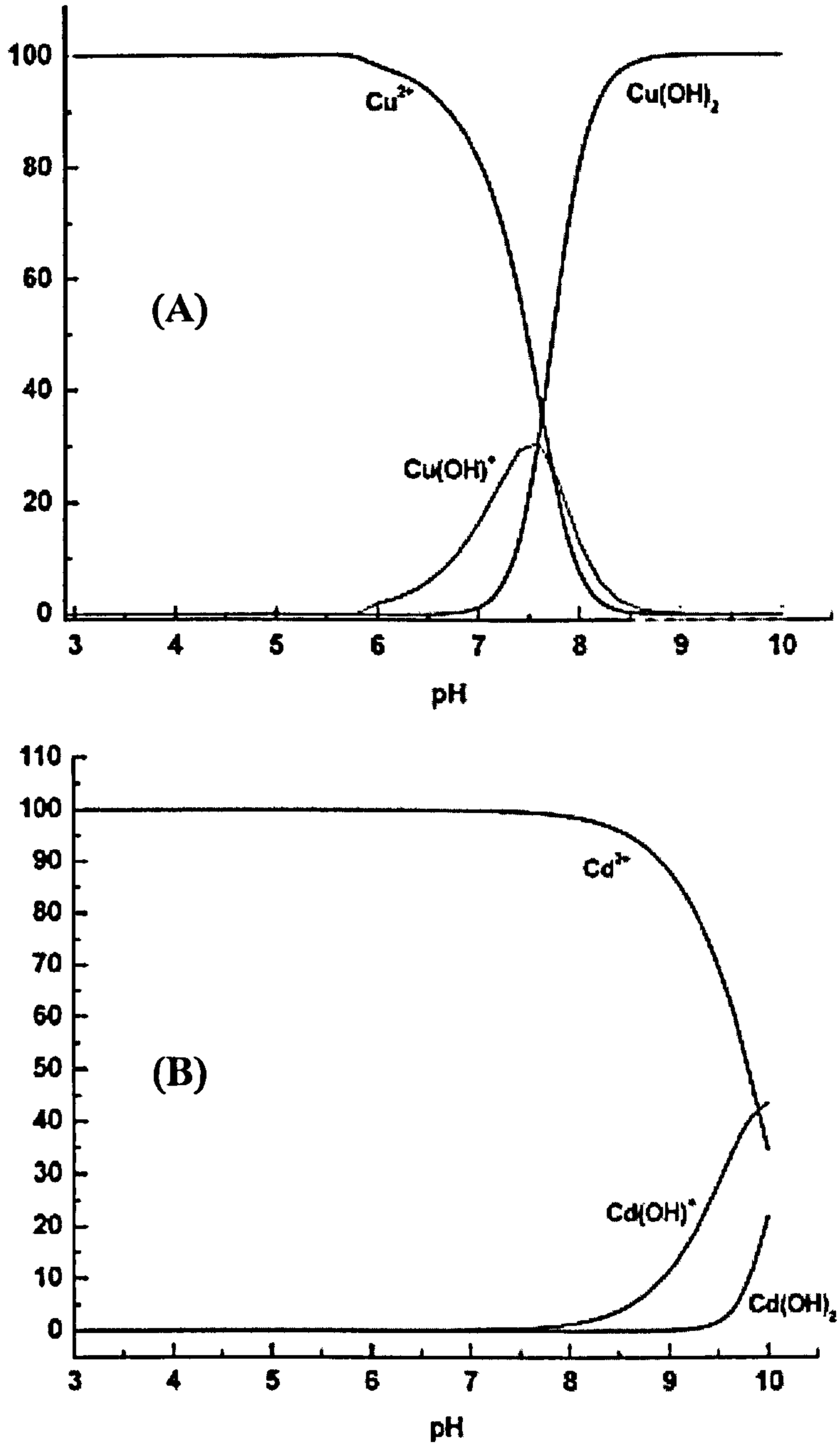

Figure 6.1: Speciation percentage of (A) Cu(II) (50 mg/l) and (B) Cd(II) (50 mg/l) at different pH values.

Adsorption was investigated by measuring the residual metal ions concentration after the adsorption process using the Perkin-Elmer atomic absorption spectrometer 3100 with multi-element hollow cathode lamps and an air-acetylene burner.

6.5.1.1 Adsorption of metal ion by MF-DTPA

(A) Batch adsorption:

The effect of initial pH was investigated by carrying out the adsorption process at five different temperatures (15, 20, 25, 30 and 35°C). For each temperature, four flasks (each flask at certain initial pH value: 3, 4, 5 and 6) with metal-ion initial concentrations of 20 mg l^{-1} were shaken for 120 minutes. From each flask, 5 ml was withdrawn and residual metal-ion concentrations were measured. An adsorption isotherm study was carried out by shaking six flasks with different initial concentrations (20, 30, 40, 50, 60 and 70 mg l^{-1}) at 20°C and an initial pH of 5. From each flask, 5 ml was withdrawn to measure the residual metal-ion concentration.

In this study, adsorption isotherm experiments were carried out using a mixture of heavy metal ions. Heavy metals are, in many situations, present in water as mixtures. Multi-element adsorption isotherm experiments may provide important data on the nature of the adsorption process such as the relative affinities for these sites. Therefore, it is crucial to understand the adsorption properties caused by competitive or synergistic effects and the underlying mechanisms of the processes to accurately predict the adsorption behaviours of mixtures of heavy metals. However, a complementary study on the adsorption of single ions is also important and this is a recommendation for future work. The same argument applies to the MF-NTA and MF-CDTA investigations.

The kinetics of adsorption (60 minutes duration) was studied at 25°C for different pH values (3, 4, 5, and 6). From each flask, 3 ml was withdrawn each 10 minutes and the residual metal-ion concentrations were measured. This withdrawn volume (3 ml) is the lowest amount required to perform absorbance measurements for the four metal elements using the atomic absorption instrument. Indeed, this withdrawn volume will have an effect on the measurements since the volume of solution in contact with the adsorbent will decrease during the experiment. However, this was unavoidable. The initial volume of solution in contact with the adsorbent was 50 ml and the final volume after 60 minutes was 32 ml. This means that the average volume over the 60 minutes was 41 ml. However, the rate of adsorption was much higher over the initial

20 minutes of the experiment. This might mean that the withdrawal process might "increase" the final adsorbed amount by about 10%. However, this effect can be considered similar for each of the four metal elements present in solution; hence relative removal data are not greatly affected. The same effect is similar for batch adsorption for MF-NTA (section 6.5.1.2) and MF-CDTA (section 6.5.1.2) cases.

It is expected that intraparticle diffusion has a limited effect on the adsorption process as average pore diameter of MF-DTPA is considerably wide and not expected to show resistance to the migration of these solutes. Hence, the experiments needed to investigate the sole effect of intraparticle diffusion (film diffusion effect can be eliminated by strong agitation) was not carried because of time limitations. The same principle was applied for MF-CDTA.

(B) Adsorption capacity (elemental analysis) and IR analysis:

The experimental load capacity of the MF-DTPA adsorbent was investigated by elemental analysis. The loading process was carried out by soaking 0.5 g of the adsorbent in 100 ml of Cu(II) solution (100 mg l^{-1}, pH 5 at 25°C) for 24 hour. To determine the salt matrix effect, the loading process was repeated with the presence of Na(I) (20 mg l^{-1}). The Cu(II) loaded adsorbent samples were washed by deionised water to remove any non-adsorbed Cu(II) which may be present in adsorbent pores. The loaded adsorbent samples then were dried and elementally analysed. The Cu(II)-loaded adsorbent sample (with no Na(I) presence) was also IR-analysed.

(C) Adsorption of Cu(II) by fresh and regenerated MF-DTPA adsorbent:

The use of mineral acids to elute adsorbed metal ions is always avoided because of the tendency of amide group to hydrolyse [72,150]. In this study, EDTA solution was used to elute metal ions from the adsorbent. EDTA has formation stability constant values (with the metal ions under study) comparable to those of adsorbing chelating agents. Hence EDTA is expected to break down the complex between the M(II)-PAPC sites [151].

The used samples of MF-DTPA for the removal of M(II) ions at 25°C were regenerated by agitating (150 rpm) each adsorbent sample (0.5 g) with 50 ml EDTA solution (concentration 0.01 M) at ambient temperature for 30 minutes. The extraction process was repeated three times, each with fresh EDTA solution. After M(II) elution, the adsorbent dose was washed twice with 50 ml distilled water by agitation. The removal process of M(II) ions was carried out again using regenerated samples under same condition of the original removal experiment. The removal percentage of Cu(II) ion was recorded and compared with the original result.

6.5.1.2 Adsorption of metal ion by MF-NTA

Batch adsorption:

The effect of initial pH was investigated by carrying out the adsorption process at different five temperatures (15, 20, 25, 30 and 35°C). For each temperature, four flasks (each flask at certain initial pH value: 3, 4, 5 and 6) with metal-ion initial concentrations of 20 mg l^{-1} were shaken for 120 minutes. From each flask, 5 ml was withdrawn and residual metal-ion concentrations were measured.

An adsorption isotherm study was carried out by shaking six flasks with different initial concentrations (20, 30, 40, 50, 60 and 70 mg l^{-1}) at 20°C and an initial pH of 5. From each flask, 5 ml was withdrawn to measure the residual metal-ion concentrations.

The kinetics of adsorption (60 minutes duration) was studied at 20°C for different pH values (3, 4, 5, and 6). From each flask, 3 ml was withdrawn each 10 minutes and residual metal-ion concentrations were measured.

6.5.1.2 Adsorption of metal ion by MF-CDTA

(A) Batch Adsorption:

To study the effect of initial pH and temperature on adsorption, a number of flasks containing solutions with initial metal-ion concentrations of 20 mg l^{-1} were shaken

for 120 minutes. The final pH and residual metal-ion concentrations were then measured.

The kinetics of adsorption (at 25° for 60 minutes duration) was carried out at different initial pH values (3, 4, 5, and 6). For each experiment, 3 ml sample was withdrawn every 10 minutes and residual metal-ion concentrations were measured. The adsorption isotherm study was carried out at 25° by shaking six flasks (pH 5) of different initial concentrations (20, 30, 40, 50, 60 and 70 mg l^{-1}). At equilibrium, 5 ml sample was withdrawn from each flask to measure the residual metal-ion concentrations.

(B) Adsorption capacity (elemental analysis):

The experimental load capacity of the MF-CDTA adsorbent was investigated by elemental analysis. The loading process was carried out by soaking 0.5 g of the adsorbent in 100 ml of Cu(II) solution (100 mg l^{-1} , pH 5 at 25°C) for 24 hour. The Cu(II) loaded adsorbent sample was washed by deionised water to remove any non-adsorbed Cu(II) which may be present in adsorbent pores. The loaded adsorbent samples then were dried and elementally analysed.

6.5.2 Continuous adsorption experiments (fixed-bed up-flow)

6.5.2.1 Removal of Cu(II) under continuous condition

The experimental set-up of the fixed-bed column is shown in **Figure 6.2**. The set-up is composed of an influent solution reservoir, an adsorbent-packed bed glass column, an effluent solution reservoir and a peristaltic pump. The height and internal diameter of the glass column were 25 and 1.4 cm respectively. The column was packed vertically with water-fluidised MF-DTPA adsorbent particles. Care was taken to guarantee good settling of particles and to avoid air entrapment.

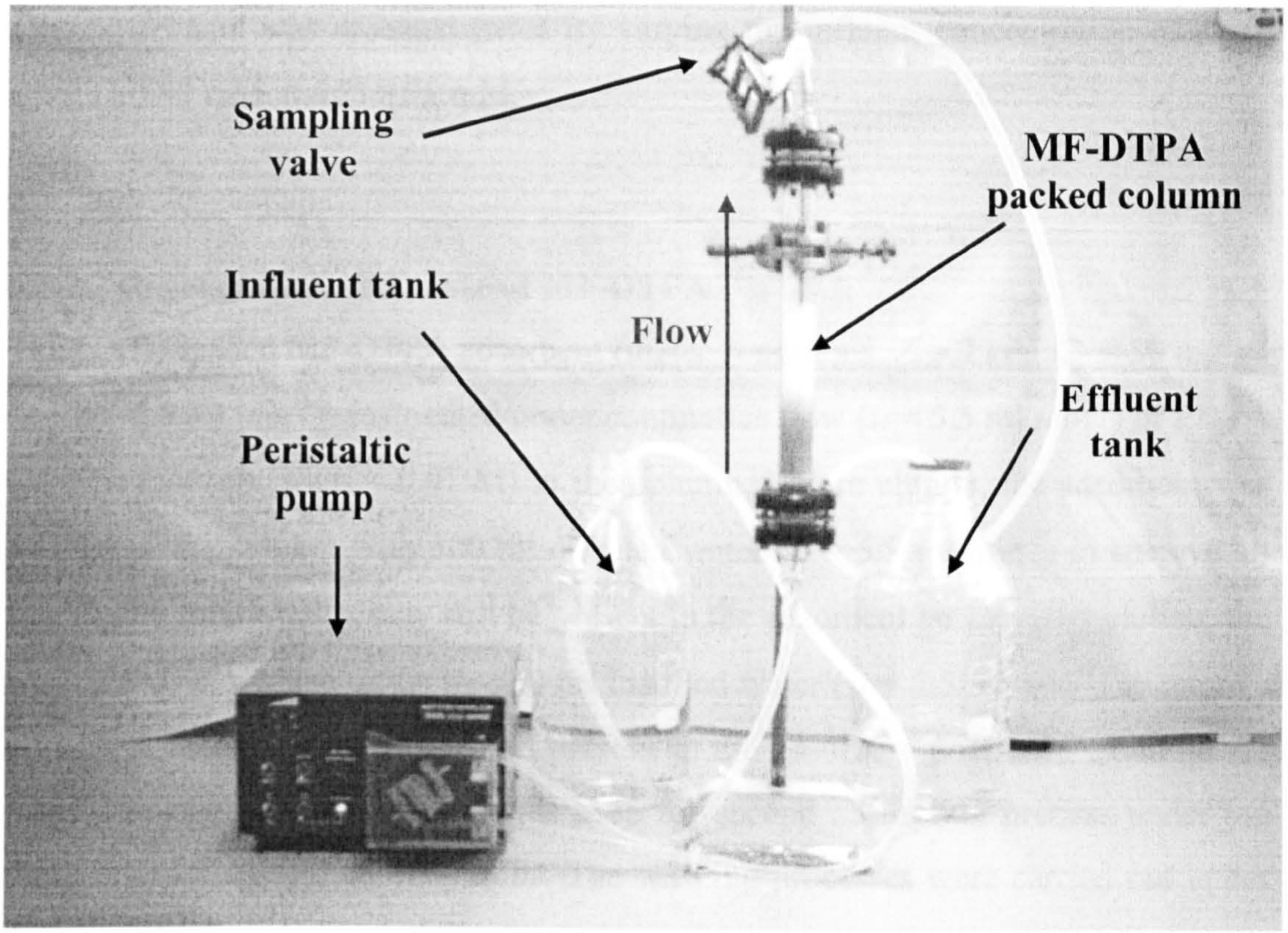

Figure 6.2: Experimental fixed-bed up-flow column setup.

Isothermal experiments (at ambient temperatures) were conducted by varying the fixed-bed height of the MF-DTPA adsorbent (5, 7 and 9 cm), flow rate (3.2, 5.5 and 8.1 ml min^{-1}) and metal ion, Cu(II), influent concentration (20, 30 and 40 mg l^{-1}). The Cu(II) solution was up-flow pumped through the fixed-bed using a peristaltic pump. The initial pH of influent Cu(II) solution was adjusted to 5–5.5. The effluent Cu(II) ion concentration was measured using atomic absorption at 324.8 nm. The adsorbent particle size was 335 – 710 μm and this size is suitable to excessive avoid pressure drop [152]. The adsorbent bed was first washed (in the column) by pumping distilled water at 3.2 ml min^{-1} for 30 minutes.

6.5.2.2 Effect of presence of citric acid in Cu(II) ion solution on adsorption

The experiment was carried out by pumping a solution of Cu(II) and citric acid through the MF-DTPA packed column using bed height of 5 cm and flow rate of 5.5 ml min^{-1}. The concentration of Cu(II) in the influent was kept constant, 30 mg l^{-1}.

The experiment was repeated twice by varying the influent concentration of citric acid: 1) 0.48 mM and 2) 0.95 mM.

6.5.2.3 Regeneration and reuse of MF-DTPA

The Cu(II)-loaded MF-DTPA adsorbent (under conditions: $Z = 7$ cm, $C_o = 30$ mg g^{-1} and $\upsilon = 5.5$ ml min^{-1}) was treated under continuous flow ($\upsilon = 5.5$ ml min^{-1}) of EDTA solution (concentration = 0.01 M) in the column. Before elution, the adsorbent was washed in the column with 500 ml distilled water ($\upsilon = 5.5$ ml min^{-1}) to remove all free Cu(II) solution that may still be present in the adsorbent pores. After elution, the adsorbent was washed again by 500 ml distilled water ($\upsilon = 5.5$ ml min^{-1}) to remove all EDTA solution which may still present in the adsorbent pores. To examine the reuse, the same adsorbent mass was used for second adsorption process under the same original adsorption conditions. The washing processes were carried out under the same flow conditions.

Chapter 7

Results and discussion I: Adsorbent characterization

This chapter presents the results of the experiments used for the preparation of MF-PAPC adsorbents (to indicate the best conditions of preparation) and the results of experimental and instrumental techniques to characterise the adsorbents.

7.1 Characterisation of MF-DTPA

7.1.1 Gelling time, water regain, elemental composition and rigidity

Some essential data of MF-DTPA adsorbent are presented in **Table 7.1**. The gelling time (G.T.) for twelve samples of MF-DTPA ranges from 12 minutes to 87 minutes depending on the reaction conditions. This is a relatively short time to prepare an adsorbent: matrix formation and active sites modification occurs in a single stage.

Generally, for a particular pH value and water content; the gelling time decreases as the temperature is increased and this may be due to fast-bridging catalyses by temperature. The value of water is high (on average, $W \approx 72\%$) which reflects the hydrophilic character of this adsorbent. This is probably due to the presence of carboxylic groups.

Table 7.1: MF-DTPA adsorbent: Gelling time and water regain elemental composition and rigidity.

T (°C)	Water content (ml)	pH	G.T. (min.)	*W*(%)	Rigidity	Elemental analysis C : H : N : O	No.
90	5	1.5	33	67.98	A (very hard)	36.1 : 5.6 : 35.8 :22.4	1
		1.3	27	66.06	B (hard)	36.3 : 5.3 : 36.1 :22.3	2
	10	1.5	55	75.67	D (soft)	35.8 : 5.5 : 36.8 :21.9	–
		1.3	87	69.68	D	35.7 : 5.3 : 37.5 :21.4	–
120	5	1.5	20	72.42	A	35.7 : 5.2 : 37.7 :21.6	3
		1.3	18	69.10	B	35.8 : 5.6 : 35.7 : 23	4
	10	1.5	30	76.19	C (fair hard)	36.1 : 5.5 : 37.1 :21.4	–
		1.3	55	71.92	D	35.8 : 5.1 : 37.2 :21.9	–
150	5	1.5	12	70.66	A	36 : 5.5 : 37.4 : 21	5
		1.3	14	70.79	B	35.8 : 5.5 : 36.4 :22.3	6
	10	1.5	16	75.32	C	35.6 : 5.5 : 38.3 :20.6	–
		1.3	41	72.09	C	35.3 : 5.4 : 37.2 :22.1	–
MF resin						35.1 : 5.12 : 42.7 : 17	

The elemental analysis of all MF-DTPA samples gives almost the same C:H:N:O ratio which is different from that of MF reference resin sample as shown in **Table 7.1**. The similarity in the elemental ratio shows that the chemical structure of the produced adsorbent samples is almost the same regardless of the preparation conditions.

It can be observed that MF-DTPA adsorbent samples have a higher ratio of oxygen compared to the MF sample, and this is because DTPA is rich in oxygen (≈41% by mass) due to the presence of five carboxylic groups in the DTPA molecule. Applying a material balance calculation using the elemental analysis data of sample number 3, the DTPA concentration is around 1.08 mmole per gram of solid MF-DTPA adsorbent.

The rigidity of samples was classified according to: A (very hard), B (hard), C (fairly hard) and D (soft). The difference in rigidity for the samples is likely to be due to the amount of cross-linking (bridging) in the synthesis process. It is reasonable to suggest that the cross-linking (bridging) between the melamine molecules starts simultaneously in many parts of the preparation solution, forming localised MF networks as long as the preparation solution is still in the liquid phase.

The formation of one hard monolithic gel matrix depends on the spacing between these localised networks. For a rigid product, this spacing is small and each localized network can form bridges with several adjacent localized networks forming a rigid monolithic gel matrix by the time of complete solidification and this is noted for samples with the lower water content (5 ml). For samples with higher water content (10 ml), the average spacing between these localised networks is increased and these managed to form only small solid agglomerates which results in a comparatively soft product (paste-like) as these agglomerates are not highly bonded to each other. Samples classified as A and B (in rigidity) in **Table 7.1** have been chosen for further characterization (BET analysis).

7.1.2 IR spectra

The IR spectra of a number of MF-DTPA adsorbent samples prepared at different conditions (pH, temperature and water content) are shown in **Figure 7.1**. It is clear that the spectra are very similar due to the presence of the same functional groups. This supports the findings from the elemental analysis about the similarity of the chemical structure for the different samples.

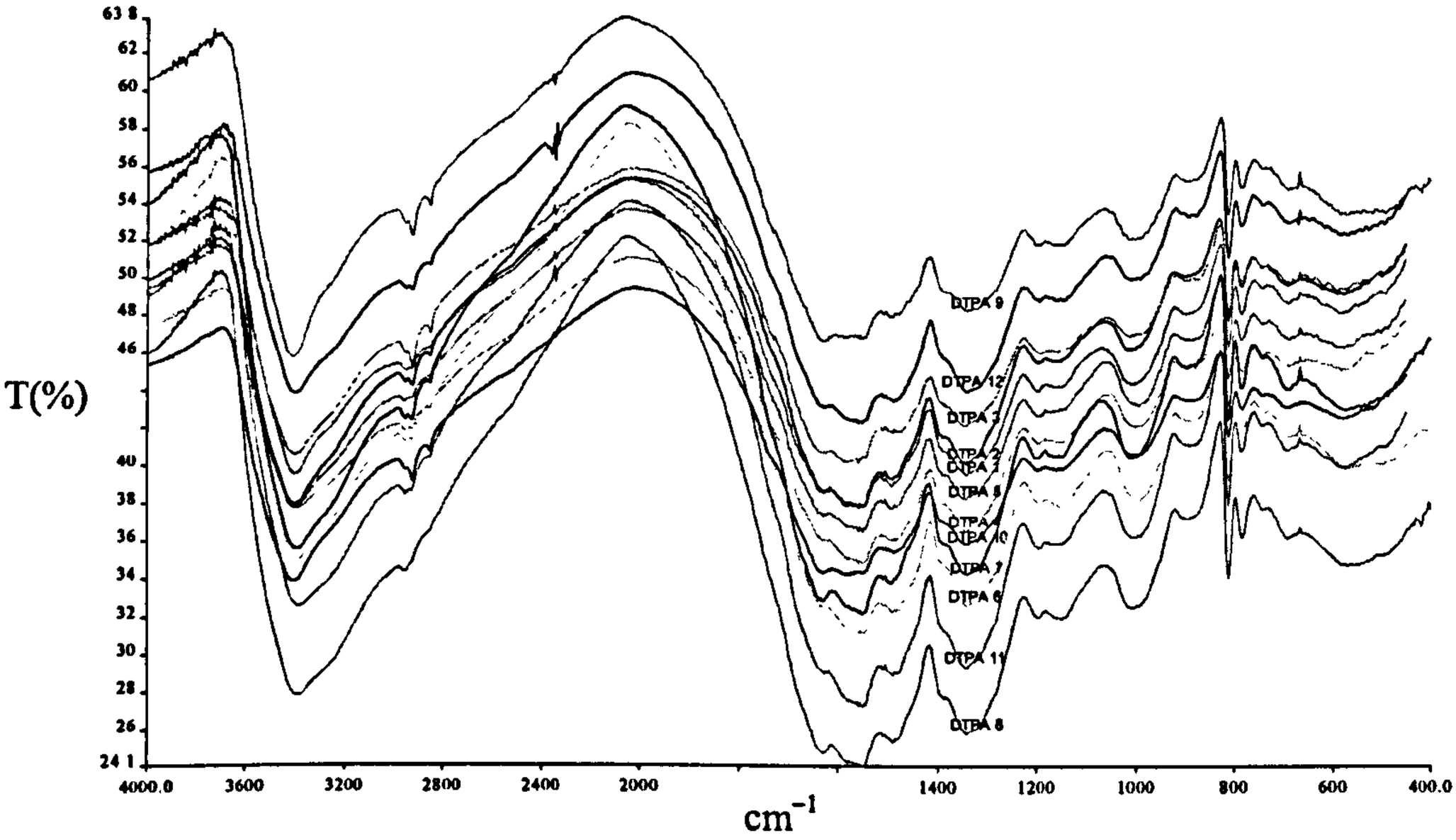

Figure 7.1: IR spectra of MF-DTPA adsorbents under different conditions (pH, temperature and water content).

To show how MF is modified by the addition of DTPA, a selected MF-DTPA spectrum (of sample number 8) is compared with the spectrum of pure MF (**Figure 7.2**).

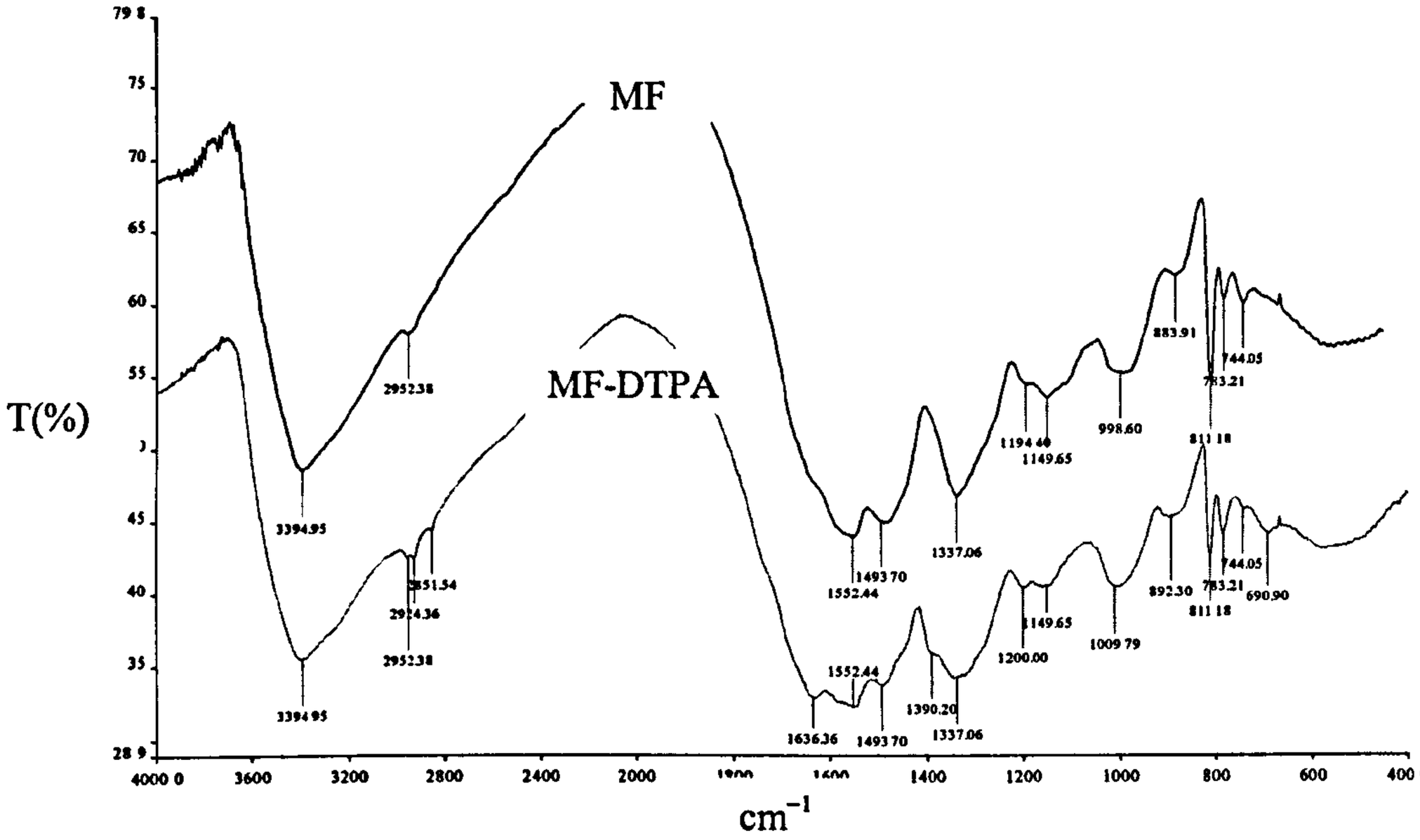

Figure 7.2: IR spectra of MF resin and MF-DTPA adsorbent.

There are common peaks due to similar groups present in both materials, such as 3394 cm^{-1} which can be assigned to the N–H stretch of the secondary amine attached to the methylene bridge. The peak at 2952 cm^{-1} can be attributed to the methylene C–H symmetric stretch (bridging methylene). The peak at 1552 cm^{-1} corresponds to the N–H bend of the bridging secondary amine. The peak at 1493 cm^{-1} is due to the methylene C–H bend. The peak at 1149 cm^{-1} may be assigned to the secondary amine C–N stretch or the stretching vibration of C–O ether bond.

However, there are important differences between the two spectra due to the anchoring of DTPA to melamine by the amide bond which appears only in the MF-DTPA spectrum: the amide carbonyl (C=O) stretch at 1636 cm^{-1}, the out-of-plane of amide (N–H) at 690 cm^{-1}, the carboxylic in-plane O–H bend appeared at 1390 cm^{-1}, the carboxylic O–H stretching at 2924 cm^{-1}. These distinguishing peaks are summarised in **Table 7.2**.

Table 7.2: IR distinguishing peaks present in MF-DTPA spectrum due to amide and carboxylic groups (not present in MF spectrum).

Functional group	MF-DTPA peaks (cm^{-1})
Amide (carboxylic)carbonyl C=O stretch	1636
Amide N–H out of plane	690
Carboxylic group In plane O–H bend	1390
Carboxylic O–H stretching	2924

The change of preparation conditions affects only some physical properties of the adsorbent, not its chemical structure.

7.1.3 TPD-MS spectrum

The adsorbent sample number 5 (freeze dried) was used to determine the mass fragments of the MF-DTPA adsorbent. Decomposition of the sample was observed to start above 100°C as noted in **Figure 7.3**. The mass number 45 appears twice at 240 and 385°C and can be attributed to the carboxylic group and/or the $NH–CH_2–O–$ bridges in the matrix. The appearance of this mass number twice at two different temperatures proves the presence of these two groups and supports the suggested chemical structure. Most of the amide groups (mass number 43) appear at 400°C. Mass number 73 (NCH_2COOH) gave a very small yield compared with its sub-fragments of mass numbers 59 (CH_2COOH) and 45 (COOH).

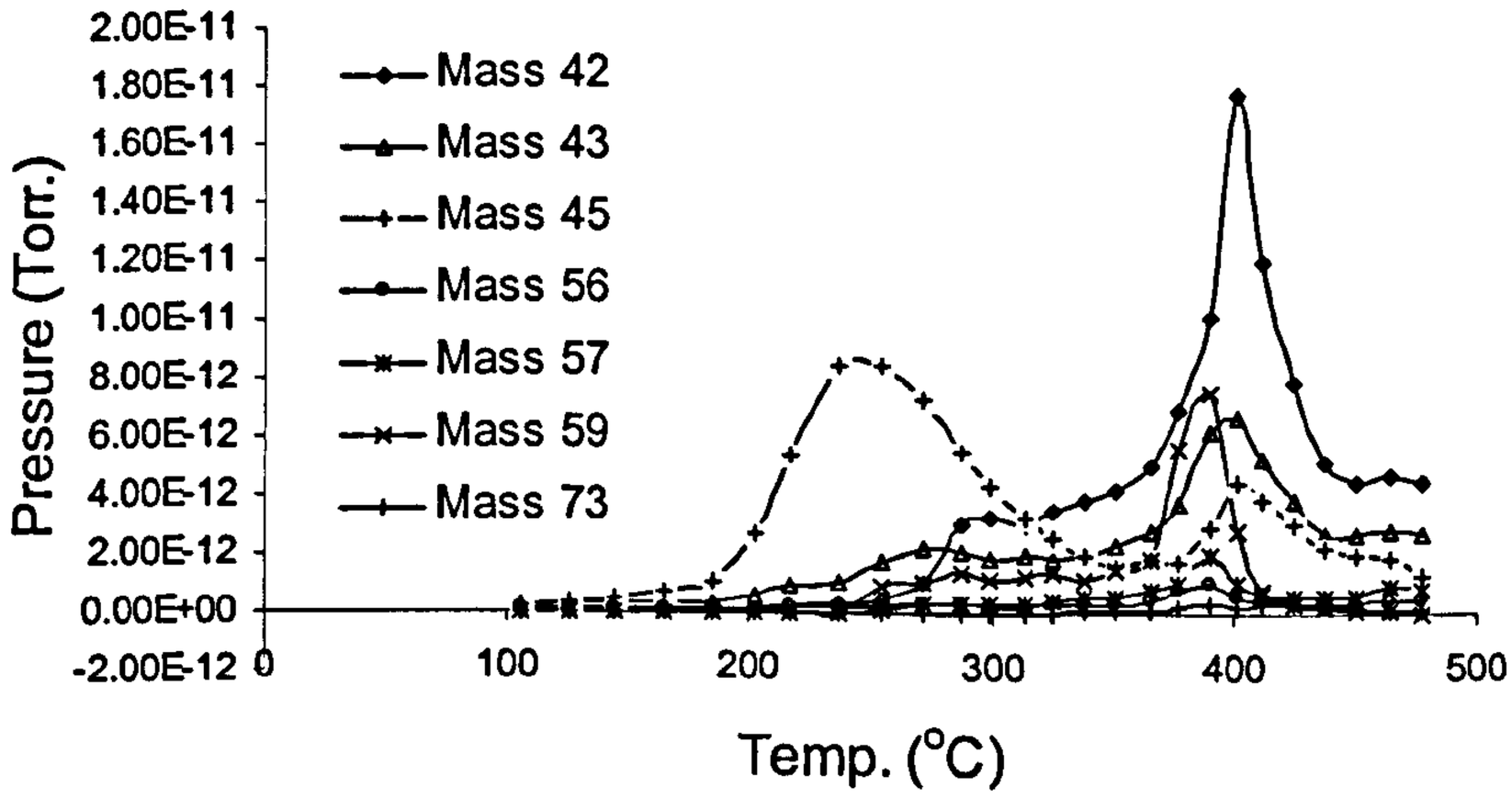

Figure 7.3: MF-DTPA fragmentation (temperature profile)

Pre-specified fragment masses were selected for the instrument according to the suggested possible structure of the MF-DTPA adsorbent. The selection considered carboxylic and amide groups. The detected mass numbers and possible related groups are summarized in **Table 7.3**. According to the suggested structure of MF-DTPA adsorbent, mass numbers related to amide group such as 42 (NCO) and 43 (NHCO) cannot be produced from MF matrix. It can be produced only from DTPA moieties in MF-DTPA adsorbent.

Table 7.3: Masses fragmented from MF-DTPA adsorbent

Fragment (group)	Mass (a.u.)
NCO	42
NHCO	43
COOH	45
$NCOCH_2$	56
$NHCOCH_2$	57
CH_2COOH	59
NCH_2COOH	73

7.1.4 NMR spectra

The ^{13}C solid-state NMR spectra of the pure MF resin and MF-DTPA adsorbent are shown in **Figure 7.4**.

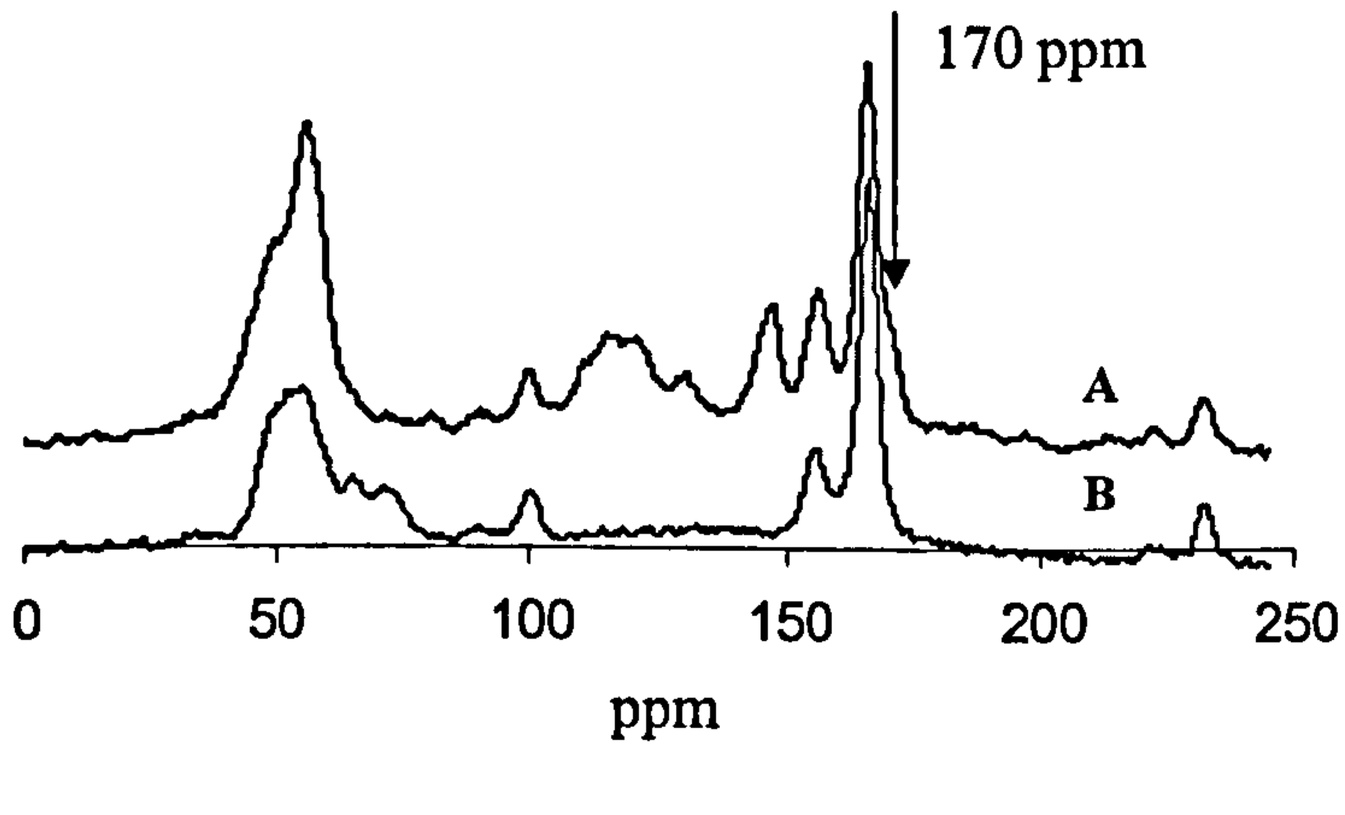

Figure 7.4: ^{13}C solid-state NMR spectra of (A) MF-DTPA adsorbent and (B) MF resin.

Both materials have the cyclic triazine ring of melamine. The three carbons in the triazine ring are in similar environment so they gave the same signals at 166.1 and

165.9 ppm for MF and MF-DTPA respectively. The signal which appears at 155.4 ppm for MF-DTPA and at 154.4 ppm for MF can be assigned to imine groups that may still be present in the matrix and not involved in the formation of bridges. The signal at 147.2 ppm for MF-DTPA distinguishes it from MF. The signal at 54.7 ppm for MF-DTPA and at 52.7 ppm for MF is consistent with the methylene ($-CH_2-$) bridges. The signal at 69.5 ppm for MF is consistent with the methylene ether ($-CH_2O-$) bridges. This signal is not present in the MF-DTPA spectrum and moreover the intensity of the methylene ($-CH_2-$) bridges signal is higher than that of the MF spectra which suggests that most of the bridging in the MF-DTPA is achieved with the methylene ($-CH_2-$) bridges.

By subtracting the two spectra (**Figure 7.5**) a high frequency signal appeared at about 170 ppm for MF-DTPA which strongly relates to the carbonyl carbon in carboxylic and/or amide groups. Furthermore, this spectral difference points to the modification in the structure caused by anchoring of DTPA to the MF matrix.

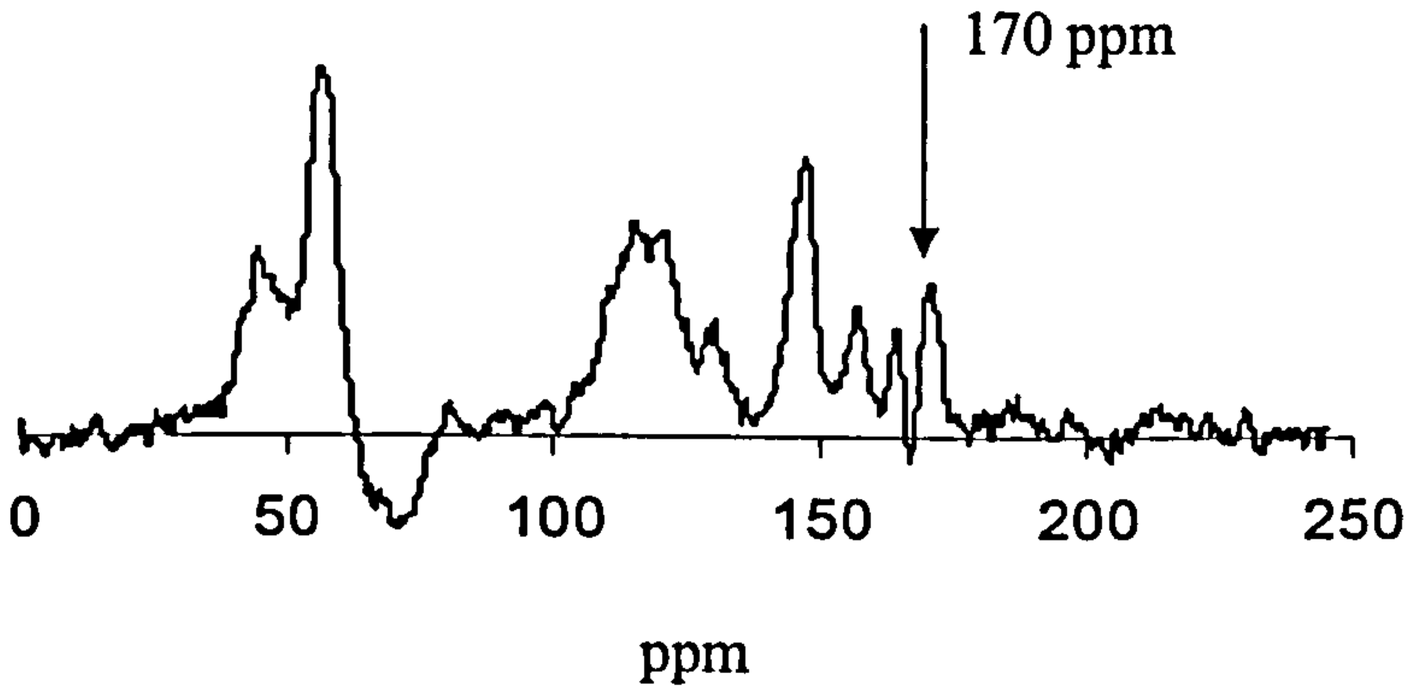

Figure 7.5: ^{13}C solid-state NMR spectral difference of MF-DTPA adsorbent and MF resin.

The ^{15}N solid-state NMR spectra of the pure MF resin and the MF-DTPA adsorbent are shown in **Figure 7.6**. The signal at –207.3 ppm for MF and at –211.3 ppm for MF-DTPA is due to triazine nitrogen. The signal at –281.3 ppm for MF and at –282.2 ppm for MF-DTPA is due to nitrogen present in the amine bridge. The

shoulder which appears in the spectrum of MF-DTPA at –268.9 is probably due to amide nitrogen.

Figure 7.7 shows the suggested structure of MF-DTPA according to the conclusions of IR, NMR and the elemental analysis.

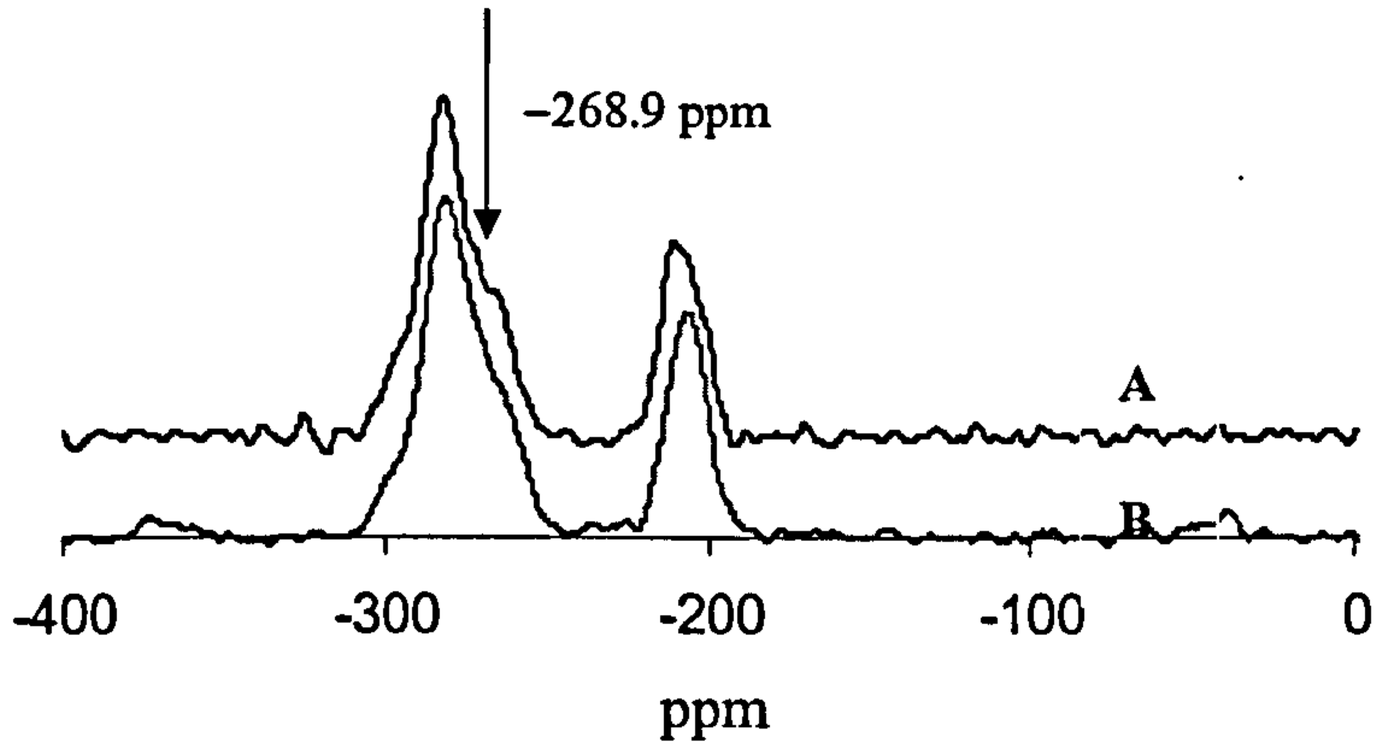

Figure 7.6: ^{15}N solid-state NMR spectra of (A) MF-DTPA adsorbent and (B) MF resin.

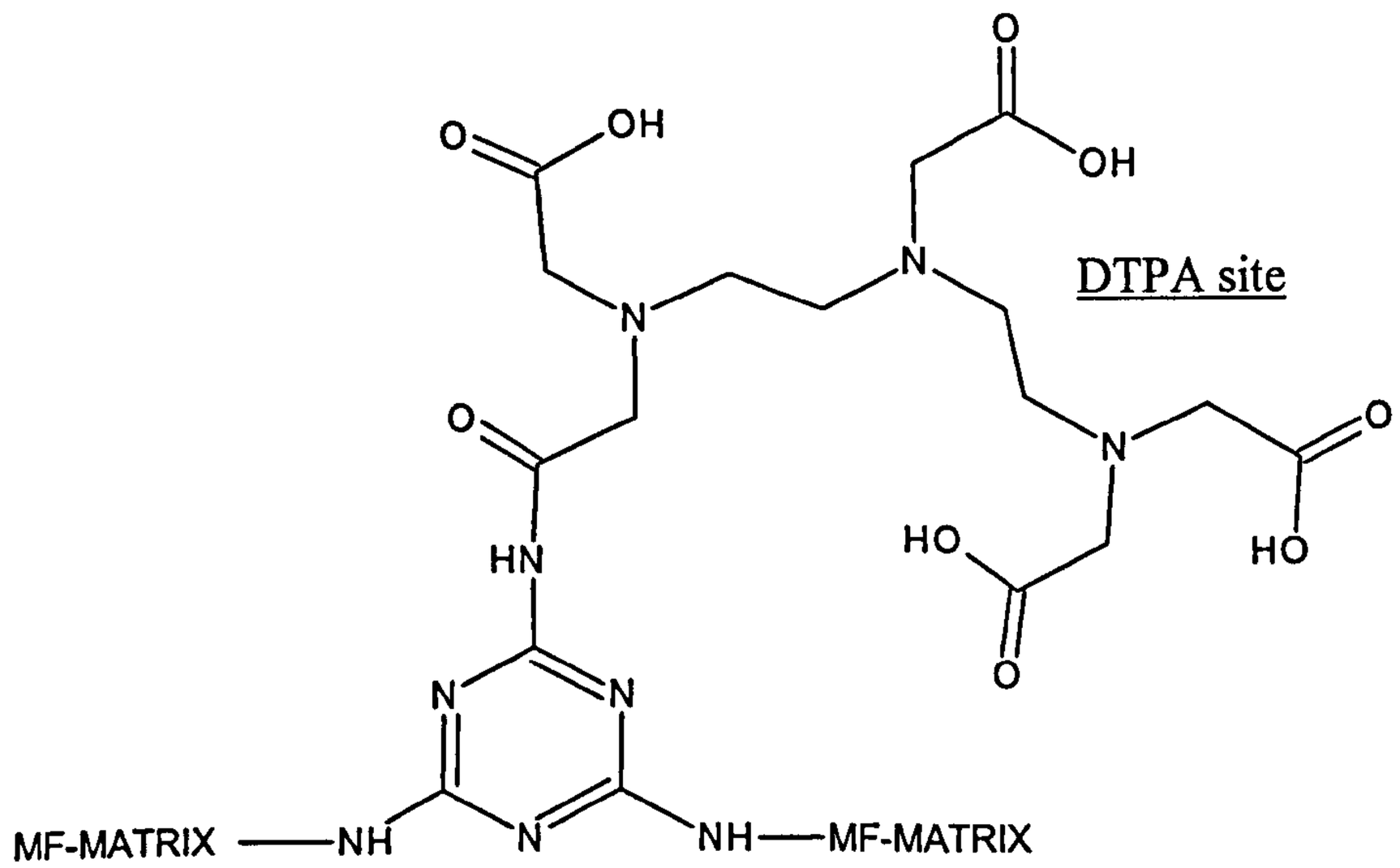

Figure 7.7: Suggested structure of MF-DTPA adsorbent.

7.1.5 Porosity (BET characterization)

The porosity characteristics for the various MF-DTPA adsorbent samples are given in **Table 7.4**. From the table, it can be concluded that surface area is sensitive to preparation conditions as it varies widely from 6 to 162 m^2/g. Sample numbers 2, 4 and 6 – which were prepared at lower pH – have lower surface areas compared to the corresponding sample numbers 1, 3 and 5 (**Tables 7.1** and **7.4**). This indicates that the acidity is a significant catalyst to aid bridging. The higher the acidity, the lower is the surface area due to the increased cross-linking.

The average pore diameter also changes with the conditions but with a smaller range of 65 to 165 Å, which is still wide enough for the M(II) ions to transfer easily through the pores; the hydrated–M(II) radius is approximately 4 Å. The micropore surface area is extremely small and can be taken as zero which is favourable for the adsorption of metal ions.

The negative values of micropore area may originate from the fact that the microporosity is too low to be detected by the instrument. This can be supported by observing the similar values for MF-CDTA adsorbent (**Tables 7.10**). For this adsorbent, the values are positive but very low.

Table 7.4: Porosity parameters for MF-DTPA selected samples (numbers 1–6)

No.	BET surface area (m^2/g)	Micropore area (m^2/g)	BJH Adsorption cumulative pore volume (cm^3/g)	Average pore diameter (Å)
1	42.6	–2.9	0.125	115.8
2	6.2	–0.3	0.026	164.6
3	161.9	0.3	0.396	94.7
4	6.8	–0.7	0.011	64.5
5	78.9	–0.6	0.251	125.1
6	114.6	0.0	0.322	112.2

The nitrogen adsorption/desorption hysteresis loop of sample number 3 is shown in **Figure 7.8**. This typical shape indicates an open pore structure arising mainly from non-crystalline intra-aggregation and inter-particle contacts of adsorbent material and allow us to characterise the adsorbent as mesoporous [154–156].

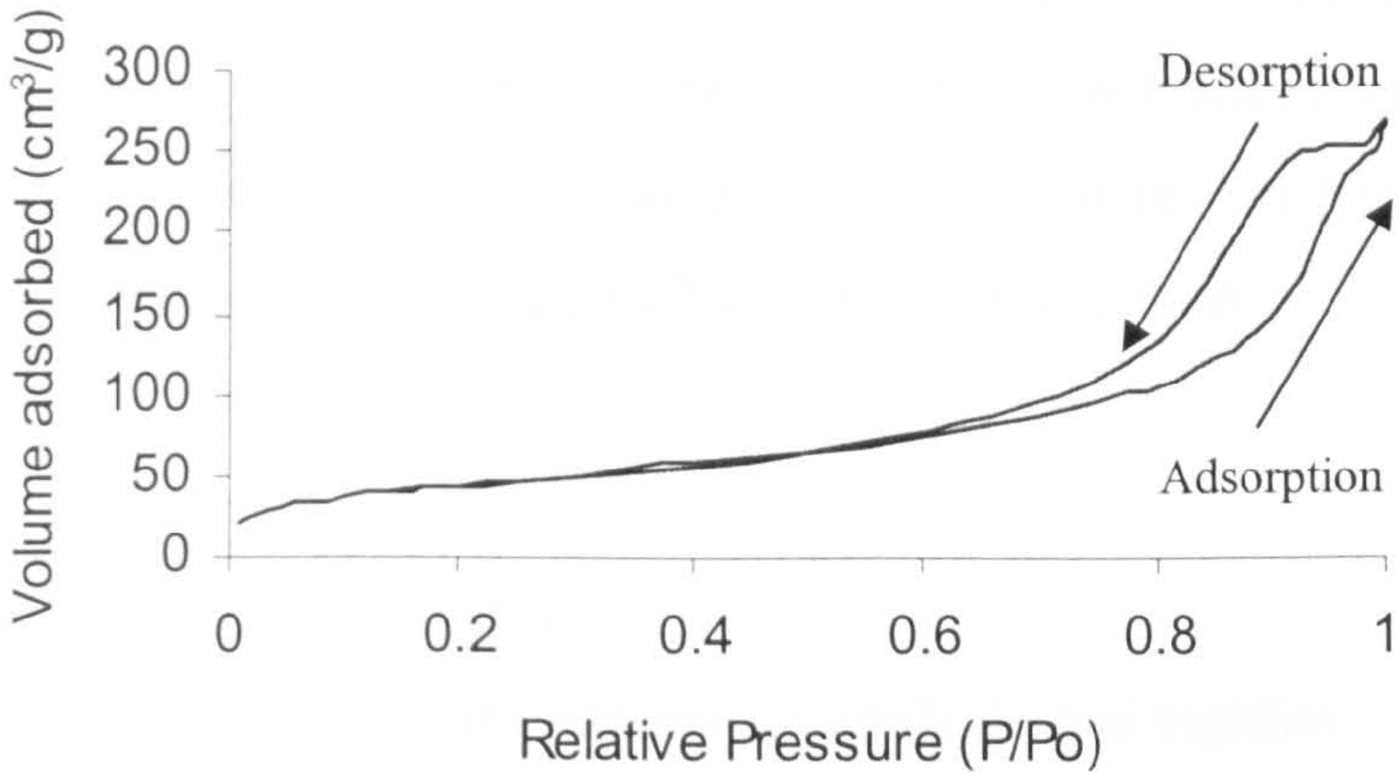

Figure 7.8: Adsorption/desorption hysteresis loop of MF-DTPA (sample No.3).

The dark areas observed in the FE-SEM image of the MF-DTPA adsorbent, **Figure 7.9**, are likely represent the intraparticle voids and cavities. This open structure facilitates solution flow in the adsorbent, which in turn gives reasonable adsorption kinetics.

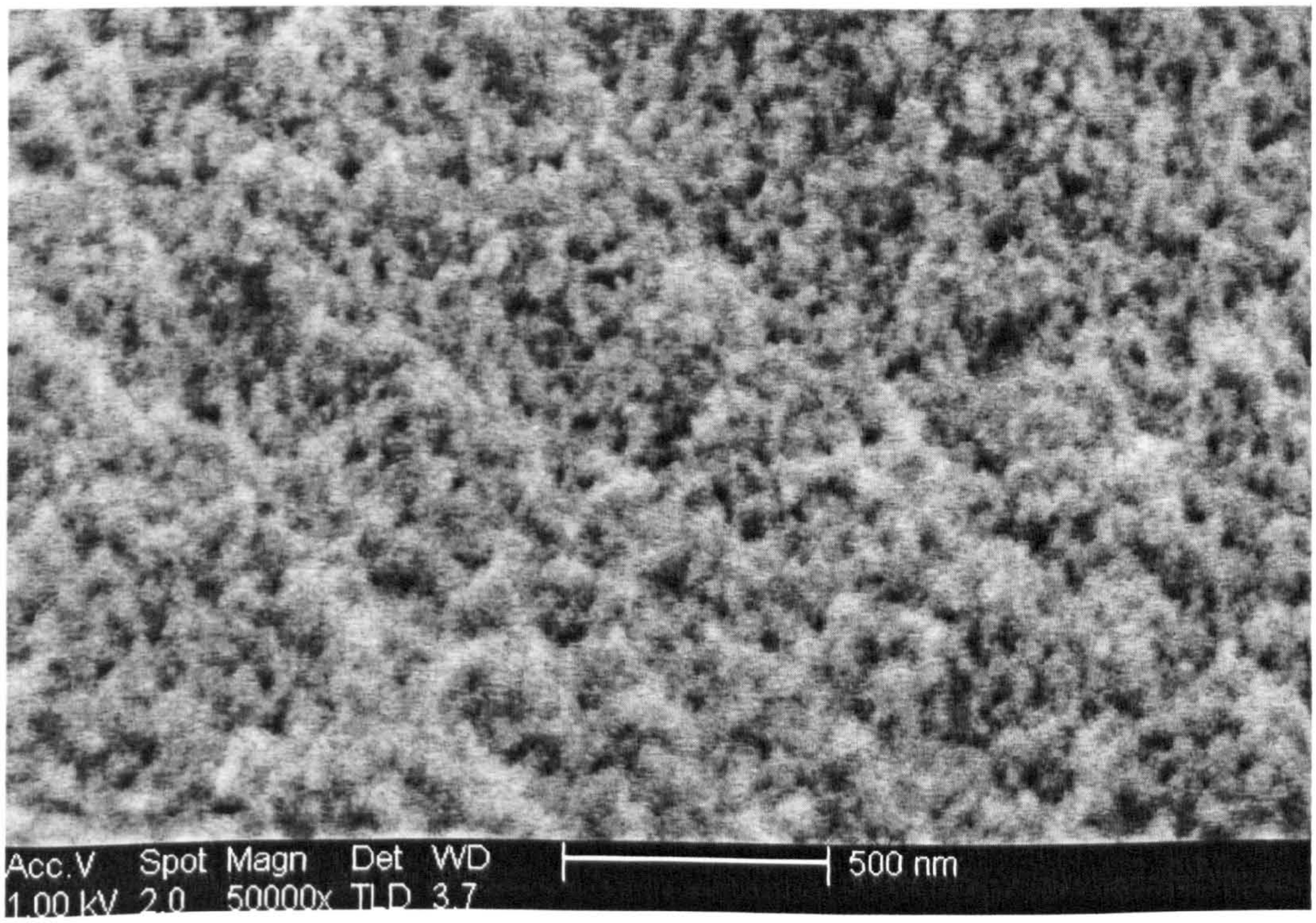

Figure 7.9: FE–SEM surface image of MF-DTPA adsorbent (sample number 3).

The adsorption experiments were carried out using sample number 3 as this sample showed the highest surface area (162 m^2 g^{-1}) with a pore volume of 0.40 cm^3/g, average pore diameter of 95 Å and a suitable rigidity to withstand water hydraulic-stress. Considering the average pore diameter, the adsorbent can be classified as a mesoporous material according to the IUPAC pore-classification.

7.2 Characterisation of MF-NTA

7.2.1 Gelling time, water regain, elemental analysis and rigidity

The gelling time of the various samples ranges from 10 to 110 minutes as shown in **Table 7.5**. Samples with a water content of 10 ml have the higher gelling time. The higher water content increases the distance between the reactants and this means more time for matrix formation. The water regain (on average, $W \approx 77\%$) shows the hydrophilic character of this adsorbent.

Table 7.5: MF-NTA adsorbent: Gelling time and water regain elemental composition and rigidity

T (°C)	Water content (ml)	pH	G.T. (min.)	*W*%	Rigidity	Elemental analysis C : H : N : O	No.
90	5	1.5	67	65	A (very hard)	34.5:5.19:41.35:18.9	1
		1.3	60	80	A	34.9:5.19:40.73:19.2	2
	10	1.5	75	86	C (fair hard)	–	–
		1.3	107	83	D (soft)	–	–
120	5	1.5	10	78	A	34.8:4.68:40.85:19.65	3
		1.3	20	78	B (hard)	34.87:4.87:41.58:18.7	4
	10	1.5	36	82	D	–	–
		1.3	110	81	C	–	–
150	5	1.5	17	72	A	34.74:4.92:40.45:19.99	5
		1.3	21	77	A	35.1:4.84:40.03:20.03	6
	10	1.5	45	90	C	–	–
		1.3	71	75	D	–	–
MF resin						35.1:5.12:42.7:17	

The elemental analysis of all the MF-NTA samples gives almost the same C:H:N:O ratio indicating the same chemical structure. This ratio is different from that of MF resin due to the modification by NTA. The oxygen ratio in MF-NTA is higher than that in MF due to the anchoring of NTA which has three carboxylic groups – NTA

has 50% oxygen. By applying a material balance calculation (using sample number 6), the NTA concentration was found to be about 1.24 mmole/g of dry adsorbent. It was noted that samples with the higher water content are less rigid due to the increased spacing in the matrix. In **Table 7.5**, the samples classified as A and B (for rigidity) have been chosen for porosity characterisation by the BET method.

7.2.2 IR spectra

The IR spectra of the twelve MF-NTA samples are shown in **Figure 7.10**. All samples have the same peaks due to same groups, so the variation in preparation conditions has no effect on the chemical structure.

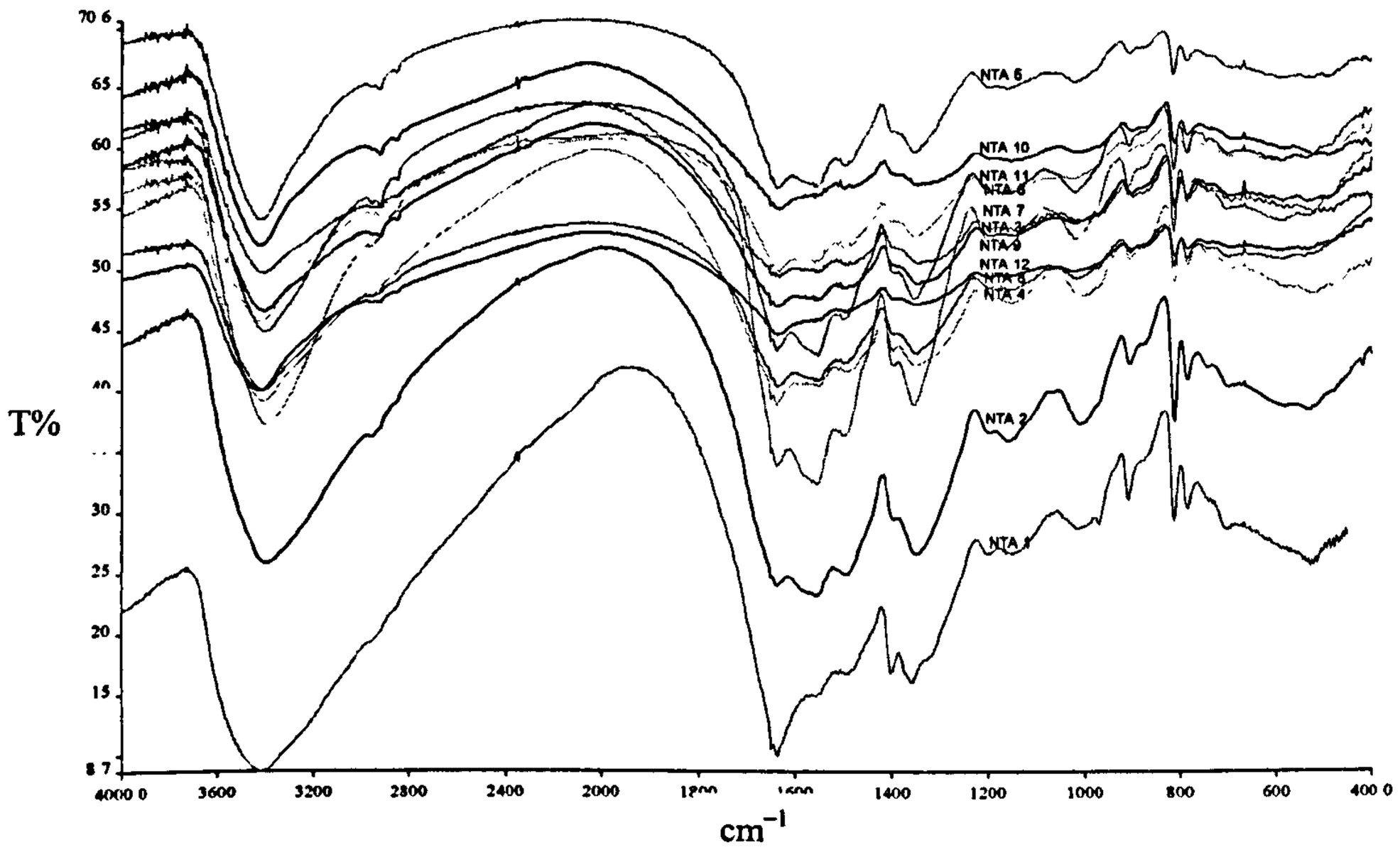

Figure 7.10: IR spectra of MF-NTA adsorbents under different preparation conditions.

Comparing one of these spectra (sample number 9) with the MF spectrum, as shown in **Figure 7.11**, shows that there are common peaks due to the common groups present in both materials but that there are also important differences between both spectra due to the anchoring of NTA into the MF matrix through the amide bond. This information is summarised in **Table 7.6**.

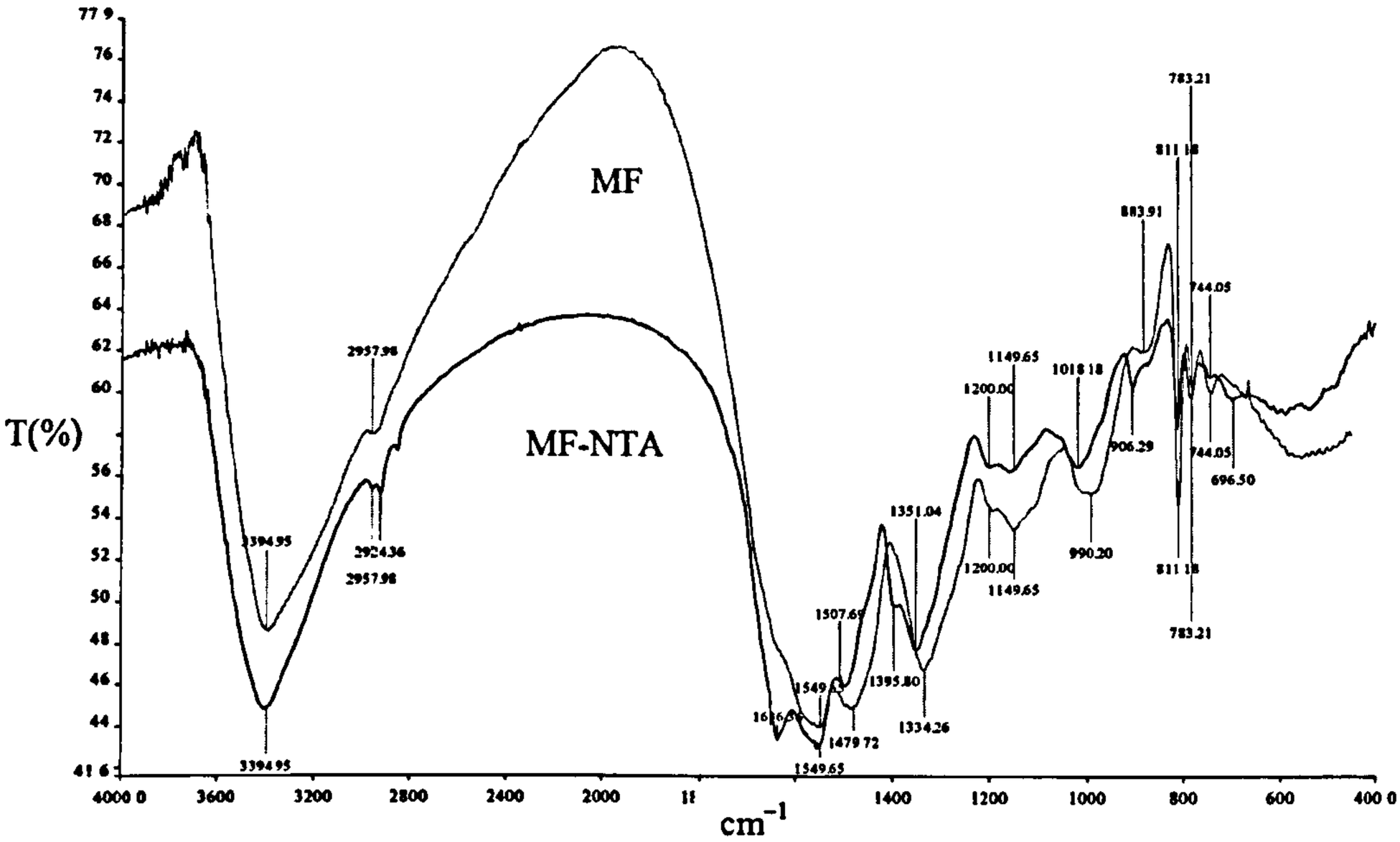

Figure 7.11: IR spectra of MF resin and MF-NTA adsorbent.

Table 7.6: IR peaks present in MF-NTA spectrum due to amide and carboxylic groups and not present in spectrum of MF.

Functional group	MF-NTA peak (cm^{-1})
Amide (carboxylic) carbonyl C=O stretch	1636
Amide N–Hout of plane	696
Carboxylic group In plane O–H bend	1395.8
Carboxylic O–H stretching	2924

A possible chemical structure of MF-NTA adsorbent is shown in **Figure 7.12.**

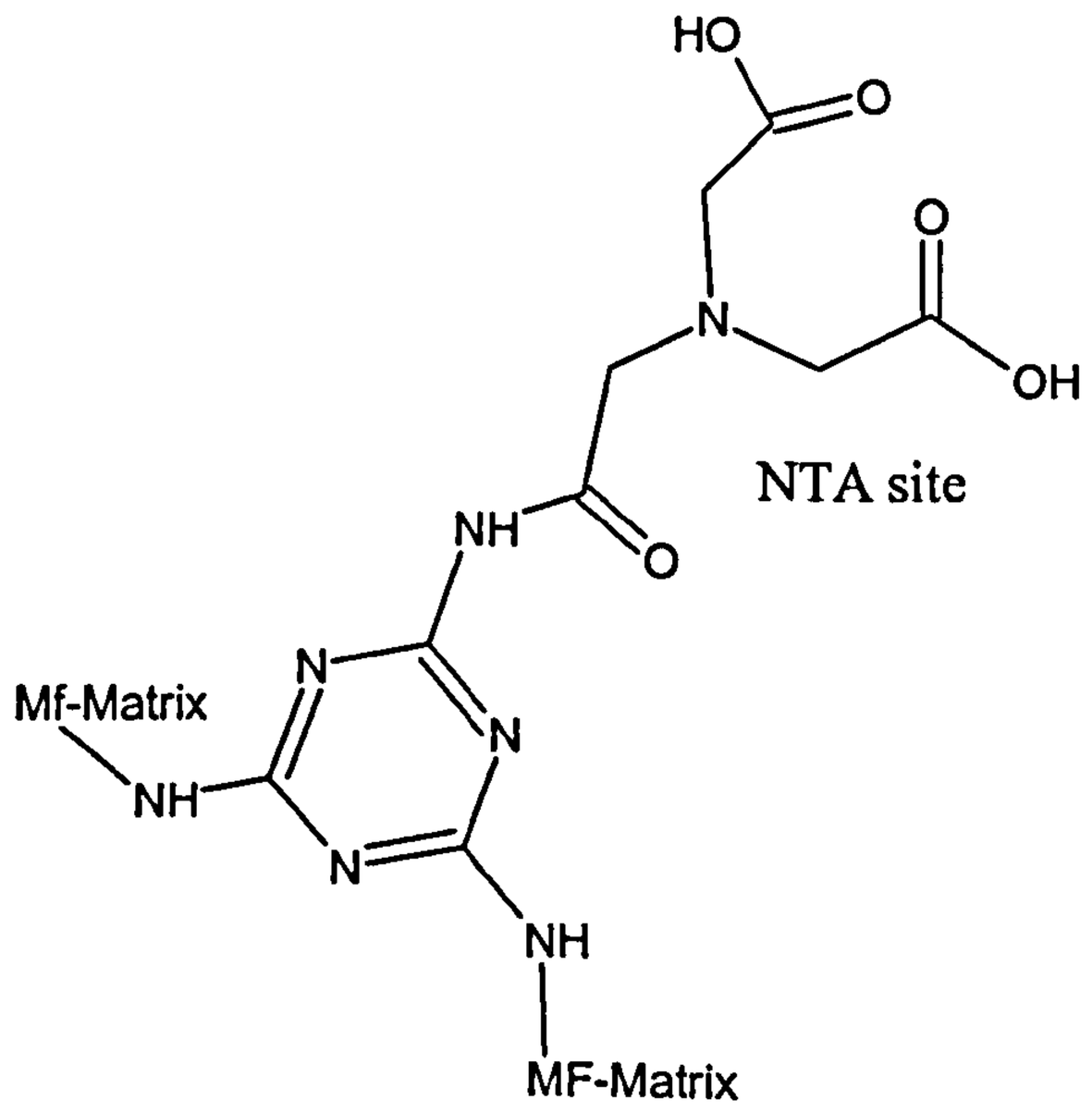

Figure 7.12: Suggested structure of MF-NTA adsorbent.

7.2.3 Porosity (BET characterization)

The porosity information of the MF-NTA samples is given in **Table 7.7**. Sample numbers 1, 2, 3, 5 and 6 have relatively high surface areas of 91, 102, 94, 143 and 159 m^2/ g respectively whereas sample number 4 has a surface area of only 15 m^2/g. The surface area is independent of pH opposed to the case of MF-DTPA which may indicate the effect of another factor. The average pore diameter is in the narrow range of 127 to 158 Å which corresponds to mesoporous classification.

Table 7.7: Porosity parameters for MF-NTA selected samples (numbers 1–6)

No.	BET surface area (m^2/g)	Micropore area (m^2/g)	BJH Adsorption Cumulative Pore Volume (cm^3/g)	Average pore diameter (Å)
1	90.7	6.3	0.364	158.7
2	102.1	3.9	0.356	137.6
3	94.2	6.6	0.337	140.9
4	14.8	1.4	0.058	127.6
5	142.7	9.0	0.483	133.2
6	159.3	8.7	0.528	130.4

For all samples, the very low porosity in the microporous range means that most of porosity corresponds to mesoporous range. This is suitable for adsorption of metal ions from solution.The adsorption/desorption hysteresis loop of sample number 6 is shown in **Figure 7.13.** The hysteresis loop has parallel vertical lines. This indicates an open cell structure of mainly mesopores [154–156].

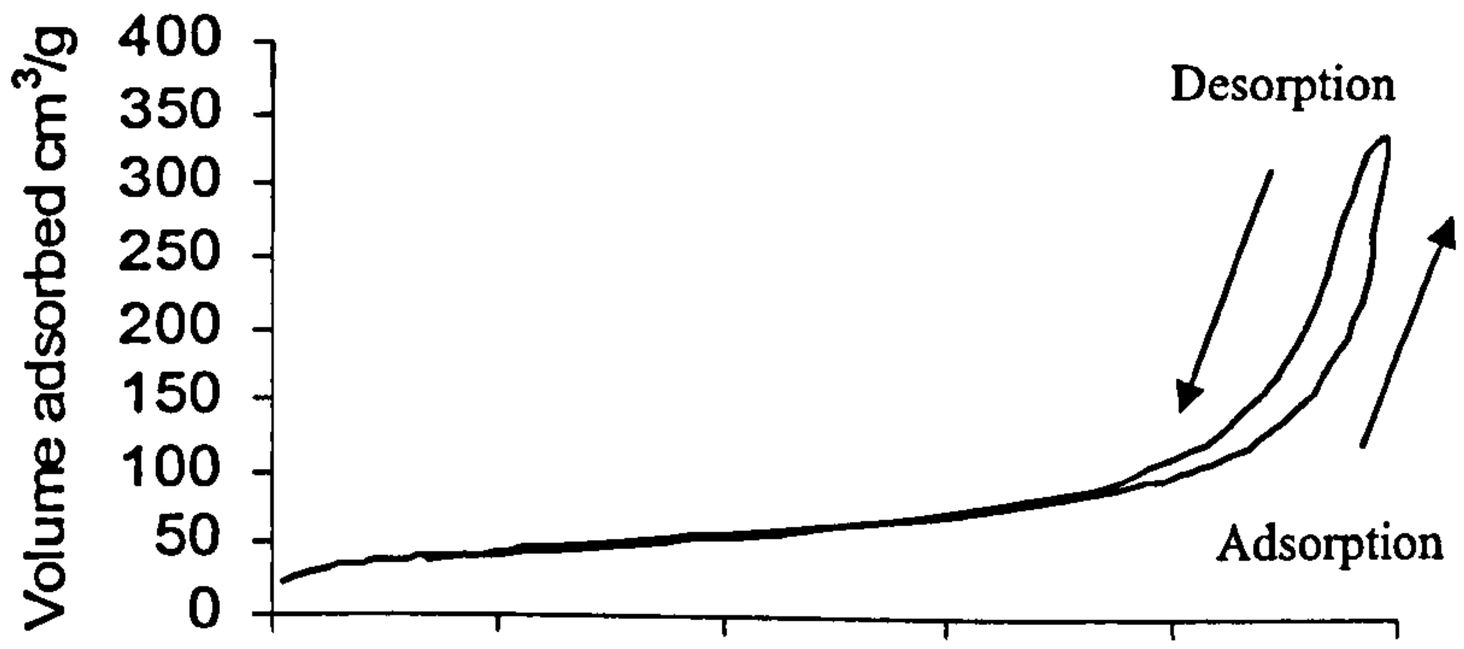

Figure 7.13: Adsorption/desorption hysteresis loop of MF-NTA, sample No.6.

The SEM image of sample number 6 is shown in **Figure 7.14**. It is clear from the image that the pores of the MF-NTA adsorbent are wider than those of MF-DTPA and MF-CDTA adsorbents (**Figures 7.9** and **7.19** respectively). Furthermore, the SEM image indicates the presence of macropores. As sample number 6 has the highest surface area (159 m^2/g) with a suitable average pore diameter (130 Å), this was considered suitable for the subsequent adsorption experiments.

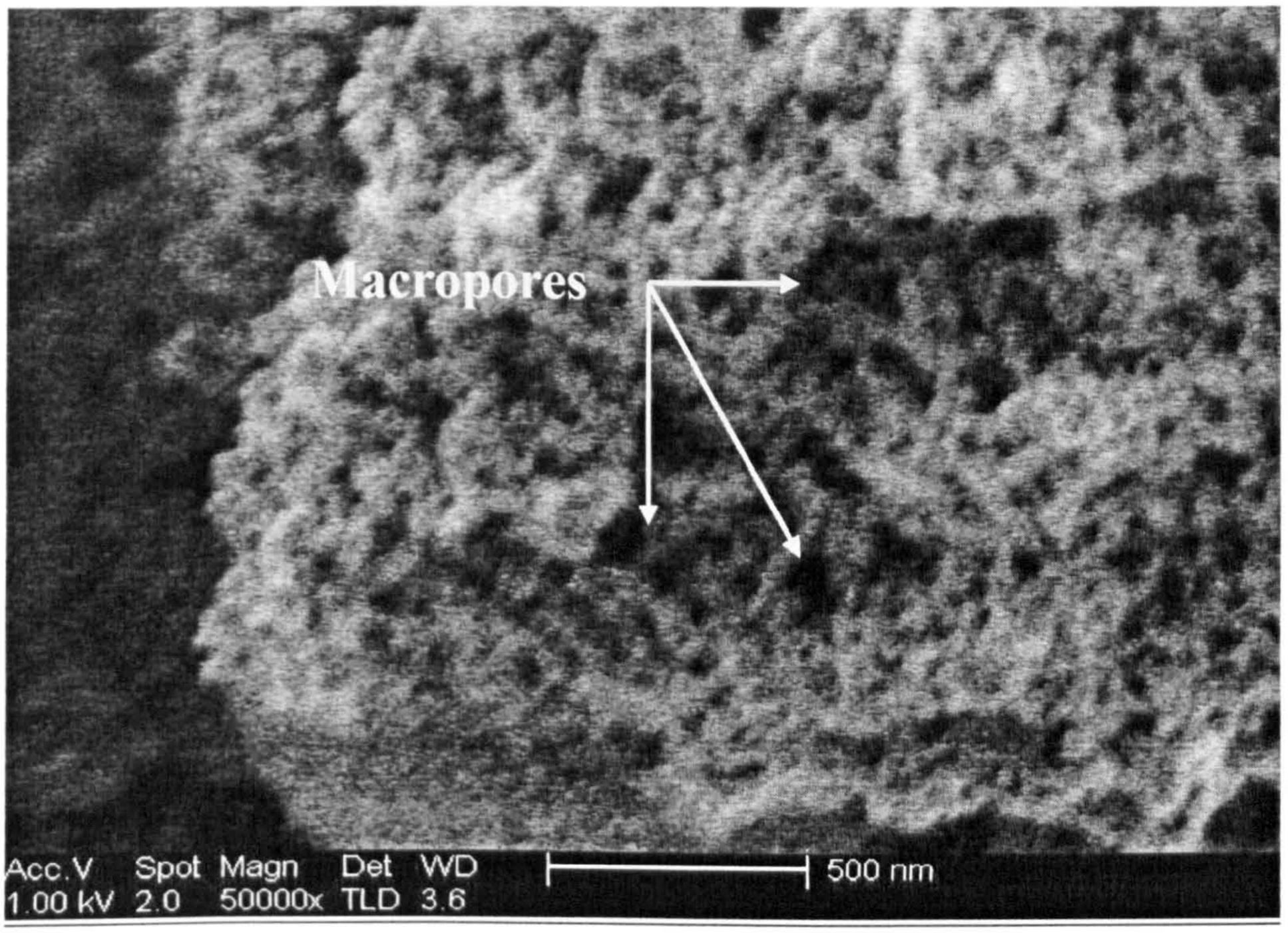

Figure 7.14: FE-SEM surface image of MF-NTA adsorbent (sample No.6).

7.3 Characterisation of MF-CDTA

7.3.1 Gelling time, water regain, elemental analysis and rigidity

The gelling time, rigidity and elemental analysis of various MF-CDTA samples are given in **Table 7.8**. The average water regain is 69% which reflects the hydrophilic character of this adsorbent. The elemental analysis showed a variation in the C:H:N:O ratio between the MF-CDTA samples. This variation is markedly different to that for MF-DTPA and MF-NTA. This behaviour for MF-CDTA may be attributed to the presence of the cyclic part of the CTDA molecule. The ratios for the MF-CDTA samples are different from that of the pure MF resin. Applying a mass

balance calculation for sample number 8, CDTA concentration is 2.28 mmole/g of dry adsorbent.

Table 7.8: MF-CDTA adsorbent: Gelling time, water regain, elemental composition and rigidity.

T (°C)	Water content (ml)	pH	G.T. (min.)	*W* %	Rigidity	Experimental C : H : N : O	No.
120	5	1.5	20	65	A	37.85:5.55:28.17:28.43	1
		1.3	30	78	B	31.81:5.13:40.47:22.59	2
	10	1.5	93	64	D	40.04:6.20:23.2:30.56	3
		1.3	112	69	D	39.20:6.14:25.16:29.5	4
150	5	1.5	19	67	A	35.86:5.64:32.44:26.06	5
		1.3	21	75	A	32.02:5.11:40.29:22.58	6
	10	1.5	109	69	B	36.12:5.71:32.28:25.89	7
		1.3	123	68	B	37.64:5.80:28.78:27.78	8
MF resin						35.1:5.12:42.7:17	

7.3.2 IR and XRD analysis of the MF-CDTA

The IR spectra of MF and MF-CDTA were determined and are shown in **Figure 7.15.** The figure also include the spectrum of Cu(II) Loaded-MF-CDTA which will be discussed later.

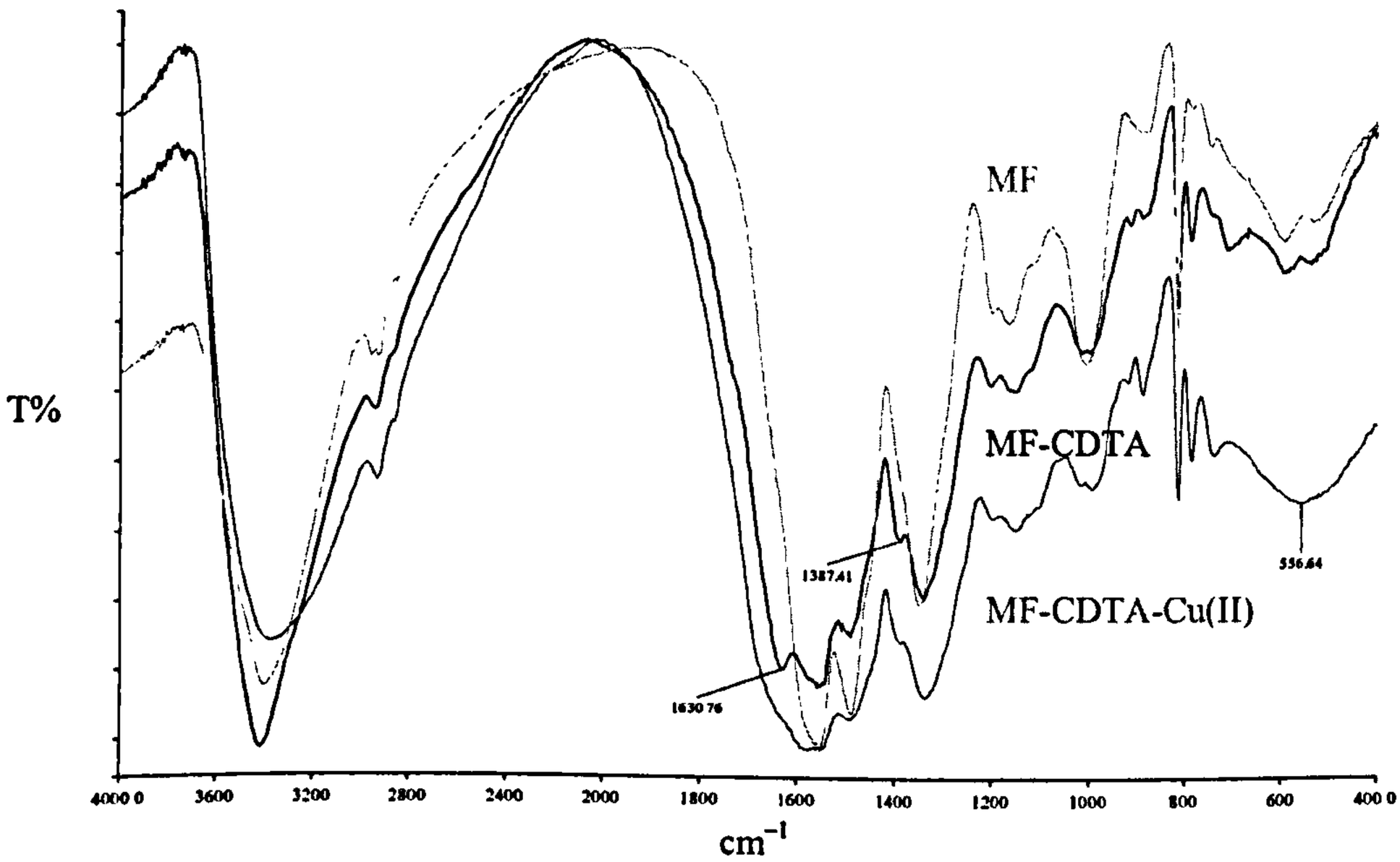

Figure 7.15: IR spectra of MF resin, MF-CDTA adsorbents and Cu(II)-loaded MF-CDTA adsorbent.

Both spectra exhibited common peaks due to common groups present in both: 3421 cm^{-1} (N–H stretch of secondary amine attached to methylene bridge), 2935 cm^{-1} (methylene C–H asymmetric stretch), 1560 cm^{-1} (N–H bend of bridging secondary amine) and 1488 cm^{-1} (methylene C–H bend). However, there are two distinguishing new peaks (**Table 7.9**) for MF-CDTA due to the CDTA anchoring to melamine: the peak at 1630 cm^{-1} (amide carbonyl C=O stretch) and the peak at 1387 cm^{-1} (carboxylic in plane O–H bend).

Table 7.9: IR peaks present in MF-CDTA spectrum due to the amide and carboxylic groups and not present in the spectrum of MF.

Functional group	MF-CDTA peaks (cm^{-1})
Amide (or carboxylic) carbonyl C=O stretch	1630
Carboxylic group In plane O–H bend	1387

The XRD diffractograms of MF and MF-CDTA (as well as the Cu(II) Loaded MF-CDTA diffractogram which will be discussed later) are shown in **Figure 7.16**. Only two weak peaks are noted for the diffractograms at 2θ values of 44.2 and 64.6. This means that the materials are mainly amorphous and that the MF structure was not affected by anchoring CDTA to MF matrix. The suggested structure of the MF-CDTA adsorbent is shown in **Figure 7.17**.

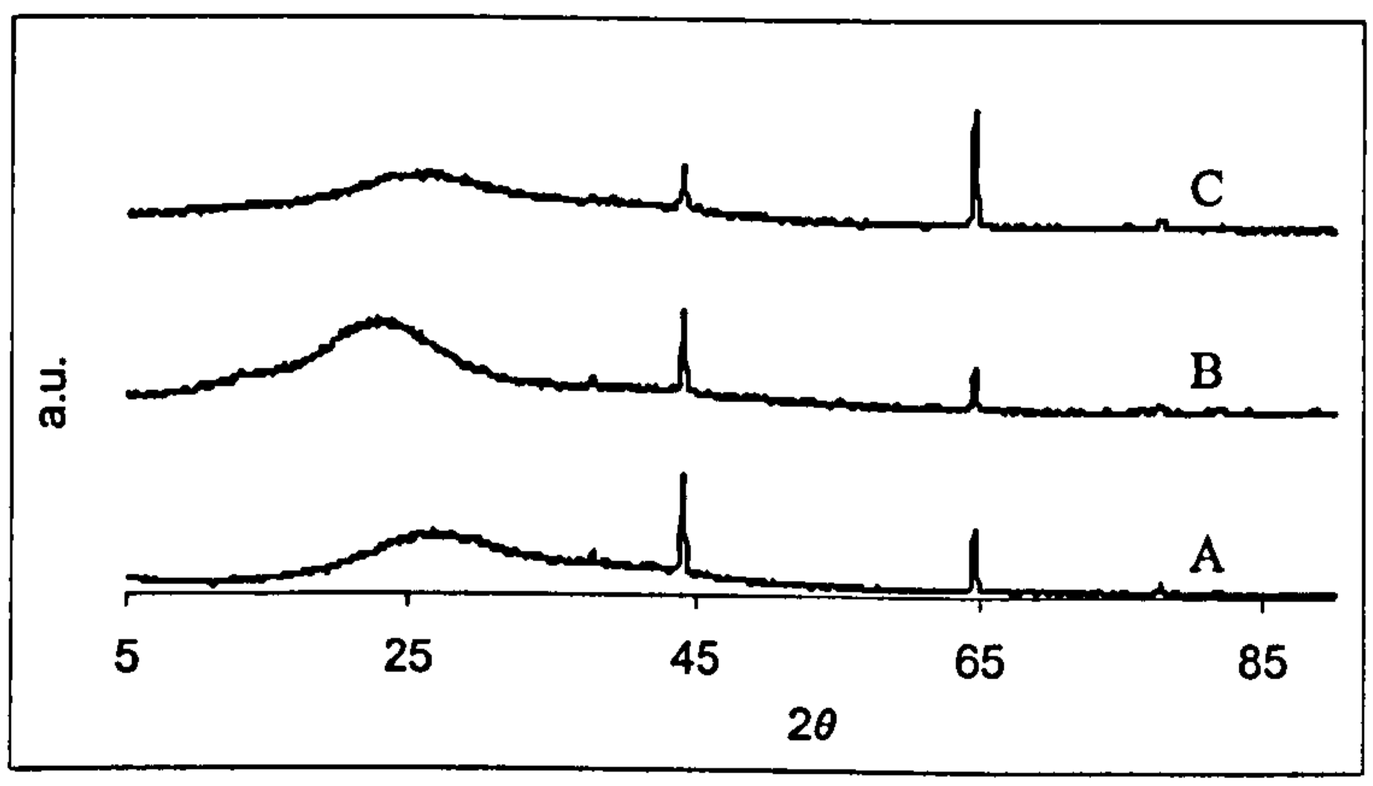

Figure 7.16: The XRD pattern of (A) MF, (B) MF-CDTA and (C) MF-CDTA-Cu(II).

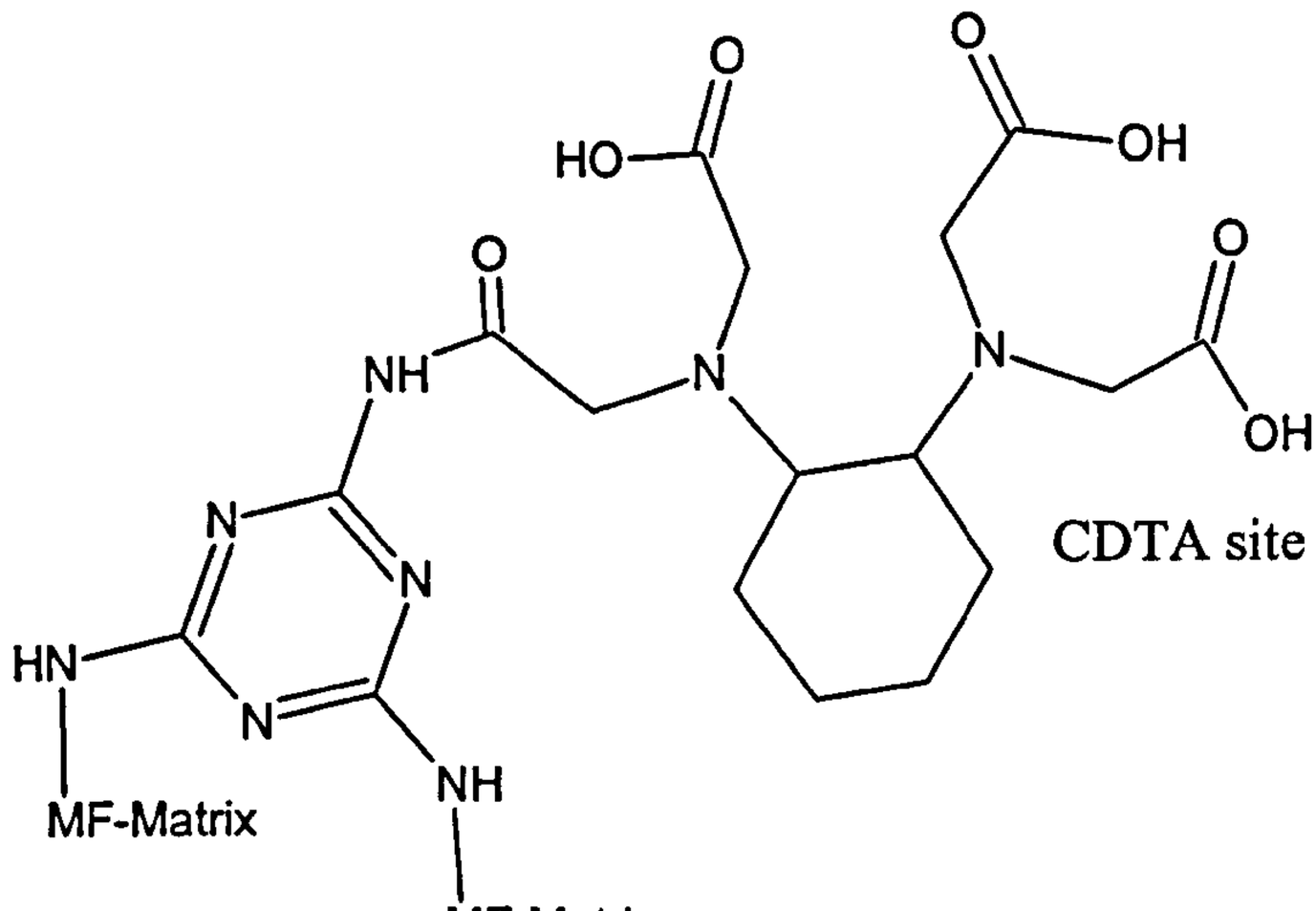

Figure 7.17: Suggested structure of the MF-CDTA adsorbent.

7.3.3 Porosity (BET characterization)

The porosity information of the MF-CDTA adsorbent samples is given in **Table 7.10**. The surface areas and the average pore diameters of the samples are very different which implies that this adsorbent is very sensitive to preparation conditions.

Table 7.10: Porosity parameters of MF-CDTA selected samples (Number 1–8).

No.	BET surface area (m^2/g)	Micropore area (m^2/g)	BJH Adsorption Cumulative Pore Volume (cm^3/g)	Average pore diameter (Å)
1	2.2	0.6	0.004	84.8
2	23.3	0.1	0.073	12.4
3	173.8	2.0	0.676	154.2
4	139.4	5.3	0.667	19.0
5	8.7	0.2	0.024	10.9
6	5.0	0.9	0.010	8.3
7	32.7	1.5	0.074	8.8
8	179.2	3.9	0.868	19.2

The highest BET surface area is 179 $m^2\ g^{-1}$ which corresponds to sample number 8. It has micropore area of 3.9 $m^2\ g^{-1}$, pore volume of 0.87 $cm^3\ g^{-1}$ and an average pore diameter of 19 Å which is on the mesopore boundary. The nitrogen adsorption/desorption hysteresis loop of the adsorbent (sample number 8) is shown in **Figure 7.18.** It indicates a mesoporous material with an open pore structure (parallel

vertical lines). This open structure originates from the textural porosity where intra-aggregate voids exist due to intra-particle contacts [154–156].

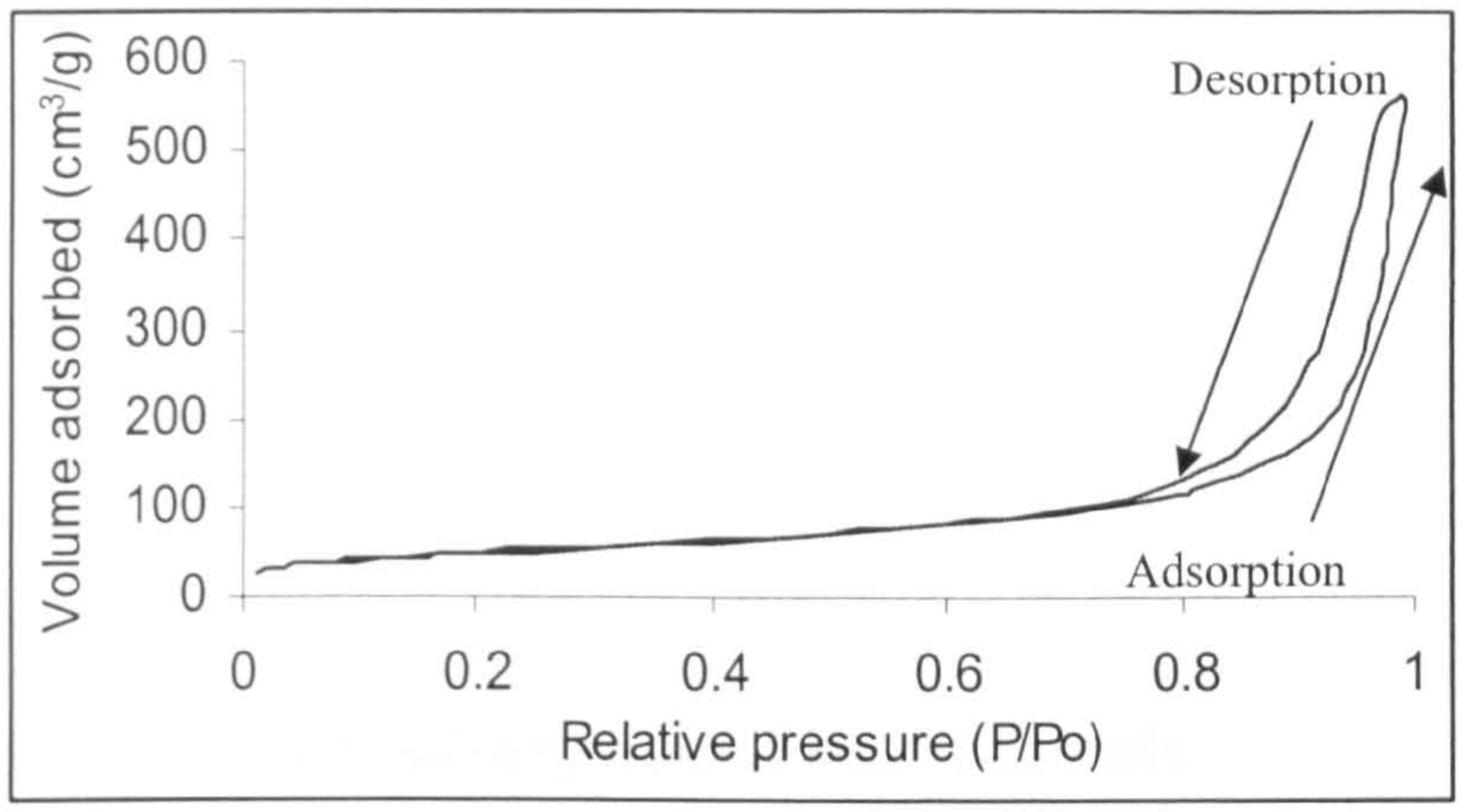

Figure 7.18: Adsorption/desorption hysteresis loop of MF-CDTA (sample No.8).

The SEM image of the MF-CDTA adsorbent is shown in **Figure 7.19.** The dark areas in the image may represent the intraparticle openings and cavities. Comparing this image to those of MF-DTPA and MF–NTA (**Figures 7.9** and **7.14** respectively), it can be observed that MF-CDTA has a compact texture and this may be due to its smaller average pore diameter.

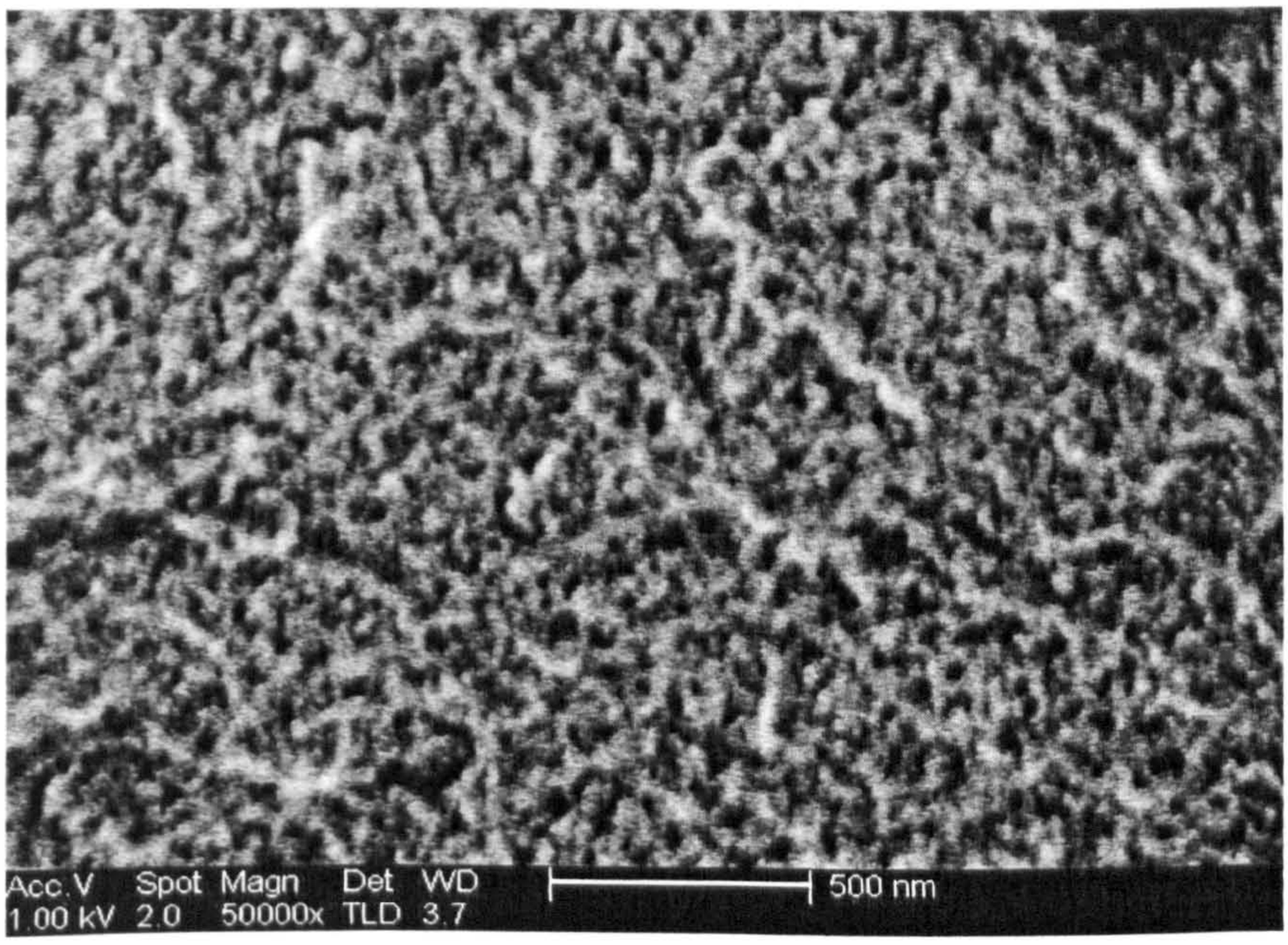

Figure 7.19: FE-SEM surface image of MF-CDTA adsorbent (sample number 8).

Chapter 8

Results and discussion II: Adsorption of heavy metals

This chapter presents the results of the simultaneous-batch adsorption of Co(II), Cd(II), Zn(II) and Cu(II) from synthetic wastewater using the synthesised MF-DTPA, MF-NTA and MF-CDTA adsorbents. The adsorption results were analysed as a function of the initial pH, temperature and initial concentration. Conventional kinetic and isotherm models were applied to investigate the removal behaviour. IR, elemental analysis and C^{13}-NMR were measured for some loaded-adsorbent samples to help understand the adsorption process. The adsorption thermodynamic parameters were then calculated.

The removal of Cu(II) by a fixed-bed packed with MF-DTPA using up-flow method was also studied and results are presented to investigate the removal of M(II) ions under continuous mode.

8.1 MF-DTPA adsorption behaviour (Batch method)

8.1.1 Characterization of metal loaded adsorbent sample (IR and elemental analysis)

The MF-DTPA adsorbent is white in colour. The colour changes upon adsorption to blue for octahedral Cu(II)–DTPA and pink for octahedral Co(II)–DTPA complexes when treated with Cu(II) and Co(II) ion solutions respectively (**Figure 8.1**) [81,104,152,157].

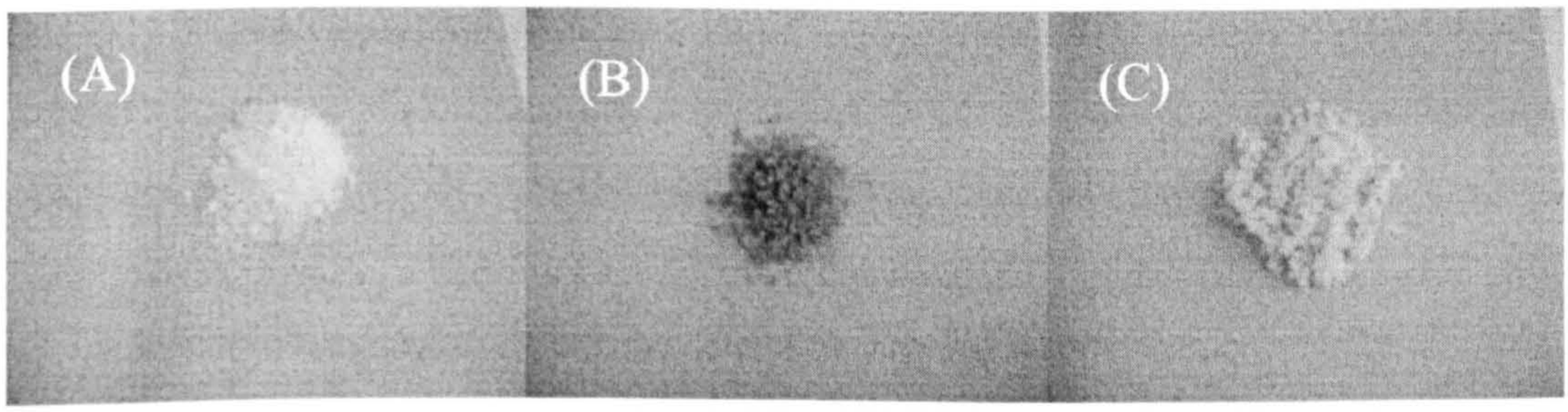

Figure 8.1: (A) White MF-DTPA, (B) Blue Cu(II)-Loaded MF-DTPA and (C) Pink Co(II)-Loaded MF-DTPA.

Most Cu(II) complexes have a distorted octahedral structure and their colour is blue or green. The Cu(II) ion has d^9 electronic configuration which leaves only one vacant orbital into which an electron may be promoted (d–d excitation), and hence has a

single absorption band which corresponds to the blue colour [104,157]. This observation suggests that the chelating mechanism strongly contributes to the adsorption process. A similar explanation can be given for the Co(II)–DTPA complex as Co(II) ion has d^7 electronic configuration and vacant orbitals are available for electron promotion. The octahedral complexes of Co(II) are commonly pink which is the case here [104].

The Cd(II) and Zn(II) complexes would not show colour change due to their d^{10} configuration. This configuration does not give a vacant *d*-orbital to allow electron promotion hence no *d–d* jump and no colour [104,157].

The IR spectrum of Cu(II)-loaded MF-DTPA sample is shown in **Figure 8.2.** It shows a change when compared with the spectrum of MF-DTPA (**Figure 7.2**) which is most evident at 1636 cm^{-1} (carbonyl C=O stretch) which became broadened after Cu(II)-loading. This indicated the involvement of amide (and/or carboxylic) groups in coordination of Cu(II) ion. The peak at 2924 cm^{-1} (carboxylic O–H stretching) became stronger after Cu(II)-loading. Also, two peaks at 600 and 530 cm^{-1} can be seen, which may be due to the coordinations Cu–N and Cu–O respectively [158].

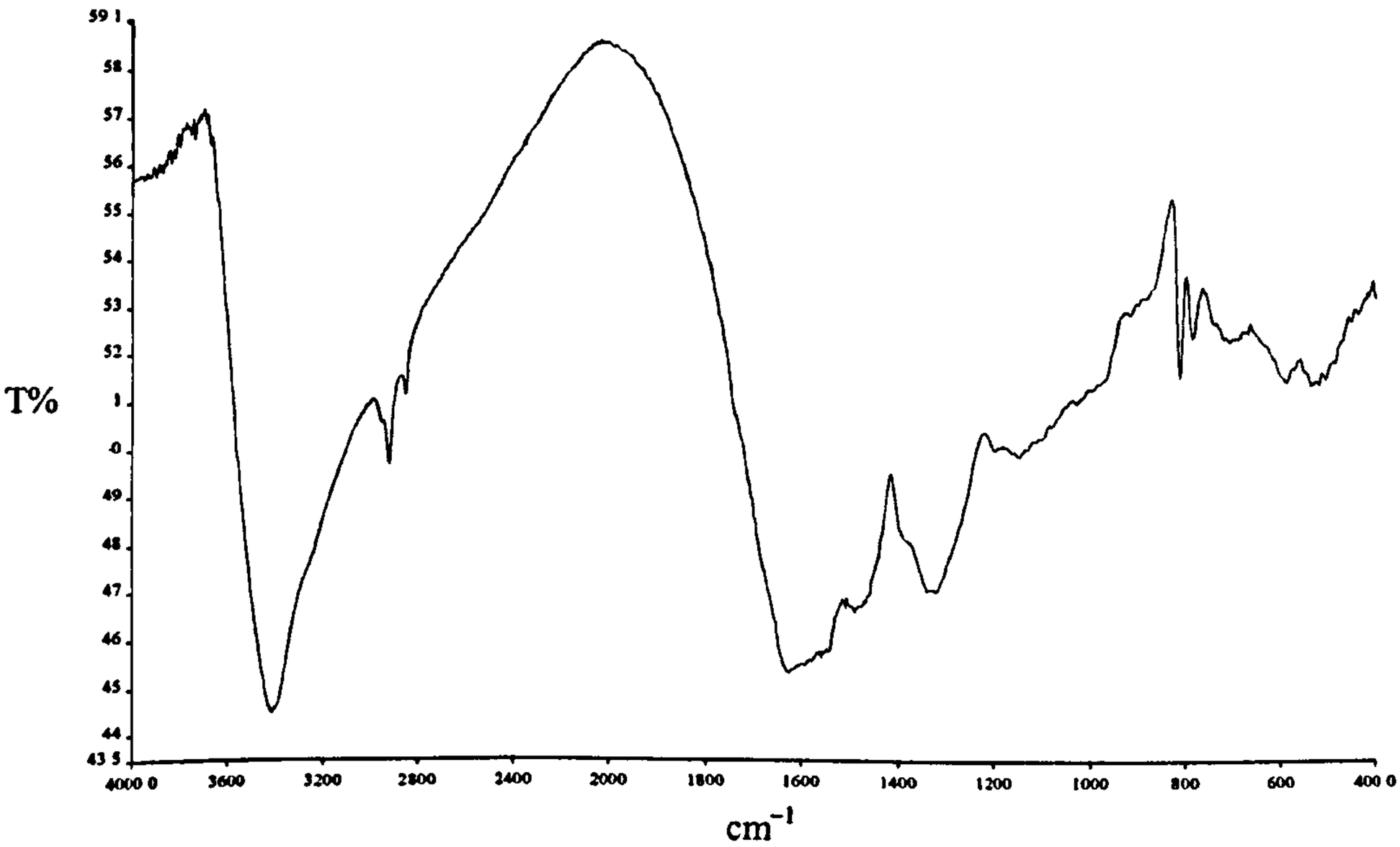

Figure 8.2: IR spectrum of Cu(II)-loaded MF-DTPA sample.

The results of elemental analysis of MF-DTPA and Cu(II)-loaded MF-DTPA samples are presented in **Table 8.1**. The similar elemental ratio of Cu(II) in the presence and absence of Na(I) ion in adsorption solution indicates that Na(I)-presence (20 mg l^{-1}) does not significantly affect the uptake of Cu(II). However, higher concentration-Na(I) needs to be studied to replicate its industrial performance [159,160].

Table 8.1: MF-DTPA and MF-DTPA-Cu(II) elemental ratio.

Sample	C	H	N	O (calculated)	Cu(II) (calculated)
MF-DTPA	35.7	5.1	37.7	21.5	—
MF-DTPA-Cu(II)	33.6	5.0	35.2	20.1	6.1
MF-DTPA-Cu(II) (Na(I) present in solution)	33.7	5.1	35.3	19.9	6

The material balance calculation revealed the uptake of about 61 mg Cu(II) per gram of adsorbent. The adsorbent therefore has a maximum M(II)-load (capacity) equivalent to 0.97 mmole per gram of the adsorbent. If chelation in molar ratio is 1:1 [(Cu(II) : DTPA], it can be concluded that Cu(II) ion chelated with about 90% of the DTPA (1.08 mmole /g adsorbent) present in the adsorbent. This shows that most of chelating sites are readily accessible to the treated solution.

8.1.2 Effect of pH and temperature (Thermodynamics) on adsorption

The initial pH and temperature of the treated solution affect the adsorption process. According to the chemical structure of the MF-DTPA adsorbent and its active sites, the most probable adsorption mechanisms are coordination (metal-chelate formation with DTPA molecules by several coordinations) and ion exchange (with available carboxylic groups of DTPA moieties). At equilibrium adsorption on MF-DTPA, the measured final pH values for different initial pH and temperatures can give an indication about the contribution of possible adsorption mechanisms. The final pH values were measured and are presented in **Table 8.2**. From the table, it is observed that ΔpH (initial pH – final pH) indicates an increase of acidity for all initial pH and temperature values. Generally, both adsorption mechanisms cause an increase of acidity of treated solution due to liberation of H^+ ions into solution which is clearly

noted from **Table 8.2** [53,116]. However, chelation can produce more acidity than ion exchange due to more liberation of H^+ ions per M(II) ion to bind.

Table 8.2: Final pH values after M(II)-adsorption on MF-DTPA (equilibrium).

Initial pH	Final pH±0.02				
	15°C	20°C	25°C	30°C	35°C
3	2.91	2.90	2.70	2.62	2.52
4	3.05	2.97	2.81	2.65	2.55
5	3.07	3.00	2.85	2.73	2.57
6	3.10	3.06	2.95	2.75	2.60

Effect of initial pH:

The initial pH influences both the chemistry of metal ions and functional groups of the adsorbent [77]. In acidic media (studied range: pH 3–6) metals have soluble solvated ions [$M^{2+}(H_2O)_n$] as the main dominating form in the solution [17,161]. The adsorbent functional groups (carboxylic and amine groups for the MF-PAPC adsorbents) are being gradually deprotonated as the initial pH increases. At lower initial pH, coordinating groups (lone pair bearing groups: carboxylic and amine of DTPA) are protonated (–COOH and $-NR_2H^+$), and M(II) ion exchange and chelation mechanisms are competed by abundant H^+ ion. However, adsorption occurred efficiently as ΔpH values (**Table 8.2**) and metal removal percentages indicate (**Figure 8.3**). The ΔpH values at lower initial pH are smaller than those of higher initial pH, hence it is suggested that ion exchange (with carboxylic groups) has a considerable contribution (*besides chelation*) at lower initial pH. At higher initial pH, active groups are deprotanated producing more negatively functional groups ($-COO^-$ and $-NR_2$), hence affinity towards the M(II) ions increases due to electrostatic attraction and both ion exchange and chelation mechanisms can occur efficiently. However, the ΔpH values at higher initial pH are larger than those of lower initial pH, hence it is suggested that chelation completely dominates higher initial pH.

Effect of temperature:

The ion exchange mechanism is favoured at higher temperatures due to its endothermic nature [162]. The endothermicity originates from the dispatching of water molecules from M(II)-hydrated ion (heat absorbing process) which overcomes

the exothermic binding of M(II) with an ion exchange site [163]. On the other hand, the chelation mechanism favours lower temperatures due to its exothermic nature [164–166]. The heat released due to the formation of several coordination bonds of the chelate overcomes the heat absorbed for the M(II)-dehydration process [164]. Accordingly, it is believed that chelation is the main mechanism for the studied initial pH and temperature ranges with some participation of ion exchange mechanism at lower initial pH and higher temperature. This can be considered as a general rule for MF-PAPC adsorbents due to their similar structure.

The initial-pH adsorption profiles at equilibrium for metal ions for different temperatures are shown in **Figure 8.3**. The removal percentage of M(II) ions *slightly* increased with the increase of initial pH for all temperatures studied. Hence from a practical application point of view, this behaviour facilitates the use of this adsorbent for removal in this pH range with no need for adjustment for an optimal pH value. This advantage is not seen for many adsorbents, especially those which exhibit an ion exchange mechanism, where removal is optimum over a narrow pH range [53,77].

The lower adsorption percentages at lower initial pH values may be attributed to H^+ ion abundance at adsorbent surface which can repel M(II) ions. Also, the probable formation of hydrogen bonding (due to abundant presence of electronegative elements, O and N) can cause some shrinkage of the adsorbent surface, which in turn, acts as a barrier slowing down the adsorption amount of M(II) ions [77].

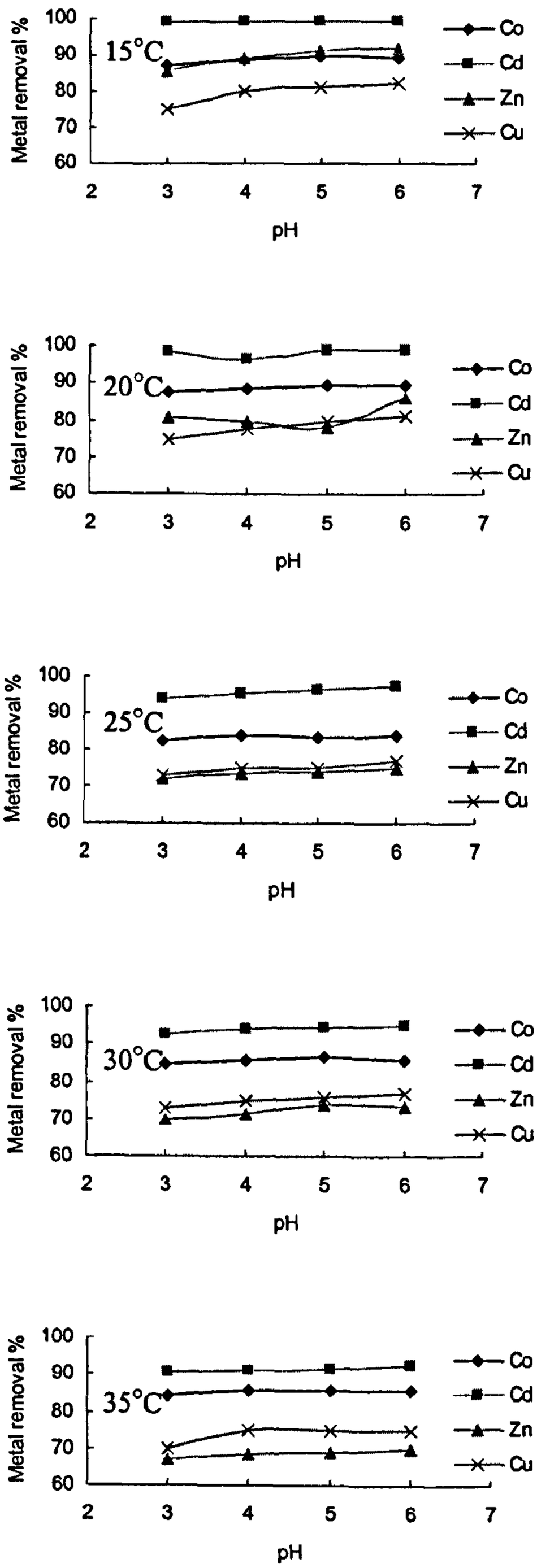

Figure 8.3: The adsorption pH-profile of Co(II), Cd(II), Zn(II) and Cu(II) on MF-DTPA (M(II)-initial concentration: 20 mg l^{-1}) at temperatures 15, 20, 25, 30 and 35°C.

The metal removal percentage increased at lower temperatures for the four elements. Considering Cd(II) as an example, it can be seen that: at pH 5 the removal is 91.7, 94.7, 96.4, 99 and 100% at temperatures of 35, 30, 25, 20, and 15°C respectively. This reflects the exothermic character of the adsorption process.

It is observed that the Cd(II) ion has a higher removal percentage at all conditions followed by Co(II), Cu(II) then Zn(II). However, exceptions are observed at lower temperatures: 1) Zn(II) removal slightly exceeded that of Cu(II) at 20 and 15°C (chelation-dominated zone) 2) Zn(II) removal exceeds Co(II) at 15°C for pH 5 and 6. This change in preference for adsorption with temperature may depend on several factors such as M(II)-chelate formation stability constants, enthalpies and entropies of adsorption, enthalpies of M(II)-dehydration and type of M(II)-DTPA chelate.

The values of the free energy of adsorption (ΔG^{ads}) are given in **Table 8.3**. The values are negative for all conditions confirming that the adsorption process is spontaneous. The absolute values for all M(II) ions at 15 and 20°C are higher than those at 30 and 35°C which suggest that adsorption is more favourable at lower temperatures [137,167]. It shows an increase with initial pH which suggests better adsorption process as solution became more neutral. The values of ΔG^{ads} suggest adsorption affinity order: Cd(II) > Co(II) > Zn(II) ≥ Cu(II) [168].

Table 8.3: Free energy of adsorption of M(II) on MF-DTPA.

T (°C)	pH	$-\Delta G^{ads}$ (kJ mole^{-1})			
		Co(II)	Cd(II)	Zn(II)	Cu(II)
15	3	4.58±0.03	11.00±0.08	4.20±0.03	2.63±0.02
	4	4.91±0.03	11.00±0.08	5.29±0.04	3.32±0.02
	5	5.09±0.03	11.00±0.08	5.50±0.04	3.47±0.02
	6	5.03±0.03	11.00±0.08	5.66±0.04	3.63±0.03
20	3	4.80±0.03	10.49±0.07	3.45±0.02	2.68±0.02
	4	4.98±0.03	8.02±0.05	3.33±0.02	3.08±0.02
	5	5.25±0.04	11.19±0.08	3.09±0.02	3.38±0.02
	6	5.26±0.04	11.19±0.08	4.43±0.03	3.53±0.02
25	3	3.84±0.03	6.84±0.05	2.32±0.02	2.46±0.02
	4	4.14±0.03	7.69±0.05	2.56±0.02	2.72±0.02
	5	4.06±0.03	8.12±0.05	2.59±0.02	2.72±0.02
	6	4.10±0.03	8.99±0.06	2.72±0.02	2.99±0.02
30	3	4.29±0.03	6.33±0.04	2.14±0.01	2.51±0.02
	4	4.55±0.03	7.07±0.05	2.32±0.02	2.77±0.02
	5	4.77±0.03	7.26±0.05	2.64±0.02	2.90±0.02
	6	4.53±0.03	7.49±0.05	2.58±0.02	3.04±0.02
35	3	4.29±0.03	5.80±0.04	1.81±0.01	2.17±0.01
	4	4.57±0.03	6.04±0.04	1.98±0.01	2.81±0.02
	5	4.62±0.03	6.14±0.04	2.06±0.01	2.81±0.02
	6	4.62±0.03	6.53±0.04	2.14±0.01	2.81±0.02

The plots of $\ln K_C$ against $1/T$ for Co(II), Cd(II), Zn(II) and Cu(II) ions at pH 3, 4, 5 and 6 are shown in **Figure 8.4**. The values of enthalpy change (ΔH^{ads}) and entropy change of adsorption (ΔS^{ads}) of adsorption of M(II) ions on MF-DTPA are given in **Table 8.4.**

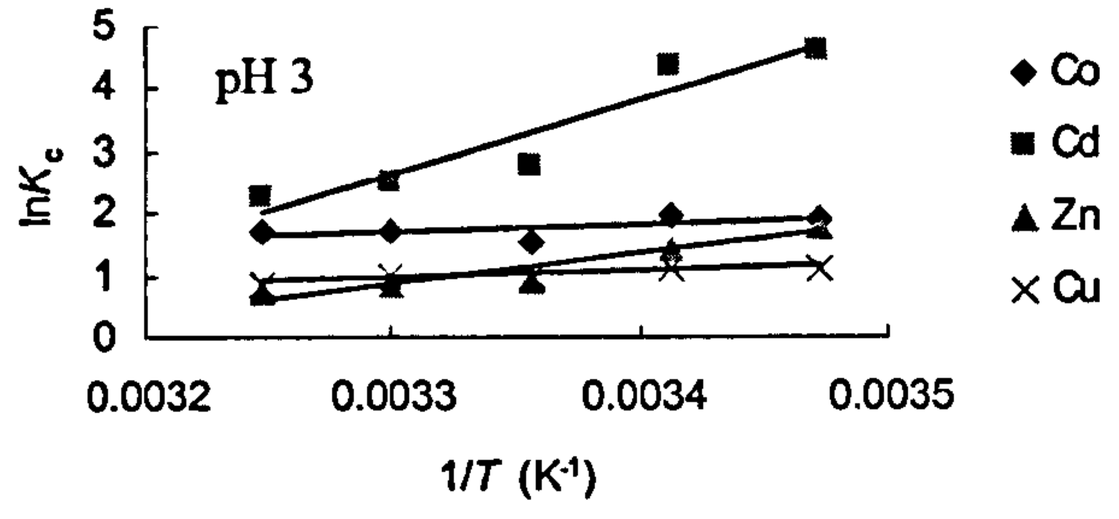

Figure 8.4: The plots of lnK_C against $1/T$ for Co(II), Cd(II), Zn(II) and Cu(II) adsorption on MF-DTPA at pH 3, 4, 5, and 6.

Table 8.4: Thermodynamic parameters of the adsorption of M(II) on MF-DTPA (ΔH^{ads} and ΔS^{ads}).

pH	Co(II)		Cd(II)		Zn(II)		Cu(II)	
	$-\Delta H^{ads}$ kJmol^{-1}	$-\Delta S^{ads}$ J mol^{-1} K^{-1}	$-\Delta H^{ads}$ kJmol^{-1}	$-\Delta S^{ads}$ J mol^{-1} K^{-1}	$-\Delta H^{ads}$ kJmol^{-1}	$-\Delta S^{ads}$ J mol^{-1} K^{-1}	$-\Delta H^{ads}$ kJmol^{-1}	$-\Delta S^{ads}$ J mol^{-1} K^{-1}
3	11.0	22.4	95.6	293.7	40.2	125.5	8.9	21.5
4	11.4	22.8	73.6	220.3	49.3	155.2	11.1	27.2
5	13.6	29.5	90.2	273.4	47.7	149.5	13.9	36.4
6	14.3	32.4	84.2	252.4	57.2	180.2	15.9	42.7

The parameters ΔH^{ads} and ΔS^{ads} have negative values for all conditions. The negative values of enthalpy change confirm an exothermic chemical process. Hence, the chelation mechanism (exothermic) may generally dominate over the ion exchange mechanism (endothermic). The values of ΔH^{ads} for M(II) ions, especially Cd(II) and Zn(II), are high enough to be caused by chemical bond formation (coordination) [169]. For the Co(II), Zn(II) and Cu(II) ions, ΔH^{ads} increases with initial pH and this reflects favourable adsorption for neutral solutions.

As a rule, the enthalpy change of chelate formation is remarkably negative for neutral ligands (these are not hydrated, and so energy is not required to dehydrate the ligands) and is close to zero for charged ligands (hydrated, and dehydration of the ligands consumes energy) [164]. The ligands present in MF-DTPA are carboxylic (and/or amide) and amine groups. It can be inferred from IR, TPD-MS and NMR analysis of MF-DTPA (chapter 7: sections 7.1.2, 7.1.3 and 7.1.4) that many of the carboxylic groups are anchored in the MF matrix forming amide groups. Under this situation, the amine groups may control the charge of the adsorbent-surface. Accordingly, it is suggested that amine groups become more charged at lower pH values, where there is more hydration of the active site. For Co(II), Zn(II) and Cu(II) ions, ΔH^{ads} decreases with increased acidity which means that more energy is needed to dehydrate the surface at lower pH values.

The entropy change results from a change in water-M(II) environment created during adsorption when M(II)-hydration sphere(s) move between the solution and the adsorbent surface [168]. The negative values of entropy change mean more order at the adsorbent/solution interface. This liberation of water molecules of hydrated-M(II)

is an essential pre-step for the chelation of M(II). This liberation causes an increase of disorder (positive entropy change) if water molecules are freely mobile [16]. But as the surface is hydrophilic, the liberated water molecules were restricted to the adsorbent surface causing a decrease of disorder, i.e. a negative entropy change. Furthermore, the decrease of internal entropy of the ligands due to the chelate formation may contribute to this phenomenon [166].

Although the negative entropy change means resistance to the adsorption process, it gives indication about the feasible nature of desorption process (i.e. ease of regeneration).

The free energy is a resultant of enthalpy and entropy of adsorption. In this study, the negative values of free energy originate from a larger contribution of enthalpy over entropy. For example, the Cd(II) ion has negative values of ΔH^{ads} indicating favourable adsorption, but at the same time it has the negative values of ΔS^{ads} which indicates resistance to adsorption. But as the enthalpy shares more in the free energy than entropy, the resultant negative free energy in this manner indicates spontaneous exothermic process, i.e. chelation-adsorption.

This theory can be supported by reviewing a study in which melamine-formaldehyde-NTA gel adsorbent was used to adsorb the Cu(II) ion. This adsorbent was prepared in the presence of guaiacol as a poring agent [94]. This adsorbent showed two obvious distinct adsorption behaviours depending on the temperature:

1. The ion exchange mechanism was believed to dominate the higher temperature range, 25–35°C, and was associated with positive enthalpy and entropy changes. The positive enthalpy change (endothermic adsorption) characterises the ion exchange mechanism due to the loss of M(II)-hydrating water molecules (endothermic process). The positive entropy change (higher disorder) may have originated from release of two H^+ ions per one Cu(II) ion adsorbed [94].
2. The chelation mechanism was believed to dominate the lower temperature range, 15–25°C, and was associated with negative enthalpy and entropy changes. The negative enthalpy (exothermic adsorption) characterises coordination bond

formation (more than one coordination bond for M(II)-chelate formation: heat evolves due to formation of covalent bonds) and negative entropy (lower disorder) may have originated from the restriction of Cu(II) upon chelate formation [94].

This change in mechanism with temperature is probably due to the presence of ion exchange site of guaiacol. For MF-PAPC under discussion here, the adsorbents preparation did not incorporate an ion exchange-bearing agent and so there are no ion exchange active-adsorbing sites except those of PAPC agents (carboxylic groups). Hence, chelation is almost the adsorption mechanism (although ion exchange is suggested for certain conditions).

8.1.3 Relative affinity of MF-DTPA towards M(II) ions

The relative M(II)-removal percentage reflects the affinity of the adsorbent towards M(II) ions present simultaneously in solution. Suggesting that adsorption follows mainly chelation-sorption, the adsorbent matrix-pendent DTPA molecules may have a tendency to react with metal ions in a similar way to the homogenous solution [172]. This implies that the M(II)-complex formation stability constants solely control the adsorption affinity order. However, other important factors have to be considered as well: enthalpy and entropy of chelation, ion radius, hydrophilicity of adsorbent surface, M(II)-dehydration enthalpy and complex coordination number.

Table 8.5 gives the factors that can affect the chelation-adsorption: standard formation stability constant (Log K) of M(II)-DTPA, enthalpy ($\Delta H^{chelate}$) and entropy ($\Delta S^{chelate}$) of chelate formation of DTPA with stated ions in single solutions [172], hydrated-ion radius and enthalpy of M(II)-dehydration.

Table 8.5: M(II)-DTPA complex formation parameters [172].

M(II)	Log K (25°C)	$\Delta H^{chelate}$ (20°C) (kcal/mole)	$\Delta S^{chelate}$ (25°C) (cal/mole. °C)	M(II) Hydrated-radius (Å)	Enthalpy of M(II)-dehydration (kcal/mole)
Co(II)	19.15	–9.4	65	4.23	476.9
Cd(II)	19	–12.4	46	4.26	431.8
Zn(II)	18.29	–8.8	54	4.30	488.9
Cu(II)	21.38	–13.6	52	4.19	501.8

It can be inferred from the log K values that DTPA forms complexes with M(II) in the order Cu(II) > Co(II) > Cd(II) > Zn(II): that is the complexes yield is directly proportional to the formation stability constants. The situation is different for M(II) chelation on MF-DTPA surface. The removal percentage results (**Figure 8.3**), gives the adsorption affinity of MF-DTPA as Cd(II) > Co(II) > Cu(II) ≥ Zn(II).

This affinity of MF-DTPA towards the M(II) ions studied can be explained as follows: as Cd(II) and Zn(II) readily form stable tetrahedral complexes (four-coordinations) and Cu(II) readily forms octahedral complexes (six-coordinations), each DTPA site on the adsorbent (has eight coordination positions) would favour formation complexes with two ions of either Cd(II) and/or Zn(II) rather than a complex with only one ion of Cu(II). This is justified from the enthalpic point of view due to the exothermic nature of process. As an approximation, the following absolute values of enthalpy are assumed: $\Delta H^{chelate}_{Cd_2-DTPA} = 2 \times 12.4 = 24.8 > [\Delta H^{chelate}_{Cu-DTPA} = 1 \times 13.6 = 13.6$ (**Figure 8.5**). That is, the chelation adsorption of Cd(II) produces more heat than that for Cu(II) .

The chelation of Cd(II) is highly favourable over Zn(II) due to the difference of their chelate formation stability constants (log K_{Cd} > log K_{Zn}) and enthalpy of chelate formation ($\Delta H^{chelate}{}_{Cd} > \Delta H^{chelate}{}_{Zn}$). Also, the chelation entropy change of Cd(II) is considerably lower than that of the other ions (specially when related to corresponding enthalpy) which favours Cd(II) adsorption because its chelation is accompanied by less released water molecules (Cd(II) ion has the lowest enthalpy of dehydration, **Table 8.5**, indicating the lowest amount of hydrating water molecules),

i.e. less need to accommodate these liberated water molecules on the adsorbent surface. The adsorption of the Cd(II) ion is also more favoured than Co(II), having an almost similar log K, due to enthalpy of chelation. It is worthy to note that according to experimental conditions, the Cd(II) ion has the lowest molar-concentration but still has adsorption-priority regardless of its lower concentration driving force.

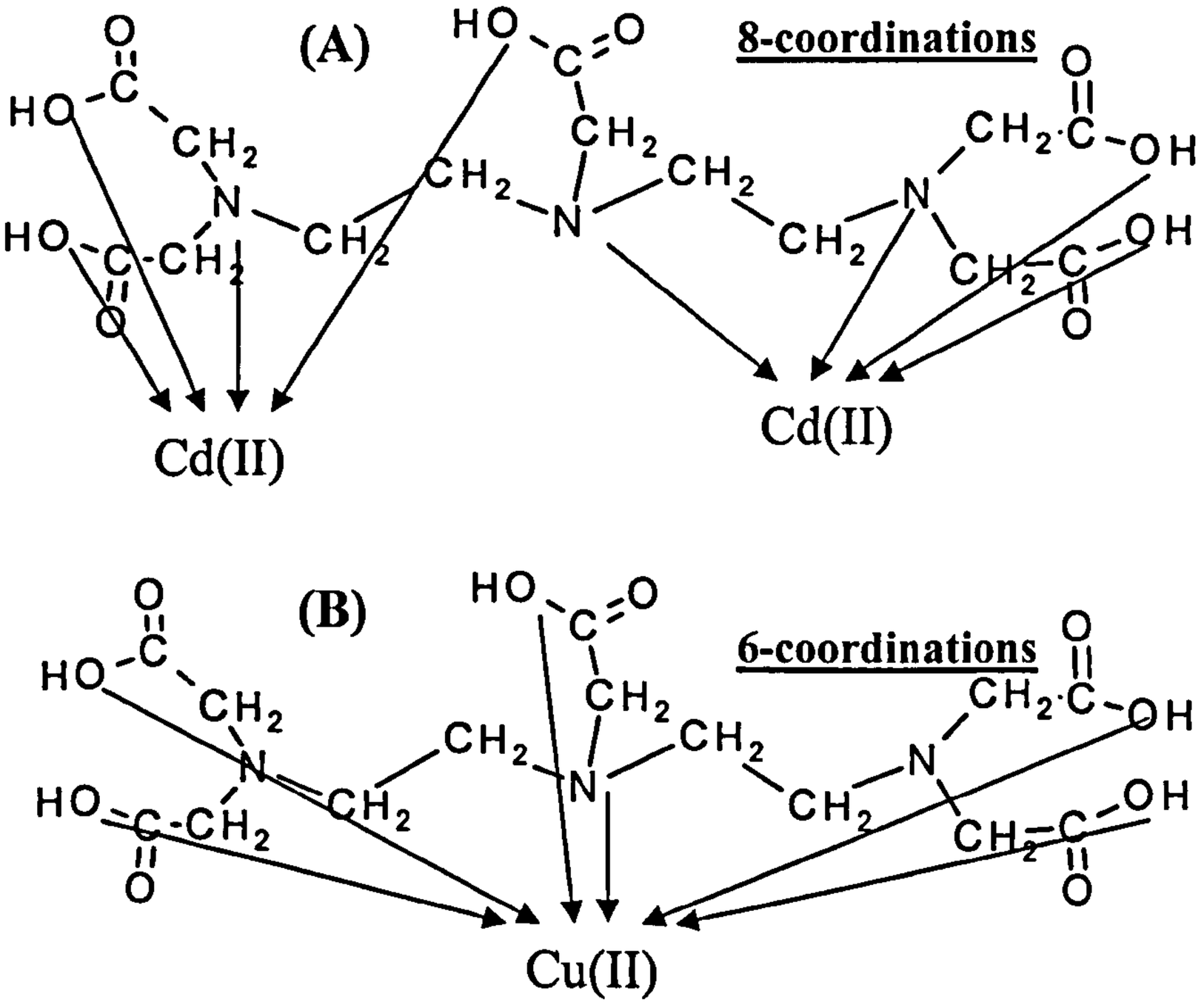

Figure 8.5: Scheme of: (A) favoured chelation of two Cd(II) ions and (B) less-favoured chelation one Cu(II) ion with DTPA under adsorption conditions.

Co(II) ion is second in affinity order. Co(II) mostly forms tetrahedral and octahedral complexes on equal terms, it is favoured to bind two Co(II) ions (tetrahedrally) with DTPA (enthalpy preference) over binding only one Cu(II) ion (assume absolute value of enthalpy: $[\Delta H^{\text{chelate}}_{\text{Co}_2\text{-DTPA}} = 2 \times 9.4 = 18.4] > [\Delta H^{\text{chelate}}_{\text{Cu-DTPA}} = 1 \times 13.6 = 13.6]$). The Co(II) ion is preferred over Zn(II) due to its higher complex formation constant enthalpy and entropy. One exceptional case is observed at 15°C (pH ≥ 4) where Zn(II) shows a higher removal percentage than Co(II) (**Figure 8.3**). The Cu(II) and Zn(II) ions show affinity competitiveness but Cu(II) is more favourably adsorbed

especially at higher temperature which reflects the ion exchange contribution at these temperatures. The Zn(II) ion is favoured over Cu(II) at lower temperature for the same reason as that of Cd(II) ion.

Accordingly, it can be concluded that enthalpy and entropy of chelation determine the M(II)-adsorption affinity when the chelation site can complex more than one M(II) ion and the formation stability constant is the controller when only one M(II) ion is bound.

Dehydration is an important early step for a complex formation process. The detachment of water shell(s) surrounding the M(II) ion is an essential process for chelation to occur. The absolute value of enthalpy of dehydration increases as: Cd(II) < Co(II) < Zn(II) < Cu(II) which is preferred thermodynamically and this is in agreement with removal order observed at lower temperature (15 and 20°C) where the chelation mechanism dominates (**Figure 8.3**).

The hydrated-radii of these ions are very similar (≈4 Å) when compared to the average pore diameter of MF-DTPA (95 Å) hence, no expected dependence of adsorption preference on pore diffusion was noted. The contribution of ion-dehydration and entropy in the adsorption is critical and play significant role in the process [168].

This suggested rule (priority of adsorption based on thermodynamic parameters of complex formation) become relatively less applicable as temperature increases due to the more involvement of the ion exchange mechanism at the expense of the chelation mechanism. This can be observed from gradual increase of Cu(II) adsorption over Zn(II) with temperature (**Figure 8.3**).

It is important to mention another two probable phenomena that may alter the M(II)-complex formation order on MF-DTPA adsorbent with respect to complex formation in homogenous M(II) solution:

(1) For MF-DTPA, the IR spectrum recorded the carbonyl groups at 1636 cm^{-1} which is suggested to belong to the amide group whereas the carbonyl of carboxylic groups (normally 1735 cm^{-1}) was not detected suggesting that most carboxylic groups may involve in anchoring with the MF matrix. This may influence a change in the chelation behaviour of DTPA towards M(II), that is affect the affinity order towards M(II) ions in accordance with the stability constants of M(II)-DTPA chelates in aqueous solutions. Since DTPA is chemically bound by several bonds to the rigid matrix, their free motions are greatly restricted and as a result the complex formation tends to be different from that observed in a solution [104,173].

(2) The highly probable contribution of nitrogen atoms present in the triazine ring and bridges of adsorbent matrix for the M(II)-coordination may alter the chelate behaviour of the DTPA site and affect the affinity. By comparing the peak at 3394 cm^{-1} in **Figures 7.2** and **8.2,** it can be suggested that there is some contribution of the secondary amine attached to the methylene bridge in chelation due to the observed sharper peak after Cu(II)-adsorption.

Inoue *et al* [92] mentioned this chelation deviation. Although they found that chitosan-EDTA and chitosan -DTPA adsorbents present adsorption towards divalent metal ions in an order in accordance with the stability constants of the metal chelates of EDTA and DTPA, the polyallylamine-EDTA and polyallylamine-DTPA adsorbents did not give the same order. The authors suggested that polyallylamine-EDTA and polyallylamine-DTPA have poor selectivity regarding stability constants of the metal chelates of EDTA and DTPA due to "non-effective" incorporation of carboxyl groups in the chelate formation with the metal ions [92]. Their discussion did not cover the influence of the physical properties of these materials.

It is crucial to mention that the interactive effects of a metal ion mixture on an adsorbent are complex and depend on adsorbent type, number of metal ions competing for binding sites, metal combination, metal ions concentration, agitation time and experimental conditions [80]. However, it can be generally concluded that the main factors controlling adsorption-affinity on MF-DTPA are: M(II)-chelate

formation stability constants, chelate-adsorption enthalpy and entropy, enthalpy of M(II) dehydration and coordination number.

8.1.4 Effect of metal ions initial concentration on adsorption

The influence of initial concentrations on adsorption of M(II) ions was investigated for initial concentrations (20, 30, 40, 50, 60 and 70 mg l^{-1}) with a constant adsorbent amount (0.5 g, conditions: T= 20°C and pH =5). **Table 8.6** gives the M(II)-removal percentages against initial concentrations. It is observed that removal percentage decreases with increasing initial concentration.

Table 8.6: Effect of initial-M(II) concentration on removal percentage by MF-DTPA.

Initial concentration (mg l^{-1})	Removal percentage ±0.3%			
	Co(II)	Cd(II)	Zn(II)	Cu(II)
20	95	95	90	95
30	93	93	87	90
40	88	88	78	83
50	80	84	70	76
60	72	75	65	68
70	67	69	59	63

At lower initial-M(II) concentration, the chelating sites are relatively more available and so removal percentage is high. At higher concentration, the chelation sites are less available compared to amount of M(II) ions in solution and so the removal percentage is less.

Figure 8.6 shows the equilibrium adsorption capacity versus initial concentration. The adsorption capacity (q_e) gradually and smoothly increased with initial concentration (C_i). The saturation plateau may start at $C_i \geq 70$ mg l^{-1}. The capacity increase with initial concentration has been noted previously [80,174]. This may reflect the driving force of concentration on the adsorption process and that the process is reversible.

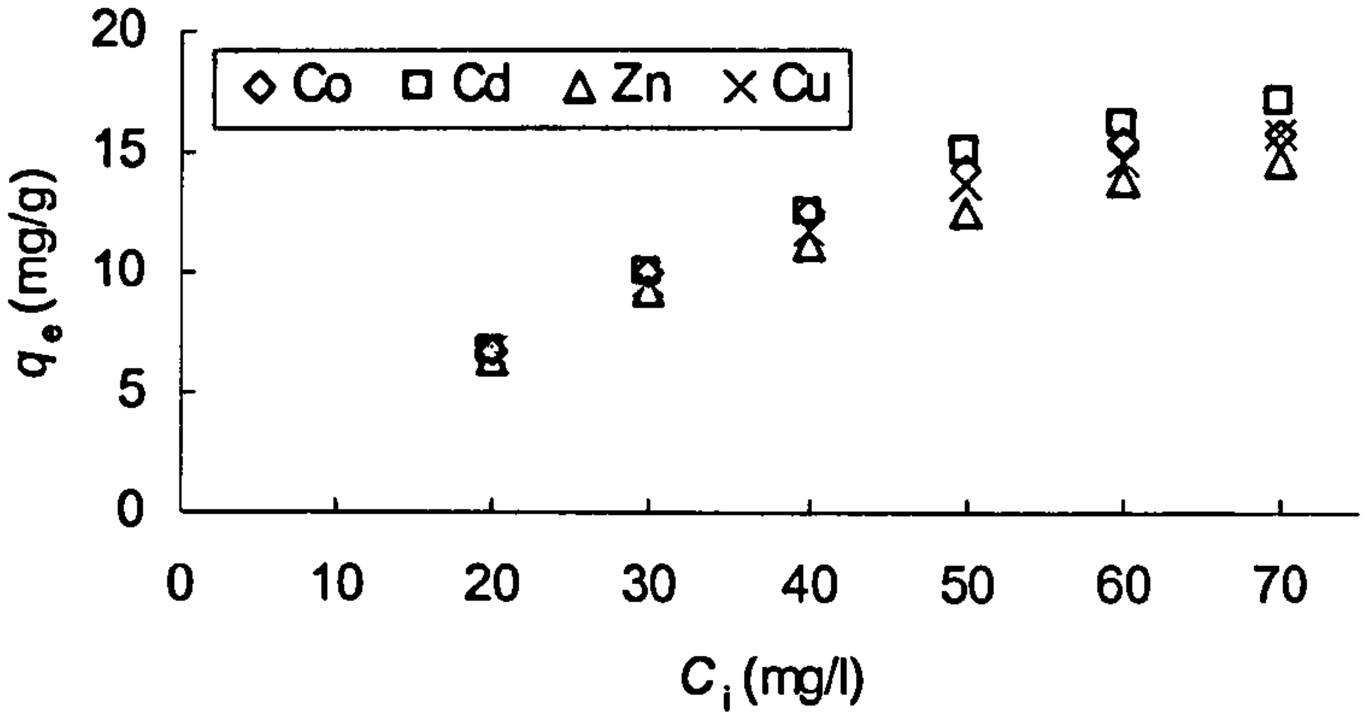

Figure 8.6: Effect of metal ions initial concentration on adsorption capacity for Co(II), Cd(II), Zn(II) and Cu(II) adsorption at pH 5 and T= 20°C.

8.1.5 Adsorption Kinetics

Time profiles (60 minutes) for M(II) ions removal for different initial pH values (T=25°C) are shown in **Figure 8.7**. The curves are smooth and continuous (especially for Co(II) and Zn(II) ions) leading to saturation. This may suggest a monolayer adsorption process [175]. The plots show that the rate of uptake of metal ions onto MF-DTPA is quite rapid and most of adsorption of M(II) ions occurs within the first 30 minutes.

Also, it can be observed that Cd(II) and Cu(II) removal is characterised by having two adsorption-stages (**Figure 8.7**). The first is a highly rapid stage which extends for about 10 minutes where most removal occurs and the second stage follows for the remaining 50 minutes. The rapid adsorption of Cd(II) can be correlated to its highest affinity, compared with other M(II) ions (section 8.1.3), where it is highly probable to bind with most DTPA sites available on the external surface of adsorbent particles. For the Cu(II) ion, its initial rapid adsorption is correlated to its higher chelate formation stability constant. After this first rapid stage for Cu(II) ion (≈10 minutes), Co(II) adsorption superimposes Cu(II) adsorption due to dynamic reversible nature of the adsorption process. For Co(II) and Zn(II), the removal smoothly increases with time.

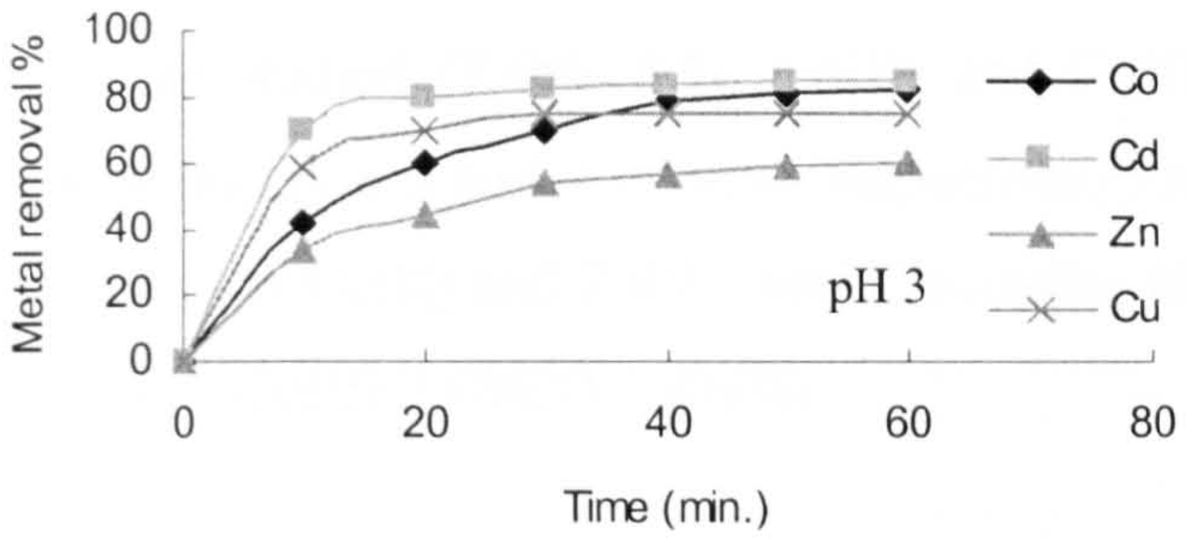

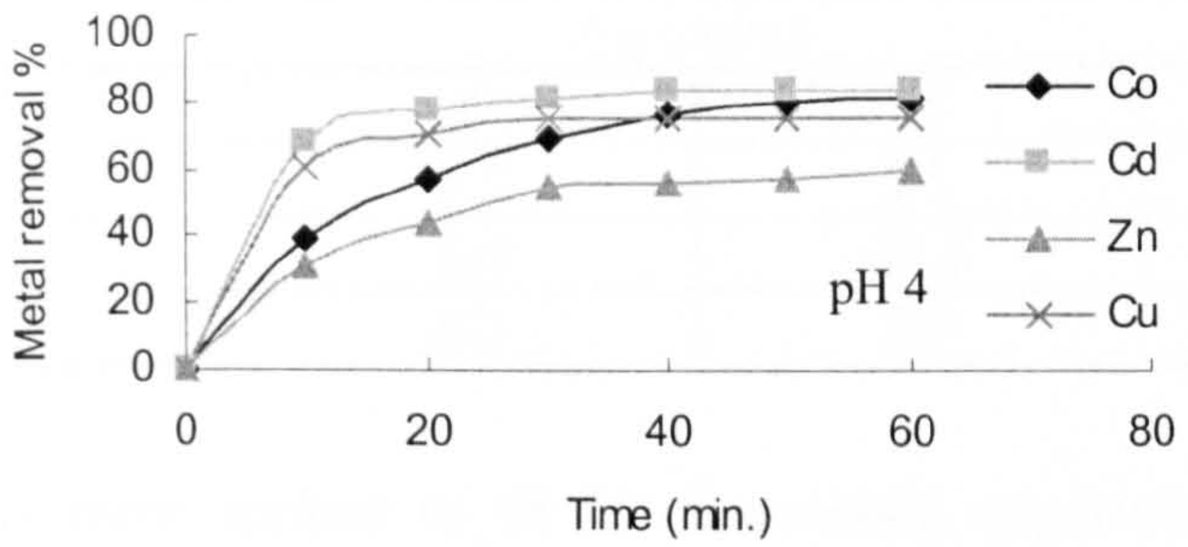

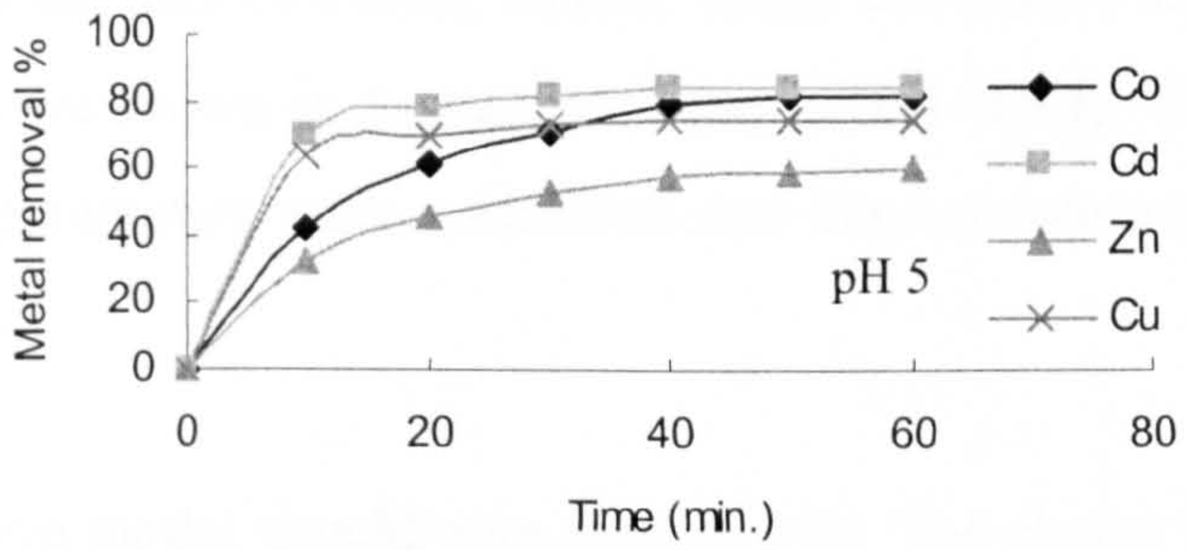

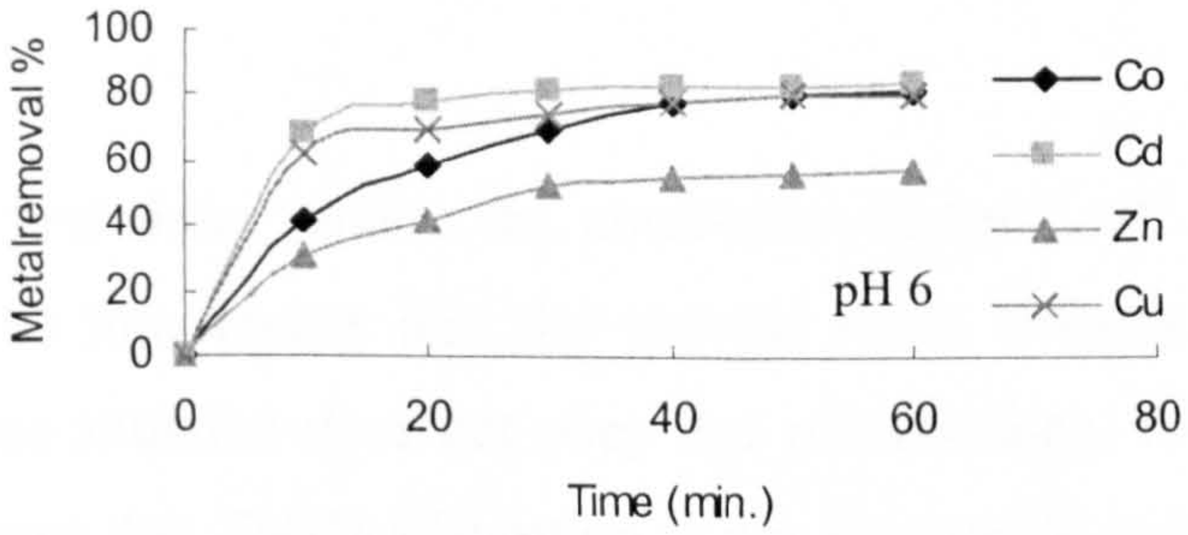

Figure 8.7: Time profile of adsorption on MF-DTPA for Co(II), Cd(II), Zn(II) and Cu(II) at 25°C at different pH values.

The time of half-load, $t_{1/2}$ (min), of metal ions is generally below 28 minutes and has not been significantly affected by the initial pH which reflects the stability of the process over the pH range studied (**Table 8.7**). Cd(II) and Cu(II) ions have the lowest $t_{1/2}$ values (approximately 6.5 and 7 minutes respectively) with considerable difference from those values of Co(II) and Zn(II) ions. Generally, at equilibrium, the order of removal is: Cd(II) > Co(II) > Cu(II) > Zn(II).

Table 8.7: Half load time $t_{1/2}$ of metal ions on MF-DTPA (25°C).

pH	Co(II)	Cd(II)	Zn(II)	Cu(II)
	$t_{1/2}$ (min.)			
3	13	6	25	7.5
4	15	6.5	25	7.5
5	13	6.5	26.5	6
6	13.5	6.5	28	7.5

Four kinetic models were applied to fit the time-based experimental results: the reversible first-order, the pseudo first-order, the pseudo second-order and the Elovich models. The adsorption data of Co(II), Cd(II), Zn(II) and Cu(II) ions were fitted by these models (plots are shown in Appendix: **Figures 10.1–10.4**). The corresponding adsorption-kinetic parameters were calculated and they are summarized in **Tables 8.8** and **8.9**.

A good representative model should give a linear plot. The choice of the model that highly represents the adsorption process depends on the magnitude of the correlation coefficient (R^2).

For the reversible first order model: the correlation factor is $R^2 > 0.9$. The ratio $k_1/k_2>1$ for all M(II) ions means that the process shifts towards adsorption over desorption. Only one situation does not obey this phenomenon: for Zn(II) at pH 6, $k_1/k_2 < 1$ which means that Zn(II)-adsorption is not favourable under this condition. Generally, the k_1/k_2 ratio values points to ease of desorption for regeneration purposes [11].

Table 8.8: Parameters of reversible first-order and pseudo first-order for adsorption on MF-DTPA.

pH	M(II)	$q_{exp.}$±3%	pseudo first order			reversible first order			
			k_L	q_e	R^2	k_R	k_1	k_2	R^2
3	Co	6.27	0.071	6.68	0.980	0.071	0.059	0.012	0.980
	Cd	7.05	0.123	4.91	0.954	0.123	0.103	0.020	0.976
	Zn	5.75	0.080	4.68	0.987	0.080	0.048	0.032	0.987
	Cu	5.36	0.140	4.42	0.951	0.141	0.106	0.035	0.951
4	Co	6.33	0.080	4.68	0.987	0.067	0.057	0.010	0.979
	Cd	6.89	0.133	6.22	0.954	0.134	0.112	0.022	0.954
	Zn	5.69	0.063	3.79	0.968	0.063	0.038	0.025	0.968
	Cu	5.69	0.140	4.20	0.951	0.139	0.105	0.034	0.951
5	Co	6.40	0.073	6.91	0.981	0.072	0.062	0.010	0.981
	Cd	7.07	0.123	4.69	0.989	0.127	0.106	0.021	0.989
	Zn	5.56	0.080	5.12	0.974	0.086	0.051	0.035	0.974
	Cu	5.58	0.127	3.80	0.978	0.120	0.090	0.030	0.977
6	Co	6.40	0.069	6.77	0.982	0.069	0.059	0.010	0.982
	Cd	7.07	0.122	4.82	0.994	0.122	0.104	0.018	0.994
	Zn	6.15	0.091	4.95	0.986	0.091	**0.026**	**0.065**	0.986
	Cu	5.79	0.116	6.48	0.908	0.116	0.093	0.023	0.908

Table 8.9: Parameters of pseudo second-order and Elovich models for adsorption on MF-DTPA.

pH	M(II)	$q_{exp.}$±3%	Pseudo second order				Elovich model		
			k_H	q_e	h	R^2	α	β	R^2
3	Co	6.27	0.0083	7.66	0.487	0.9993	0.9968	0.5740	0.9945
	Cd	7.05	0.0697	6.26	2.731	0.9998	410	1.7376	0.9052
	Zn	5.75	0.0165	5.19	0.444	0.9973	0.9965	0.8981	0.9745
	Cu	5.36	0.0649	5.67	2.086	0.9989	58	1.544	0.8519
4	Co	6.33	0.0049	8.86	0.385	0.9900	0.7741	0.4889	0.9902
	Cd	6.89	0.0588	6.29	2.326	0.9998	151	1.5586	0.9253
	Zn	5.69	0.0161	5.15	0.427	0.9952	0.9062	0.8800	0.9585
	Cu	5.69	0.0735	5.64	2.338	0.9992	143	1.7358	0.8672
5	Co	6.40	0.0103	7.30	0.549	0.9964	1.119	0.6060	0.9763
	Cd	7.07	0.0659	6.29	2.607	0.9998	352	1.7056	0.9299
	Zn	5.56	0.0158	5.24	0.434	0.9982	0.9231	0.8668	0.9768
	Cu	5.58	0.0853	5.59	2.665	0.9998	993	2.1441	0.9253
6	Co	6.40	0.0093	7.36	0.504	0.9959	1.018	0.5937	0.9795
	Cd	7.07	0.0606	6.27	2.382	0.9999	211	1.6268	0.9266
	Zn	6.15	0.0168	4.98	0.417	0.9942	0.8782	0.9086	0.9578
	Cu	5.79	0.0389	6.14	1.467	0.9997	27	1.3219	0.9849

The Cd(II) ion shows a higher ratio compared to other ions which indicates its higher adsorption. The desorption rate constant for Zn(II) is the highest (k_2/k_1 ≈0.66) which reflects its less affinity towards the adsorbent and this implies that the adsorption has chemical dynamic-equilibrium character. The rate constant (k_R) values do not follow the suggested removal order. The values of the correlation factor (R^2) and the rate constant (k_R) are very similar to the corresponding values for the pseudo-first order model. This similarity may be due to the same relation of adsorbed amount or concentration versus time for both models [111].

For the pseudo first-order: although $R^2 > 0.9$, its estimated adsorption capacity values (q_e) do not satisfactorily match the experimental capacity values (q_{exp}) when compared to the matching of the pseudo second-order model. The model rate constant values (k_L) do not follow the affinity order.

The Elovich model has R^2 values > 0.85 which is the lowest. The values of initial adsorption rate (α) for Cd(II) and Cu(II) are the highest and this is in agreement with what is observed in the first 10 minutes as shown in **Figure 8.7**. The values seem to be not reasonable as ranged from <1 to >200. However, the model can give an indication about the role of diffusion in the adsorption process. As α values are very different, the diffusion may have a role in the process. The values of desorption constant (β) are directly proportional to initial adsorption rate (α) which can give indication about reversibility of the adsorption process. The model is useful in describing adsorption on heterogeneous adsorbents [122]; hence its lower R^2 values may suggest homogenous adsorbents.

The pseudo second-order model best represents the adsorption process as it shows the highest correlation factor, R^2> 0.99. Besides, the model highly estimated the adsorption capacity: estimated values (q_e) highly match the experimental capacity values (q_{exp}). The values of initial adsorption rate (h) are in agreement with the initial adsorption rate of the Elovich model (α) with respect to corresponding M(II) and represent the adsorption behaviour in the initial stage (10 minutes) from the removal order point of view. Moreover, these values are reasonable as they range from 0.326

to 2.731. However, the model rate constant values (k_H) do not follow the affinity order.

Best fits of data to the pseudo second-order model strongly confirm the chemisorption character of the process which involve sharing (or exchange) of electrons between MF-DTPA and M(II) ions [111,169]. Besides, it is suggested that chemisorption is the main step that controls the adsorption process [176].

Azizian [177] reported a derivation of pseudo first- and second-order models based on the assumption of a *chemisorption reversible* (adsorption/desorption) process. Derivation assumed monolayer coverage of adsorbent. The condition for pseudo first-order was the very high initial concentration of solute compared to the active sites on the surface of adsorbent. On the contrary, for pseudo second-order the initial concentration is comparable with the concentration of active sites on the surface of the adsorbent. Furthermore, derivation stated that rate constants k_L and k_H are functions of initial concentration and include the rates of adsorption and desorption (that is k_L and k_H are not intrinsic rate constants for respective models). As kinetic data fits the pseudo second-order model, *reversibility* of the process can be suggested. Also, it can be concluded that the applied initial concentration in this study is comparable with adsorbent maximum capacity. It can be concluded that the maximum capacity of MF-DTPA adsorbent is sufficiently effective to remove M(II) of total initial concentration of 80 mg l^{-1}. This information is essential to design a M(II)-removing system. Monolayer adsorption behaviour is concluded from the isotherm study (section 8.1.6) which strongly suggests pseudo second-order to be good representative of the process.

A careful study of the values of the rate constants k_R, k_L and k_H (at the same conditions of initial pH) indicates that they do not represent the affinity order suggested (Cd(II > Co(II) > Cu(II) ≥ Zn(II)). Also, they do not represent the order of adsorption during the early stages of the process. This behaviour may reflect the effectiveness of the reversible chemisorption nature of the process where different adsorbed M(II) ions can swap with each other.

For practical purposes, the reversible first order model can be applied to represent the adsorption process (especially to calculate the rate constants, adsorption (k_1) and desorption (k_2)) with support by the pseudo second-order model to estimate the adsorption capacity (q_e).

Diffusion is a common phenomenon for adsorption, and investigating its role in the removal process is important to increase understanding about the adsorption mechanism. Plots of adsorbed amounts of M(II) (q_t) against time at different temperatures and initial pH values (Appendix: **Figure 10.5**) suggest that adsorption has, generally, two stages: initial stage (0–30 minutes) where film diffusion may dominate and latter stage (30–60 minutes) where pore diffusion dominate.

Plots of adsorption data using **equation (18)** for film diffusion and **equation (19)** for pore diffusion were determined (Appendix: **Figures 10.6** and **10.7**). The corresponding film and pore diffusion coefficients, D_1 and D_2, were calculated and are presented in **Table 8.10**.

Michelson et al [178] reported that film diffusion coefficient values (D_1) should be in the range of 10^{-6} to 10^{-8} cm^2 s^{-1} and pore diffusion coefficient values (D_2) should be in the range of 10^{-11} to 10^{-13} cm^2 s^{-1}. In this study, D_1 values for M(II)-adsorption on MF-DTPA belong to this range for Cd(II) and Cu(II) and are very near for Co(II) and Zn(II) **(Table 8.10)**. This means that the adsorption process depends on film diffusion. The D_2 values are out of the range and considerably higher, order $\geq 10^{-8}$, which implies that pore diffusion has no significant effect on the adsorption. This may be due to the fact that the average pore diameter of MF-DTPA (95 Å) is wide enough for M(II) pore-migration (the M(II)-hydrated radius $\approx$4 Å). Besides, the hydrophilic surface of MF-DTPA may play a role: the surface-attached water molecules enhance the attraction of hydrated-M(II) ions.

No significant correlation between type of M(II) and initial pH with film and pore diffusion coefficients can be observed and this may be due to the fact that the adsorption process is carried using multi-element solutions.

Table 8.10: Diffusion parameters of M(II) adsorption onto MF-DTPA.

pH	$(D_1 \pm 0.03) \times 10^{-9}$ ($cm^2\ s^{-1}$)				$(D_2 \pm 3) \times 10^{-8}$ ($cm^2\ s^{-1}$)			
	Co(II)	Cd(II)	Zn(II)	Cu(II)	Co(II)	Cd(II)	Zn(II)	Cu(II)
3	21.7	4.5	22.2	8.9	11.4	11.7	11.1	6.6
4	19.2	5.2	28.1	6.9	5.0	23	3.8	6.6
5	23.7	4.1	23.5	3.4	18.4	13.9	14.5	11.2
6	23.9	4.7	26.2	5.1	15.3	6.9	12.4	23

In general, the kinetic study reveals that adsorption is chemical, reversible and fast (one hour to reach equilibrium). It is considered that process is film diffusion dependent.

8.1.6 Adsorption isotherm

Figure 8.8 shows equilibrium capacity (q_e) against equilibrium concentration (C_e) at 20°C and pH 5. The M(II)-isotherms are regular, positive and concave to the concentration axis (C_e) and these are of type I according to Brunauer's classification which represents the Langmuir adsorption model [179]. The isotherm curves were fitted using experimental data excluding origin. However, the isotherm curves were extrapolated and found to pass through origin. The initial rapid increase in equilibrium capacity [for initial concentration range studied (20–70 mg l^{-1})] reflects efficiency of the adsorbent for the removal in a wide range of concentrations and indicates efficient use of the MF-DTPA adsorbent at higher M(II)-initial concentration [9]. The kinetic results conform to isotherm study. From kinetic study, k_2/k_1 is generally < 0.33 and this implies that adsorption is considerably higher than desorption. Hence (q_e) shows sharp increase with C_e.

Figures 8.9 and **8.10** present the plots of the data of adsorption isotherms according to the Freundlich and Langmuir models respectively. From these plots, related constants were calculated and **Table 8.11** summarizes them.

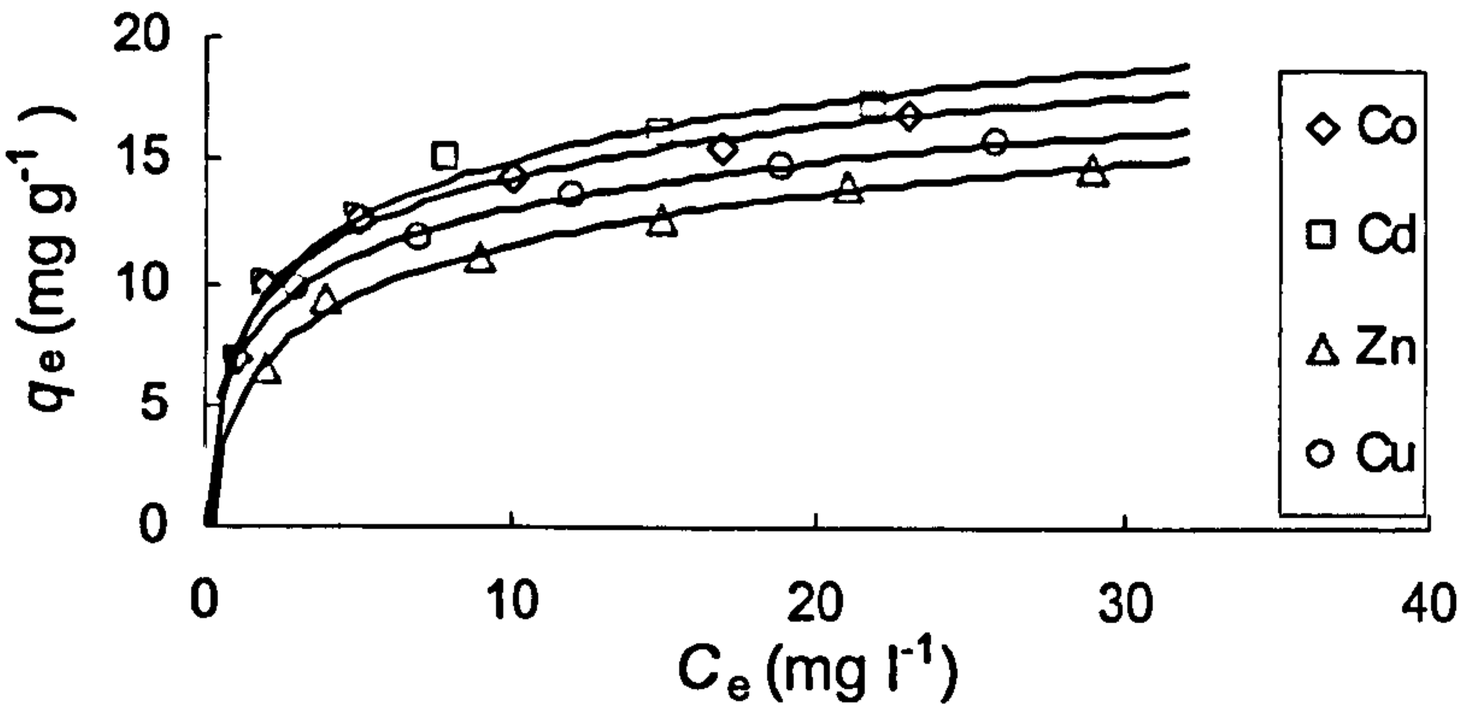

Figure 8.8: The adsorption isotherm (20°C) of Co(II), Cd(II), Zn(II) and Cu(II) on MF-DTPA at pH 5 and 120 minute equilibrium contact time.

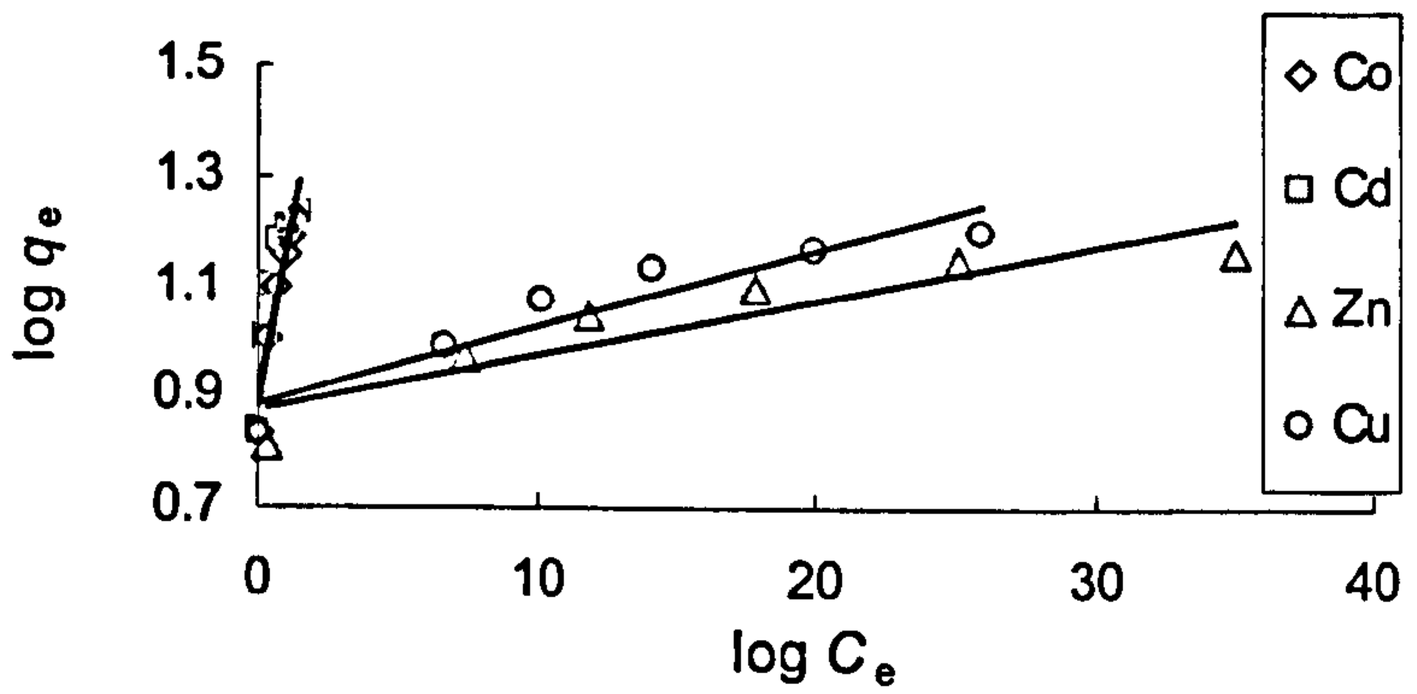

Figure 8.9: The Freundlich adsorption isotherm (20°C) of Co(II), Cd(II), Zn(II) and Cu(II) on MF-DTPA at pH 5 and 120 minute equilibrium contact time.

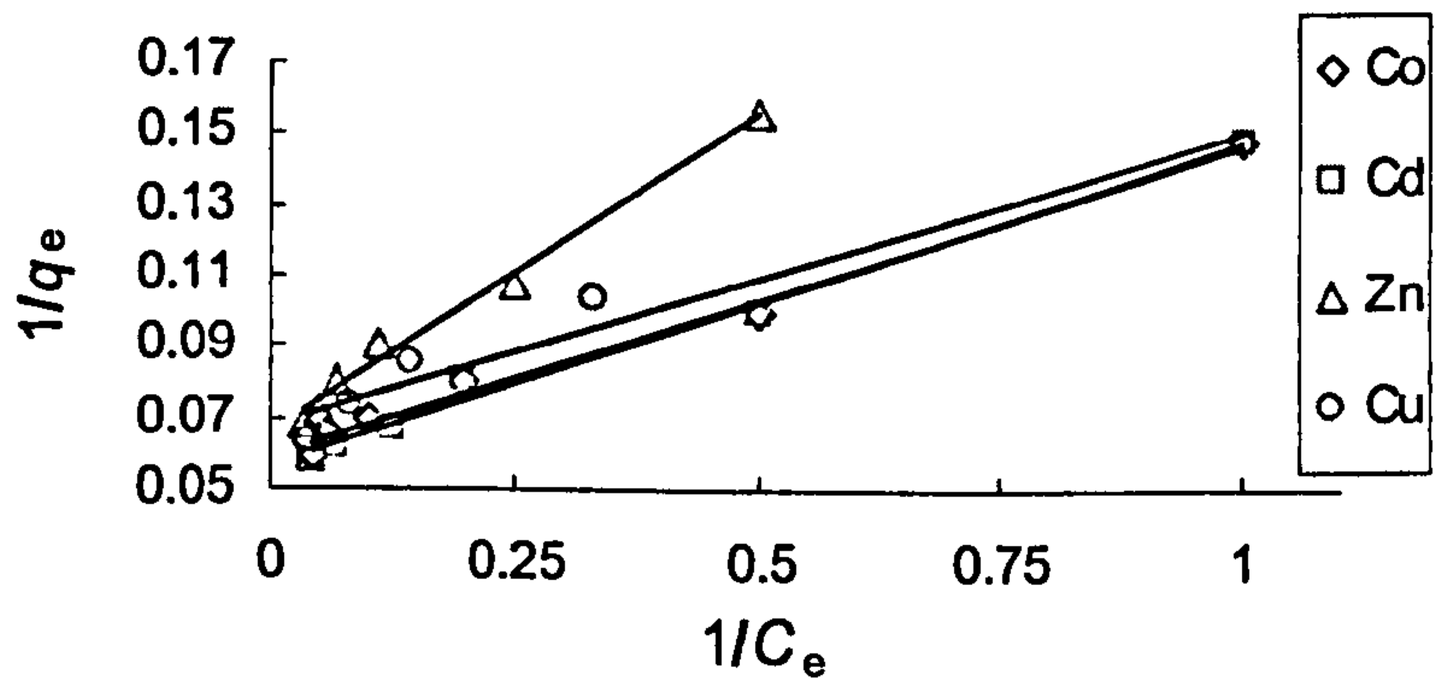

Figure 8.10: The Langmuir adsorption isotherm (20°C) of Co(II), Cd(II), Zn(II) and Cu(II) on MF-DTPA at pH 5 and 120 minute equilibrium contact time.

Table 8.11: The adsorption isotherm constants of the Freundlich and Langmuir models (MF-DTPA).

Adsorption Model	Co(II)	Cd(II)	Zn(II)	Cu(II)
Freundlich				
k_F ((mg g^{-1})(mg l^{-1})^n)	7.58	7.95	7.55	7.68
$1/n$	0.26	0.26	0.0098	0.014
R^2	0.9463	0.874	0.8483	0.8948
Langmuir				
Q_o (mg g^{-1})	16.84	17.7	15.32	14.84
Q_o (mmole g^{-1}) [total = 0.92 mmole g^{-1}]	0.29	0.16	0.24	0.23
b (l mg^{-1})	0.68	0.62	0.36	0.81
R_L	0.21	0.23	0.38	0.170
R^2	0.9932	0.9932	0.9899	0.9644

The Freundlich parameter (k_F) (which roughly indicates adsorption capacity [7]) is almost the same for the elements under study; however, cadmium shows a slight higher value indicating its priority for adsorption. The values of $1/n$ parameter are between 0 and 1 which fulfil the condition of favouring the adsorption process [9]. The parameter $n > 10$ for Cu(II) and Zn(II) may indicate they form very stable chelates on MF-DTPA surface, which suggests the need for strong eluting agent to regenerate the adsorbent from these elements [154].

The values of Langmuir simultaneous capacity (Q_o) are: Co (16.84), Cd (17.7), Zn (15.32) and Cu (14.84 mg g^{-1}). The values are in accordance with the affinity order suggested. However, they are very similar (as the Freundlich parameter k_F indicates also) which implies M(II)-universal removal behaviour. The total capacity of 0.92 mmole g^{-1} derived from the isotherm study is in agreement with total capacity of 0.97 mmole g^{-1} calculated from Cu(II)-loaded MF-DTPA elemental analysis (section 8.1.1) and with the amount of DTPA per gram of adsorbent, 1.08 mmole g^{-1} (section 7.1.1). In addition, this suggests no change in adsorption due to the presence of Na(I) as the elemental analysis suggested (section 8.1.1). The values of parameter R_L for all metal ions are in the range of favouring adoration ($0 < R_L < 1$).

The Langmuir R^2 values are higher for all elements (lowest value is 0.9644) than for the Freundlich model (highest value is 0.9463) which means that the Langmuir

model gives a better fit to the experimental data. This reflects the energetic homogeneity of the surface and shows that adsorption of M(II) is mostly monolayer [174]. Furthermore, strong bonding involving chemical forces between M(II) and MF-DTPA is strongly suggested [169] and this is in agreement with suggesting the pseudo second order model is the best to describe the adsorption kinetics. This implies that the DTPA sites in the adsorbent matrix are responsible for the main chemisorption process (chelation) to remove M(II) ions. The kinetic derivation of the Langmuir model assumes that adsorption is a reversible process. Obeying the experimental data to this model means that the chemisorption process is reversible which supports the consideration of reversible first order and pseudo second-order as the most suitable kinetic models to represent this system.

The distribution factor (D) is relatively high for all elements (**Table 8.12**) and reflects the affinity of the adsorbent towards the ions under study to be in the order of Cd(II) > Co(II) > Cu(II) > Zn(II).

Table 8.12: Distribution ratio of M(II) between MF-DTPA and solution.

	Co(II)	Cd(II)	Zn(II)	Cu(II)
D (ml/g)	730	779	505	604

8.1.7 Regeneration of MF-DTPA

The removal percentage of Cu(II) at 25°C for different initial-pH values by fresh and regenerated adsorbent doses are shown in **Figure 8.11**.

The Cu(II) removal percentage by the regenerated dose is about 90% compared to the fresh dose. The decrease of removal percentage is mostly due to partial deterioration of the active sites in the adsorbent. The deterioration mostly originates from hydrolysis of the amide bond anchoring DTPA to the MF matrix which in turn releases into water. This hydrolysis can occur during elution of adsorbed metal, washing and even during first adsorption process due to decrease in pH. Another explanation is the difficulty of the EDTA molecule to reach chelating sites present in

some small pores. This result can give a rough estimate to use the adsorbent dose for about 4–6 times for M(II)-removal.

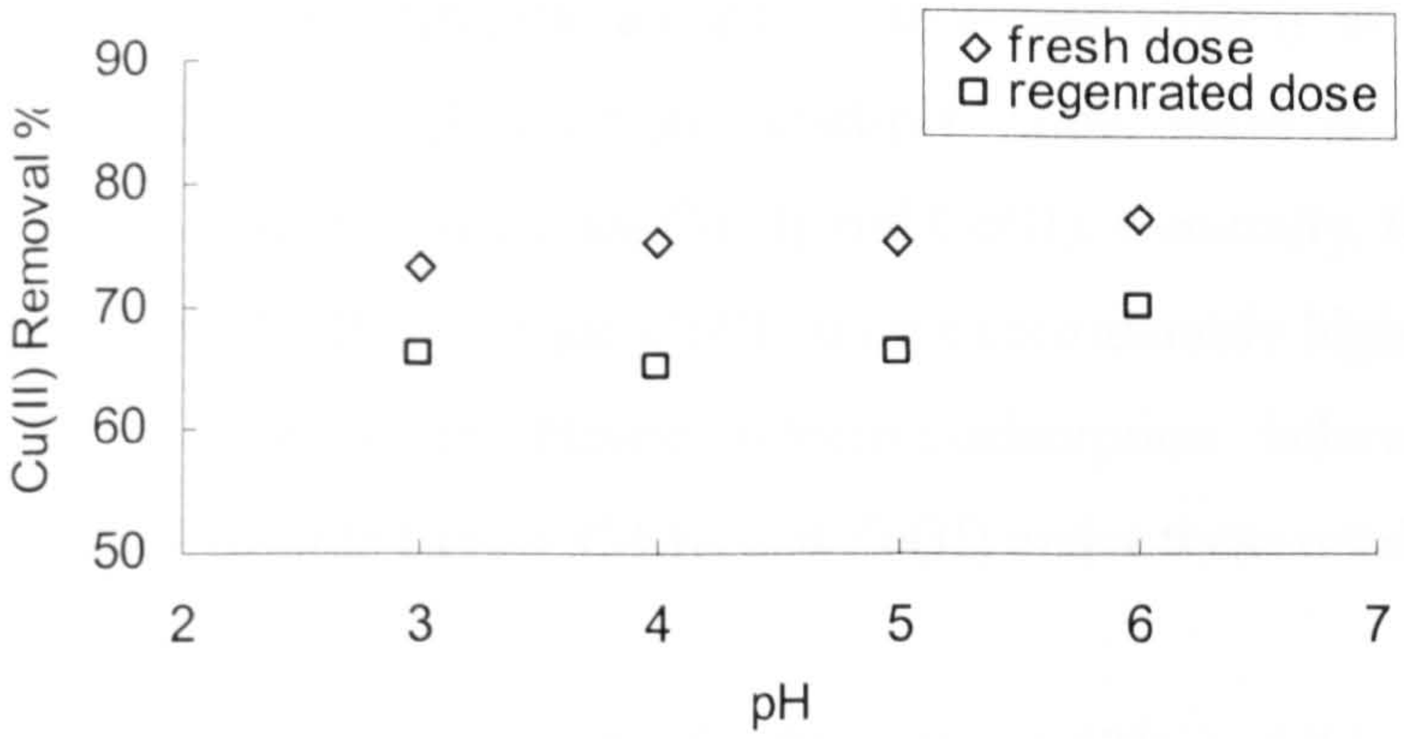

Figure 8.11: The removal percentage of Cu(II) at 25°C for different initial-pH values by fresh and regenerated MF-DTPA doses.

8.2 MF-NTA adsorption behaviour (batch method)

8.2.1 Characterization of metal loaded adsorbent sample (visual)

MF-NTA adsorbent is white in colour. The colour changes upon adsorption of Cu(II) to pale blue for Cu(II)–NTA complex (**Figure 8.12**) [81,104,152,157]. The colour is obviously different from that of MF-DTPA-Cu(II) (**Figure 8.1**) and MF-CDTA-Cu(II) (**Figure 8.25**) which suggests a different Cu(II)-complex structure.

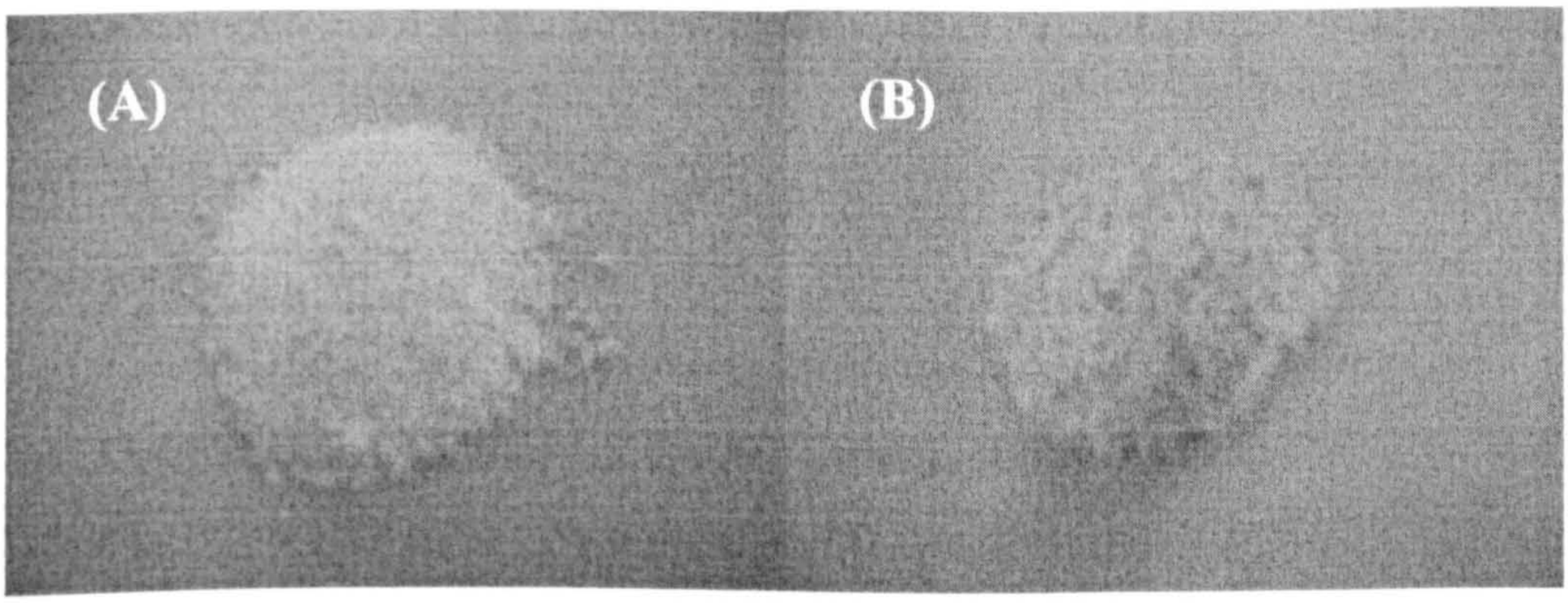

Figure 8.12: (A) White MF-NTA and (B) Pale blue Cu(II)–Loaded MF-NTA.

8.2.2 Effect of pH and temperature (Thermodynamics) on adsorption

The initial-pH adsorption profile for the temperature range under study (15–35°C) is shown in **Figure 8.13**. There is no adsorption at all for Cd(II) and Zn(II) under these conditions. For each temperature, the adsorption increases slightly as pH increases for Cu(II) and Co(II). For each solution initial-pH value, there is a decrease in adsorption with temperature increase for Cu(II) and Co(II). Generally, this behaviour is similar to that of MF-DTPA. The ion Cu(II) shows considerably higher adsorption over Co(II) for all conditions. Hence selective-adsorption behaviour can be considered for Cu(II) towards Co(II), Cd(II) and Zn(II) under these conditions.

The maximum adsorption percentage for Cu(II) is about 67% and this limited value (compared with MF-DTPA) may be due to using a small amount of adsorbent in the experiments (0.3 g wet adsorbent corresponds to solid fraction = 0.069 g) and/or shift of dynamic equilibrium point towards desorption (when compared to MF-DTPA).

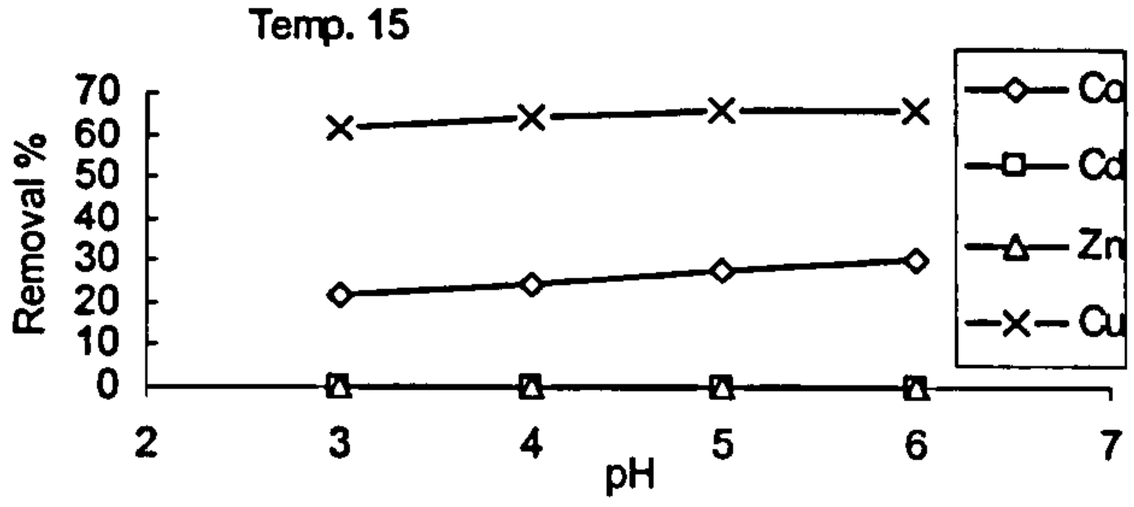

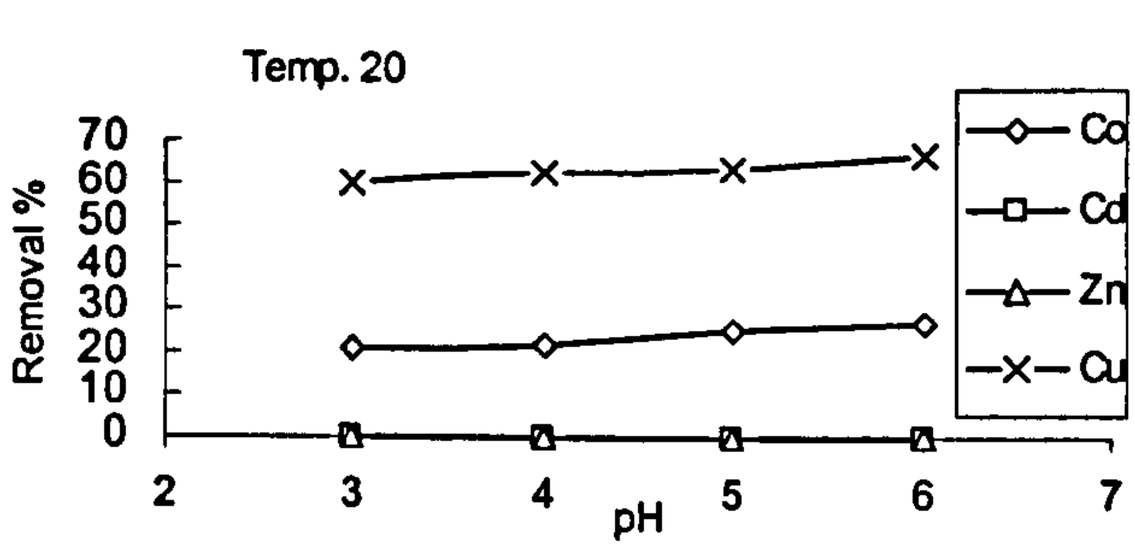

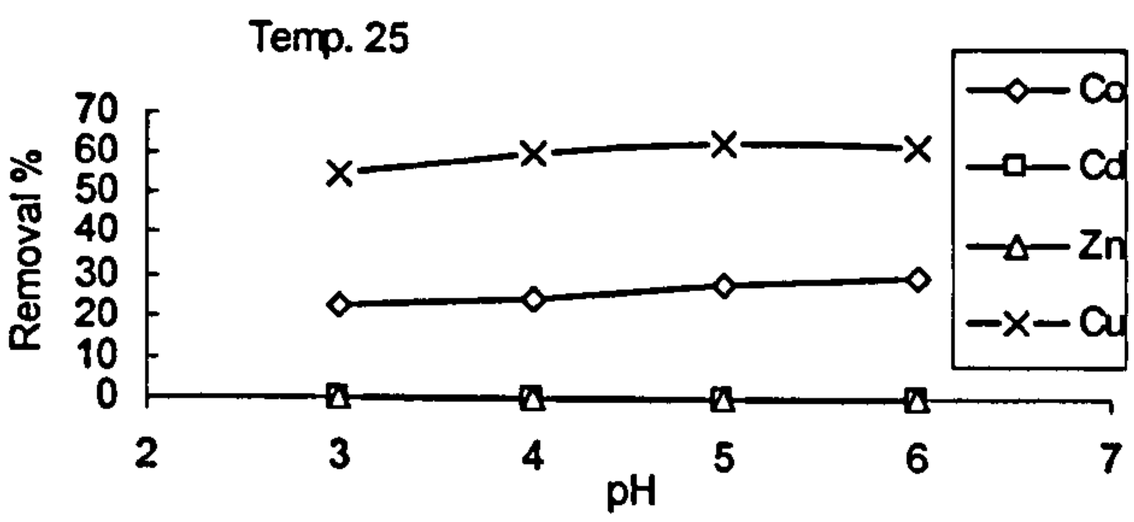

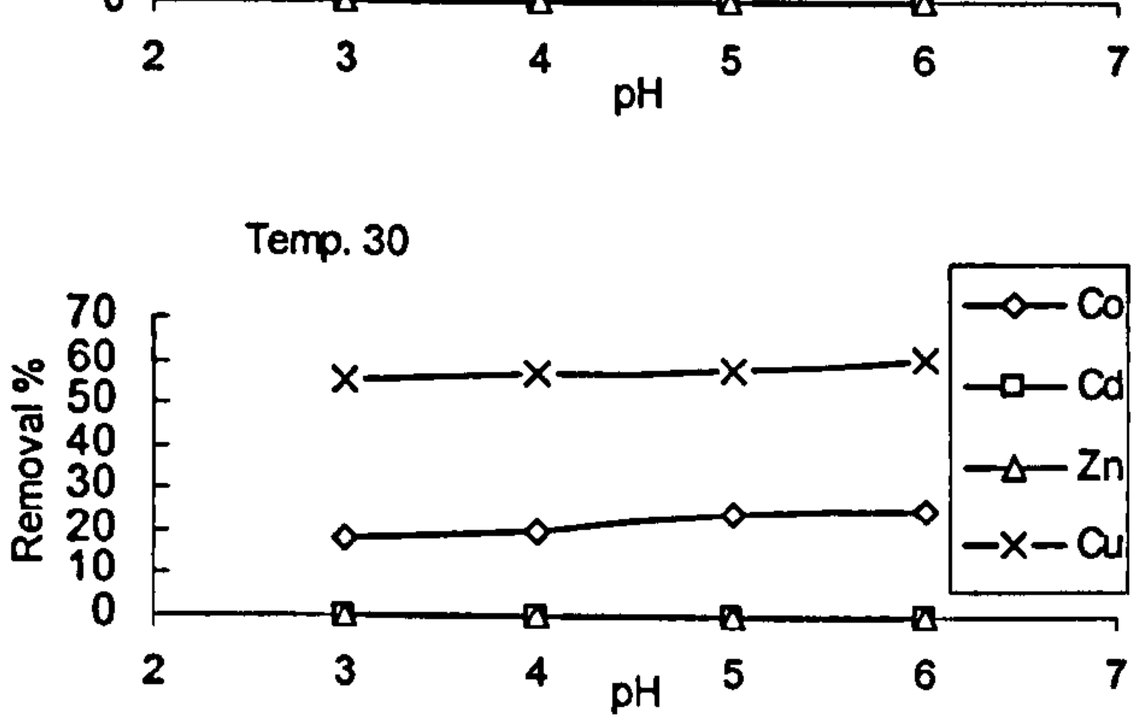

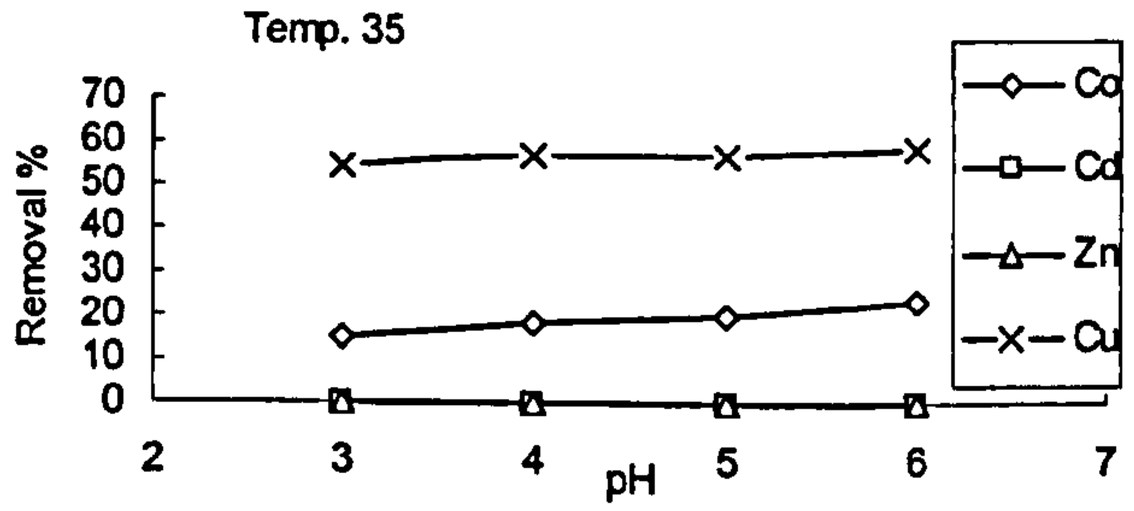

Figure 8.13: The initial-pH adsorption profile of Co(II), Cd(II), Zn(II) and Cu(II) on MF-NTA at temperatures 15, 20, 25, 30 and 35°C.

The values of free energy of adsorption for Cu(II) ion for different conditions are given in **Table 8.13**. They are negative which reflects a spontaneous adsorption and it can be observed that as temperature decreases, the absolute value of free energy increases which means that adsorption at lower temperature is more favourable. Also, the same behaviour is observed as the pH value is increased: that is adsorption favours neutral solutions [180].

Table 8.13: Free energy of adsorption for Cu(II) on MF-NTA.

T(°C)	$-\Delta G^{ads}{}_{Cu}$(kJ mol^{-1})			
	pH 3	pH 4	pH 5	pH 6
15	1.09 ± 0.01	1.38 ± 0.01	1.52 ± 0.01	1.56 ± 0.01
20	0.97 ± 0.01	1.17 ± 0.01	1.28 ± 0.01	1.64 ± 0.01
25	0.50 ± 0.00	0.97 ± 0.01	1.22 ± 0.01	1.21 ± 0.01
30	0.53 ± 0.00	0.68 ± 0.00	0.76 ± 0.01	1.06 ± 0.01
35	0.38 ± 0.00	0.67 ± 0.00	0.67 ± 0.00	0.82 ± 0.01

The plots of lnK_C against 1/T, for Cu(II) at pH 3, 4, 5, and 6, are shown in **Figure 8.14** from which the adsorption thermodynamic parameters ΔH^{ads} and ΔS^{ads} were calculated and are given in **Table 8.14**.

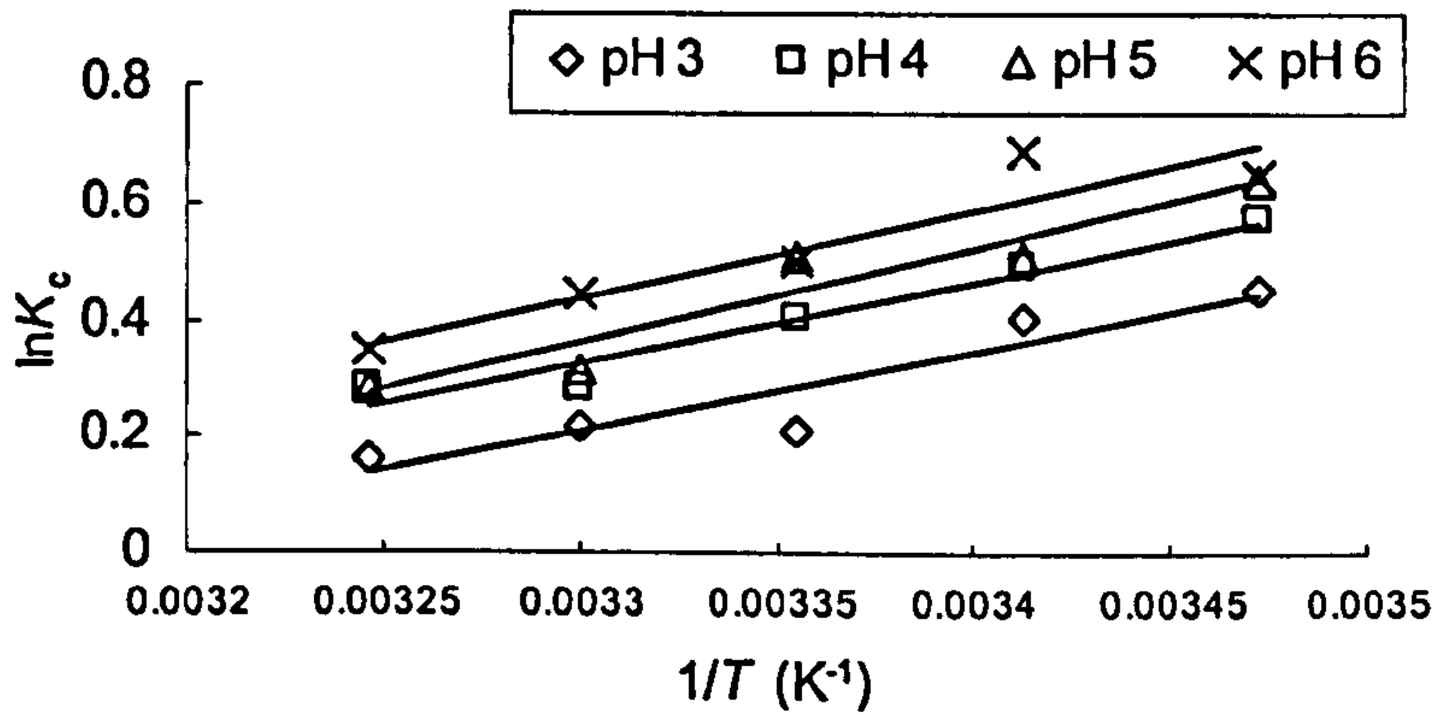

Figure 8.14: The Plots of lnK_C against 1/T for Cu(II) adsorption on MF-NTA at pH 3, 4, 5 and 6.

Table 8.14: Thermodynamic parameters of adsorption of Cu(II) on MF-NTA.

pH	3	4	5	6
$-\Delta H^{ads}$ (kJ mol^{-1})	11.43	11.74	13.34	12.54
$-\Delta S^{ads}$ (J mol^{-1} K^{-1})	35.97	36.03	41.03	37.72

The parameters ΔH^{ads} and ΔS^{ads} have negative values for all conditions. Negative enthalpy means an exothermic process and chelation adsorption is suggested to be the main mechanism. The values of ΔH^{ads} can be considered relatively low for chemisorption (and observed to be less than the corresponding values for the MF-DTPA case), but this may be due to consumption of some evolved energy for endothermic-dehydration process [164]. In the MF-DTPA case, the number of formed coordination bonds is higher than those formed by MF-NTA, hence more energy is released and compensates dehydration. The Negative value of entropy means a decrease in the degree of freedom. Hence, the entropy change resists adsorption but reflects reversibility of the process. In general, this behaviour resembles that of MF-DTPA which suggests that MF-PAPC adsorbents have the same general structure.

The maximum adsorption percentage for Co(II) is about 30%. **Table 8.15** gives adsorption free energies for Co(II) for different conditions. They are positive which reflects that Co(II)-adsorption is not favourable under these conditions, especially due to the Cu(II)-competitive uptake process onto the limited available number of chelating sites.

Table 8.15: Free energy of adsorption for Co(II) on MF-NTA.

T (°C)	ΔG^{ads}_{Co} (kJ mol^{-1})			
	pH 3	pH 4	pH 5	pH 6
15	3.03 ± 0.02	2.76 ± 0.02	2.26 ± 0.02	2.03 ± 0.01
20	3.17 ± 0.02	3.03 ± 0.02	2.63 ± 0.02	2.38 ± 0.02
25	3.31 ± 0.02	3.17 ± 0.02	2.89 ± 0.02	2.63 ± 0.02
30	3.63 ± 0.03	3.32 ± 0.02	2.76 ± 0.02	2.63 ± 0.02
35	4.15 ± 0.03	3.63 ± 0.03	3.32 ± 0.02	2.89 ± 0.02

The plots of lnK_C against 1/T, for Co(II) at pH 3, 4, 5, and 6, are shown in **Figure 8.15** from which adsorption thermodynamic parameters ΔH^{ads} and ΔS^{ads} were calculated. These parameters are given in **Table 8.16**.

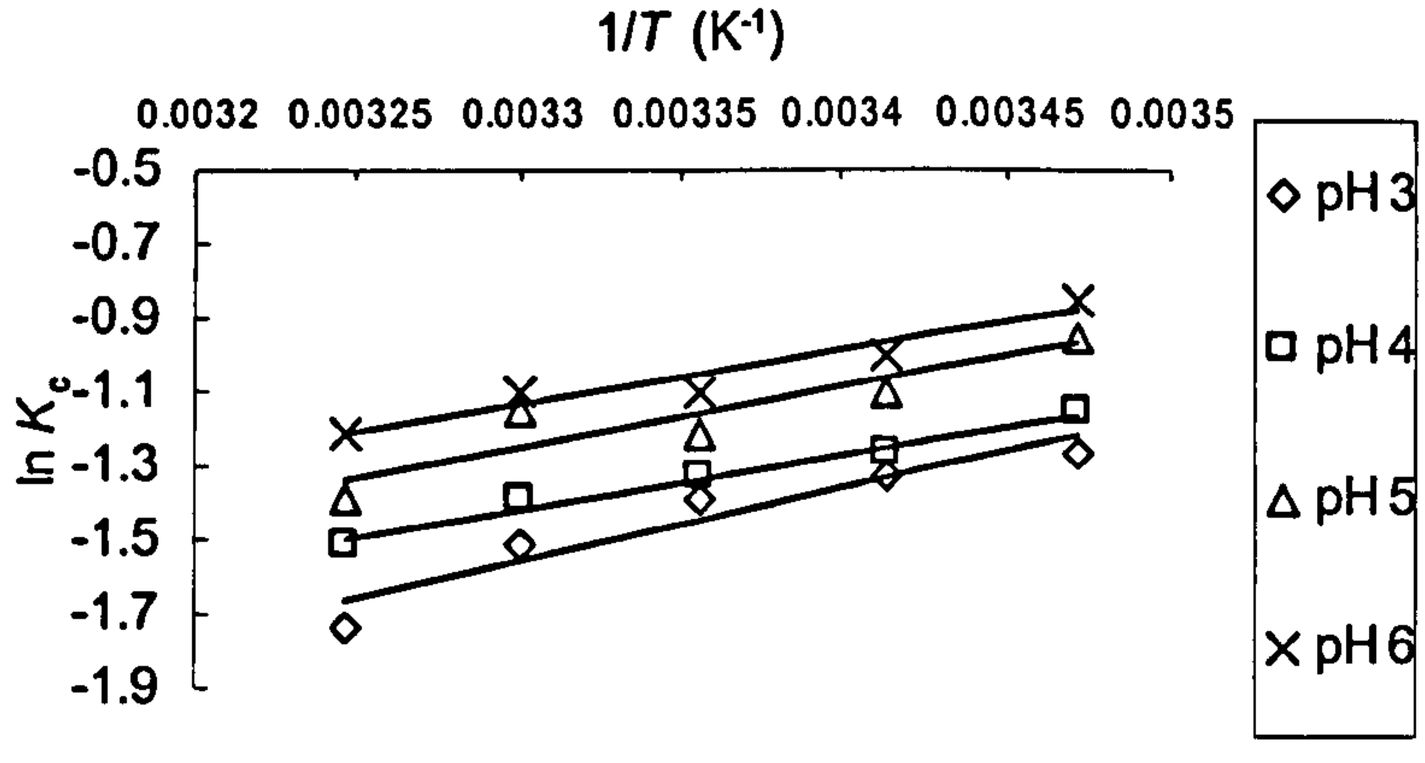

Figure 8.15: The Plots of $\ln K_C$ against $1/T$ for Co(II) adsorption on MF-NTA at pH 3, 4, 5 and 6.

Table 8.16: Thermodynamic parameters of adsorption of Co(II) on MF-NTA.

pH	3	4	5	6
$-\Delta H^{ads}$ (kJ mol^{-1})	16.57	16.57	13.83	12.23
$-\Delta S^{ads}$ (J mol^{-1} K^{-1})	67.6	67.6	56.1	49.8

The parameters ΔH^{ads} and ΔS^{ads} have negative values for all conditions. A negative enthalpy means an exothermic process (favourable) and chelation adsorption is suggested to be the main mechanism. A negative value of entropy means a decrease in the degree of freedom (non-favourable). The positive value of free energy originates from higher contribution of entropy over enthalpy in the Co(II) adsorption process. It is significant that the entropic part of Cu(II) adsorption is lower than that of Co(II) adsorption which may explain the lower adsorption of Co(II). This indicates the important role of the entropic effect associated with M(II)-adsorption on MF-PAPC adsorbents.

8.2.3 Relative affinity of MF-NTA towards M(II) ions

Standard values of M(II)-complex formation stability constants, enthalpy and entropy of chelate formation of NTA with the stated ions are given in **Table 8.17** [172]. These values concern the formation of the corresponding complexes singly in aqueous solutions. The enthalpy of dehydration and ion hydrated radius are given as well.

Table 8.17: M(II)-NTA complex formation parameters [172].

M(II)	Log K (25°C)	$\Delta H^{chelate}$ (20°C) (kcal/mole)	$\Delta S^{chelate}$ (25°C) (cal/mole °C)	M(II) Hydrated-radius (Å)	Enthalpy of M(II)-dehydration (kcal/mole)
Co(II)	10.38	–0.1	47	4.23	476.9
Cd(II)	9.78	–4.0	31	4.26	431.8
Zn(II)	10.66	–0.9	46	4.30	488.9
Cu(II)	12.94	–1.9	53	4.19	501.8

It is clear from previous results that the MF-NTA adsorbent has a high selectivity towards Cu(II) compared to Cd(II), Zn(II), and Co(II). This selectivity could be correlated to metal ion complex formation stability constants with NTA being significantly the highest. The NTA molecule has to bind only one M(II) ion due to the limited number of coordination positions it has (four coordination positions).

Since the Cu(II) ion has the highest stability constant, it is more likely to be chelated than the other M(II) ions. The rule of enthalpy of chelate formation is not effective in this case as NTA has to chelate only one M(II) ion. It is probable that Cu(II) is coordinated with two water molecules to complete its octahedral structure [180]. The Co(II) and Zn(II) ions have the same opportunity to form chelate due to similar stability chelation constants but only Co(II) showed adsorption and this may be due to its lower dehydration energy. The ion hydrated-radii cannot play a role due to the wide average pore diameter of the MF-NTA adsorbent (130 Å). It seems therefore that the enthalpy of M(II)-dehydration does not play significant role here.

8.2.4 Effect of initial concentration

The effect of initial concentration on adsorption of the Cu(II) ion was investigated by changing the initial concentration (20, 30, 40, 50, 60 and 70 mg l^{-1}) with a constant adsorbent amount (0.3 g, conditions: T= 20°C and pH =5). The removal percentage increases with initial concentration (**Table 8.18**) which is not in agreement with the behaviour of MF-DTPA (section 8.1.4) and MF-CDTA (section 8.5.3). This phenomenon may be attributed to selective-adsorption nature of Cu(II) on MF-NTA and the reversibility nature of the chelation process. As MF-NTA selectively adsorbs

Cu(II) ion, the total initial concentration of the four M(II) ions is the driving force for the Cu(II) ion only [67]. The desorption/adsorption ratio (reversibility) for Cu(II) adsorption on MF-NTA (at pH 5) is 0.63 (section 8.2.5) whereas on MF-DTPA is 0.33 (section 8.1.5). Hence, as concentration increases the chelation significantly shifts towards adsorption. These two effects can increase the removal percentage.

Table 8.18: Effect of initial concentration on Cu(II) Removal% by MF-NTA.

Cu(II)-Initial concentration	Cu(II) Removal percentage ±3%
20	52
30	55
40	56
50	58
60	59
70	61

The effect of Cu(II) initial concentration (T= 20°C and pH= 5) on equilibrium adsorption capacity (q_e) is shown in **Figure 8.16**.

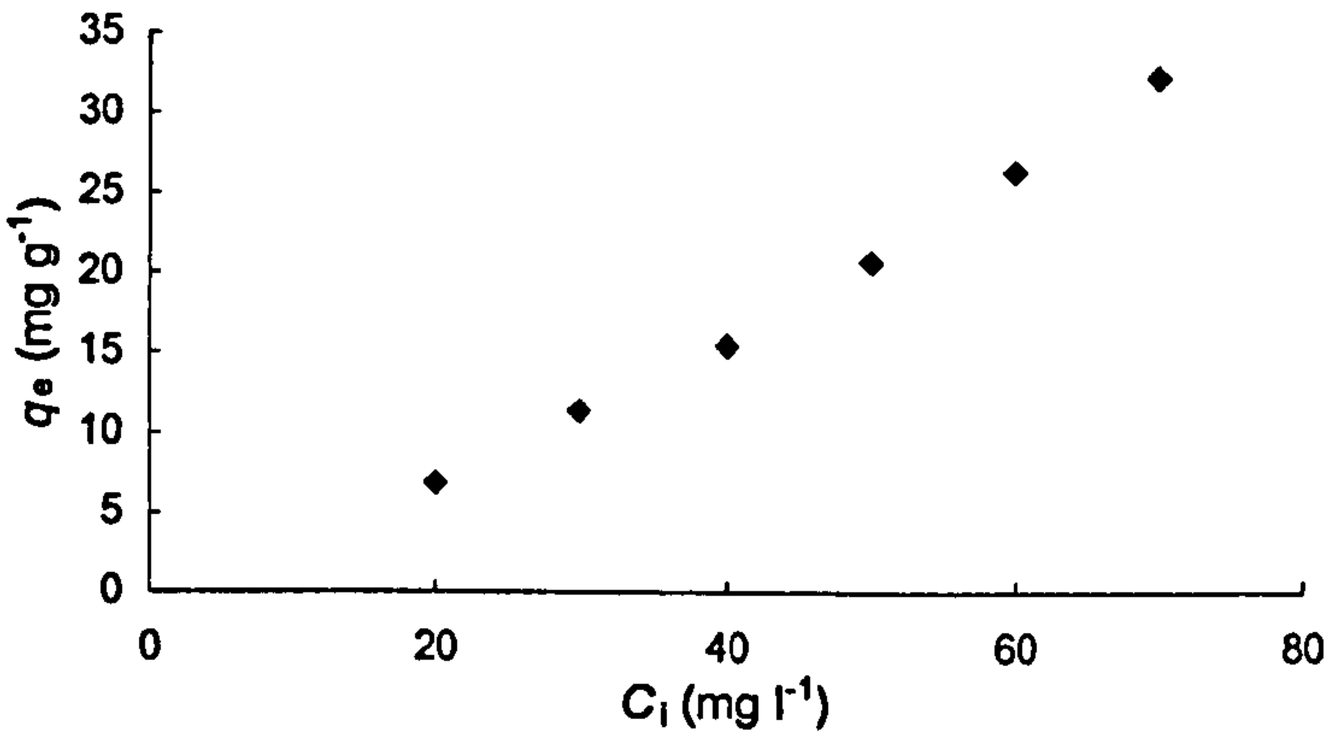

Figure 8.16: The effect of Cu(II) ion initial concentration on adsorption capacity on MF-NTA at pH 5 and T = 20°C.

The adsorption capacity increased, almost linearly, with concentration and the saturation plateau does not appear to start in this range of concentration. This indicates the dependence of adsorption on the ion concentration and may be due to higher pore volume, 0.529 cm^3 g^{-1} (for MF-DTPA: pore volume = 0.396 cm^3 g^{-1}) which means more concentration driving force.

8.2.5 Adsorption Kinetics

Adsorption time profiles of Cu(II) within 60 minutes at temperature 20°C for different pH values are shown in **Figure 8.17**. The removal increases sharply in the first 10 minutes leading to saturation and this may be due to relative high pore diameter and volume (compared to MF-DTPA for example).

The half load time, $t_{1/2}$, of Cu(II) ion is given in **Table 8.19**. It is in the range of minutes and has not been affected by pH change. This suggests that a successful adsorption process is applicable over the studied pH range.

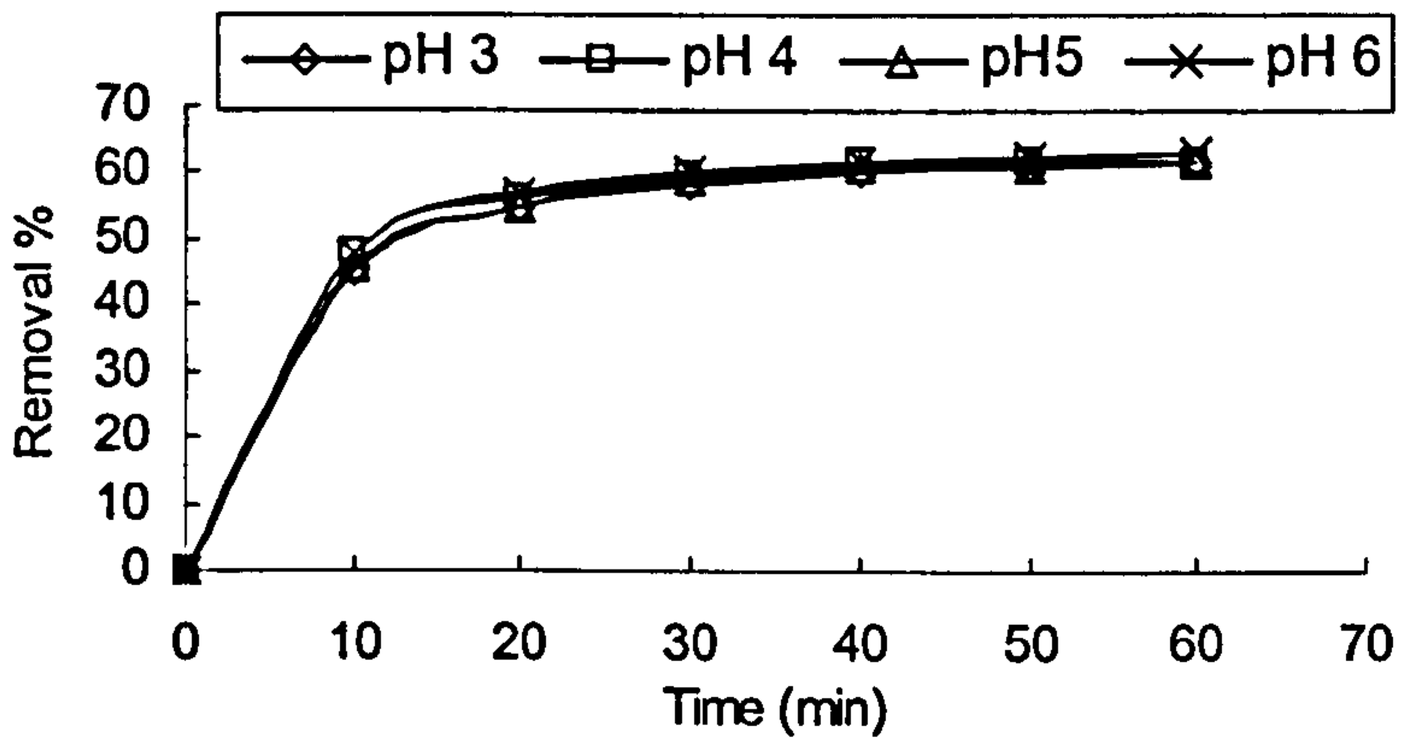

Figure 8.17: Time profile of adsorption of Cu(II) on MF-NTA at 20°C at different pH values.

Table 8.19: The half-load time of adsorption of Cu(II) on MF-NTA.

pH	3	4	5	6
$t_{1/2}$ (min.)	12	10.7	11.4	10.3

The kinetic models were used to fit the experimental results. The pseudo first-order and reversible first-order plots are shown in **Figures 8.18** and **8.19** respectively. Their constants were calculated and tabulated in **Table 8.20**. There is a good match between k_R and its corresponding k_L values as mentioned for MF-DTPA. This suggests the same kinetic behaviour of MF-PAPC adsorbents. The ratio k_1/k_2 is greater than one for Cu(II) which means that the process is shifted towards adsorption over desorption [180]. The desorption rate parameter (k_2) is about two thirds of the adsorption rate (k_1) which is a high ratio when compared to that of the

MF-DTPA case. This may explain lower the removal percentage for MF-NTA compared to that of MF-DTPA.

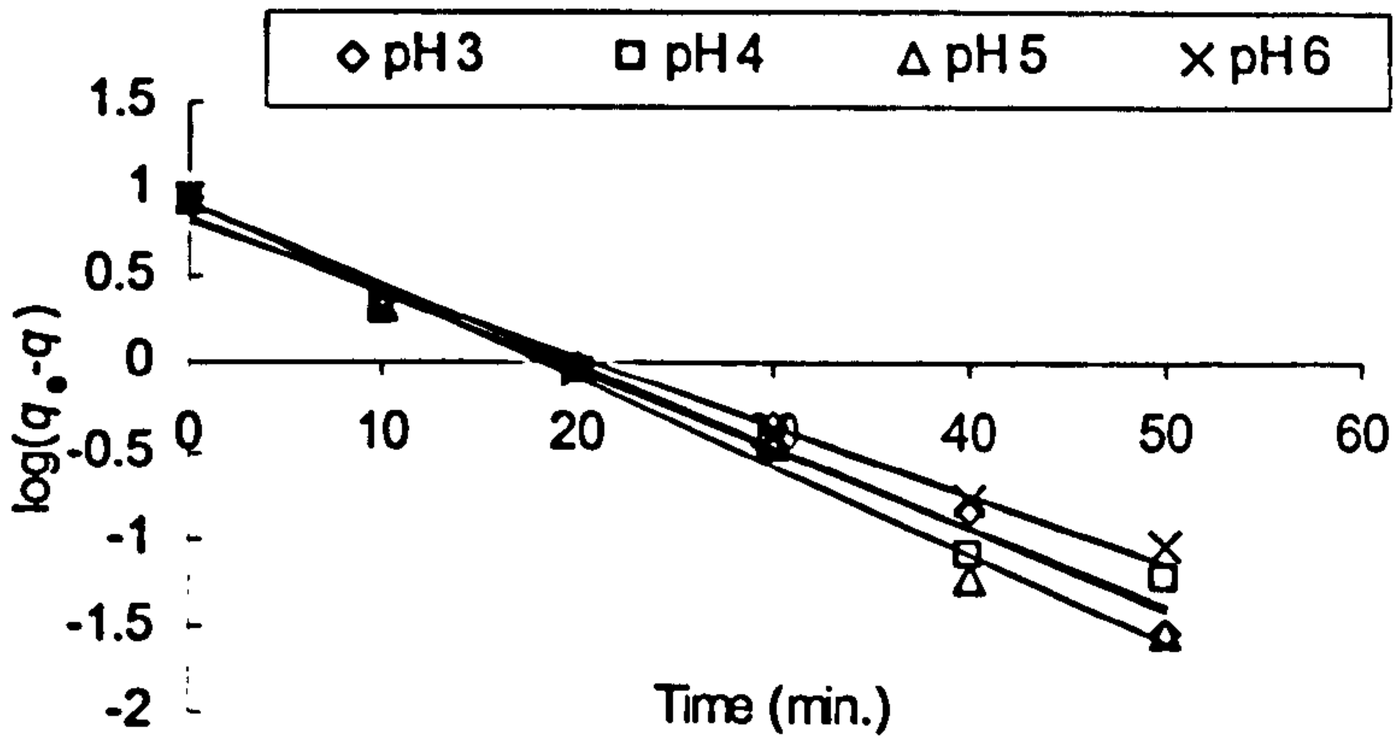

Figure 8.18: Pseudo first-order (Lagergren) plots of Cu(II) adsorption on MF-NTA at temperature 20°C and pH values 3, 4, 5 and 6.

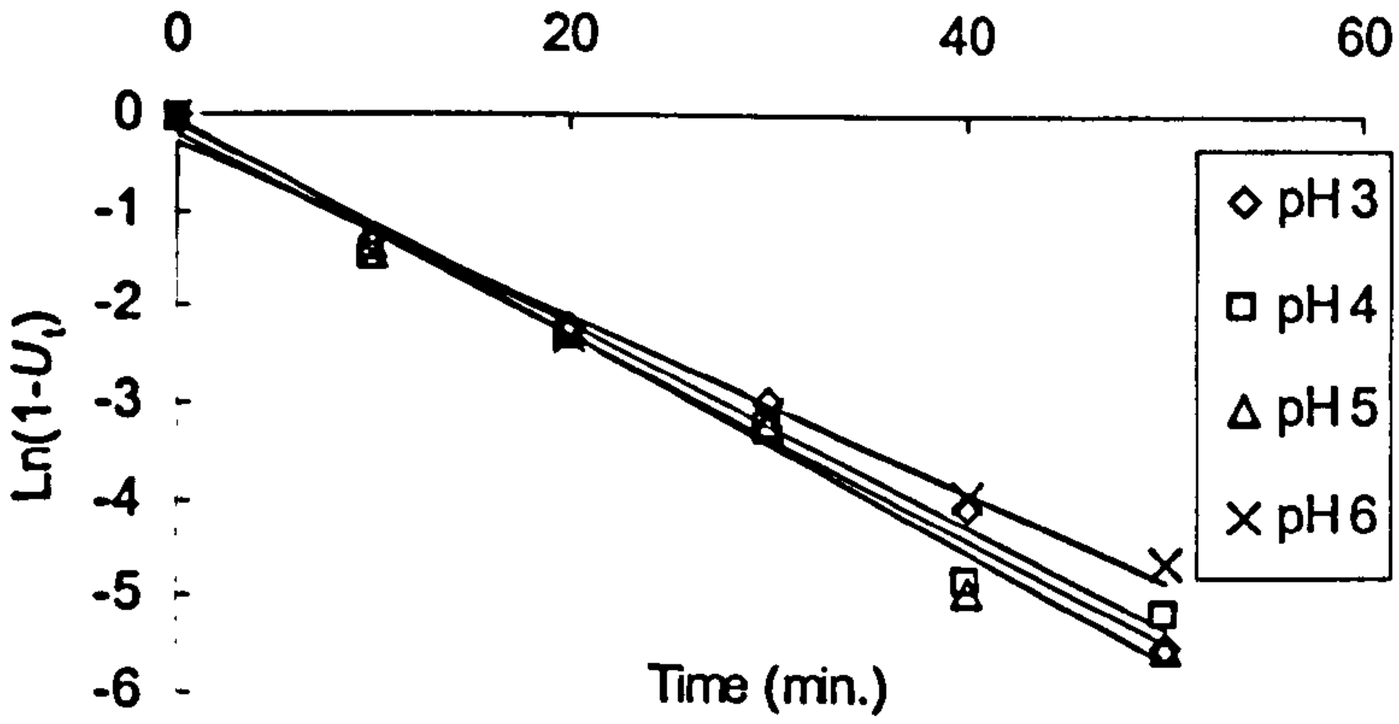

Figure 8.19: Reversible first-order plots of Cu(II) adsorption on MF-NTA at temperature 20°C and pH values 3, 4, 5 and 6.

Table 8.20: Parameters of reversible first-order and pseudo first-order of Cu(II) adsorption on MF-NTA.

pH	$q_{exp.}$±3%	pseudo first order			reversible first order			
		k_1	q_e	R^2	k_R	k_1	k_2	R^2
3	8.70	0.107	8.53	0.9875	0.104	0.064	0.040	0.9912
4	8.97	0.102	7.04	0.9794	0.105	0.065	0.040	0.9820
5	9.14	0.115	8.61	0.9892	0.112	0.068	0.043	0.9885
6	9.64	0.091	6.63	0.9839	0.090	0.057	0.033	0.9852

The plots of pseudo first-order and reversible first-order have $R^2 > 0.97$ which suggests that either might represent the adsorption process. The adsorption capacities

(q_e) estimated by the pseudo first-order model do not match the experimental capacities (q_{exp}).

Pseudo second-order and Elovich plots are shown in **Figures 8.20** and **8.21** respectively. Their constants were calculated and are tabulated in **Table 8.21**. The Elovich model confirms reversibility, as well as the reversible first order model, as the relation α/β suggests. The correlation factor $R^2 > 0.93$ is the lowest compared to the other models. The pseudo second order model gives the best fit to the data ($R^2 > 0.999$) and estimated capacity values (q_e) match better with the experimental capacity values (q_{exp}) than those of pseudo first order model. The fitting lines of the pseudo second order model almost coincide which suggest stable adsorption behaviour over the pH range studied. It is suggested that the reversible first-order and pseudo second order models are best for M(II)-adsorption on MF-NTA.

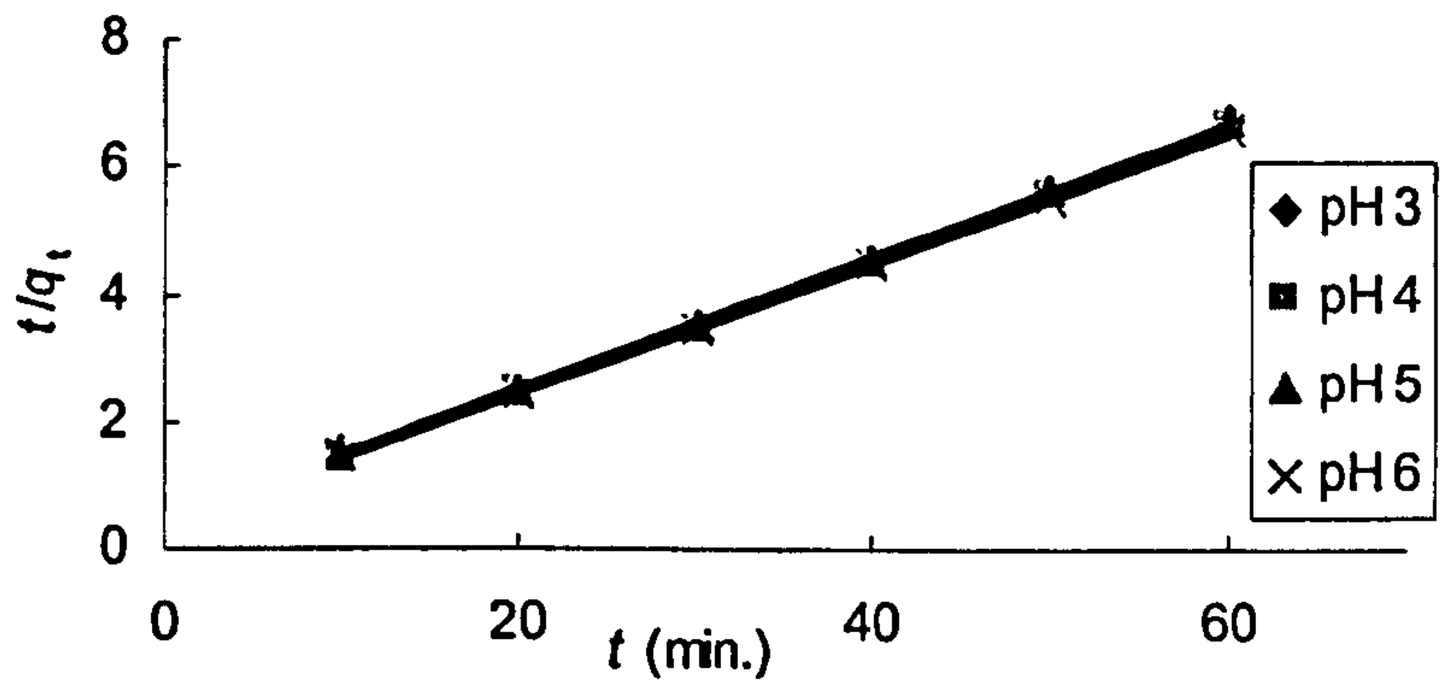

Figure 8.20: Pseudo second-order (Lagergren) plots for Cu(II) adsorption on MF-NTA at temperature 20°C and pH values 3, 4, 5 and 6.

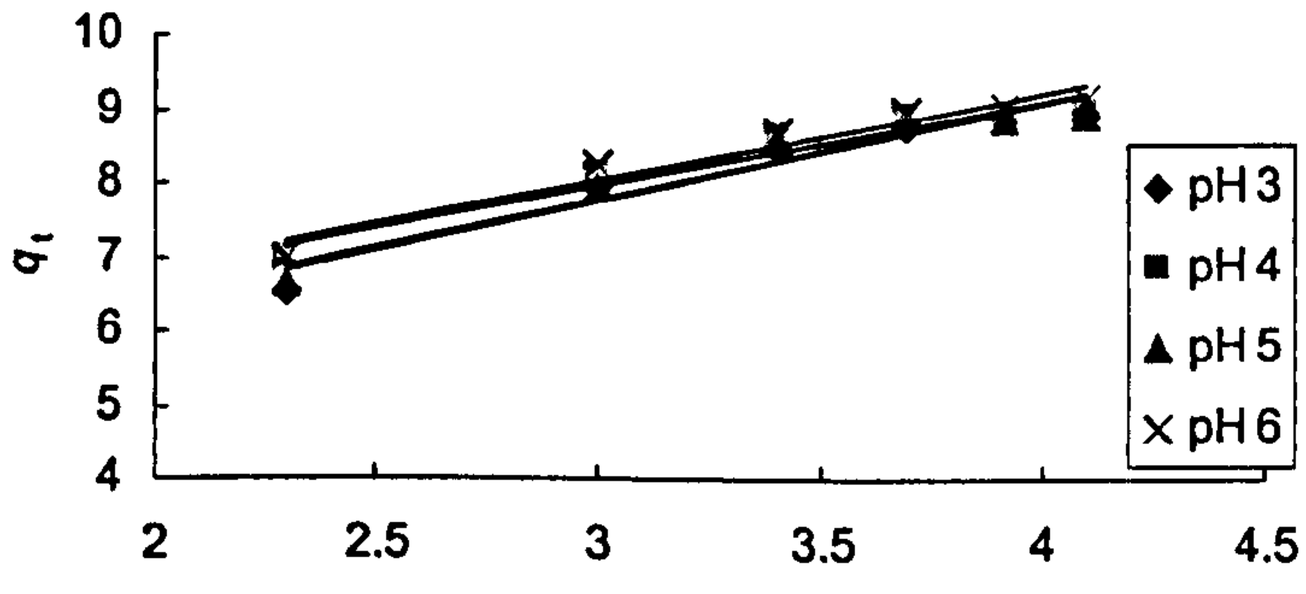

Figure 8.21: Elovich plots for Cu(II) adsorption on MF-NTA at temperature 20°C and pH values 3, 4, 5 and 6.

Table 8.21: Parameters of pseudo second-order and Elovich models of Cu(II) adsorption on MF-NTA.

pH	$q_{exp.}$±3%	Pseudo second order			Elovich model		
		k_H	q_e	R^2	α	β	R^2
3	8.70	0.0242	9.62	0.9996	2.826	0.7467	0.9348
4	8.97	0.0299	9.57	0.9997	2.745	0.8663	0.9395
5	9.14	0.0259	9.59	0.9994	2.802	0.7730	0.9329
6	9.64	0.0277	9.73	0.9999	2.764	0.8284	0.9426

8.2.6 Adsorption isotherm

Figure 8.22 shows the adsorption isotherm of Cu(II) at 20°C and pH 5. The Cu(II)-isotherm is regular, positive and concave to the concentration axis (C_e). The isotherm is of type I according to Brunauer's classification and represents the Langmuir adsorption [179]. The isotherm curve was fitted using experimental data including origin. The equilibrium capacity (q_e) increases smoothly with equilibrium concentration (C_e) which reflects a considerable desorption and reaching the plateau may occur at higher initial concentrations. The isothermal behaviour of MF-NTA is similar to that of MF-DTPA.

This result from the isotherm study supports results from the kinetic study. In the kinetic study, k_2/k_1 is generally > 0.57 and this implies that adsorption is not considerably higher than desorption. Hence, q_e shows a smooth increase with C_e (compared with the higher initial increase in the case of MF-DTPA, section 8.1.6). This confirms the reversible nature of adsorption on MF-NTA (and generally on MF-PAPC adsorbents).

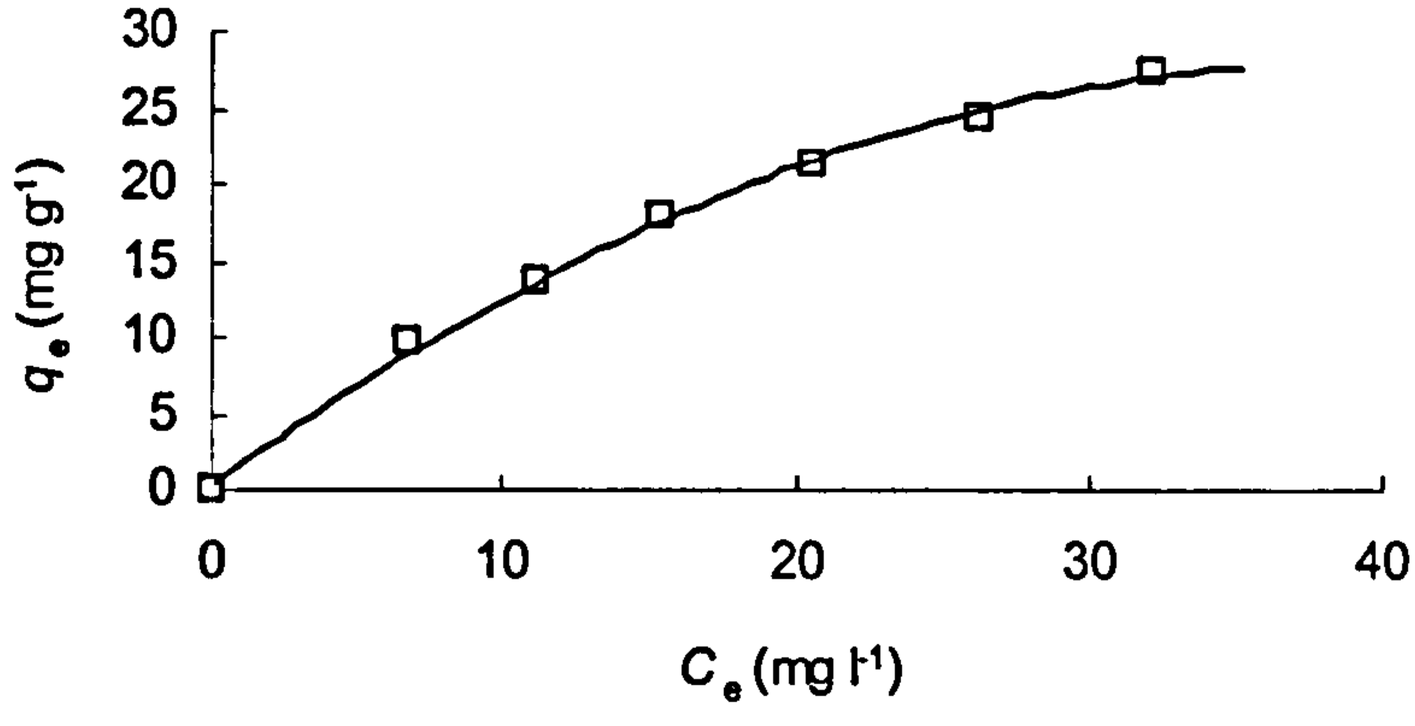

Figure 8.22: Adsorption isotherm of Cu(II) on MF-NTA (20°C) at pH 5 and 120 minute equilibrium contact time.

The plots of this adsorption isotherm data according to Freundlich and Langmuir models are presented in **Figures 8.23** and **8.24** respectively. From these plots, related constants were calculated and **Table 8.22** summarizes them.

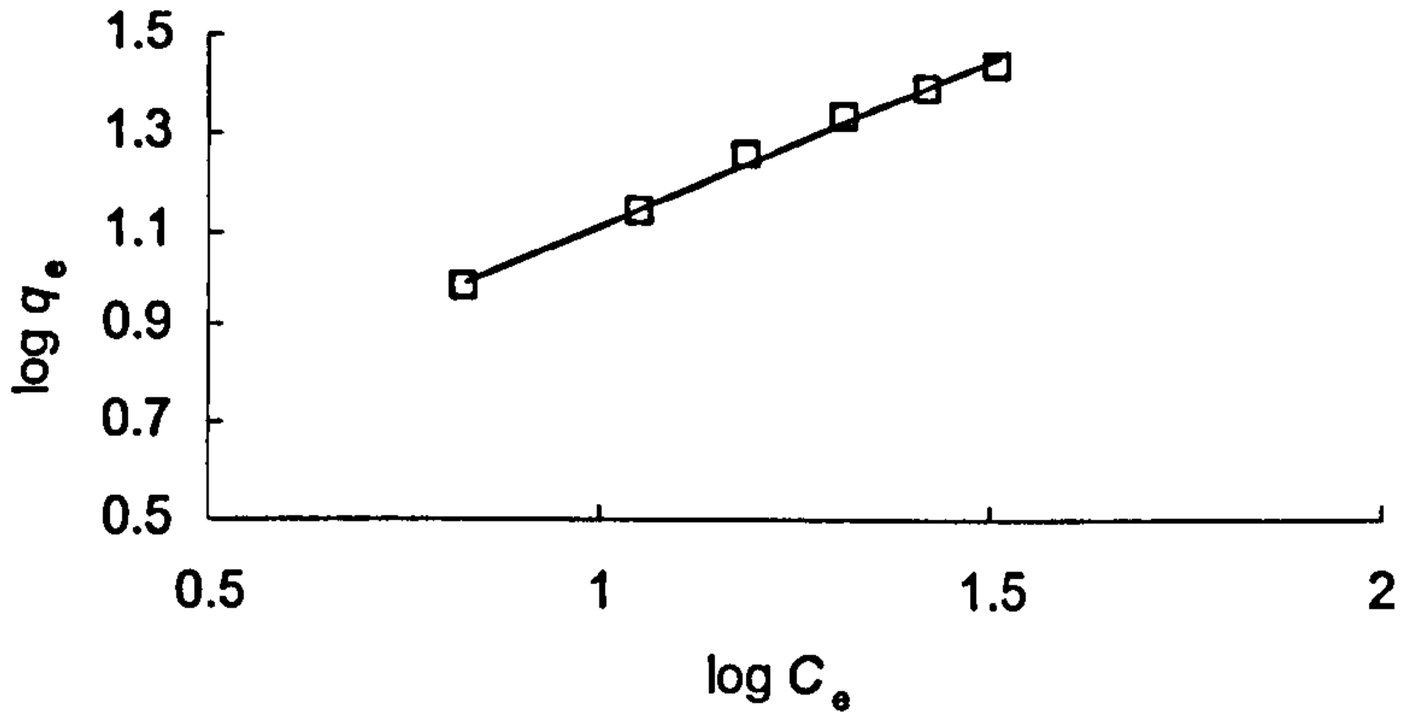

Figure 8.23: Freundlich adsorption isotherm of Cu(II) on MF-NTA (20°C) at pH 5 and 120 minute equilibrium contact time.

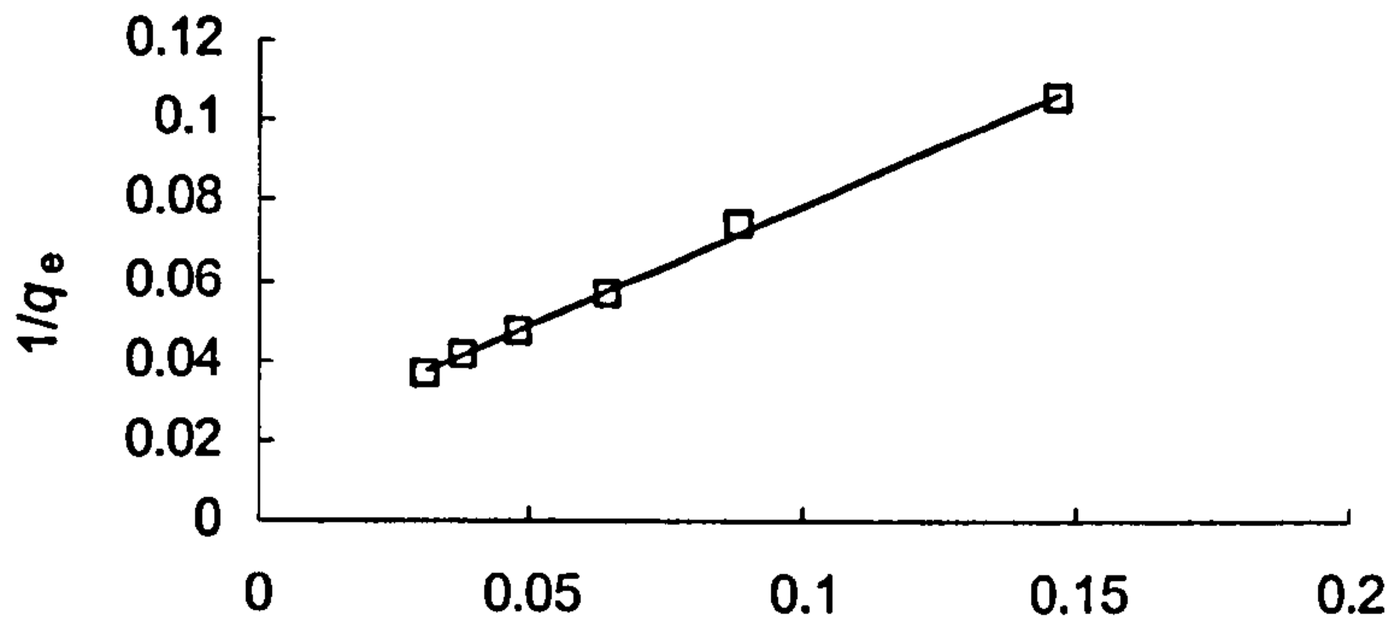

Figure 8.24: Langmuir adsorption isotherm of Cu(II) on MF-NTA (20°C) at pH 5 and 120 minute equilibrium contact time.

The Freundlich parameter ($1/n$) fulfils the condition of favouring the adsorption process, $0 < 1/n < 1$. The value of the parameter ($1 < n < 10$) indicates that adsorption of Cu(II) on MF-NTA is reversible [154]. k_F is related to the capacity but not equal to it and so as this parameter increases maximum adsorption increases and this is helpful when comparing different adsorbents or conditions. This parameter is lower than those of MF-DTPA which suggests lower removal behaviour.

The Langmuir capacity (Q_o) is 52.6 mg g^{-1}. The parameter R_L is in the range of favouring adsorption ($0 < R_L < 1$). The Langmuir correlation factor (R^2) is slightly higher than that of the Freundlich model which means that Langmuir model gives a better fit to the experimental data [180]. This reflects the homogeneity nature of the MF-NTA surface.

Table 8.22: Adsorption isotherm constants of Freundlich and Langmuir for Cu(II) adsorption on MF-NTA.

Adsorption Model						
Freundlich			Langmuir			
k_F	$1/n$	R^2	Q_o	b	R_L	R^2
2.65	0.68	0.9956	52.6	0.032	0.61	0.9968

8.3 MF-CDTA adsorption behaviour

8.3.1 Qualitative determination of adsorption (visual, ^{13}C-NMR, IR and XRD)

The MF-CDTA adsorbent is white. After soaking an adsorbent sample in Cu(II) solution, it turned dark blue (the colour of concentrated Cu(II)–CDTA complex in aqueous solution) which suggests that the chelating mechanism strongly contributes to the adsorption process **(Figure 8.25)** [81,104,152,157]. The Cu(II) solution in which the adsorbent sample was soaked cannot be detected visually due to the low concentration of Cu(II) which is 20 mg l^{-1}. The adsorbent successfully concentrated the Cu(II) ion from solution to its pendent chelating CDTA-sites giving the known deep blue colour of some Cu(II) complexes.

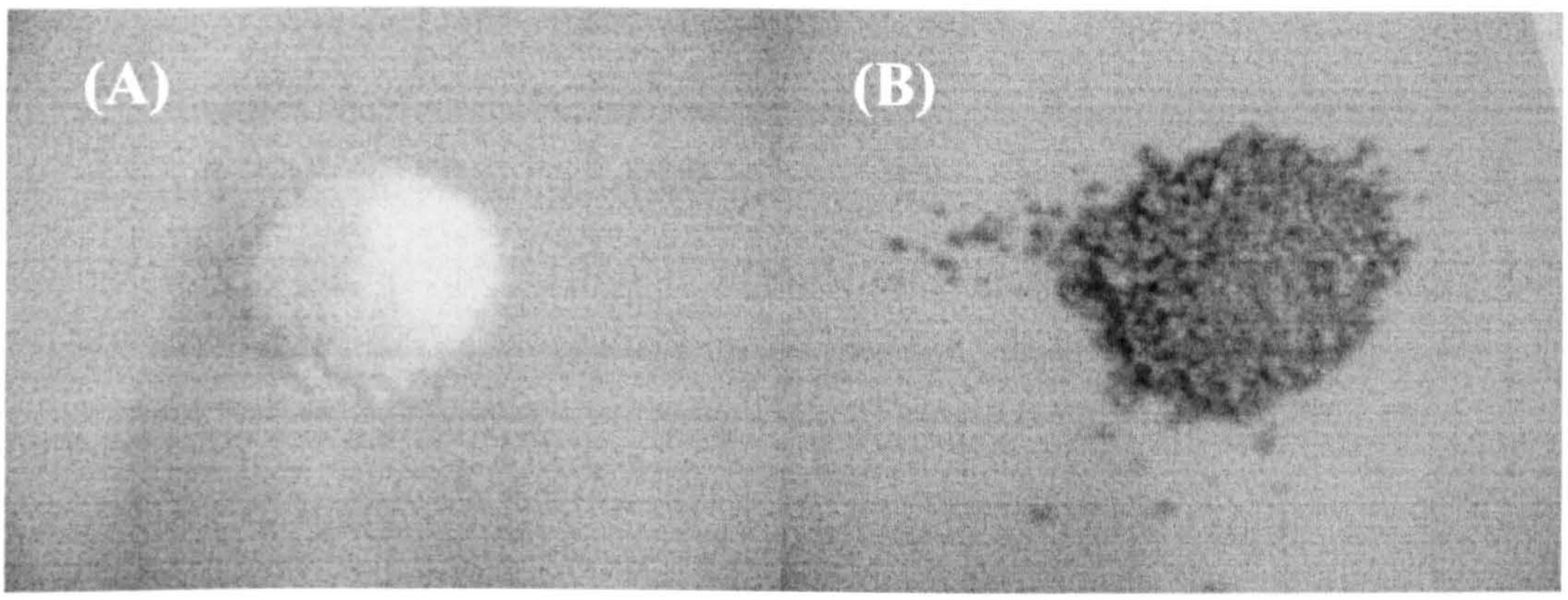

Figure 8.25: (A) White MF-CDTA and (B) Deep-blue Cu(II)-Loaded MF-CDTA.

The ^{13}C-NMR spectrum of the MF-CDTA sample shows a number of signals which are consistent with the structure (**Figure 8.26 (A)**). The intense line at 166.3 ppm presumably represents triazinic carbon (N–**C**(N)=N) and the line at 157.5 ppm refers to the amidic carbon (HN–**C**(=O)–). The line at 25 ppm accounts for aliphatic methyl groups and the broad band between 40 and 70 ppm accounts for the methyl groups bonded to nitrogen and oxygen. The broad shoulder on the 166.3 ppm line at around 175 ppm probably arises from the –**C**OOH groups. For the Cu(II)-loaded MF-CDTA spectrum (**Figure 8.26 (B)**), the intense line at 166.3 ppm of triazinic carbon (N –**C**(N)=N) is still present with the same height indicating no involvement of this ring in chelation. The line at 157.5 ppm refers to the amidic carbon (HN–**C**(=O)–) becoming weaker indicating some change of carbon environment

suggesting contribution of amidic nitrogen in chelation. The line at 25 ppm almost disappeared. The broad band between 40 and 70 ppm accounts for the CH_2s groups bonded to nitrogen and oxygen becoming significantly weaker suggesting chelation by oxygen and nitrogen. The broad shoulder at 175 ppm (–COOH groups) is not present suggesting chelation of the copper by this group.

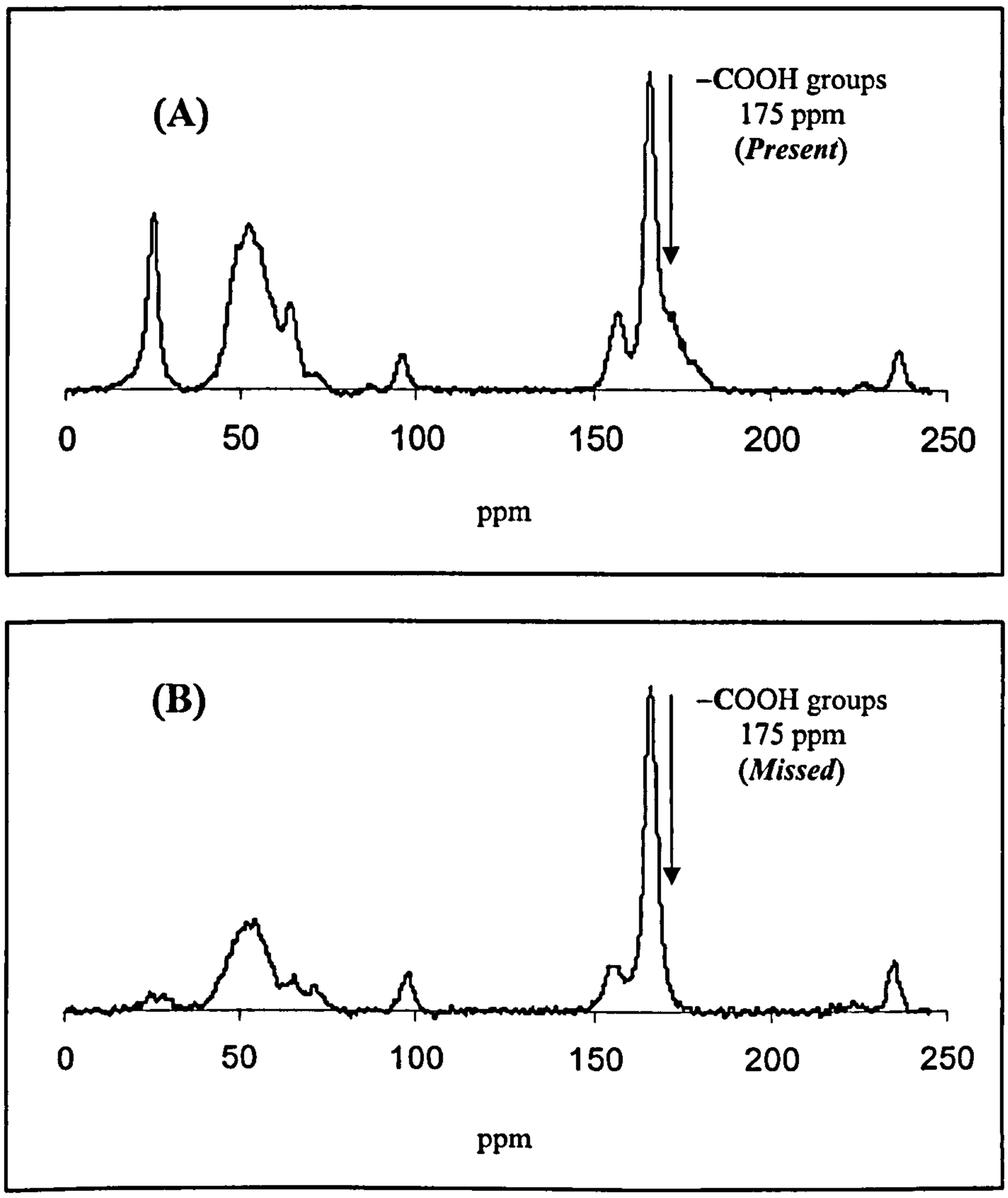

Figure 8.26: (A) ^{13}C-NMR spectrum of MF-CDTA and (B) Cu(II)-loaded MF-CDTA.

The IR spectrum of MF-DTPA-Cu(II) (**Figure 7.15**) is different from the spectrum of MF-CDTA at 1630 cm^{-1} which means contribution of amide (or carboxylic) groups in bonding Cu(II) ion. Also, for the spectrum of MF-DTPA-Cu(II), the broad peak at 556 cm^{-1} may indicate N–Cu(II) or O–Cu(II) bonding.

Figure 7.16 shows XRD diffractograms of MF-CDTA and Cu(II)-Loaded MF-CDTA. The two diffractograms have the same peaks at 2θ 44.2 and 64.6 and so Cu(II) adsorption did not affect the morphology which can indicate that Cu(II) binding occurs with anchored CDTA only and does not affect the main MF matrix.

8.3.2 Quantitative analysis of adsorption by elemental analysis

The elemental analysis of Cu(II)-loaded MF-CDTA is presented in **Table 8.23**. The calculated total adsorption load is 226 mg Cu(II) per gram adsorbent which corresponds to about 3.59 mmole M(II) per gram adsorbent. Accordingly, as the amount of chelating sites is about 2.28 mmole/ g adsorbent, most of the chelating moieties were exposed to the treated solution and accessible by metal ions, which corresponds to a good open pore structure in the adsorbent. This loading is higher than that of MF-DTPA (section 8.1.1).

Table 8.23: MF-CTPA and MF-CTPA-Cu(II) elemental ratio.

Sample / Element	C	H	N	O (calculated)	Cu(II) (calculated)
MF-CDTA	37.9	5.5	37.4	19.3	–
MF-CDTA-Cu(II)	24.3	6.3	24.3	22.5	22.6

The theoretical stoichiometric ratio (Cu(II) : CDTA) for chelation is 1:1. However, the calculated ratio was 1.6:1. This may imply that ion exchange was taking place in parallel. If this is true, the predominance of chelation over ion exchange is inferred from the total exothermic behaviour of the process: the exothermic heat for chelation exceeds the endothermic heat for ion exchange.

8.3.3 Effect of pH and temperature (thermodynamics) on adsorption

An investigation showing the change in pH on adsorption at different temperatures is presented in **Table 8.24**. From the table, it is observed that ΔpH (initial pH – final pH) increases with both the temperature and initial pH. The results suggest that at low initial pH values and high temperatures, ion exchange is significant. However, at

high initial pH values and low temperatures, chelation is totally dominant. The same behaviour is observed for MF-DTPA and MF-NTA.

Table 8.24: Final pH values after M(II)-adsorption on MF-CDTA (equilibrium).

Initial pH	Final pH±0.02		
	15°C	25°C	35°C
3	2.52	2.48	2.38
4	2.91	2.86	2.80
5	2.98	2.90	2.87
6	3.02	2.92	2.89

The pH adsorption profile at equilibrium (24 hours for complete adsorption) for temperatures 15, 25 and 35°C is shown in **Figure 8.27.**

A slight increase in removal percentage of the four elements is observed as the temperature decreases: for example, considering Cu(II) at pH 5; removal is 80% at 35°C, 85% at 25°C, and 85% at 15°C). The removal percentage was lower at pH 3 compared with pH values of 4, 5, and 6: this may be due to higher concentration of competitive H^+ ions. It is clearly observed that Cu(II) ion has the higher removal percentages at all conditions followed by Co(II), Cd(II) and then Zn(II). In general, the M(II)-removal percentages by MF-CDTA are lower than those by MF-DTPA. This can be attributed to the smaller amount of MF-CDTA used (0.25 g) compared to that of MF-DTPA (0.5 g) and the higher reversibility nature of MF-CDTA (at 25°C, the average value of $k_2/k_1 = 0.92$) compared with that of MF-DTPA (at 25°C, the average value of $k_2/k_1 = 0.45$), refer to **Tables 8.8** and **8.29**.

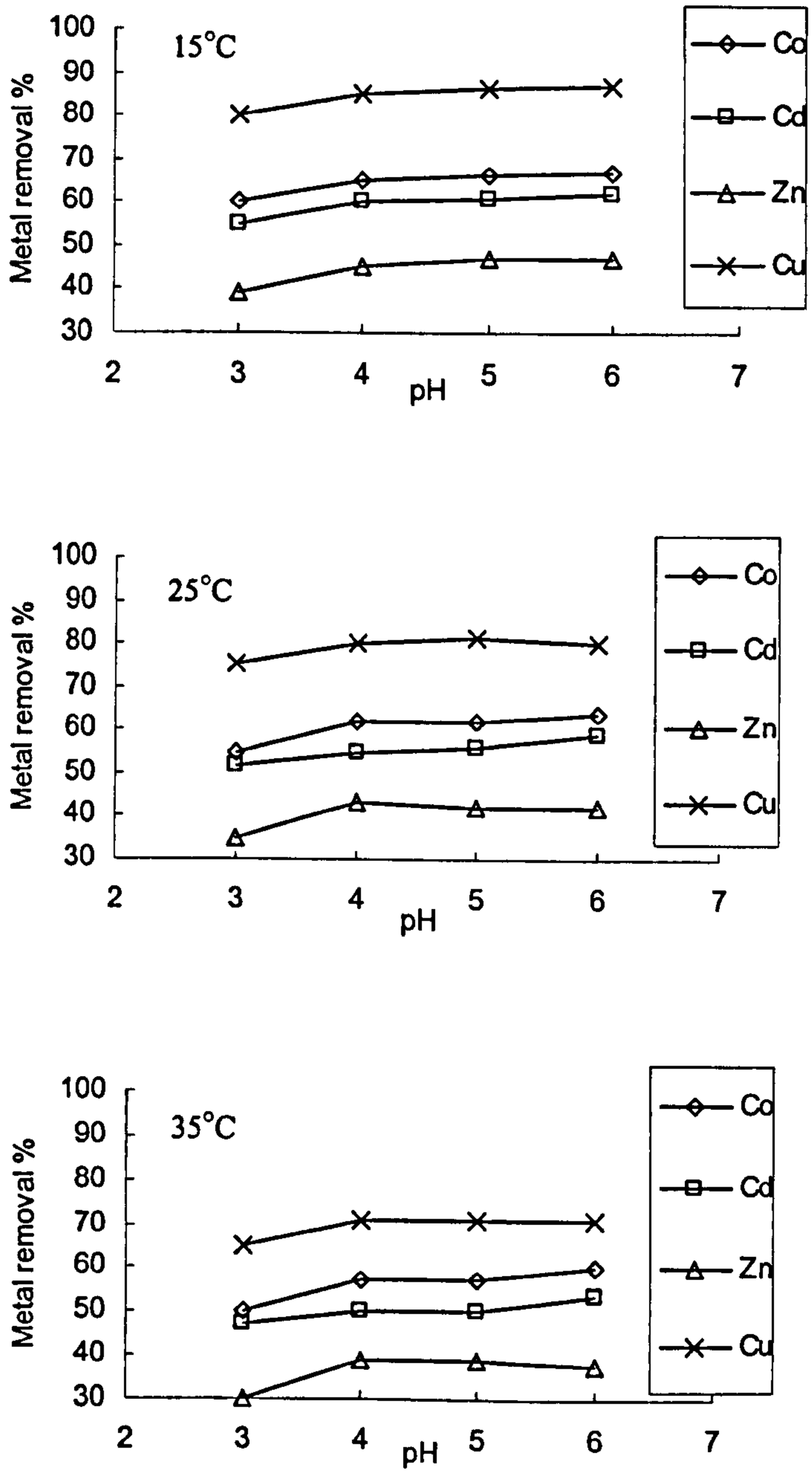

Figure 8.27: Removal percentage of Co(II), Cd(II), Zn(II) and Cu(II) by MF-CDTA at different pH values for temperatures 15, 25 and 35°C.

The adsorption is spontaneous as ΔG^{ads} has negative values for M(II) under all conditions except Zn(II) as given in **Table 8.25**. This table shows the adsorption preference as Cu(II) > Co(II) > Cd(II) > Zn(II).

Table 8.25: Free energy of adsorption of M(II) on MF-CDTA.

T (°C)	pH	$-\Delta G^{ads}$ (kJ mol^{-1})			
		Co(II)	Cd(II)	Zn(II)	Cu(II)
15	3	0.98±0.01	0.48±0.00	–1.07±0.01	3.32±0.02
	4	1.48±0.01	0.97±0.01	–0.48±0.00	4.15±0.03
	5	1.60±0.01	1.09±0.01	–0.31±0.00	4.35±0.03
	6	1.67±0.01	1.20±0.01	–0.29±0.00	4.51±0.03
25	3	0.48±0.00	0.00±0.00	–1.48±0.01	2.63±0.02
	4	0.97±0.01	0.48±0.00	–0.87±0.00	3.36±0.02
	5	1.17±0.01	0.58±0.00	–0.77±0.01	3.47±0.02
	6	1.27±0.01	0.67±0.01	–0.77±0.01	3.36±0.02
35	3	0.00±0.00	–0.10±0.00	–1.70±0.01	1.48±0.01
	4	0.97±0.00	0.48±0.00	–1.07±0.01	2.06±0.01
	5	1.07±0.00	0.58±0.00	–0.87±0.01	2.09±0.01
	6	1.17±0.01	0.67±0.00	–0.87±0.01	2.14±0.01

The adsorption is more favourable at high pH values and low temperatures as indicated by the increase in absolute ΔG^{ads} values. This behaviour conforms to the chelation mechanism.

The plots of lnK_C against 1/T, for Cu(II), Co(II), Zn(II), and Cd(II) at pH 3, 4, 5, and 6, are shown in **Figure 8.28** from which the adsorption thermodynamic parameters ΔH^{ads} and ΔS^{ads} were calculated. These parameters are given in **Table 8.26**. Both parameters have negative values at all conditions for elements under study. Absolute values of ΔH^{ads} between 7.64 and 37.33 kJ mol^{-1} suggest chemisorption as a mechanism, and the negative sign indicate an exothermic process. This specifies chelation as the chemisorption mechanism. For Cu(II) (the highest adsorbed ion), the value of ΔH^{ads} increases with pH suggesting that amine groups control the charge state of the MF-CDTA surface; the same behaviour is observed for MF-DTPA (section 8.1.2).

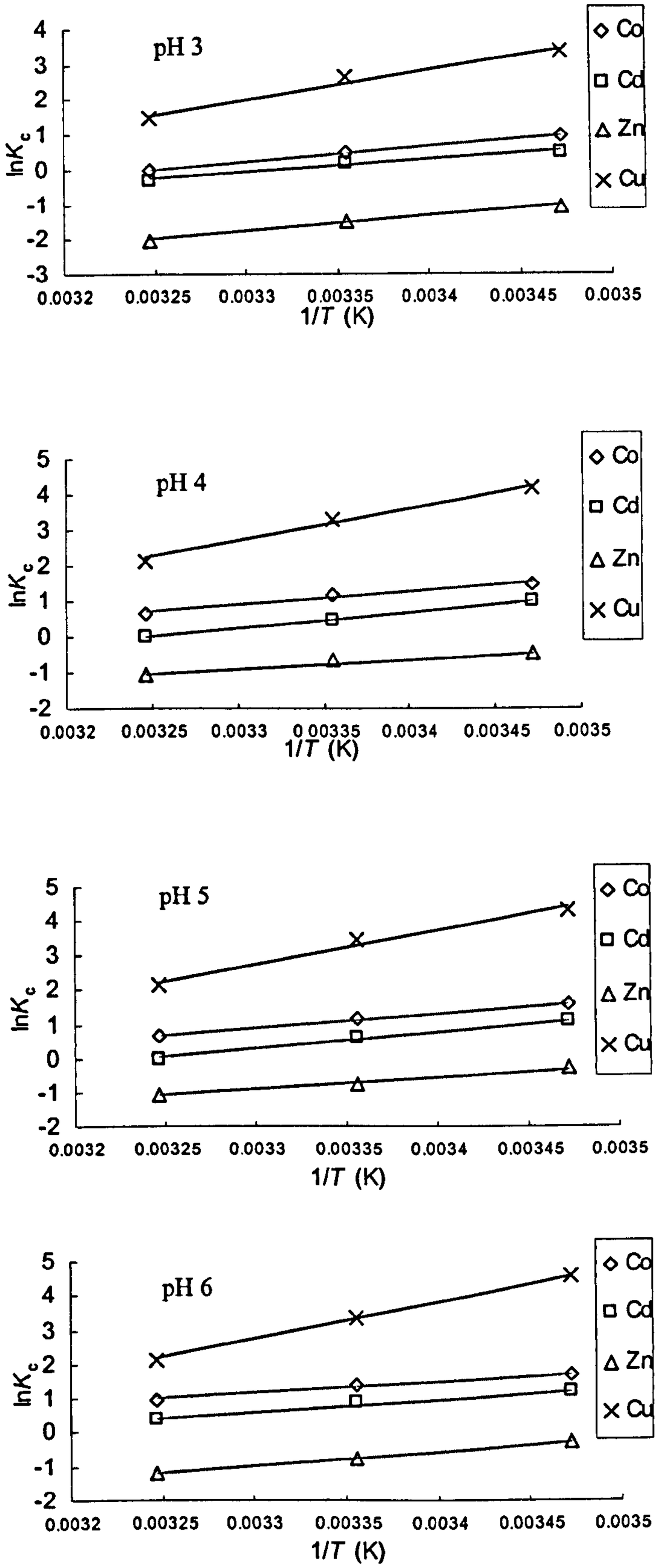

Figure 8.28: Plots of $\ln K_C$ against $1/T$ for Co(II), Cd(II), Zn(II) and Cu(II) adsorption on MF-CDTA at pH 3, 4, 5 and 6.

Table 8.26: Thermodynamic parameters of adsorption on MF-CDTA.

pH	Co(II)		Cd(II)		Zn(II)		Cu(II)	
	$-\Delta H^{ads}$ kJ mol^{-1}	$-\Delta S^{ads}$ J mol^{-1} K^{-1}	$-\Delta H^{ads}$ kJ mol^{-1}	$-\Delta S^{ads}$ J mol^{-1} K^{-1}	$-\Delta H^{ads}$ kJ mol^{-1}	$-\Delta S^{ads}$ J mol^{-1} K^{-1}	$-\Delta H^{ads}$ kJ mol^{-1}	$-\Delta S^{ads}$ J mol^{-1}K^{-1}
3	15.1	49.03	8.94	29.57	9.65	37.33	28.21	86.12
4	7.96	22.77	7.64	23.4	9.13	33.45	32.09	96.69
5	8.25	23.5	8.03	24.48	8.64	31.4	34.75	105.4
6	7.78	21.35	8.22	24.64	9.06	32.67	36.41	110.7

The negative value of entropy means a decrease in degree of freedom that reflects reversibility of the process and ease of regeneration. The role of entropy controlling the adsorption is obvious for MF-CDTA. The Zn(II) ion shows non-spontaneous adsorption as suggested by the ΔG^{ads} positive value. These positive values originate from the higher contribution of the entropy term over the enthalpy term in equation: $\Delta G^{ads} = \Delta H^{ads} - T\Delta S^{ads}$. At certain conditions, $\Delta G^{ads} = 0$ was calculated for for Cd(II) and Co(II) ions **(Table 8.25)**.

It is concluded that the adsorption process is mainly controlled by the entropy change for MF-CDTA. This phenomenon can be explained by considering the M(II)-dehydration process. The liberation of water of hydration molecules from M(II) upon adsorption is accompanied by the adsorption or attraction (restriction) on the hydrophilic surface of the adsorbent. The greater the amount of water molecules to be attracted to the surface, the lower the tendency to adsorb the corresponding M(II) ion(s). This behaviour was not observed for MF-DTPA due to the higher number of coordination positions (8 positions for DTPA and 6 for CDTA) which promotes chelation of all M(II) ions whatever the type of complex structure (tetrahedral and/or octahedral).

It would appear that the entropy change of adsorption, M(II)-dehydration and number of coordinating sites in the PAPC play an essential role in the adsorption process. Comparing the thermodynamic parameters (ΔG^{ads}, ΔH^{ads} and ΔS^{ads}) of adsorption on MF-DTPA, MF-NTA and MF-CDTA confirms the above argument.

The decrease in ΔG^{ads} values has a general order according to the PAPC type as follows: DTPA (8 coordination sites) > CDTA (6 coordination sites) > NTA (4

coordination sites). The chelate formation with 8 coordination sites is exothermic enough (ΔH^{ads}) to compensate for both the endothermic dehydration process (ΔH^{dehyd}) and negative entropy (ΔS^{ads}). This compensation becomes less effective as the number of coordination sites decreases. For chelating agents with lower number of coordination sites, the ΔH^{ads} is not large enough to compensate for the dehydration and entropy change. For example, for MF-CDTA, ΔG^{ads} is positive for Zn(II) and sometimes zero for Co(II) and Cd(II). For MF-NTA, this behaviour is more evident as NTA has only four coordination sites and the ΔH^{ads} is not sufficient to compensate in the case of Cd(II) and Zn(II), and only partially able to compensate for Co(II) and Cu(II) ions.

8.3.4 Relative affinity of MF-CDTA towards M(II) ions

Table 8.27 gives standard values of chelate formation stability constants, enthalpy and entropy of chelate formation of CDTA with stated ions [172]. These values correspond to the formation of the complexes of single ions present in aqueous solutions. Also, the enthalpy of dehydration and hydrated-radius of these ions are given in the table.

Table 8.27: M(II)-CDTA complex formation parameters [172].

M(II)	Log K (25°C)	$\Delta H^{chelate}$ (20°C) (kcal/mole)	$\Delta S^{chelate}$ (25°C) (cal/mole °C)	M(II) Hydrated-radius (Å)	Enthalpy of M(II)-dehydration (kcal/ mole)
Co(II)	19.58	–2.8	80	4.23	476.9
Cd(II)	19.84	–7.4	66	4.26	431.8
Zn(II)	19.35	–1.9	82	4.30	488.9
Cu(II)	21.92	–6.1	80	4.19	501.8

The CDTA molecule has six coordination positions, and hence can normally form 1:1 chelates. The order of removal is Cu(II) > Co(II) > Cd(II) >Zn(II). The Cu(II) ion shows the highest affinity as it requires six coordinations and has the highest formation stability constant.

The chelation-enthalpy and dehydration-enthalpy preference role is limited here as only one molecule is readily available to bind to CDTA and the formation stability constant values control the process. The Cu(II) ion has the lowest hydrated-radius which gives it higher migration probability with respect to other ions, due to the relatively small average pore diameter of MF-CDTA (19 Å). The Co(II), Cd(II) and Zn(II) ions have similar stability constants and the higher removal of Co(II) ion may be due to the smaller hydrated-ionic radius.

It is important to comment on the relation between the enthalpy of adsorption (ΔH^{ads}) and enthalpy of dehydration. The absolute values of ΔH^{ads} (exothermic, **Table 8.26**) are comparatively low with respect to the absolute values of M(II)-dehydration (endothermic **Table 8.27**) which imply that the overall process must be endothermic; however this is not the case. The M(II)–O coordination bond energy can be *assumed* to be in the order of 400 kJ mol^{-1} [181]. Hence six coordinations of M(II) produces energy equal to $400 \times 6 = -2400$ kJ mol^{-1}. The average M(II)-dehydration energy is +1980 kJ mol^{-1}. If the M(II)-dehydration process takes its energy from the coordination process, then the observed value of ΔH^{ads} would equal –420 kJ mol^{-1}. However, the tabulated values of ΔH^{ads} is lower than this, which suggests that more of the coordination-produced energy has been consumed for the dehydration of the MF-CDTA adsorbent surface (which is highly hydrophilic). Hence, the coordination energy compensates for both the dehydration of M(II) ions *and* the adsorbent surface. This explanation can be applied equally to MF-DTPA and MF-NTA.

8.3.5 Effect of initial concentration

The effect of initial concentration of M(II) ions on adsorption was investigated by changing the initial concentrations (20, 30, 40, 50, 60 and 70 mg l^{-1}) with a constant adsorbent amount (0.25 g adsorbent and conditions: T= 20°C and pH =5). **Table 8.28** presents the removal percentage with respect to the initial concentration. For M(II) ions, the removal percentage decreased with increasing initial concentration due to greater competition towards a limited number of binding sites. This behaviour agrees with that for MF-DTPA due to non-selective adsorption.

Table 8.28: Effect of initial-M(II) concentration on removal percentage by MF-CDTA

Initial concentration (mg l^{-1})	Removal percentage ±3%			
	Co(II)	Cd(II)	Zn(II)	Cu(II)
20	60	55	45	80
30	57	50	37	80
40	55	45	35	80
50	52	40	32	76
60	50	38	32	73
70	46	37	29	69

The time profile of the effect of increasing the initial concentration of M(II) (20, 30, 40, 50, 60 and 70 mg l^{-1}) on the adsorbed amount capacity (conditions: 0.25 g adsorbent, $T = 25°C$ and pH = 5) is presented in **Figure 8.29**. The plots showed that the amounts of M(II) ions adsorbed increased smoothly towards the end of the run. The Cu(II) ion shows the highest rate at the beginning especially at higher concentrations indicating its higher affinity towards the MF-CDTA adsorbent over the other M(II) ions .

For the different initial concentrations, M(II)-adsorption saturation was achieved within 20 to 25 minutes which reflect open texture of the MF-CDTA adsorbent. The initial metal concentration provides an important driving force; hence a higher initial concentration of metal ions will increase the sorption rate.

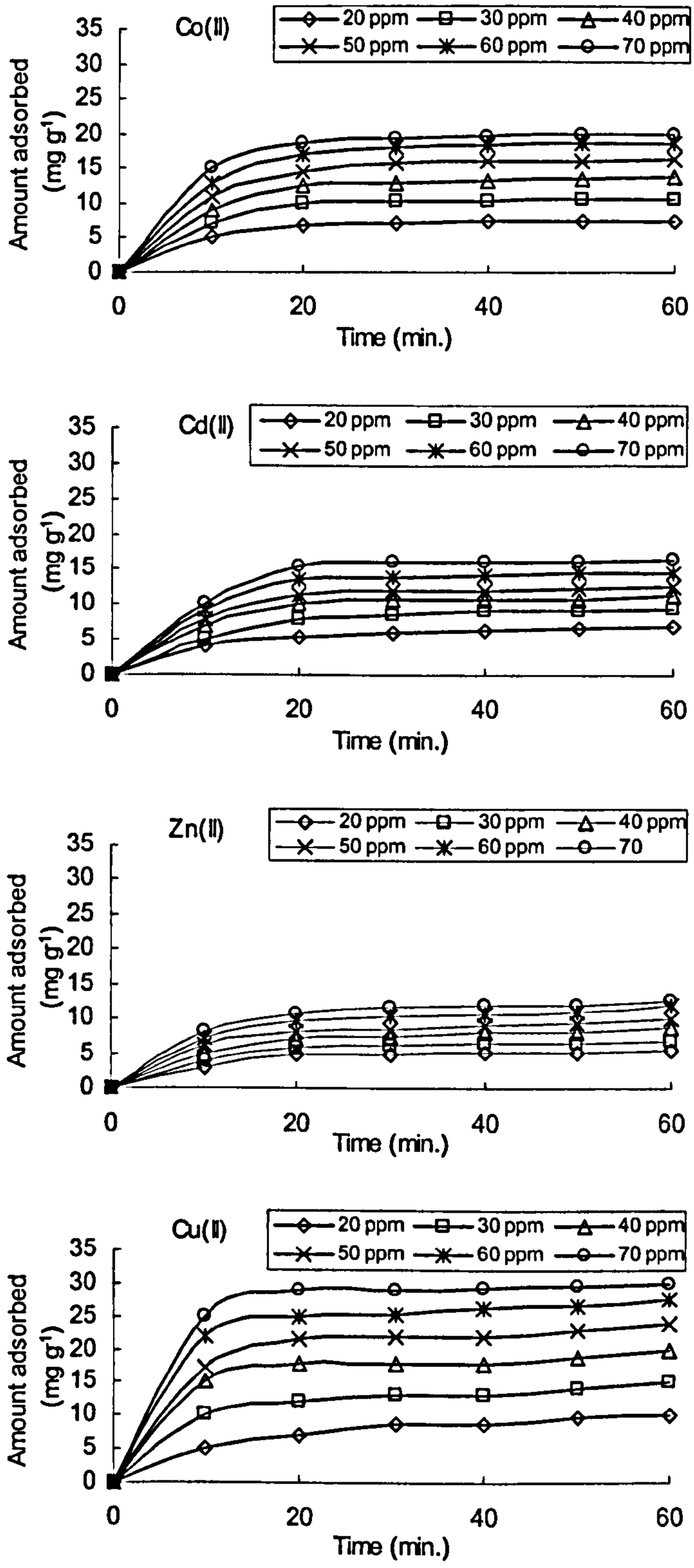

Figure 8.29: Time profile of adsorption on MF-CDTA with the effect of metal ions initial concentration on adsorption capacity at pH 5 and T= 25°C.

Figure 8.30 shows the effect of the metal ion initial concentration on equilibrium adsorption capacity. As observed from the figure, the adsorption capacity increases smoothly with initial concentration and the saturation plateau is likely to start around 70 mg l^{-1}, especially for Zn(II), Cd(II) and Co(II), which indicates the high capacity of MF-CDTA adsorbent. Also, shows a high dependence of adsorption on the ion concentration and reflects the role of the high pore volume (0.868 cm^3 g^{-1}) in the process. The higher the pore volume, the higher the enclosed amount of treated solution and the greater the probability of binding (compared to MF-DTPA).

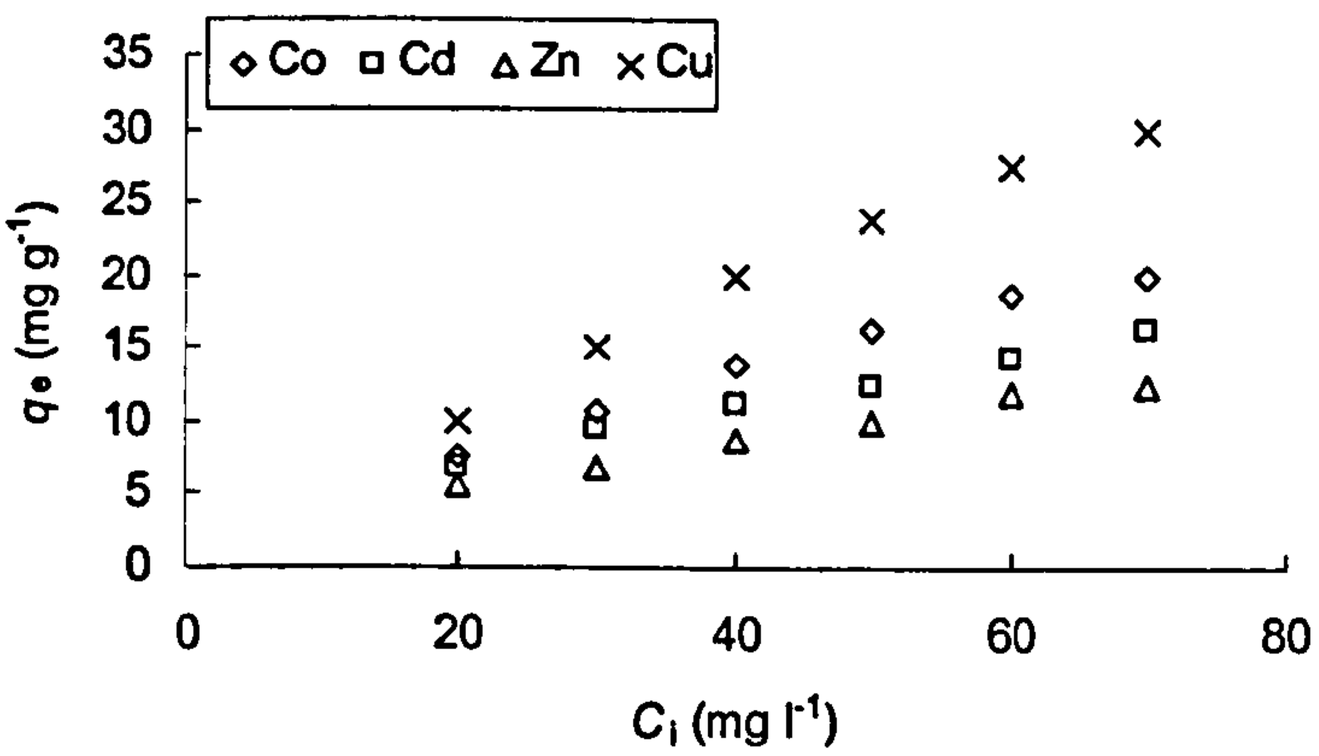

Figure 8.30: Effect of initial concentration of metal ions on adsorption capacity for MF-CDTA at pH 5 and T= 25°C.

8.3.6 Adsorption Kinetics

The variation with time of adsorbed amounts of metal ions at different pH values (3, 4, 5 and 6) and temperatures (15, 25 and 35°C) (**Figures 8.31–8.33**) revealed that Cu(II) has the highest adsorption rate and Zn(II) the lowest. The variation with time of Co(II) and Cd(II) are similar, but Co(II) has a slightly higher rate. The order of adsorption is the same for all conditions: Cu(II) > Co(II) > Cd(II) > Zn(II).

The half load time ($t_{1/2}$) is in the range of minutes (e.g. $t_{1/2}$ at 25°C and pH 5: 24, 34 and 4 minutes for Co(II), Cd(II) and Cu(II) respectively). The figures indicate, in general, that the adsorption rate is greater at lower temperatures and higher pH values.

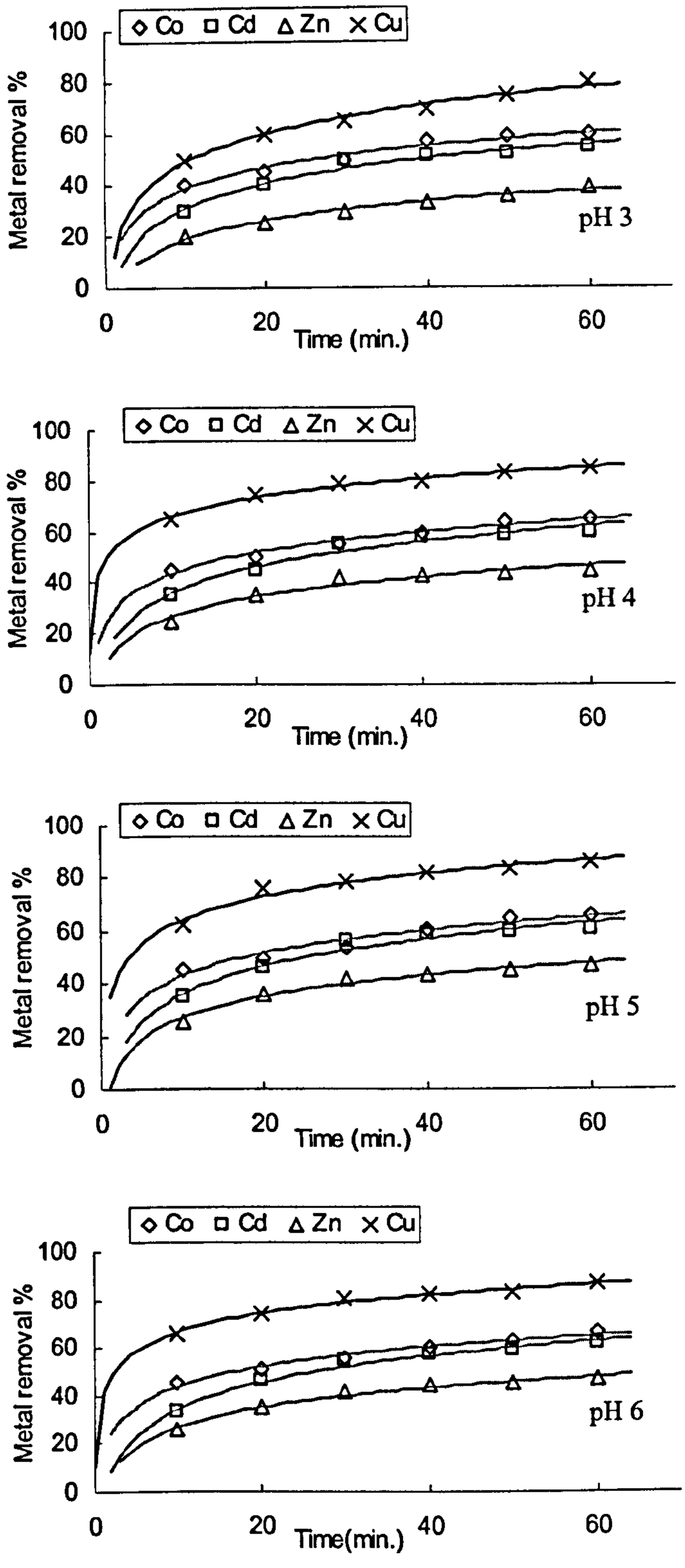

Figure 8.31: Variation of metal removal with time for Co(II), Cd(II), Zn(II) and Cu(II) on MF-CDTA at 15°C for pH 3, 4, 5 and 6.

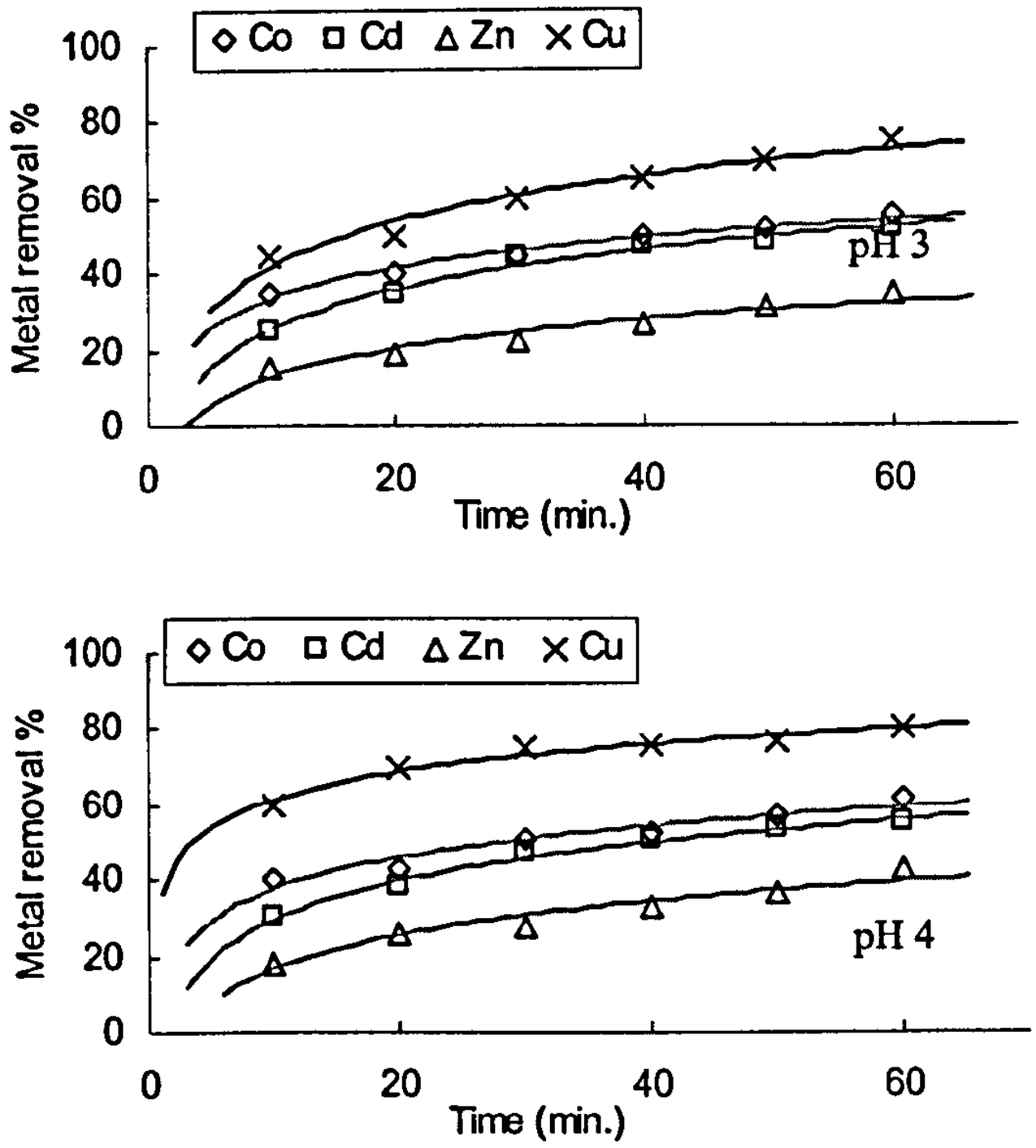

Figure 8.32: Variation of metal removal with time for Co(II), Cd(II), Zn(II) and Cu(II) on MF-CDTA at 25°C for pH 3, 4, 5 and 6.

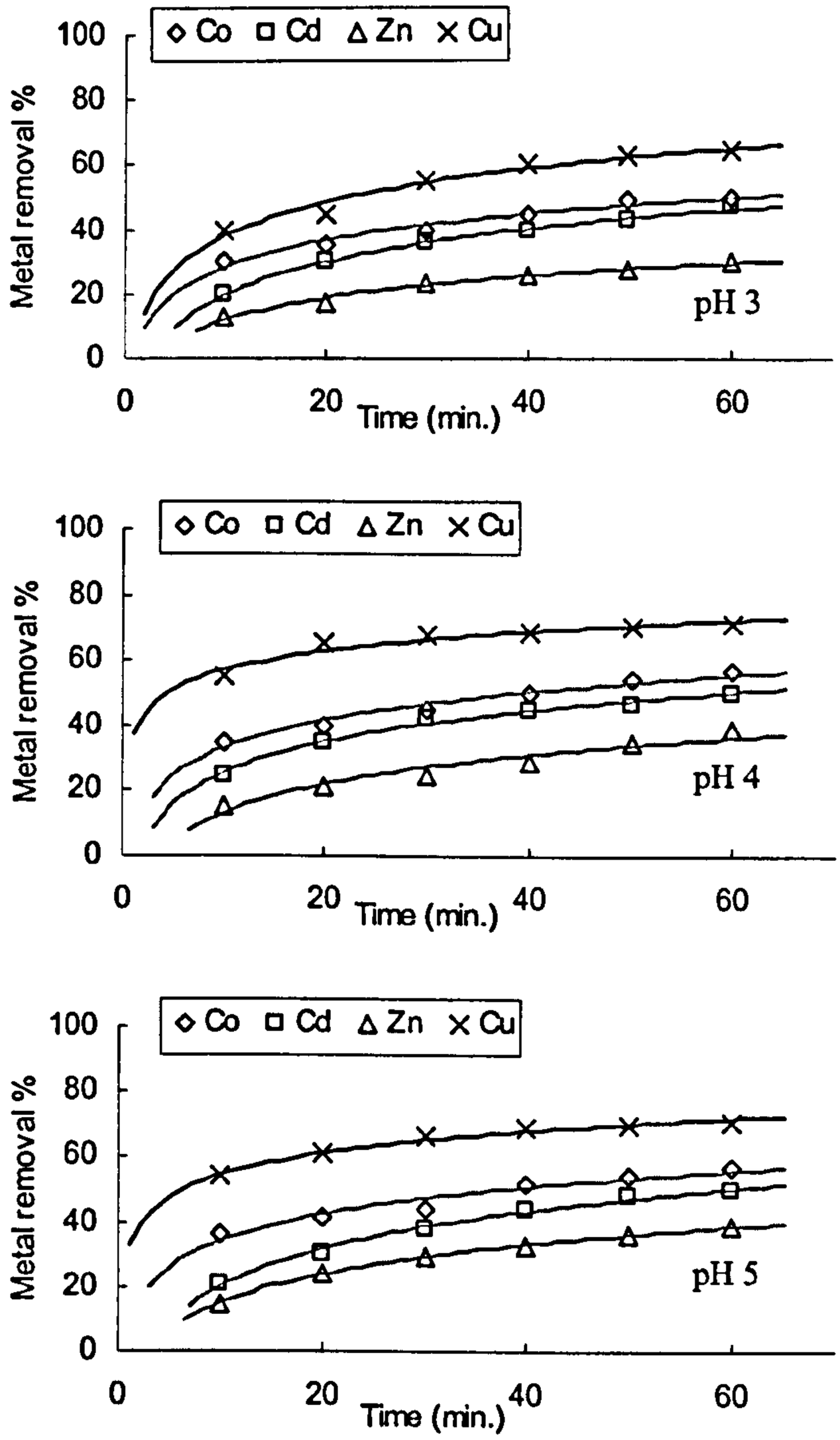

Figure 8.33: Variation of metal removal with time for Co(II), Cd(II), Zn(II) and Cu(II) on MF-CDTA at 35°C for pH 3, 4, 5 and 6.

The removal percentage for all ions increases gradually with time and Cu(II) shows the greatest initial rate. The removal order (Cu(II)> Co(II) > Cd(II) > Zn(II)) follows the order of ionic radius **(Table 8.27)**. This may be due to the pore diameter (19 Å) which affects migration of these ions.

The experimental kinetics data were fitted by the reversible first order and pseudo first order models (Appendix: **Figures 10.8–10.13)** and their constants were calculated and are summarised in **Table 8.29**.

There is a good match between the k_R values (reversible first order model) and their corresponding k_L values (Pseudo first order model) as for the case of MF-DTPA and MF-NTA which indicates same kinetic behaviour. Considering the reversible first order model, the Cu(II) ion has the ratio $k_1/k_2>1$, which means that adsorption is favourable. This is the case also for Co(II) except at one condition (pH 5, 35°C). The rate of desorption of Cd(II) ion is greater than that for adsorption especially at 35°C. For the Zn(II) ion, the rate of desorption is greater than that of adsorption for all conditions ($k_1/k_2 < 1$).

These relations reflect the chemisorption behaviour of the adsorption. The Cu(II) ion shows a higher ratio compared to other ions, and the adsorption rate constant (k_1) is also the highest. Also, fitting the data with the reversible first order model ($R^2 > 0.9$) points to a chemisorption nature of the process.

The fitting of data by the pseudo first order model has the correlation factor, $R^2 > 0.9$. The order of the rate constant values is not the same as the order of removal, and the capacities estimated by the model do not correspond to the experimental capacities

The pseudo second order and Elovich equation were also used to fit the data (Appendix: **Figures 10.14–10.19**). The parameters were calculated and are summarized in **Table 8.30**.

Table 8.29: Reversible first-order and Pseudo first-order parameters of adsorption on MF-CDTA.

M(II)	T (°C)	pH	$q_{exp.}$±3%	reversible first order				pseudo first order		
				k_R	k_1	k_2	R^2	k_L	q_e	R^2
Co(II)	15	3	7.51	0.0743	0.0455	0.0288	0.9589	0.074	7.42	0.9589
		4	8.16	0.0727	0.0472	0.0255	0.9307	0.073	7.66	0.9307
		5	8.26	0.0714	0.0482	0.0232	0.9214	0.071	8.00	0.9214
		6	8.35	0.0520	0.0341	0.0179	0.9593	0.052	6.26	0.9593
	25	3	6.88	0.0546	0.0300	0.0246	0.976	0.055	5.70	0.976
		4	7.50	0.0536	0.0280	0.0256	0.9568	0.054	5.98	0.9568
		5	7.75	0.0599	0.0371	0.0228	0.9397	0.060	7.00	0.9397
		6	7.88	0.0423	0.0280	0.0143	0.9309	0.042	5.77	0.9309
	35	3	6.25	0.0689	0.0445	0.0244	0.9234	0.069	6.68	0.9234
		4	7.50	0.0442	0.0302	0.0140	0.9593	0.044	6.34	0.9593
		5	7.63	0.0481	0.0229	0.0252	0.9445	0.048	6.78	0.9445
		6	7.75	0.0413	0.0326	0.0087	0.9789	0.041	6.66	0.9789
Cd(II)	15	3	6.88	0.0604	0.0332	0.0272	0.9568	0.060	5.86	0.9568
		4	7.50	0.0833	0.0500	0.0333	0.9935	0.083	7.82	0.9935
		5	7.65	0.0827	0.0512	0.0315	0.9838	0.083	8.07	0.9838
		6	7.79	0.0602	0.0378	0.0224	0.9718	0.060	6.75	0.9718
	25	3	6.25	0.0673	0.0279	0.0394	0.9834	0.067	5.70	0.9834
		4	6.88	0.0751	0.0412	0.0339	0.9675	0.075	7.79	0.9675
		5	7.00	0.0882	0.0494	0.0388	0.9513	0.088	8.18	0.9513
		6	7.13	0.0573	0.0289	0.0284	0.9935	0.057	6.25	0.9935
	35	3	6.13	0.0536	0.0226	0.0310	0.9878	0.054	6.48	0.9878
		4	6.88	0.0647	0.0279	0.0368	0.9859	0.065	7.68	0.9859
		5	7.00	0.0566	0.0190	0.0376	0.9771	0.057	7.61	0.9771
		6	7.13	0.0556	0.0435	0.0121	0.9813	0.056	7.38	0.9813
Zn(II)	15	3	4.88	0.0478	0.0186	0.0292	0.9856	0.048	4.50	0.9856
		4	5.63	0.0776	0.0363	0.0413	0.9871	0.078	5.34	0.9871
		5	5.84	0.0676	0.0300	0.0376	0.9907	0.068	5.28	0.9907
		6	5.88	0.0644	0.0301	0.0343	0.9873	0.064	5.20	0.9873
	25	3	4.38	0.0394	0.0138	0.0256	0.9601	0.039	4.33	0.9601
		4	5.13	0.0389	0.0156	0.0233	0.9822	0.039	4.80	0.9822
		5	5.25	0.0369	0.0155	0.0214	0.9871	0.037	4.82	0.9616
		6	5.25	0.0357	0.0150	0.0207	0.9770	0.036	4.75	0.977
	35	3	4.13	0.0481	0.0159	0.0322	0.9889	0.048	4.33	0.9889
		4	4.88	0.0408	0.0159	0.0249	0.9445	0.041	5.03	0.9445
		5	5.13	0.0433	0.0161	0.0272	0.9816	0.043	4.93	09816
		6	5.13	0.0499	0.0186	0.0313	0.9774	0.050	5.35	0.9774
Cu(II)	15	3	10	0.0498	0.0398	0.0100	09628	0.050	7.90	0.9628
		4	10.63	0.0676	0.0569	0.0107	0.9262	0.068	6.57	0.9262
		5	10.75	0.0701	0.0603	0.0098	0.9611	0.070	7.39	0.9611
		6	10.85	0.0595	0.0513	0.0082	0.8979	0.60	6.43	0.8979
	25	3	9.38	0.0496	0.0372	0.0124	0.9732	0.050	8.05	0.9732
		4	10.04	0.0608	0.0504	0.0104	0.9013	0.061	5.94	0.9013
		5	10.13	0.0947	0.0696	0.0251	0.9616	0.095	8.77	0.9616
		6	10.04	0.1206	0.0671	0.0535	0.9479	0.121	11.19	0.9479
	35	3	8.13	0.0655	0.0426	0.0229	0.9800	0.065	7.83	0.9800
		4	8.79	0.139	0.0817	0.0573	09510	0.139	7.28	0.9510
		5	8.81	0.11	0.0663	0.0437	0.9839	0.110	7.37	0.9839
		6	8.88	0.0821	0.0579	0.0242	0.9446	0.082	5.75	0.9446

The Elovich model predicts that the initial adsorption rate for Cu(II) is the highest. It is observed that, for most conditions, the initial-adsorption rate (α) is higher for pH 4 and 5, which suggests that these values are preferable for the removal process. For Co(II), Cd(II) and Zn(II) ions, the value of α increases as the temperature is decreased (especially for pH= 4, 5 and 6) suggesting that chelation is the dominant mechanism of adsorption. For the Cu(II) ion, there is no specific trend suggesting that adsorption of the Cu(II) ion occurs by chelation and ion exchange. For Co(II) and Cd(II) ions, the values of β are similar (for each ion) at different temperatures suggesting that temperature does not affect the stability of the chelated ions on the adsorbent surface. However, the ratio β/α decreases with decreasing temperature suggesting a greater surface coverage at lower temperatures [114]. For the Z(II) ion, the values of β (compared to α) shows that removal process is shifted towards desorption, especially at 35°C. In general, the values of α and β follow the adsorption order suggesting a good representation of this model for the adsorption process. The values of α are reasonable at representing the adsorption process when compared to the corresponding values for the MF-DTPA system. Furthermore, the correlation factor for MF-CDTA ($R^2 > 0.92$) is in general higher than that for MF-DTPA ($R^2 > 0.85$). These observations may indicate that the MF-CDTA surface is less homogeneous than that of MF-DTPA.

The fitting of data with the pseudo second order model has an R^2 value greater than 0.91 (except for Zn(II) at three different conditions) but for Cu(II), the R^2 about 0.99. The rate constants do not represent the removal order as in the case of the pseudo first order model. The estimate of capacity (q_e) with respect to experimental values (q_{exp}) by this model is better than that for the pseudo first order model. The values of the initial-adsorption rate (h) are generally lower than the corresponding values of α, but follow the removal order. The values of the pseudo second order model are supposed to be more reliable than those of the Elovich model.

According to the fitting, it is recommended that the reversible first order model is used to calculate the rate constants with the aid of the pseudo second-order model to estimate the adsorption capacity (q_e) and initial adsorption rate.

A careful study of the values of the rate constants k_R, k_L and k_H (at the same conditions of temperature and initial pH) indicates that they do not represent the affinity order suggested (Cu(II) > Co(II) > Cd(II) > Zn(II)). Also they do not represent the order of the adsorption sequence during early stages of the process. This behaviour may reflect the effectiveness of the reversible chemisorption nature of the process, where different M(II) ions can swap with each other as in the case of MF-DTPA (section 8.1.5). This gives an indication of the similar behaviour of MF-PAPC adsorbents due to their similar structure.

Furthermore, it is observed that the values of the rate constants k_R, k_L and k_H are higher at the lowest temperature for Co(II), Cd(II) and Zn(II) which suggests chelation to be the main mechanism of adsorption. On the contrary, Cu(II) shows the higher removal at higher temperature. This means that the ion exchange mechanism is significant for Cu(II) adsorption, and that the affinity order is not dependent on the chelation parameters (M(II)-CDTA formation stability constant, enthalpy of chelation). The contribution of ion exchange was also expected from elemental analysis (section 8.3.2). This investigation reflects the complex situation of simultaneous removal of M(II) ions by a particular adsorbent. A single-component adsorption for each M(II) ion would give more understanding of the process.

Generally, for the MF-PAPC adsorbents, the pseudo second-order model gave the highest correlation to the experimental data. This suggests that these sorption systems are controlled by chemisorption, which involves valence forces through sharing or exchange of electrons between sorbent and sorbate, i.e. coordination [111]. It is important to comment that for many adsorption systems, the chemical reaction is significant as the rate-controlling step, with some contribution from mass transfer. The pseudo second-order model provides the best fit to the corresponding experimental data of such cases [111,182].

Table 8.30: Pseudo second order and Elovich parameters of adsorption on MF-CDTA.

M(II)	T (°C)	pH	$q_{exp.}$ ±3%	pseudo second order			Elovich			
				k_H	q_e	h	R^2	α	β	R^2
Co(II)	15	3	7.51	0.028	7.87	1.734	0.9829	0.661	0.661	0.9610
		4	8.16	0.029	8.42	2.056	0.9862	5.838	0.676	0.9697
		5	8.26	0.026	8.59	1.918	0.9817	4.89	0.639	0.9490
		6	8.35	0.028	8.51	2.0278	0.9857	5.685	0.663	0.9794
	25	3	6.88	0.028	7.11	1.415	0.9804	2.75	0.703	0.9768
		4	7.50	0.028	7.70	1.660	0.9811	3.408	0.660	0.9310
		5	7.75	0.024	8.04	1.551	0.9775	3.176	0.629	0.9584
		6	7.88	0.026	7.92	1.631	0.9772	2.91	0.606	0.9715
	35	3	6.25	0.025	6.61	1.092	0.9717	1.643	0.676	0.9697
		4	7.50	0.020	7.70	1.186	0.9607	2.224	0.641	0.963
		5	7.63	0.019	7.90	1.186	0.9559	2.552	0.664	0.9403
		6	7.75	0.016	8.01	1.027	0.9522	1.402	0.514	0.9667
Cd(II)	15	3	6.88	0.025	7.27	1.321	0.978	0.571	0.571	0.9589
		4	7.50	0.025	8.01	1.604	0.9825	2.095	0.543	0.9617
		5	7.65	0.023	8.22	1.554	0.9799	2.042	0.524	0.9605
		6	7.79	0.021	8.26	1.433	0.9774	1.71	0.498	0.9759
	25	3	6.25	0.022	6.78	1.011	0.9684	1.029	0.533	0.9734
		4	6.88	0.021	7.42	1.156	0.9712	1.36	0.539	0.9852
		5	7.00	0.024	8.04	1.551	0.9775	1.393	0.514	0.9599
		6	7.13	0.024	7.48	1.343	0.9791	1.286	0.500	0.9913
	35	3	6.13	0.014	6.82	0.651	0.9289	0.707	0.543	0.9979
		4	6.88	0.015	7.63	0.873	0.9474	1.085	0.577	0.9936
		5	7.00	0.011	7.92	0.690	0.9179	0.688	0.474	0.9916
		6	7.13	0.011	8.04	0.711	0.9196	0.805	0.428	0.9516
Zn(II)	15	3	4.88	0.025	5.14	0.660	0.9554	0.758	0.758	0.9814
		4	5.63	0.034	6.00	1.224	0.9824	1.481	0.706	0.9451
		5	5.84	0.031	6.19	1.188	0.9818	1.51	0.687	0.9724
		6	5.88	0.031	6.22	1.199	0.9812	1.435	0.676	0.9752
	25	3	4.38	0.017	4.69	0.374	0.8843	0.443	0.732	0.9202
		4	5.13	0.018	5.14	0.476	0.9173	0.59	0.621	0.9402
		5	5.25	0.017	5.51	0.516	0.9120	0.6	0.646	0.9359
		6	5.25	0.017	5.49	0.512	0.9115	0.578	0.635	0.9435
	35	3	4.13	0.017	4.67	0.371	0.8886	0.416	0.810	0.9789
		4	4.88	0.014	5.33	0.398	0.8714	0.444	0.614	0.9424
		5	5.13	0.018	5.50	0.545	0.9265	0.507	0.604	0.9989
		6	5.13	0.016	5.63	0.507	0.9211	0.477	0.619	0.9889
Cu(II)	15	3	10.00	0.020	10.22	2.089	0.9804	0.495	0.495	0.9824
		4	10.63	0.045	10.78	5.229	0.9968	64.658	0.748	0.9775
		5	10.75	0.037	10.99	4.469	0.9958	23.783	0.624	0.9579
		6	10.85	0.041	10.96	4.925	0.9959	51.074	0.709	0.9734
	25	3	9.38	0.017	9.73	1.609	0.9689	2.516	0.468	0.9542
		4	10.04	0.018	10.15	1.854	0.9962	43.477	0.755	0.9623
		5	10.13	0.039	10.45	4.259	0.9957	13.605	0.598	0.9779
		6	10.04	0.048	10.33	5.122	0.9972	63.339	0.765	0.9479
	35	3	8.13	0.021	8.58	1.546	0.9764	2.357	0.539	0.9655
		4	8.79	0.076	9.01	6.170	0.9979	79.729	0.942	0.9247
		5	8.81	0.065	9.03	5.300	0.9978	31.128	0.814	0.9867
		6	8.88	0.055	9.09	4.545	0.9966	16.99	0.730	0.9519

The magnitude of activation energy may give an idea about the type of adsorption. The Arrhenius plots (adsorption rate constant k_1 of reversible first order model) of Co(II), Cd(II), Zn(II) and Cu(II) on MF-CDTA at pH 5 are shown in **Figure 8.34.**

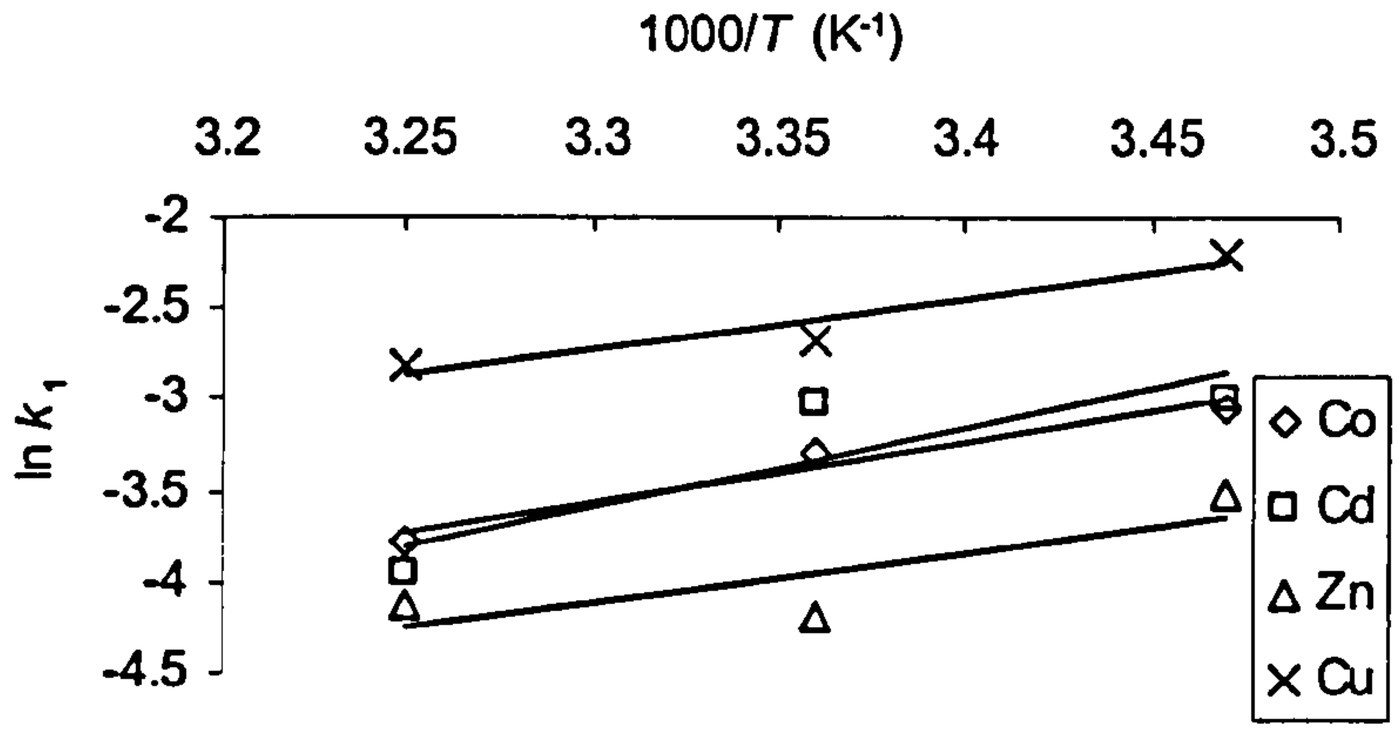

Figure 8.34: Arrhenius plots of Co(II), Cd(II), Zn(II) and Cu(II) adsorption onto MF-CDTA at pH 5.

The plots have positive slopes (negative values of E_a) corresponding to exothermic adsorption. The activation energies (E_a) of adsorption were calculated from the slopes of these plots and the absolute values were found to be 28, 36, 23 and 22 kJ mol^{-1} for Co(II), Cd(II), Zn(II) and Cu(II) respectively. These values are in the range of physisorption but as kinetic models highly suggest a chemisorption process, we can conclude that these values indicate high affinity of adsorbent to M(II) ions. The order of these values agrees with the affinity order except for Zn(II).

Plots of M(II)-adsorbed amounts (q_t) against time at different temperatures and initial pH values were determined (Appendix: **Figures 10.20–10.22**). From figures, an initial stage (0–30 minutes) for film diffusion and a latter stage (30–60 minutes) for pore diffusion are possibilities. Plots of adsorption data using **equations (18)** and **(19)** were determined (Appendix: **Figures 10.23–10.28**). From these figures, the corresponding film and pore diffusion coefficients (D_1 and D_2) were calculated and are presented in **Table 8.31.**

Table 8.31: Diffusion parameters of adsorption of M(II) on MF-CDTA.

Temp. (°C)	pH	$(D_1 \pm 0.03) \times 10^{-9}$ ($cm^2\ s^{-1}$)				$(D_2 \pm 3) \times 10^{-8}$ ($cm^2\ s^{-1}$)			
		Co(II)	Cd(II)	Zn(II)	Cu(II)	Co(II)	Cd(II)	Zn(II)	Cu(II)
15	3	5.3	25.2	12.5	6.9	13.8	3.1	6.6	6.6
	4	4.5	21.1	27.6	5.4	13.8	9.6	6.6	6.6
	5	3.6	22.6	22.5	7.9	14.9	9.4	5.5	7.5
	6	5.2	24.3	22.3	5.7	6.1	5.1	5.5	2.4
25	3	6.3	28.1	7.7	7.4	7.2	3.4	7.1	6.6
	4	5.8	18.1	10.8	6.9	4.7	12.5	5.5	3.1
	5	5.0	24.3	10.6	8.5	10.7	10.7	9.8	10.7
	6	7.9	20.4	11.0	7.0	4.2	4.7	4.2	8.3
35	3	7.6	22.5	20.8	9.8	13.8	6.1	7.5	9.6
	4	5.8	22.3	12.7	6.7	8.3	5.9	7.5	6.6
	5	3.8	22.1	25.1	5.5	8.8	9.6	10.7	7.2
	6	8.9	40.1	19.2	7.9	9.2	10.7	10.7	7.8

For Cd(II) and Zn(II) ions, the D_1 values are in the range of film diffusion [178] and are very near to this range for Co(II) and Cu(II). This means that the overall process depend on film diffusion. The D_2 values are out of the range of pore diffusion [178] and considerably greater than typical values. This implies that pore diffusion has a limited effect on the rate of adsorption compared to film diffusion. This may originate from the M(II)-attracting hydrophilic surface of MF-CDTA. The D_2 values of MF-DTPA (section 8.1.5) are generally higher than those for MF-CDTA and this may be due to the higher average pore diameter of MF-DTPA.

No significant correlation between the type of M(II), pH and temperature with film and pore diffusion coefficients can be observed and this may be due to the fact that the adsorption process is carried out using multi-element solutions. This phenomenon was observed for MF-DTPA as well.

In general, the kinetics shows that adsorption is chemical, reversible, considerably fast (one hour duration) and dependent on film diffusion.

8.3.7 Adsorption isotherm

Figure 8.35 shows adsorption isotherm of Co(II), Cd(II), Zn(II) and Cu(II) at 25°C and pH 5 where q_e increases with C_e. The Cu(II)-isotherm is higher than the other M(II) isotherms. The M(II)-isotherms are positive and concave to the concentration axis. The isotherms are of type I (Langmuir adsorption according to Brunauer's classification). The isotherm curves were fitted using experimental data excluding origin. However, the isotherm curves were extrapolated and found to pass through origin.

The equilibrium capacity (q_e) of Cu(II) increases rapidly with equilibrium concentration (C_e) indicating greater affinity for adsorption over other M(II) ions. Also, the slow approach to equilibrium at higher M(II) concentrations is expected due to the higher MF-CDTA capacity. Comparing these isotherms with those for MF-DTPA (**Figure 8.8**), it is clear that MF-CDTA has a higher equilibrium capacity for all M(II) ions.

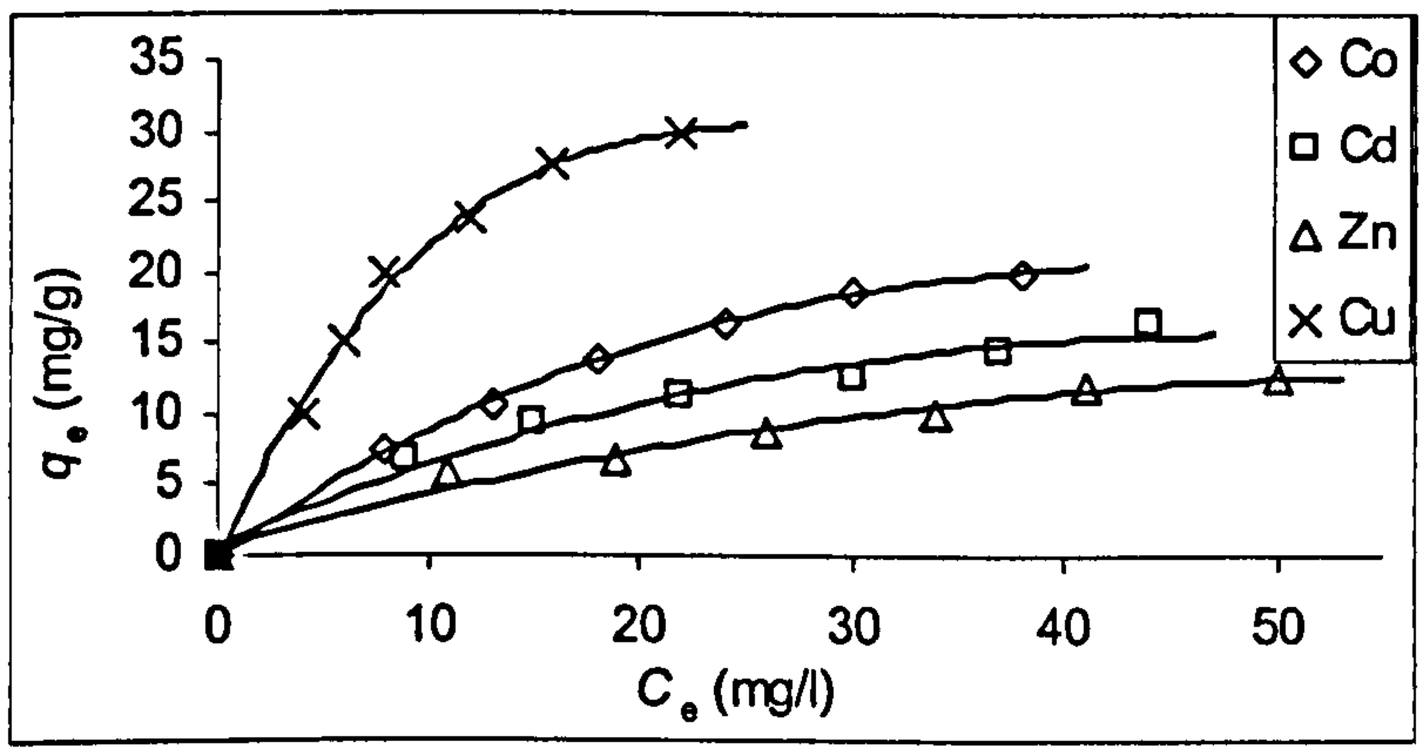

Figure 8.35: Adsorption isotherm (25°C) of Co(II), Cd(II), Zn(II) and Cu(II) on MF-CDTA at pH 5 and 120 minute equilibrium contact time.

The plots of the MF-CDTA adsorption isotherm data according to Freundlich and Langmuir are shown in **Figures 8.36** and **8.37** respectively. From these plots, the related constants were calculated and these are summarised in **Table 8.32**.

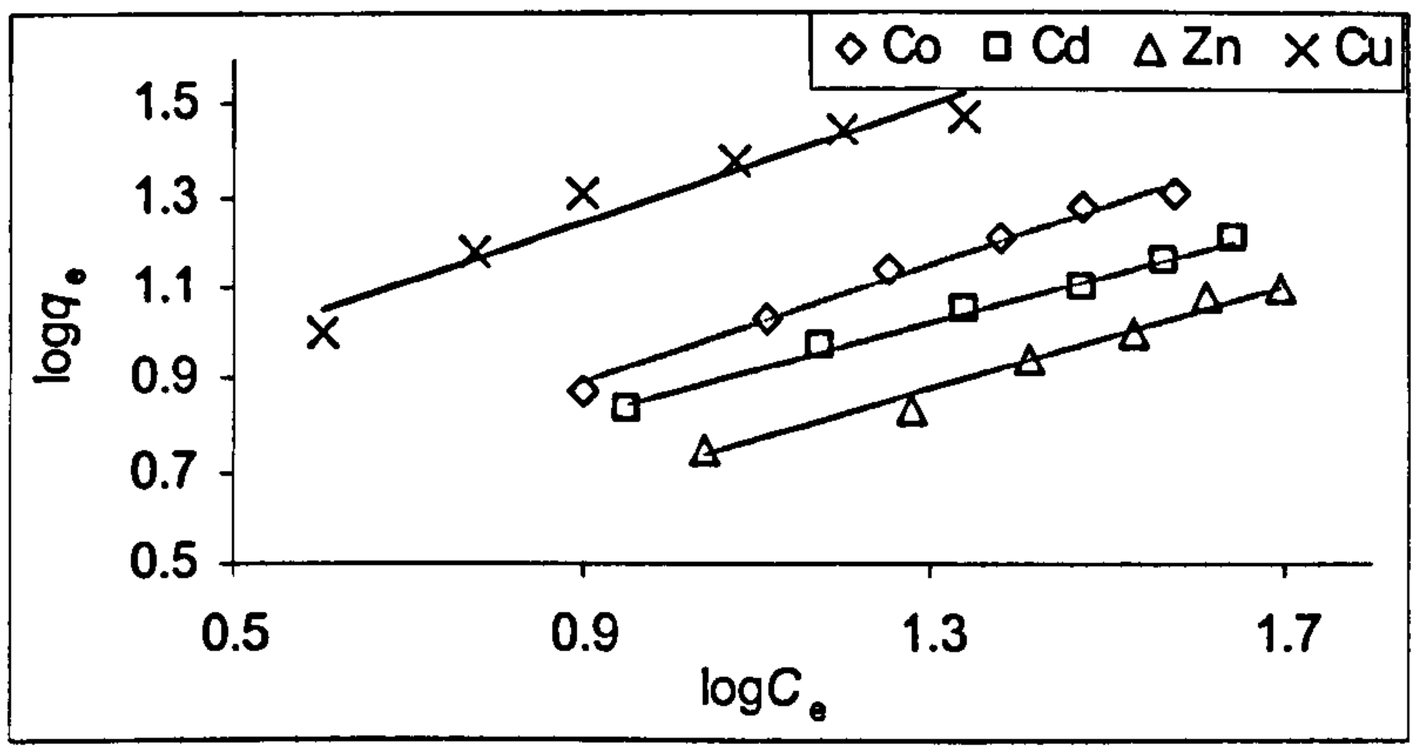

Figure 8.36: Plot of adsorption data using Freundlich (25°C) of Co(II), Cd(II), Zn(II) and Cu(II) on MF-CDTA at pH 5.

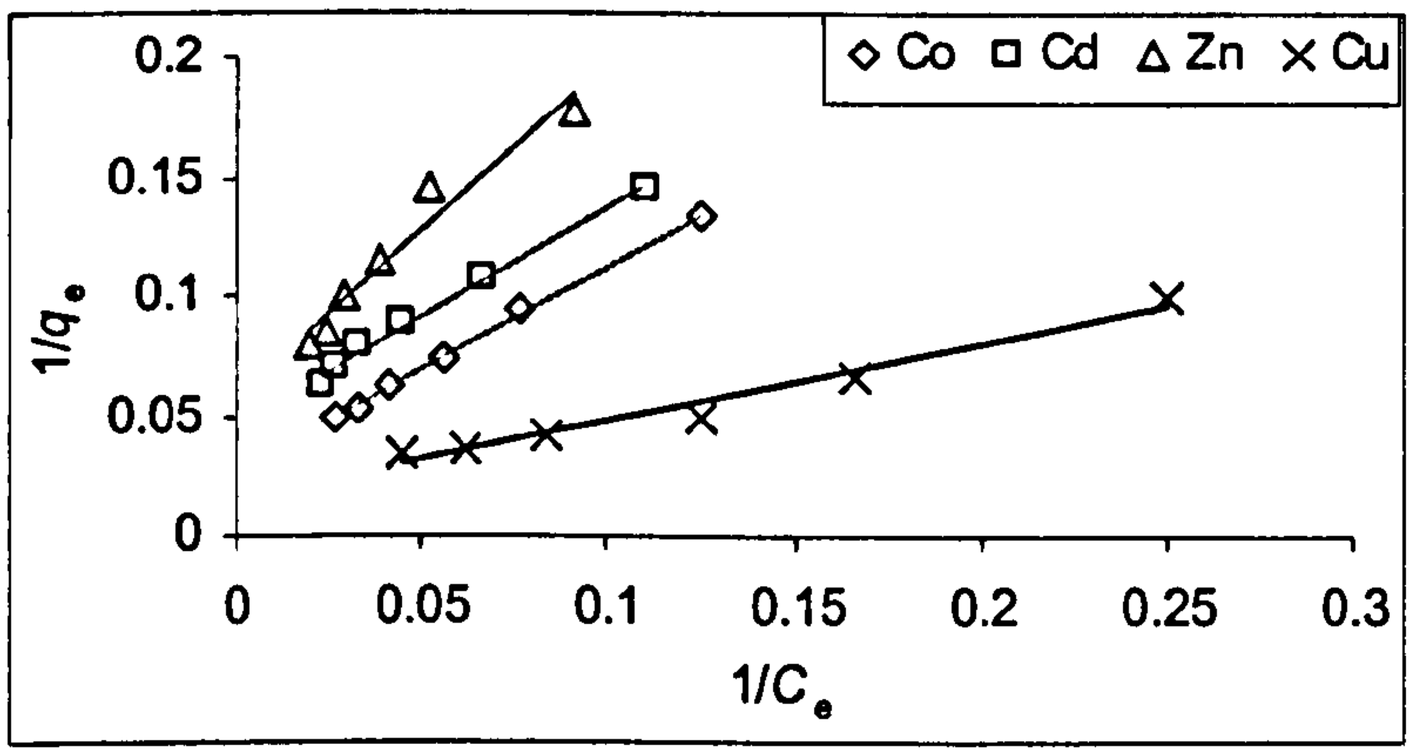

Figure 8.37: Plot of adsorption data using Langmuir (25°C) of Co(II), Cd(II), Zn(II) and Cu(II) on MF-CDTA at pH 5.

Table 8.32: The adsorption isotherm constants for the Freundlich and Langmuir models (MF-CDTA).

Adsorption Model	Co(II)	Cd(II)	Zn(II)	Cu(II)
Freundlich				
k_F ((mg g^{-1})(mg l^{-1})^n)	2.01	2.24	1.42	4.68
$1/n$	0.65	0.52	0.56	0.63
R^2	0.9876	0.9924	0.9821	0.9463
Langmuir				
Q_o (mg g^{-1})	38.6	21.9	17.6	66.7
Q_o (mmole g^{-1}) (total = 2.17 mmole g^{-1})	0.66	0.19	0.27	1.05
b (l mg^{-1})	0.03	0.05	0.04	0.05
R_L	0.32	0.22	0.26	0.22
R^2	0.9983	0.9904	0.9520	0.9793

The value of the Freundlich parameter $1/n$ indicates favourable adsorption for all ions ($0 < 1/n < 1$). The values of n between 1 and 10 indicate that adsorption is reversible for all M(II) ions [154]. The Freundlich parameter k_F is related to capacity and so as this parameter increases, so does the maximum capacity. Here, the values are different (contrary to the MF-DTPA case) and to some extent represent the order of adsorption.

The Langmuir capacity (Q_o) values are: Co (38.6), Cd (21.9), Zn (17.6) and Cu (66.7 mg g^{-1}), which is equivalent to 2.12 mmole M(II) per gram of adsorbent. This value is lower than the value calculated from elemental analysis (3.59 mmole M(II)/gram adsorbent, section 8.3.2). This difference may originate from the difference in the M(II) ions used for experiments. The values of M(II) capacities for MF-CDTA are not similar, which is not the case for MF-DTPA. This indicates a more selective behaviour for MF-CDTA.

For elemental analysis (section 8.3.2), Cu(II) was present solely in solution and the chelate formed was Cu(II)-CDTA. However, the isotherm study was carried out using a mixture of M(II) ions. The predicted capacity according to the isotherm is in agreement with elemental analysis (the calculated concentration of CDTA is 2.28 mmole/g adsorbent, section 7.3.1). However, this agreement does not necessarily mean that chelation follows the ratio of 1:1 [M(II) : CDTA].

The effect of Na(I) in solution on the adsorption appears to be negligible. The parameter R_L is in the range of favourable adsorption for all metal ions ($0 < R_L < 1$). The Langmuir correlation factors are, in general, higher than these for the Freundlich model (namely for Cu(II) and Co(II) which have the highest adsorption capacities). This suggests that the Langmuir model best represents the adsorption process. This reflects a homogeneous surface due to the main role of CDTA sites for adsorption, and that the chemisorption process is reversible. The reversible nature of this adsorption process originates from the fact that metal ions are present in solution in complex form as $M^{2+}(H_2O)_n$ (for example; $Cu^{2+}(H_2O)_6$), and the energy state of this complex form is comparable to that of the M(II)-chelated form. Hence, it is possible

that there is a certain equilibrium position for the M(II) ion between the aqueous phase and adsorbed phase.

The Freundlich model gives a better representation for adsorption for MF-CDTA than for MF-DTPA. This may imply that MF-CDTA has a more heterogeneous surface than MF-DTPA, and this can be confirmed by the results of the Elovich model for both adsorbents (sections 8.1.5 and 8.3.6).

The *batch experiments* the adsorption of M(II) ions on MF-PAPC adsorbents infers that the adsorption behaviour depends on the type of PAPC anchored to the MF matrix. The selectivity order is different for MF-DTPA, MF-NTA and MF-CDTA and does not solely depend on the chelate formation constants, but also depends on other physical properties such as chelation enthalpy and entropy, enthalpies of M(II)-dehydration, M(II)-radii (especially for MF-CDTA) and the contribution of the ion exchange mechanism.

The M(II)-adsorption capacity of MF-PAPC is suitable for practical applications. The overall process is chemisorption (chelation and ion exchange), exothermic, reversible and does *not* depend on the initial pH. Regeneration of the adsorbents is achieved using a solution of chelating agent.

8.4 Adsorption of Cu(II) on MF-DTPA (continuous method)

8.4.1 Adsorption process (in up-flow MF-DTPA packed column)

Initially in the up-flow mode, when Cu(II) solution was introduced into the blank adsorbent bed, almost all Cu(II) ions were bonded to the chelating sites of the bottom layer of the adsorbent, which can be imagined as a slice of the adsorbent and can be recognised as adsorption-zone. As operation continued, this slice became saturated by Cu(II) ions so that the adsorption-zone moved upwards to the next slice. This ascending process is smooth and slices are merging, not discrete. The process continued until it reached the top of the adsorbent bed where the last slice became saturated and concentration of Cu(II) started to increase in the effluent until it was equal to the initial influent concentration [139]. The process is shown in **Figure 8.38.**

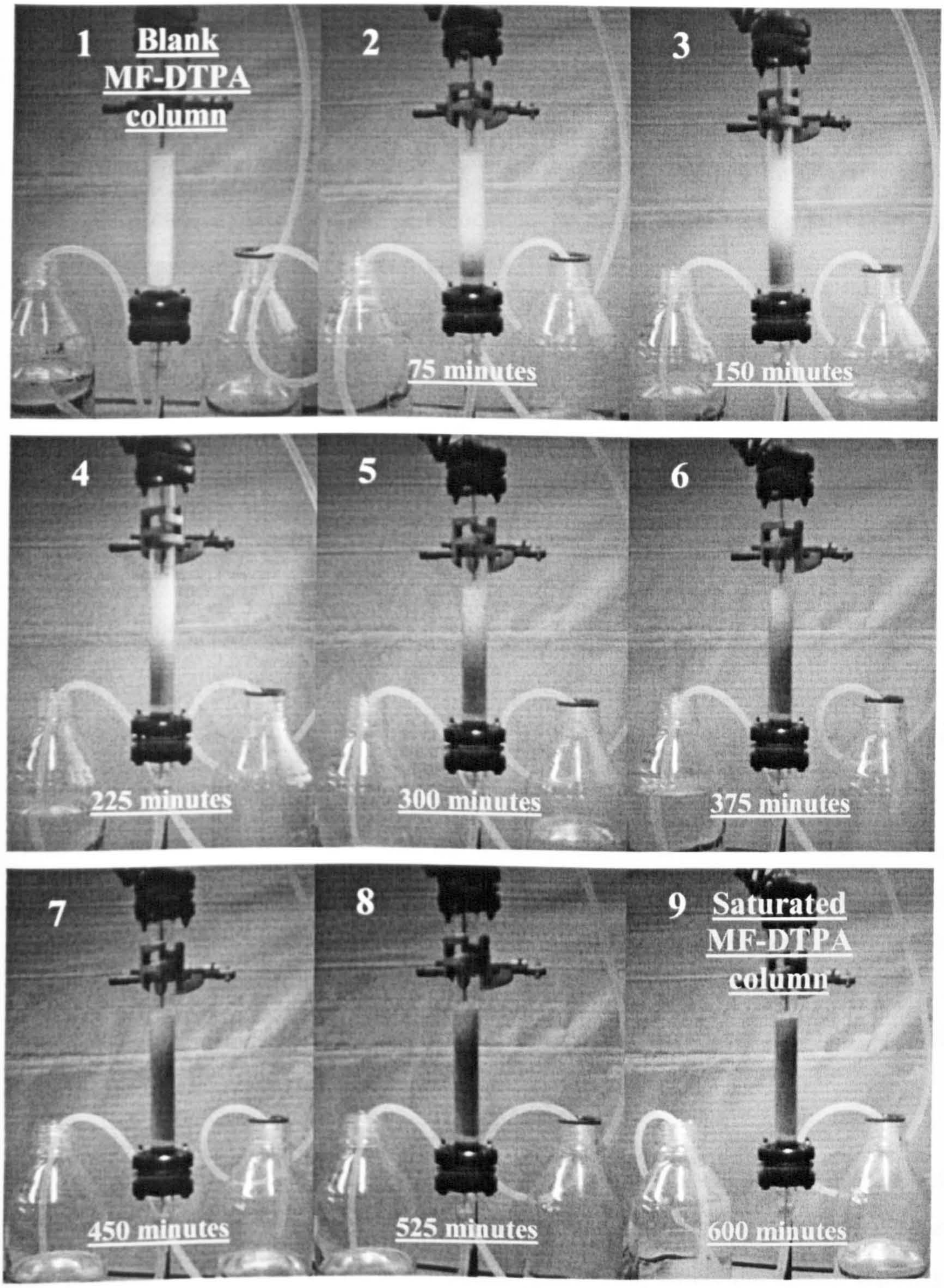

Figure 8.38: Cu(II)-adsorption stages on MF-DTPA in up-flow backed column system (9 cm).

8.4.2 Effect of bed height on adsorption

The adsorption of Cu(II) in the fixed-bed column is largely dependent on the quantity of adsorbent inside the column. The breakthrough curves (C_t/C_o versus time) of Cu(II) adsorption on MF-DTPA adsorbent-packed column for the bed heights 5, 7 and 9 cm at Cu(II)-solution flow rate of 5.5 ml min^{-1} and initial concentration of 30 mg l^{-1} are shown in **Figure 8.39**. They have the "S" shape profile characterizing ideal adsorption system which is associated with adsorbate of small diameter compared to adsorbent pore diameter [145,183].

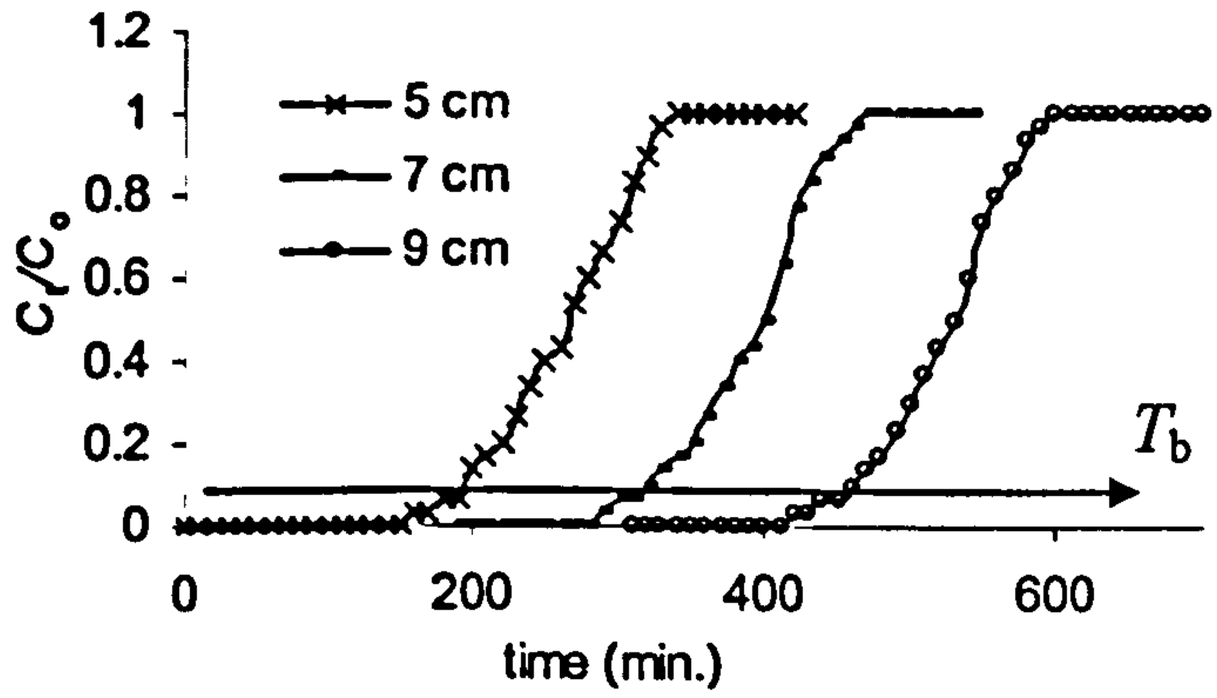

Figure 8.39: Breakthrough curves for Cu(II) adsorption on MF-DTPA at three different bed heights.

From the curves we can observe that the break-point, T_b at C_t/C_o= 0.1, increases as bed height increases. The increase of bed height means an increase of the amount of adsorbent in column which causes increase of amount of chelating sites. This result in a longer time for activity and more solution volume to be treated [144]. The T_b values were 195, 320 and 460 minutes and treated volumes were 1072, 1788 and 2530 ml for bed height 5, 7 and 9 cm respectively **(Table 8.33)**.

Theoretically, the equilibrium capacity (q_m) should be constant as the amount of removed Cu(II) should increase linearly with bed height (adsorbent amount). This ideal behaviour was observed for some studies [184–186] where the uptake capacity remains "almost" identical for different bed heights. For these studies, it is clearly observed that the breakthrough curve becomes steeper as the bed height is decreased. However, this is not true for cases when the effect of radial dispersion of M(II) in the

bed is considerable. For the MF-DTPA column, this effect seems to a play a role as the equilibrium capacity, q_m, shows an increase with bed height **(Tables 8.33)**.

The phenomenon can be explained by considering the role of mass transfer in the process. For smaller bed height, axial dispersion dominates for mass transfer and this reduces the radial diffusion of M(II) ions. But as bed height increases, radial dispersion has a larger contribution to mass transfer which means more time for M(II) ions to diffuse into the adsorbent pores. This lead to more active sites to be accessed for M(II)-binding, hence increase of capacity [145]. In other words, this behaviour can be regarded as a result of increase of residence time (more contact time duration with adsorbent) of each unit volume of the solution being treated. The steepness of the breakthrough curves did not change with bed height, which indicates no broadening of the active zone (Z_o) with increase of adsorbent mass in the column [187]. Non-broadening of the active zone confirms the role of radial mass transfer in the increase of capacity with bed height.

Table 8.33: Experimental results of up-flow column adsorption considering bed height, influent concentration and influent flow rate.

[Z(cm), C_o (mg l^{-1}), υ (ml min^{-1})]	V_{eff} (ml)	T_b (min.)	q_m±3% (mg g^{-1})
[5, 30, 5.5]	1072	195	23
[7, 30, 5.5]	1788	320	27
[9, 30, 5.5]	2530	460	30
[7, 20, 5.5]	2475	450	25
[7, 40, 5.5]	1403	255	29
[7, 30, 3.2]	2212	660	34
[7, 30, 8.1]	1296	160	20

The increase of treated volume (V_{eff}) and break-point (T_b) is linear with bed height **(Figure 8.40)** and this behaviour reflects that although the adsorbent is mesoporous type (which may suggest difficulty to M(II)-mobility), it is accessible for Cu(II) ions.

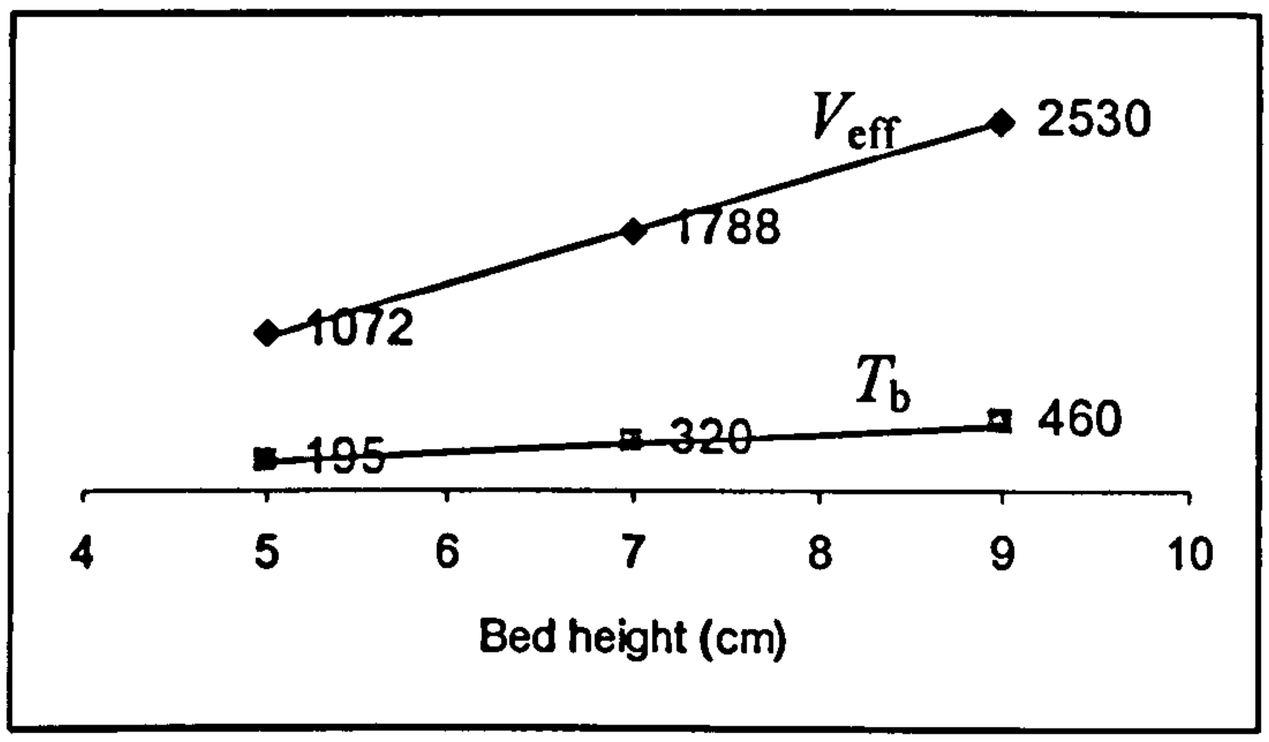

Figure 8.40: The linear increase in V_{eff} and T_b with bed height.

8.4.3 Effect of initial concentration on adsorption

The effect of changing Cu(II)-influent concentration (20, 30 and 40 mg l^{-1}) on breakthrough curves at bed height of 7 cm and flow rate of 5.5 ml min^{-1} is shown in **Figure 8.41**.

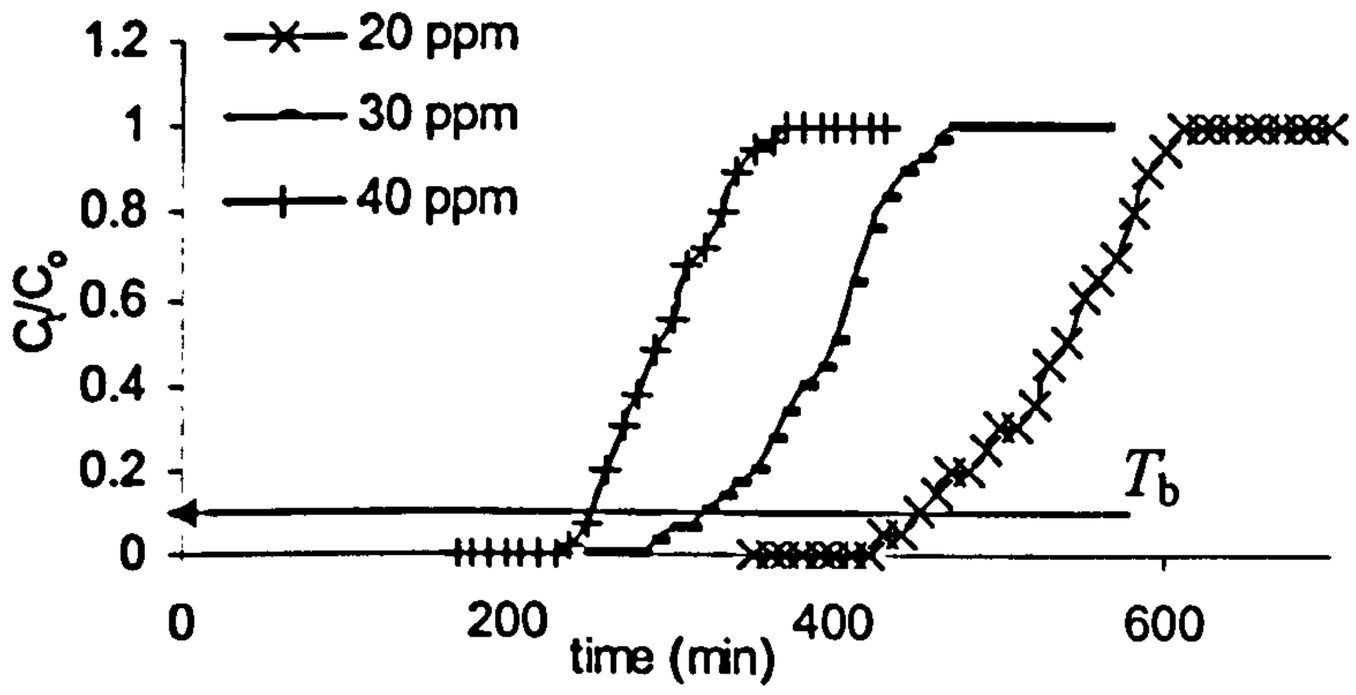

Figure 8.41: Breakthrough curves for Cu(II) adsorption on MF-DTPA at three different influent concentrations.

It can be observed from the curves that as influent concentration increases, the break-point (T_b) were reached earlier as the increase of concentration increases the rate of occupation of chelation sites [145]. The treated volume (V_{eff}) increased as influent concentration decreased **(Table 8.33)** because the amount of Cu(II) enters per unit time is smaller and presence of vacant sites for more incoming Cu(II) ions are more

available. The capacity (q_m) increases with the increase of concentration (**Table 8.33**) which gives indication about the driving force of initial concentration on the adsorption process [145]. This phenomenon was also observed for batch experiments.

The larger the influent concentration, the steeper the slope of breakthrough curve, indicating a thinner active zone. In this case, diffusion is concentration dependent. This phenomenon demonstrates that the change of concentration gradient affects the saturation rate, i.e. adsorption is concentration dependent [60].

8.4.4 Effect of flow rate on adsorption

The effect of a number of different flow rates (3.2, 5.5 and 8.1 ml/min) on breakthrough curves for a fixed bed height of 7 cm and influent concentration of 30 mg g^{-1} is shown in **Figure 8.42**.

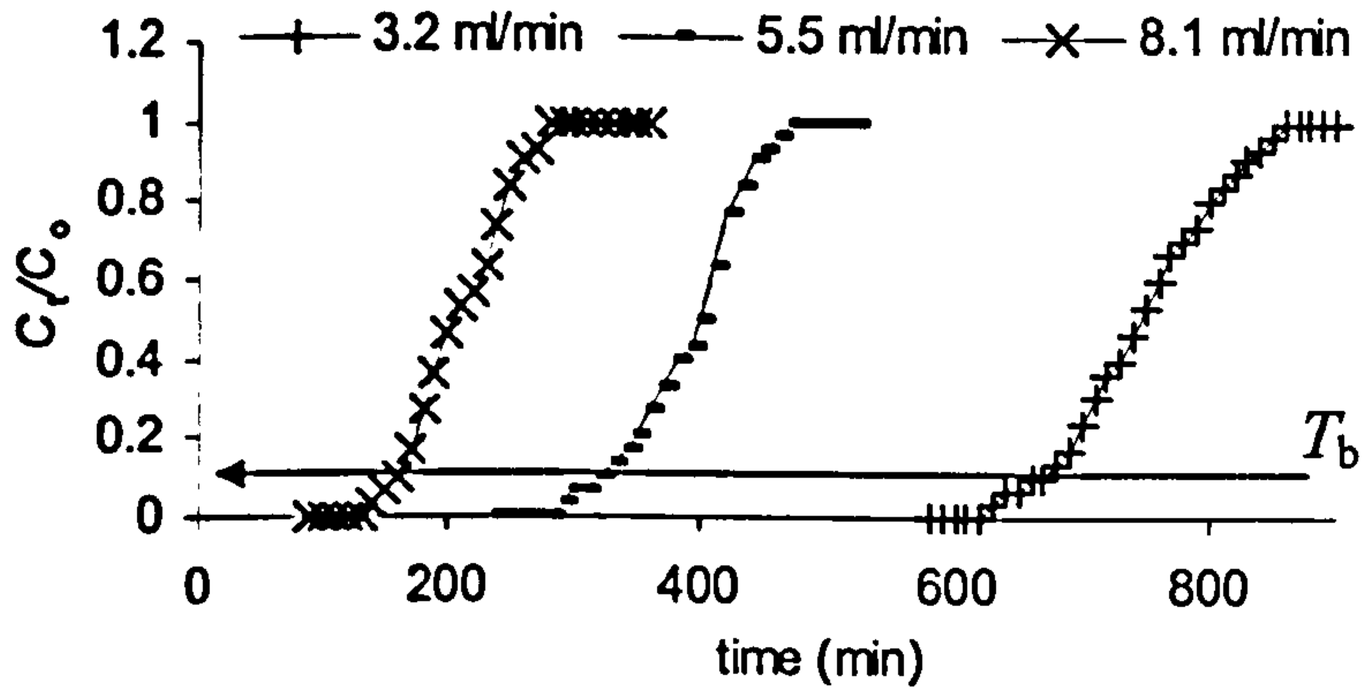

Figure 8.42: Breakthrough curves for Cu(II) adsorption on MF-DTPA at three different flow rates.

It can be observed from the curves that as flow rate increases, the break-points (T_b) were reached earlier due to the higher amount of Cu(II) ions entering the bed per unit time causing a higher rate of chelation. The treated volume and capacity increased with flow rate (**Table 8.33**) due to increase of contact time between Cu(II) ions and adsorbent, and this also reflects the importance of radial mass transfer which starts to play an important role at lower flow rates. As the flow rate is decreased, the Cu(II)

ions have more time for radial diffusion and so a higher opportunity to reach many of the available chelating sites.

Also, the breakthrough curve was steeper for higher flow rate, implying smaller active zone and high diffusion. At higher flow rate the boundary layer around the particles is thinner which reduces film resistance. The breakthrough curves were less steep for lower flow rate indicating a larger active zone, longer service time for the column and more prominent effect of film transfer resistance [187]. This suggests that diffusion may have a role in the process.

Steep slopes of breakthrough curves were obtained for systems that exhibit high film transfer coefficients and high internal diffusion coefficients [183]. The breakthrough curves of continuous Cu(II) adsorption on MF-DTPA can be considered that steep compared to many other studies [145] and accordingly it is suggested that chemisorption is the main adsorption step.

8.4.5 Thomas model analysis

The Thomas model was used to fit the experimental results with respect to different bed height, influent concentration and influent flow rate. For bed heights 5, 7 and 9 at flow rate of 5.5 ml min^{-1} and influent concentration of 30 mg l^{-1}, model plots show linearity as shown in Figure 8.43.

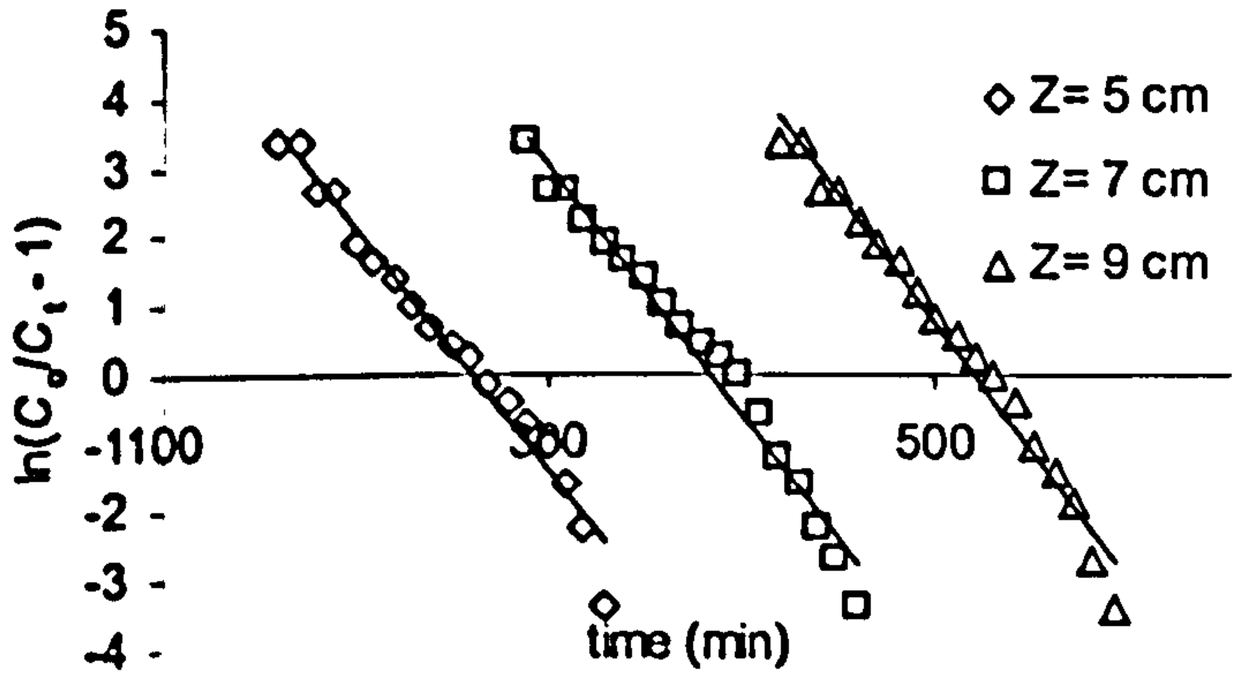

Figure 8.43: Thomas model fitting Cu(II) adsorption on MF-DTPA at three different bed heights.

Form **Table 8.34** it can be observed that Thomas model capacity (Q) increased with bed height which means that increasing bed height has positive influence on the process. This observation is in agreement with experimental capacity (q_m) **(Table 8.33)**. The Thomas capacities (Q) reasonably match experimental capacities (q_m). The rate constant (k_{Th}) increase with bed height which may reflect the effect of radial mass transfer in the process and confirms no broadening of the active zone.

Table 8.34: Parameters predicted from Thomas model considering bed height, influent concentration and influent flow rate.

[Z(cm), C_o (mg l^{-1}), v (ml min^{-1})]	k_{Th} (l mg^{-1} min^{-1})	Q (mg g^{-1})	R^2
[5, 30, 5.5]	1.17×10^{-3}	21.97	0.9748
[7, 30, 5.5]	1.21×10^{-3}	32.30	0.9766
[9, 30, 5.5]	1.25×10^{-3}	43.75	0.9800
[7, 20, 5.5]	1.50×10^{-3}	29.69	0.9593
[7, 40, 5.5]	1.32×10^{-3}	33.16	0.9702
[7, 30, 3.2]	0.91×10^{-3}	36.55	0.9923
[7, 30, 8.1]	1.42×10^{-3}	26.13	0.9847

For Cu(II) influent concentrations (20, 30 and 40 mg l^{-1}) at flow rate of 5.5 ml min^{-1} and bed height of 7 cm, Thomas model give linear plots as shown in **Figure 8.44.**

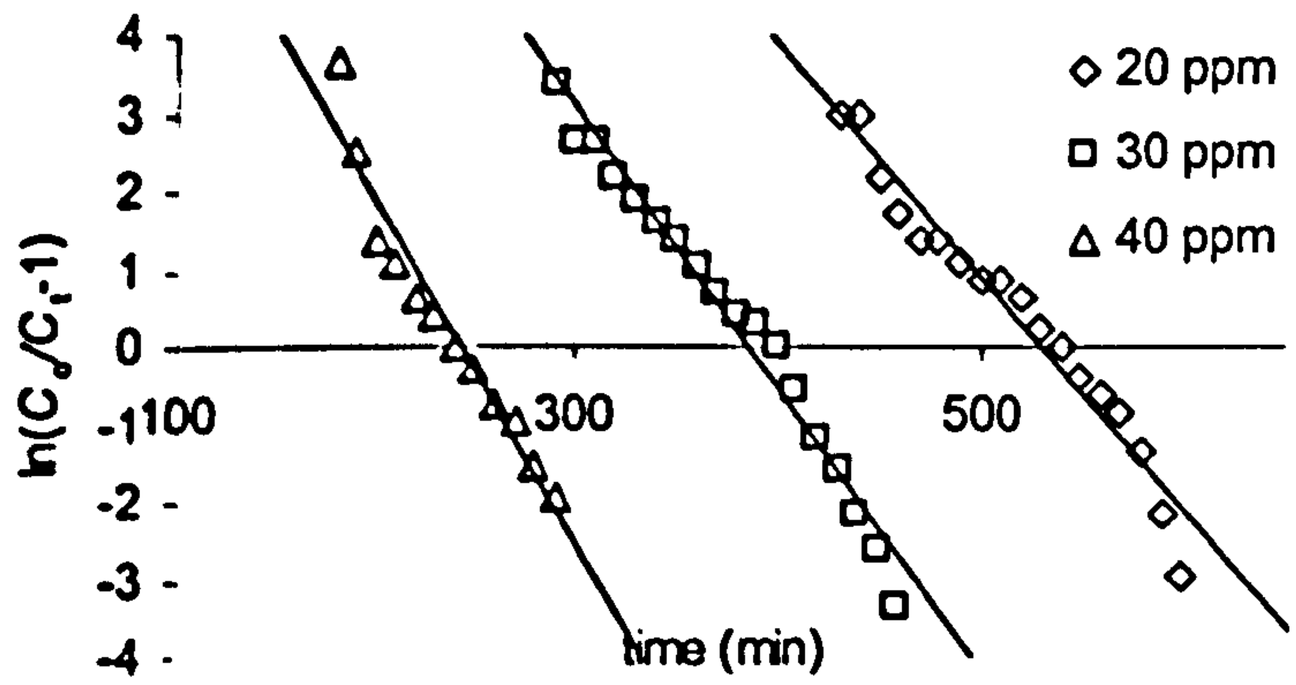

Figure 8.44: Thomas model fitting Cu(II) adsorption on MF-DTPA at different influent concentrations.

With the increase of influent concentration, rate constant (k_{Th}) did not give a trend but column capacity (Q) showed an increase **(Table 8.34)** and this agrees with experimental capacity (q_m) **(Table 8.33)**. This also suggests the influence of initial concentration as a driving force for adsorption.

For influent flow rates (3.2, 5.5 and 8.1 ml min^{-1}) at bed height of 7 cm and influent concentration of 30 mg l^{-1}, model gives linear plot as shown in **Figure 8.45**.

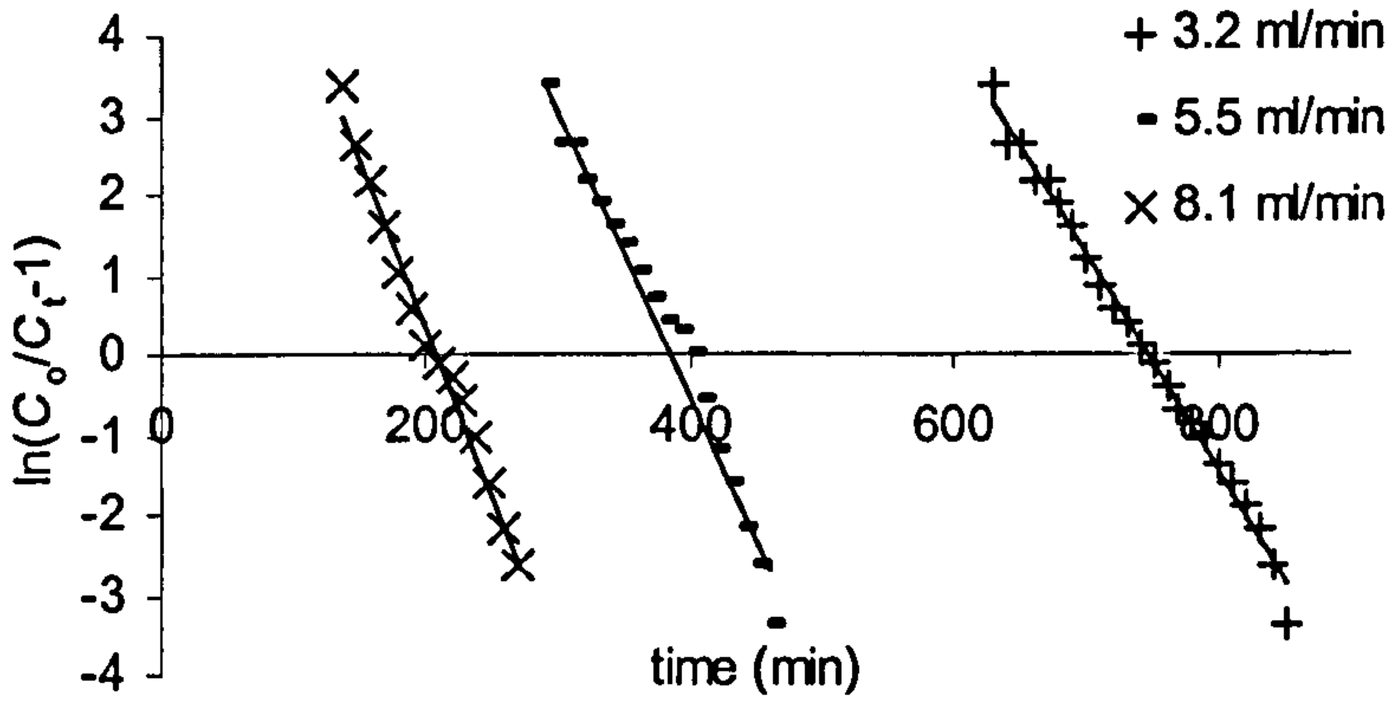

Figure 8.45: Thomas model fitting Cu(II) adsorption on MF-DTPA at different influent flow rates.

Table 8.34 summarises corresponding Thomas parameters, rate constant (k_{Th}) and capacity (Q). If the process is pore diffusion controlled, a slower flow rate favours the adsorption and when the process is external mass transfer controlled; the higher flow rate decreases the film resistance [188]. The rate constant (k_{Th}) increased with flow rate which suggest contribution of film diffusion in the process. This is in agreement with batch study (section 8.1.5).

Decrease in flow rate has a positive influence on adsorption from the capacity point of view and also this agrees with experimental capacity, (q_m) **(Table 8.33)**.

Generally, the estimated capacities by the model (Q) are lower than that calculated for batch-removal and this phenomenon is always observed.

The reasonable agreement of the Thomas model estimated parameter with experimental values suggests the model can represent the continuous removal of Cu(II) by a column packed with MF-DTPA adsorbent and can be applied for the purpose of designing practical removal unit that employ MF-DTPA adsorbent. Furthermore, it confirms that MF-DTPA follows Langmuir isotherm and reversible-adsorption reaction as batch study suggested. Deviation of model capacity values (Q)

from experimental values (q_m) may originate form the role of diffusion on the process which is not considered for Thomas model.

8.4.6 BDST model analysis

From the breakthrough curves considering different bed heights shown in **Figure 8.39**, the BDST plots were determined for C_t/C_o = 0.033, 0.1, 0.5 and 0.9 as shown in **Figure 8.46.**

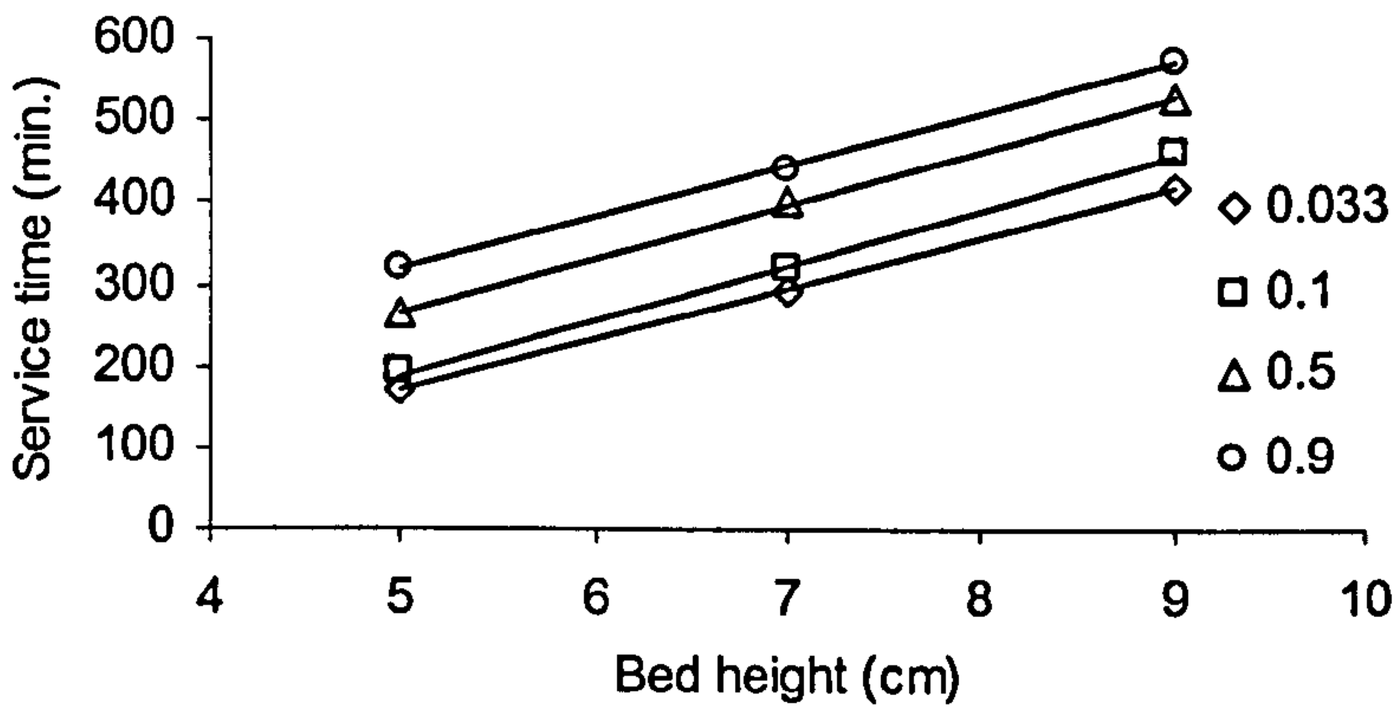

Figure 8.46: The BDST plots at C_t/C_o= 0.033, 0.1, 0.5 and 0.9.

The BDST equations of these lines are as follows:

$T_s = 62.5\ Z - 144.17$ for C_t/C_o= 0.033 (R^2= 0.9995)

$T_s = 67.5\ Z - 149.17$ for C_t/C_o= 0.1 (R^2= 0.9995)

$T_s = 66.3\ Z - 65.417$ for C_t/C_o= 0.5 (R^2= 0.9999)

$T_s = 63.\ 8\ Z - 1.25$ for C_t/C_o= 0.9 (R^2= 0.9988)

The slopes are very similar which means, according to **equation (36)**, that N_o value did not change with bed height which means that adsorption zone is moving up the column at a constant speed [189]. For C_t/C_o= 0.1, k_B was calculated using **equation (36)** and the minimum column height necessary to give effluent of concentration C_b = 3 mg g^{-1}, Z_o, was also calculated using **equation (39).**

Design parameters were found to be, N_o= 7232 mg ml^{-1} (correspond to 25.8 mg per gram of solid adsorbent), $k_B = 4.91\times 10^{-4}$ l mg^{-1} min^{-1}. The parameter Z_o can help to control the wanted bed height. For this study, Z_o= 2.2 cm and so the least bed height should not be smaller than these value to guarantee not miss breakthrough. The Correlation factor, $R^2 > 0.998$, is high which means good fit of data with the model.

8.4.7 Examining BDST model with influent concentration and flow rate

Comparison of experimental service time and predicted service time according to BDST model with respect to different influent concentration at $C_t/C_o = 0.1$, flow rate 5.5 ml min^{-1} and bed height of 7 cm is given in **Table 8.35**. Also, comparison of experimental results and predicted service time according to BDST model with respect to different influent flow rate at $C_t/C_o = 0.1$, influent concentration 30 mg g^{-1} and bed height of 7 cm are given in the table.

Equations (40) – (42) were used to calculate the new intercepts and slops. Applying the new slopes and intercepts in **equation (36)** to predict service times was carried out. These comparisons can indicate the applicability of this model to represent the MF-DTPA column.

Table 8.35: The BDST model fitting the influent concentration and influent flow rate conditions.

[Z(cm) ,C_o (mg l^{-1}) , υ (ml min^{-1})]	Experimental service time (min.)	T_S (min.)
[7, 20, 5.5]	450	485
[7, 30, 5.5]	320	324
[7, 40, 5.5]	252	243
[7, 30, 3.2]	660	663
[7, 30, 8.1]	160	172

We can conclude from the table that BDST model satisfactorily predicts service time with good agreement to that of experimental results. This in turn implies the usefulness of this model for practical employment of enlargement of experimental set into an industrial removal unit.

8.4.8 Effect of presence of citric acid in Cu(II) ion solution on adsorption

The presence of chelating agents with heavy metal in wastewater is important for some industrial application such as electroplating and electroless copper plating of printed circuit boards. The use of precipitation or ion exchange for the removal or recovery of the metal from this type of wastewater effluents is ineffective in the presence of chelating agents [190,191].

Wang et al [190] found that the adsorption of Cu(II) by Copoly(GMA-DVB-HEMA-grafted-PEHA) decreases as EDTA concentration in Cu(II)/EDTA solution increases. When the Cu(II)/EDTA ratio exceeds 0.75, the removal efficiency is limited.

Matejka and Zitkova [191] studied the removal of heavy metals from solutions containing EDTA, a powerful chelating agent. The removal was successful at optimum conditions using acrylamide adsorbents having oligo(ethyleneamine)–OEA– moieties due to stability constants of M(II)–OEA complexes which are comparable or even higher than the stability constants of M(II)–EDTA complexes.

Citric acid is a chelating agent that may be present in many water effluents and can stabilize M(II) ion in the mobile phase and so may retard the M(II) adsorption on MF-DTPA. The effect of citric acid presence with Cu(II) ion in influent solution is shown in **Figure 8.47.**

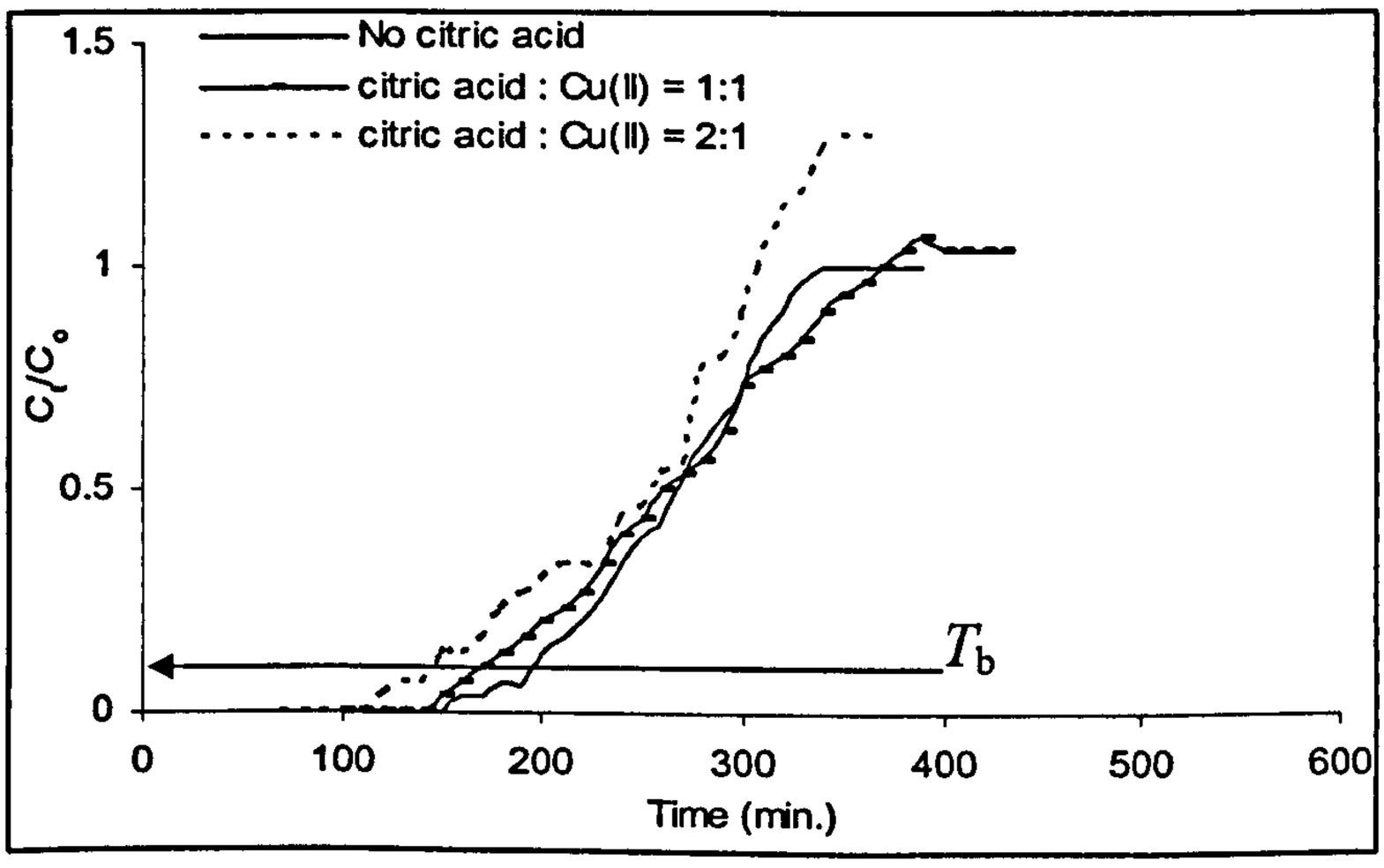

Figure 8.47: Effect of presence of citric acid in Cu(II) ion solution on adsorption.

As the citric concentration increases, T_b was reached earlier (**Table 8.34**). But, even presence of two times concentration of citric acid as Cu(II) does not stop considerable amount of Cu(II) ions to be adsorbed by the adsorbent. This indicates the ability of DTPA to chelate Cu(II) in the presence of some organic pollutants in the treated wastewater and suggests the possible separation of heavy metals ion.

Table 8.36: Effect of citric acid presence on the Break-point (T_b) of Cu(II) adsorption

Citric acid concentration	Break-point T_b min. (C_t/C_o= 0.1)
No citric acid	195
0.47 mM	180
0.95 mM	150

8.4.9 Column regeneration and reuse

Figure 8.48 shows an elution cycle using EDTA solution. The elution is very fast in the first ten minutes which may correspond to removal of Cu(II) ions from external surface of adsorbent particles. The latter part may be due to the elution of Cu(II) from inner pores which needs more time due to the migration of EDTA into adsorbent pores because of its relatively high dimension. This slow mobility also explains the residence of about 16% of Cu(II) in the adsorbent after elution which may be due to the presence of this percentage in pores of tiny dimensions not accessible by for EDTA. Another explanation could be the *stable* chelate of Cu(II)-DTPA formed on adsorbent (section 8.1.6).

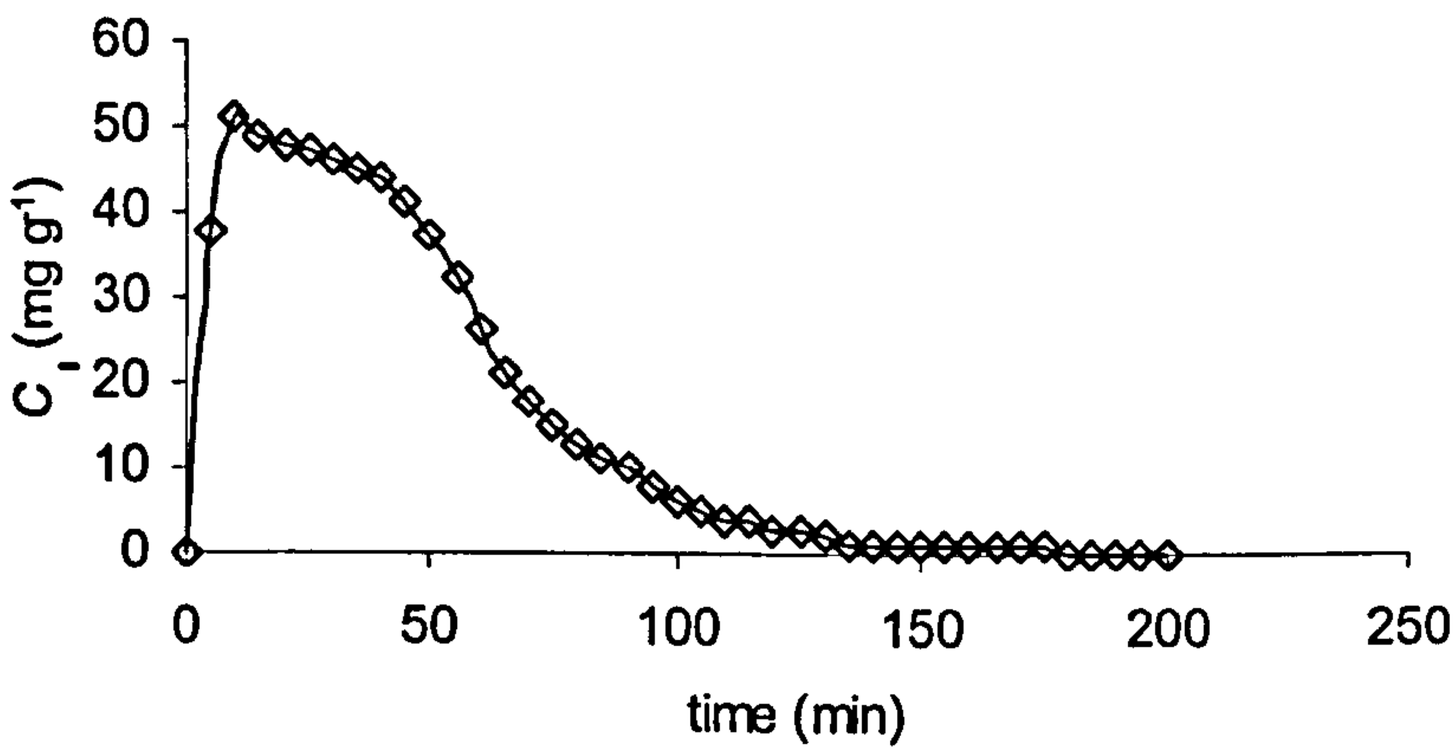

Figure 8.48: Time profile of Cu(II) concentration during its elution from saturated MF-DTPA sample by 0.01 M EDTA solution.

About 1100 ml of EDTA solution was accumulated after completed elution process of Cu(II) ion from loaded MF-DTPA dose. The Cu(II) ion concentration of this solution was 48 mg l^{-1}. This means that removal from the total dose mass of the adsorbent is 52.8 mg (Cu(II)) which corresponds to 26.94 mg g^{-1}. First adsorption process gave q_m = 32.26 mg g^{-1} and by calculation, the elution efficiency is 84%. Most of Cu(II) ions were eluted in the fist 100 minutes which corresponds to 9.3 bed volumes. The number of bed volumes is an important parameter from design point of view as it suggests the amount of eluting solution to be used.

Figure 8.49 shows the first (fresh sample) and second (same sample after elution) adsorption processes with the same conditions (Z= 7 cm, C_o= 30 mg g^{-1} and υ= 5.5 ml min^{-1}). The second adsorption process has T_b= 290 minutes (at C_t/C_o= 0.1) which is less than that of first adsorption process by 30 minutes and V_{eff}= 1595 ml which is less than that of first adsorption process by 165 ml. Adsorption capacity, q_m, was calculated and found to be 25.48 mg g^{-1} which means 79% of the first adsorption capacity. This decrease in performance can be attributed to blocked sites because of non-eluted Cu(II) and deterioration of the adsorbent because of loss of active sites which mainly occurred by hydrolysis of DTPA during adsorption process, elution and washing.

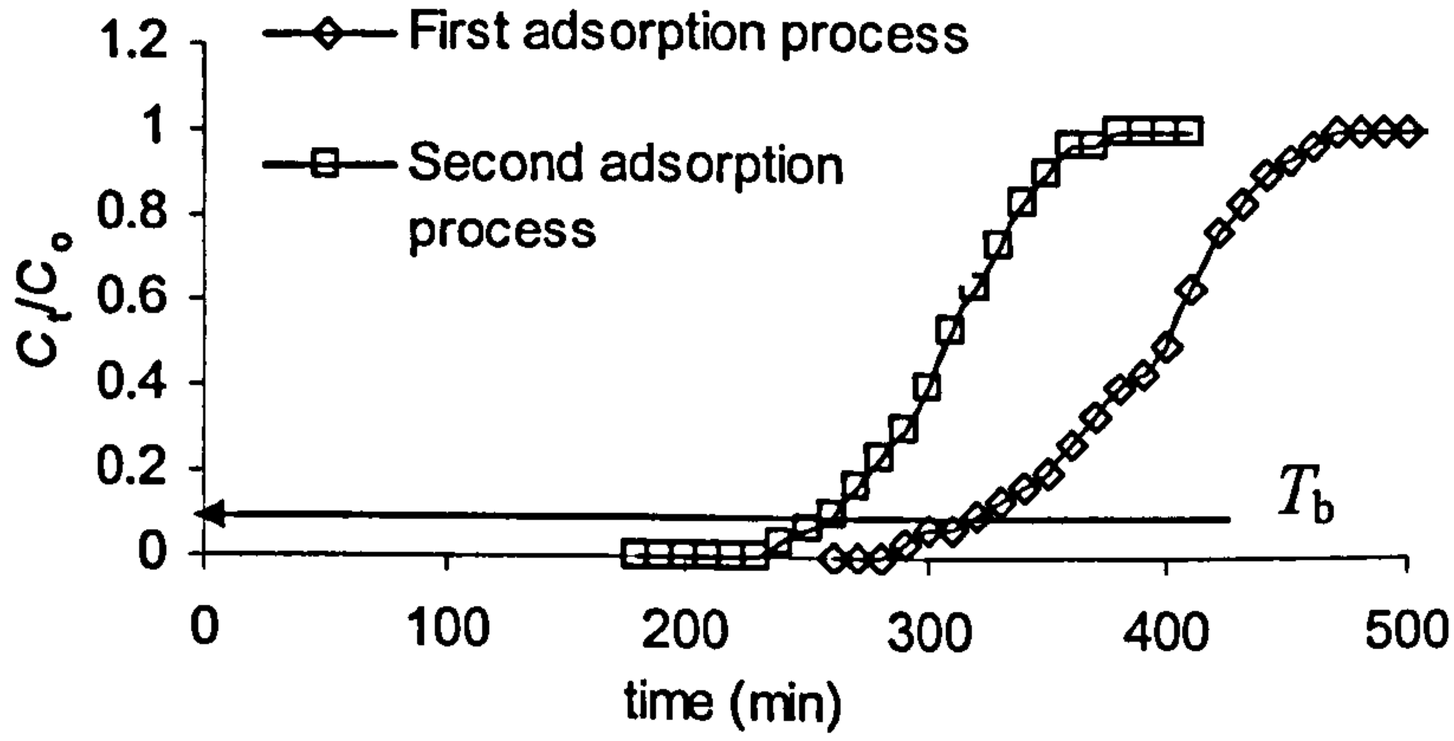

Figure 8.49: First and second adsorption breakthrough curves (Z= 7 cm, C_o= 30 mg g^{-1} and υ= 5.5 ml min^{-1}).

From the previous discussion, it can be inferred that MF-DTPA adsorbent is promising to be used as a removal medium for M(II) ions from wastewater effluents applying continuous mode. The parameters of adsorption process (adsorption rate, capacity, active zone) can be detected according to essential variable (bed height, flow rate, influent concentration) using simple standard models which enable the production of practical design.

Chapter 9

Conclusions

9.1 MF-PAPC adsorbents synthesis and characteristics

New MF-PAPC chelating adsorbents were successfully synthesised by mixing melamine, formaldehyde and a polyamine-polycarboxylic acid in acidic water, as a solvent and porogen, at elevated temperatures. The reaction consists of the bridging of melamine molecules by formaldehyde and the anchoring PAPC with melamine. The products are gels of monolithic MF-PAPC. A variety of instrumental tests (IR, NMR, TPD-MS and elemental analysis) have shown the success of the modification of the melamine-formaldehyde matrix (MF) by anchoring polyamine-polycarboxylic acid (PAPC) to the matrix through the amide bond. According to this preparation method, the produced MF-PAPC adsorbents are functionalised with chelating sites able to multi-coordinate (chelate) heavy metals and remove them from wastewater.

The amount of PAPC per gram of dry adsorbent is 1.08, 1.24 and 2.28 mmole for MF-DTPA, MF-NTA and MF-CDTA respectively. The physical properties of these adsorbents (porosity and rigidity) of MF-PAPC adsorbents depend on the preparation conditions (pH, temperature and water content) whereas the chemical properties are constant. The preparation of the monolith sample of MF-PAPC takes only about one hour.

Generally, the synthesised MF-PAPC adsorbents can be classified as mesoporous, rigid, hydrophilic materials and chemically active towards heavy metal. The surface areas (162, 159 and 179 m^2 g^{-1} for MF-DTPA, MF-NTA and MF-CDTA respectively) and average pore diameters (95, 130 and 19 Å for MF-DTPA, MF-NTA and MF-CDTA respectively) suggest that these adsorbents are well suited to the adsorption of heavy metals from solutions.

MF-PAPC adsorbents texture consist of agglomerates of very tiny material-particles and this is responsible for the porosity. The MF-PAPC adsorbents are hydrophilic (the average water regain is greater than 69%) which is a preferred characteristic for the application of heavy metal removal from solutions.

The porosity parameters (average pore diameter, pore volume and surface area) are strongly dependent on the preparation conditions (pH, temperature and water content) which implies that further study is required. It is helpful to be able to synthesise these adsorbents with larger pore diameter and a higher surface area which will in turn enhance the kinetics of adsorption and reduce the contact time required.

9.2 Adsorption of heavy metals M(II) on MF-PAPC adsorbents

The white colour of MF-PAPC adsorbents turns to the respective colour of the corresponding M(II)-PAPC complex when treated with Cu(II) and Co(II) solutions. This fact reflects the chelation behaviour of these adsorbents.

The initial pH value of the M(II)-treated solution has an insignificant effect on the removal percentage of M(II) ions by MF-PAPC adsorbents. However, the pH may affect the chemical mechanism of the removal where chelation dominates at the higher pH values and ion exchange has some contribution at the lower pH values.

The increase of the acidity of treated solutions suggests a chemisorption process (chelation and ion exchange).

Generally, the decrease in temperature causes an increase of M(II) removal which suggests adsorption by chelation. However, it is thought that ion exchange has some effect at higher temperature. The contribution of ion exchange in the adsorption process was suggested due to the nature of the active moieties present in the adsorbent (presence of carboxylic groups), and was confirmed by observing a change in the M(II)-affinity of MF-DTPA as the temperature increases. The presence of Na(I) ions (20 mg l^{-1}) in solution does not affect the removal of M(II) from solutions. However, higher concentrations have to be studied to conform to some practical cases.

Thermodynamic studies confirm the spontaneous (ΔG^{ads} is negative), and exothermic (ΔH^{ads} is negative) nature of the adsorption process with few exceptions. The exothermic nature of the adsorption process – over the temperature range studied – strongly suggests that chelation is the main mechanism of adsorption due to multi-exothermic coordinations. The entropy of adsorption (ΔS^{ads} is negative) indicates that the system becomes less disordered during the adsorption process. It is suggested that the hydrophilic surface of the adsorbents attracts the displaced water molecule from the hydrated metals. Also, the negative entropy change indicates the feasibility of regeneration of the adsorbents which is an essential procedure to allow the adsorbents to be used repeatedly in practical situations. It is suggested that chelation-enthalpy and chelation-entropy and M(II)-dehydration determine the adsorption affinity when the chelation site can complex more than one M(II) cation, and the formation constants of M(II)-complexes is the main factor when the chelation site can complex only one M(II) cation.

The removal percentage of M(II) by MF-DTPA and MF-CDTA decreases with M(II)-initial concentration. At higher concentrations, the chelation sites are less available compared to the amount of M(II) cations in solution and so the removal percentage decreases. On the contrary, the removal percentage of Cu(II) by MF-NTA increases with M(II)-initial concentration. This phenomenon may be attributed to the selective-adsorption nature of Cu(II) on MF-NTA and the reversible nature of the chelation process. As MF-NTA selectively adsorbs Cu(II) ion, the total initial concentration of the four M(II) ions is the driving force for The Cu(II) ion only.

The adsorption maximum *capacity increases with* M(II)-initial concentration for MF-DTPA, MF-NTA and MF-CDTA and this reflects *the driving force of concentration* on the adsorption process.

Time profiles of M(II)-removal by MF-PAPC adsorbents at different conditions (pH and temperature) show that the rate of uptake of metal ions is quite rapid, < 60 minutes. This is mainly because of the suitable pore diameter and hydrophilic character of the adsorbents.

The kinetics of adsorption of M(II) onto MF-PAPC adsorbents is well represented by pseudo second-order and reversible first-order models as the correlation factor

indicates. The reversible first-order model represents the reversible nature of the adsorption process. The pseudo second-order model is suitable to represent the adsorption maximum capacities. The good fit of these models confirms the reversible nature of the adsorption process.

For all MF-DTPA adsorbents, the pseudo second-order model shows the highest correlation factor (R^2) with experimental data and this suggests that the process is controlled by chemisorption involving valencey forces through sharing or exchange of electrons between adsorbent and sorbate, i.e. coordination.

It is believed that film diffusion may contribute in the adsorption process due to the hydrophilic character of the adsorbents. Pore diffusion has no significant effect for MF-DTPA and MF-NTA due to their wide pore diameter (95 and 130 Å respectively). For MF-CDTA, pore diffusion may have an effect due to its smaller pore diameter (19 Å). The rate of uptake of metal cations onto MF-PAPC is quite rapid and most of the adsorption of M(II) is achieved within less than one hour. The adsorption process is more reversible for MF-NTA and obviously depends on initial concentration.

Isotherm studies indicate that the Langmuir model gives a better fit to experimental data for adsorption of M(II) on MF-PAPC adsorbents. In general, this reflects the homogeneous energy distribution of the surface and shows that adsorption of M(II) is mostly of the monolayer type. This implies – in addition to the kinetic study – that the pendent PAPC sites in the adsorbent matrix are responsible for the main chemisorption process (chelation) to remove the M(II) cations from solutions.

The maximum adsorption capacities of MF-PAPC adsorbents are encouraging for their future use for the removal of heavy metals from contaminated water effluents. The capacities of MF-DTPA adsorbent are approximately 17, 18, 15 and 15 mg g^{-1} for Co(II), Cd(II), Zn(II) and Cu(II) respectively. The capacity of MF-NTA for Cu(II) is approximately 53 mg g^{-1}. The capacities of MF-CDTA are approximately 39, 22, 18 and 67 mg g^{-1} for Co(II), Cd(II), Zn(II) and Cu(II) respectively. The total capacity of MF-CDTA is the highest (2.17 mmole g^{-1}) followed by MF-NTA (1.1 mmole g^{-1}) and then MF-DTPA (0.92 mmole g^{-1}). This capacity order is in agreement with PAPC concentration in their corresponding adsorbents.

In general, the adsorption behaviour of MF-PAPC towards M(II) depends on the type of the PAPC anchored to the MF matrix. The selectivity order is different for MF-DTPA, MF-NTA and MF-CDTA and does not solely depend on the chelate formation constants, but also depends on other physical properties such as chelation enthalpy and entropy , enthalpies of M(II)-dehydration and M(II)-radii (especially for MF-CDTA).

The EDTA solution is suitable for the elution and generation of the MF-PAPC adsorbents. The removal percentage by the regenerated sample is lower than the original sample which is due to the partial deterioration of the active sites in the adsorbent. This deterioration originates from hydrolysis of the amide bond which

anchors PAPC to the MF matrix. This hydrolysis can occur during elution of the adsorbed metal, washing and even during the first adsorption process.

In general, it can be concluded that MF-DTPA can be used for the universal removal of Co(II), Cu(II), Cd(II) and Zn(II) as they have similar adsorption capacities. Further adsorption studies for various metal ions can confirm this behaviour. MF-NTA shows selectivity towards Cu(II), under conditions of the experiments, hence MF-NTA needs more study to understand its selectivity for specific practical conditions. MF-CDTA can be considered as a universal adsorbent and it is favoured due to its higher capacity.

The adsorption capacities of MF-PAPC adsorbents are higher than many chelating adsorbents: 0.63 [71], 0.6 [78], 1.23 mmole g^{-1} [80].

The adsorption of Cu(II) – as a representative of M(II) – in the fixed-bed column was studied according to the following parameters: bed height, solution flow rate and initial-Cu(II) concentration. Cu(II) removal is largely dependent on the quantity of adsorbent inside the column. The capacity increase with bed height suggests an increase of horizontal mass transfer with bed height. The capacity increases with the influent concentration which gives an indication about the driving force of initial concentration on the adsorption process. This phenomenon was also observed for batch experiments. The capacity increases as flow rate decreases due to the increase of contact time between Cu(II) cations and adsorbent and this also reflects the importance of the horizontal mass transfer effect which starts to play a role at lower flow rates.

The treated water volume increases with bed height and decreases with influent concentration and flow rate.

The adsorption active zone becomes thinner with flow rate and influent concentration. The change of breakthrough curve steepness with flow rate and influent concentration implies the contribution of film diffusion in the adsorption process. This confirms the role of film diffusion in adsorption derived from the batch study.

The reasonable agreement of estimated capacities of the Thomas model with the experimental values suggests that the model provides a successful representation of the continuous removal of Cu(II) ions by a column packed with MF-DTPA adsorbent, and can be applied for the purpose of designing a practical removal system. The adsorption rate constant (k_{Th}) increases with bed height and flow rate suggesting horizontal mass transfer and the contribution of film diffusion in the process respectively.

The BDST model gives prediction of the service time ($R^2 > 0.998$) that show good agreement with the experimental results. This, in turn, implies the usefulness of this model to scale-up the experimental arrangement into an industrial unit. At a flow rate of 5.5 ml min^{-1} and influent concentration of 30 mg g^{-1}, adsorption active zone was found to be 2.2 cm. The BDST parameters were found to be, dynamic bed capacity:

N_o= 7232 mg ml^{-1} (corresponding to 25.8 mg per gram of solid adsorbent) and adsorption rate constant: $k_B = 4.91 \times 10^{-4}$ l mg^{-1} min^{-1}.

The presence of organic compounds is a potential problem, since these can chelate heavy metals and stabilize them in solution. However, the successful removal of Cu(II) in the presence of citric acid by the MF-DTPA column suggests that removal of heavy metals is possible under these conditions.

The elution of Cu(II) from the exhausted column was successfully accomplished by EDTA. The adsorption capacity, after the elution step, was observed to decrease by 21%.

As an example of a practical application approach, it is suggested that MF-DTPA adsorbent will satisfactorily remove Cu(II) ions (126 mg l^{-1}) from wastewater of a copper plating facility [52], whereas the removal of Co(II) ion (996 mg l^{-1}) from wastewater of a cobalt plating facility may be accomplished by using MF-CDTA adsorbent [52].

9.3 Suggested future work

1) A more detailed study of the MF-PAPC adsorbents synthesis conditions (higher temperature and optimum initial amount of PAPC) would be instructive. Also, it is important to try alternate organic solvents instead of water (or mixture). The overall aim is to produce adsorbents of higher surface areas and more active sites.

2) Use of instrumental techniques that can give more understanding about the chemical structure of MF-PAPC adsorbents and the mechanism of adsorption. X-ray photoelectron spectroscopy (XPS), for example, can provide chemical bonding information of the blank and M(II)-loaded adsorbent samples. Binding energies can be used to determine the contribution of N and O atoms in coordination.

3) The interactive effects of a metal ion mixture on the adsorption of these metals on a chelating adsorbent can be determined by conducting complementary batch adsorption experiments for single-ion solutions of these four metals. The results of these experiments, with the results of the present study, may give a better understanding about how the chelates are formed, the effect on adsorption kinetics and the effect on adsorption capacity. Furthermore, the affinity order can be made clearer by this study.

4) Conduct continuous adsorption experiments (column method) for multi-cation solutions and make a comparison with batch experiments and continuous adsorption for a single cation. This comparative study would give a comprehensive understanding of adsorption process, i.e. kinetics and affinity. Also, this can help for design purposes for applications in which mixtures of metal cations are present.

5) The investigation of the adsorption of lanthanides and actinides under the presence of competitive ions that help in the separation technology of precious metals.

6) A preliminary synthesis process to produce MF-DTPA in foamy monolithic disc form was carried out. The foamy structure was achieved by using ether as a porogen. The monolithic form will make it easy to use MF-PAPC as a cartridge. This foamy structure with density 0.16 g cm^{-3} will allow a reasonable flow of water through the monolith which will be helpful in practical/industrial situations. **Figure 9.1** shows a sample after adsorbing Cu(II) ions. The kinetics of Cu(II)-adsorption indicate a high rate of removal and the experimental capacity for this sample was found to be about 15 mg g^{-1}. Furthermore, the picture shows clearly that the blue colour (Cu(II)-DTPA chelate) is equally distributed through the sample as observed from the outer surface and cross-section. Further research for this form is likely to produce a more efficient adsorbent cylinder, and this would be promising for practical use for the removal of heavy metals using a continuous flow system.

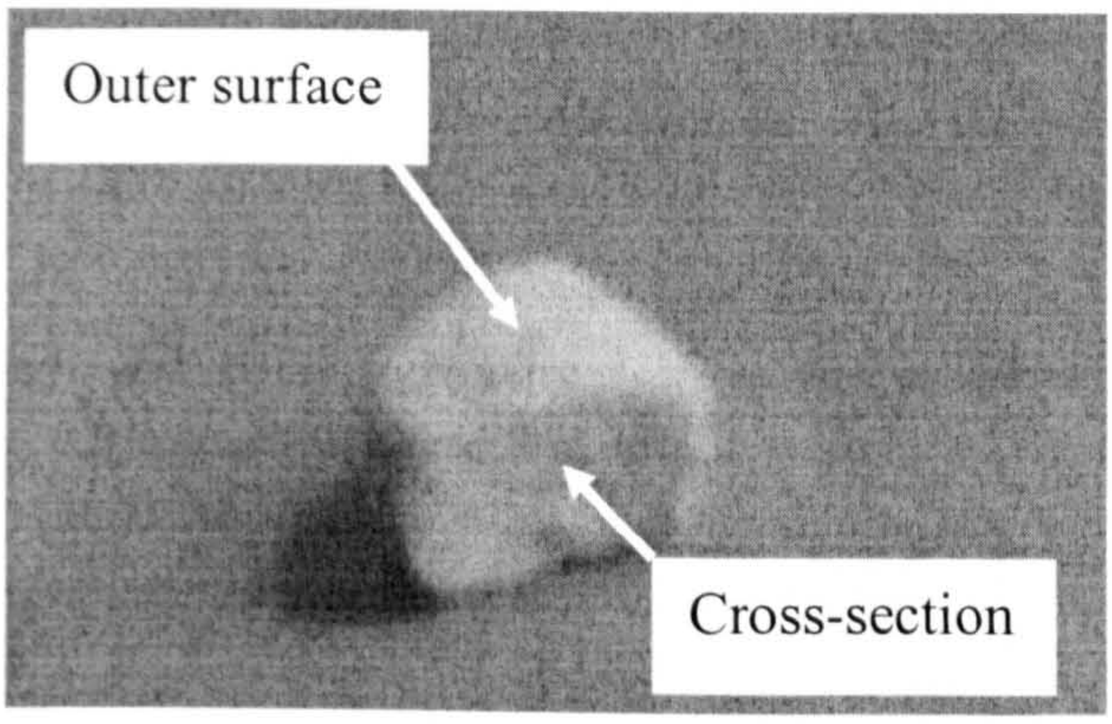

Figure 9.1: Foamy monolithic MF-DTPA after adsorbing Cu(II).

7) Enhancement of preparation methods to avoid hydrolysis of chelating sites in the adsorbent.

Chapter 10

Appendixes

Appendix A: Reference figures.

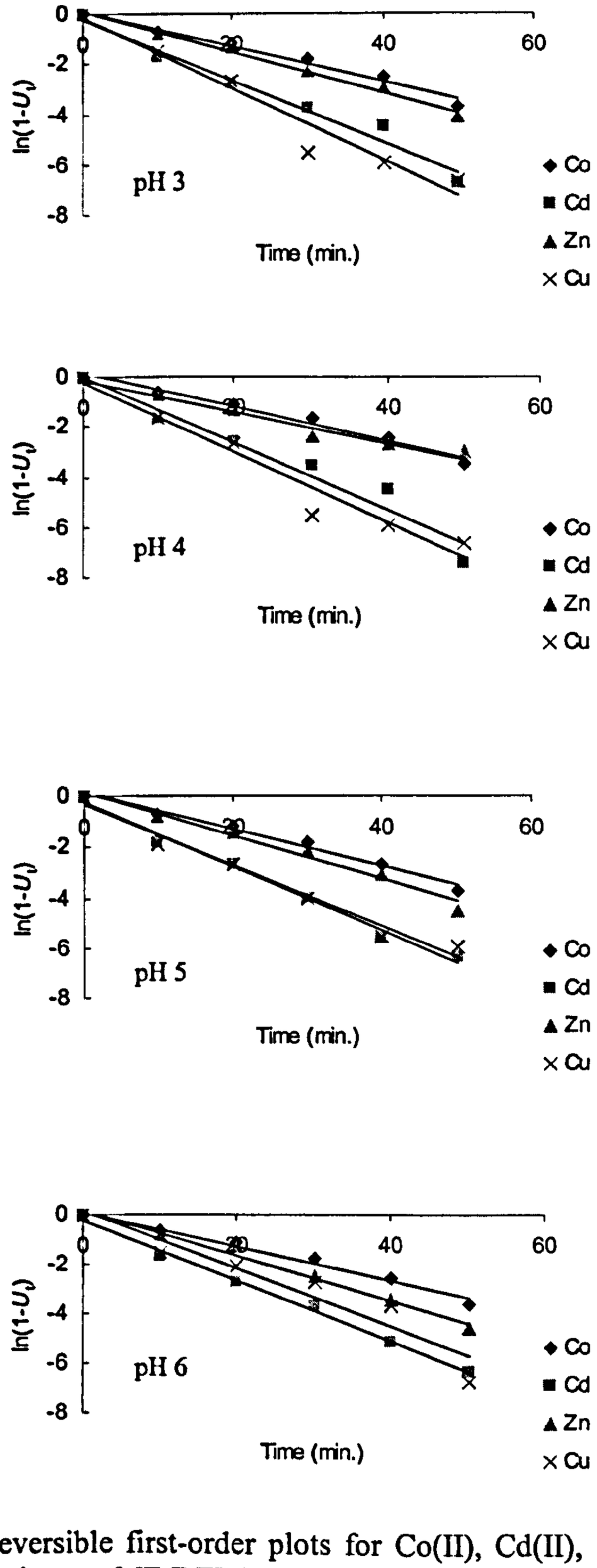

Figure 10.1: The reversible first-order plots for Co(II), Cd(II), Zn(II) and Cu(II) adsorption on MF-DTPA at temperature 25°C and pH values 3, 4, 5 and 6.

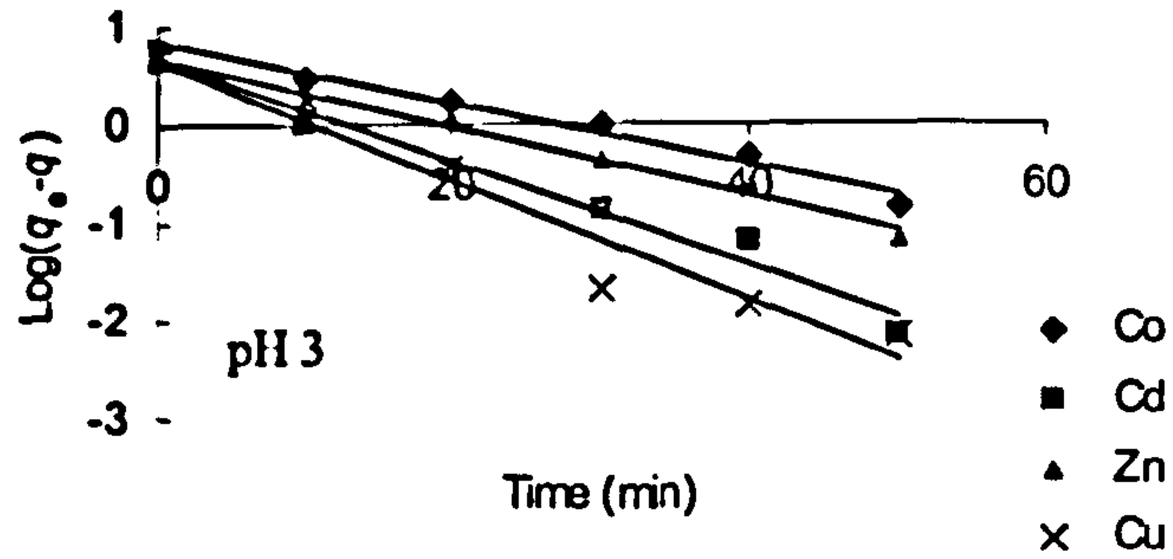

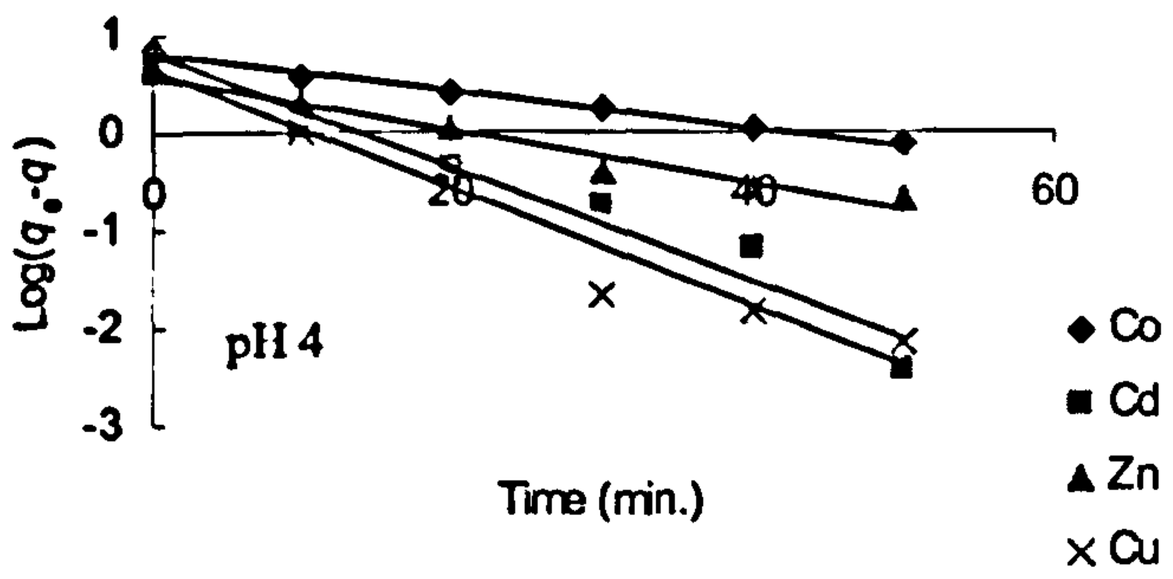

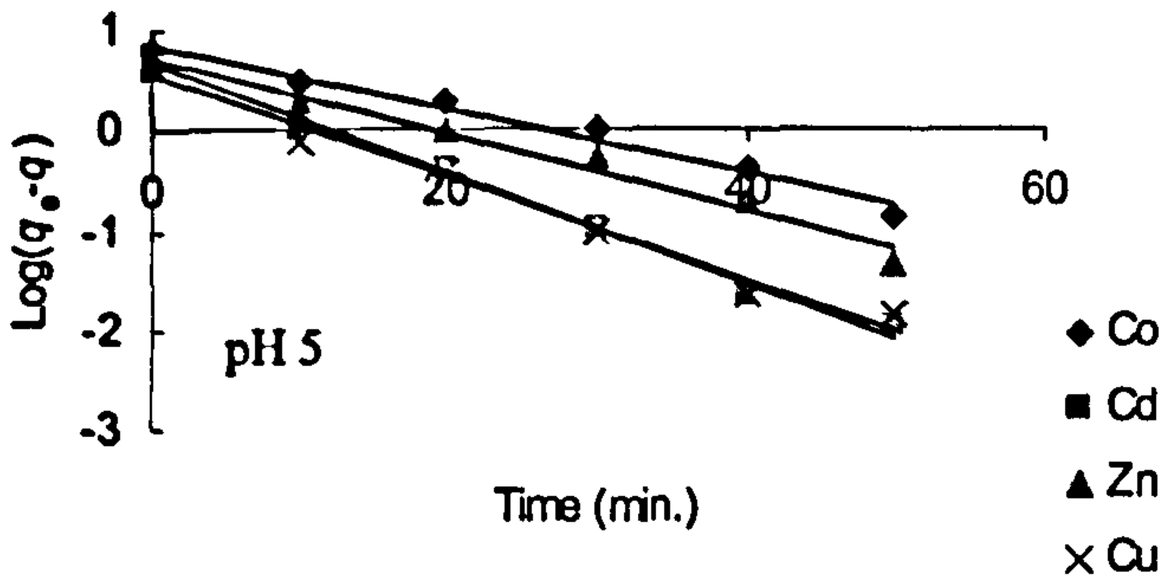

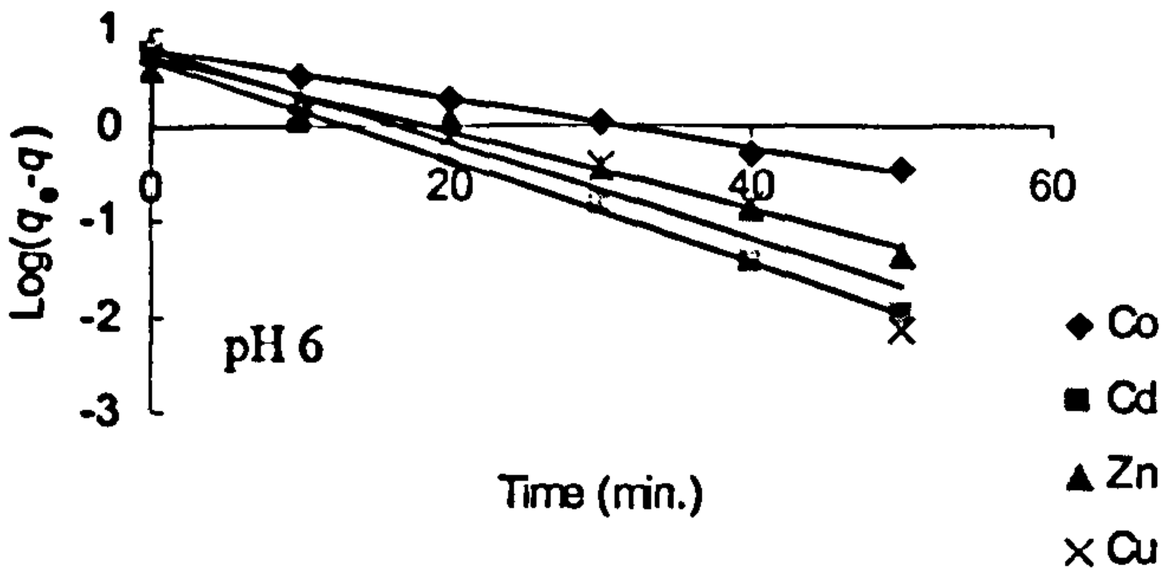

Figure 10.2: The pseudo first-order plots for Co(II), Cd(II), Zn(II), and Cu(II) adsorption on MF-DTPA at temperature 25°C and pH values 3, 4, 5 and 6.

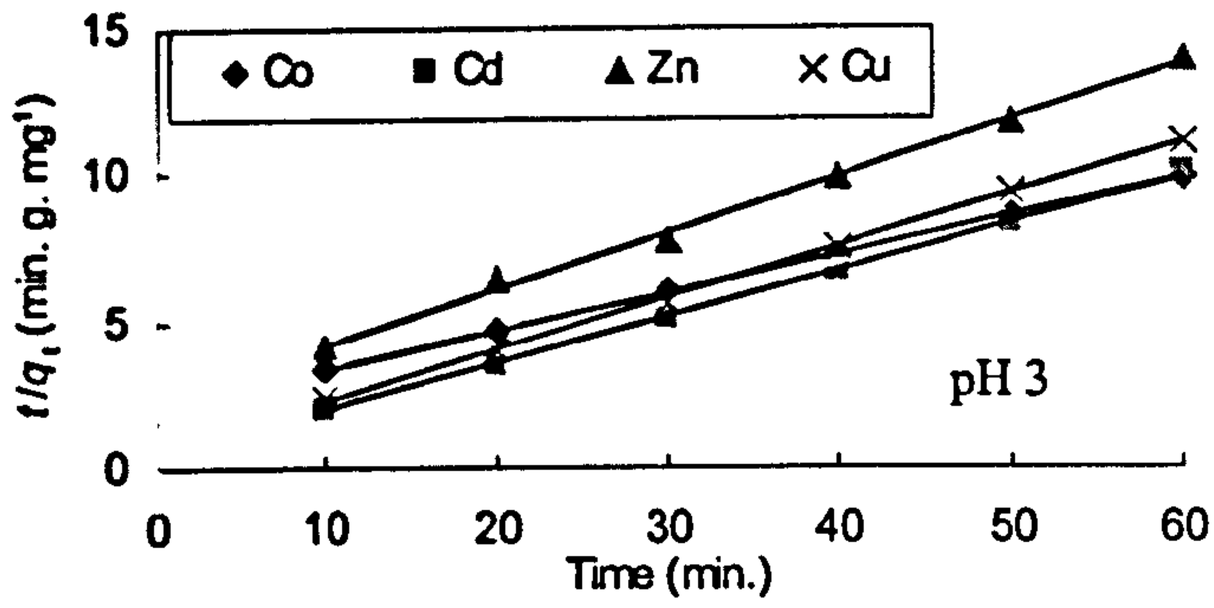

Figure 10.3: The pseudo second-order plots for Co(II), Cd(II), Zn(II) and Cu(II) adsorption on MF-DTPA at temperature 25°C and pH values 3, 4, 5 and 6.

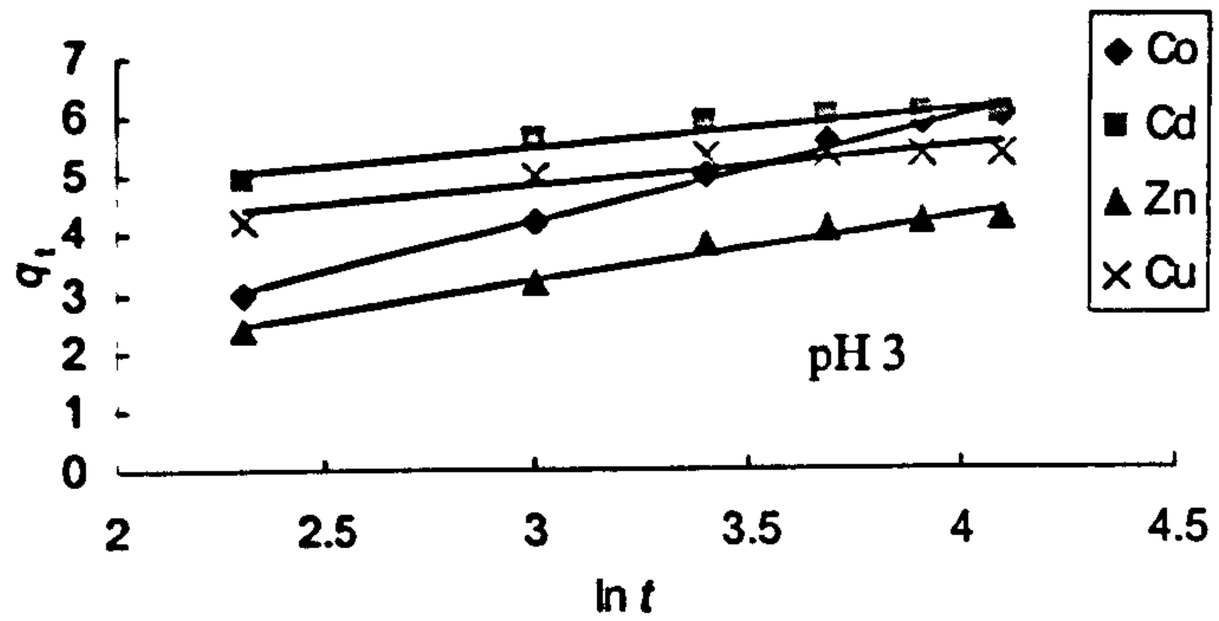

Figure 10.4: The Elovich plots for Co(II), Cd(II), Zn(II) and Cu(II) adsorption on MF-DTPA at temperature 25°C and pH values 3, 4, 5, and 6.

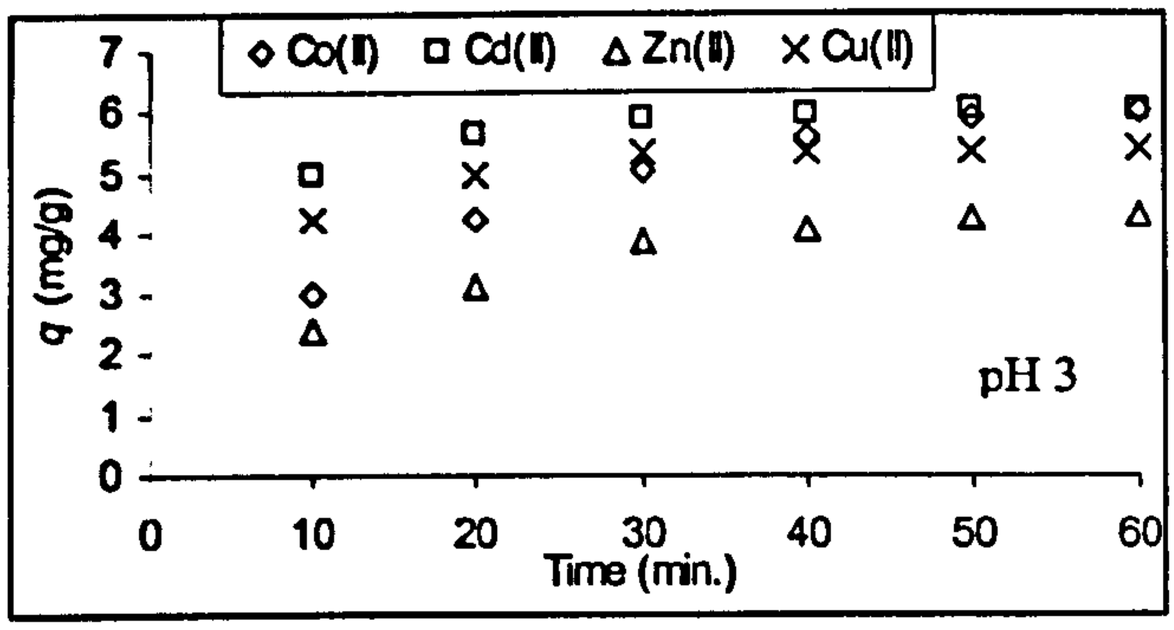

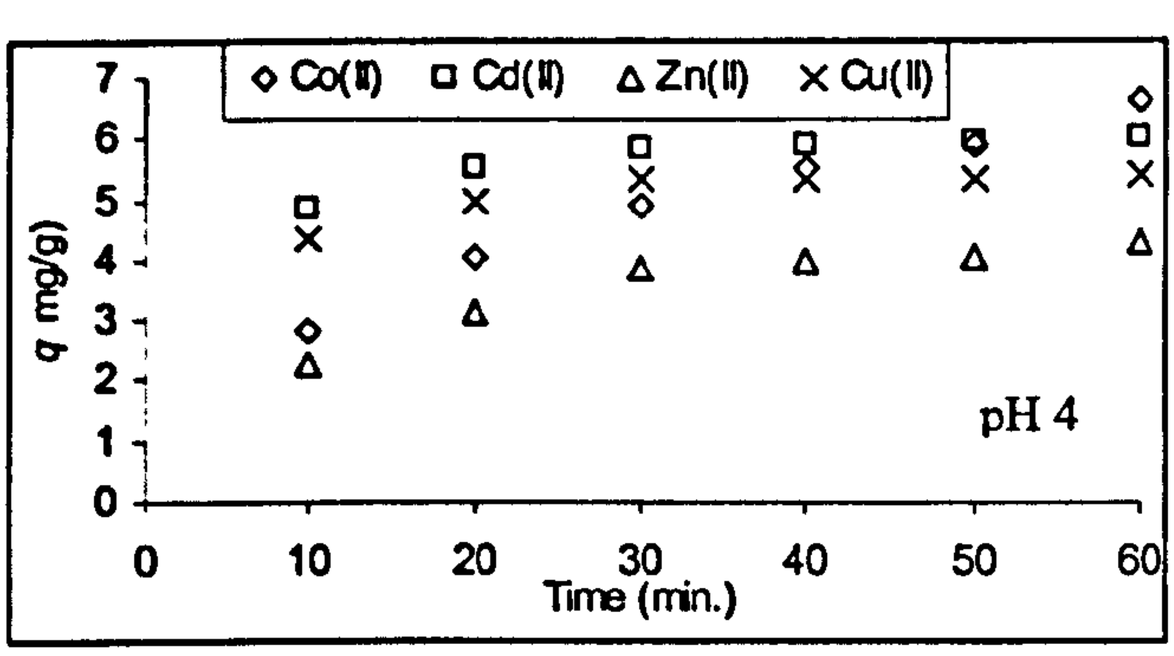

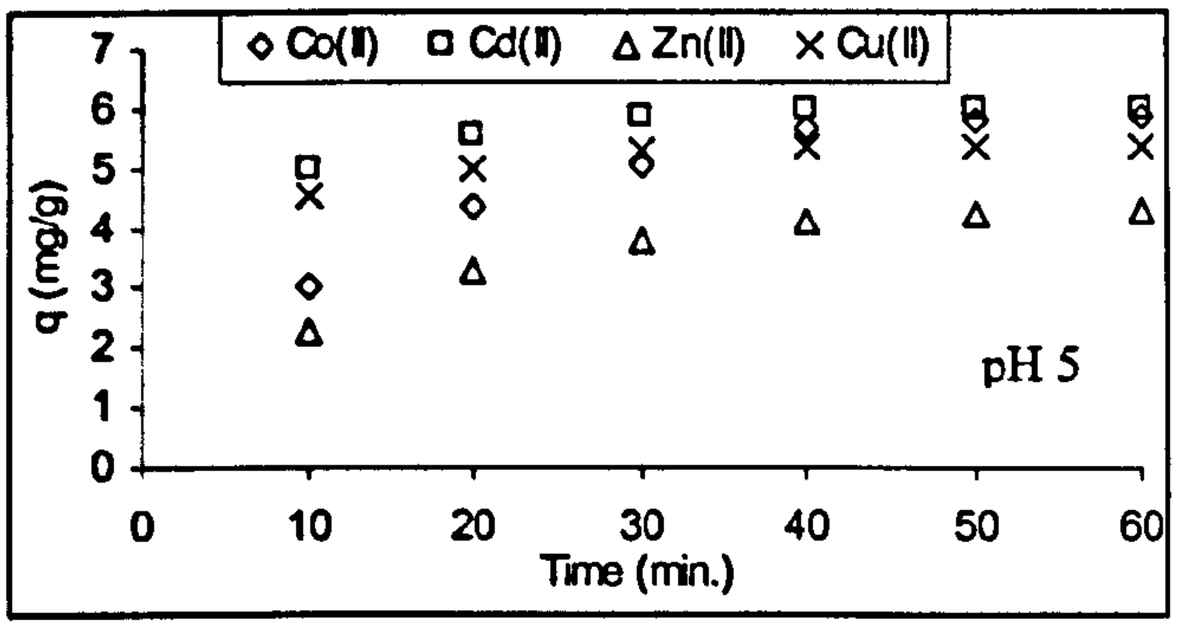

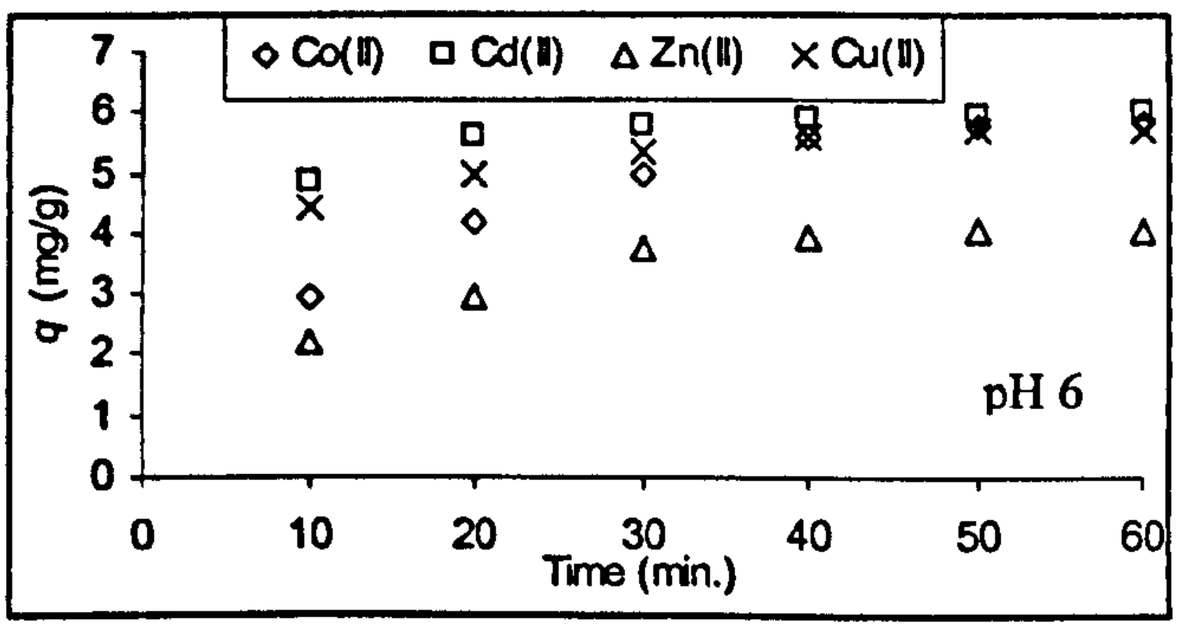

Figure 10.5: Increase of adsorbed amount of M(II) on MF-DTPA with time at different initial pH values (25°C).

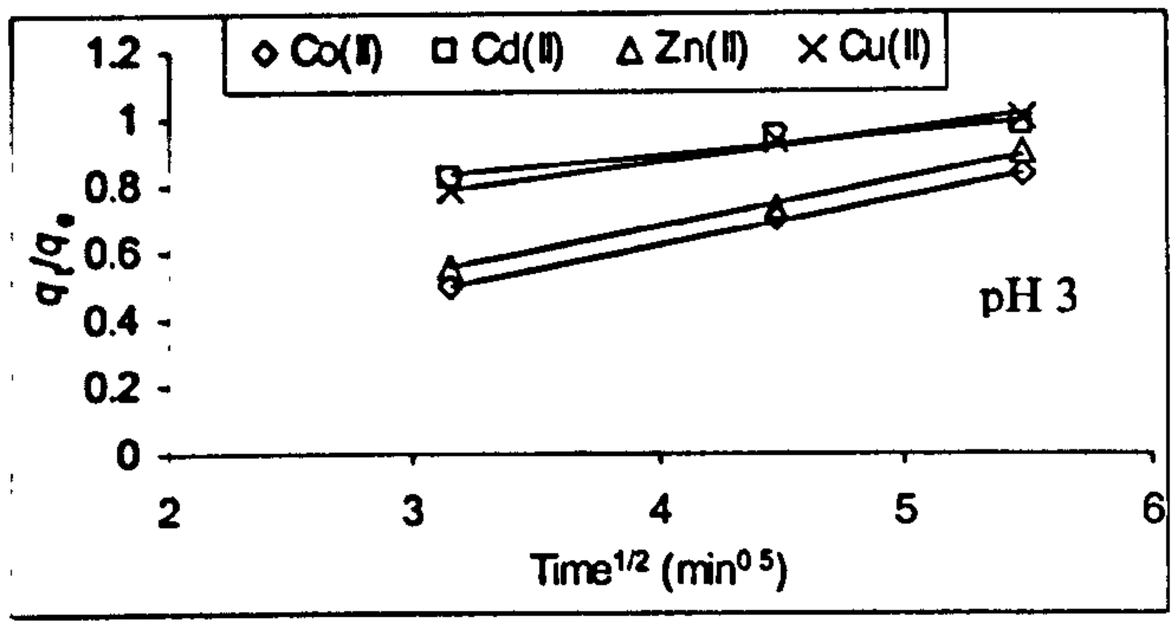

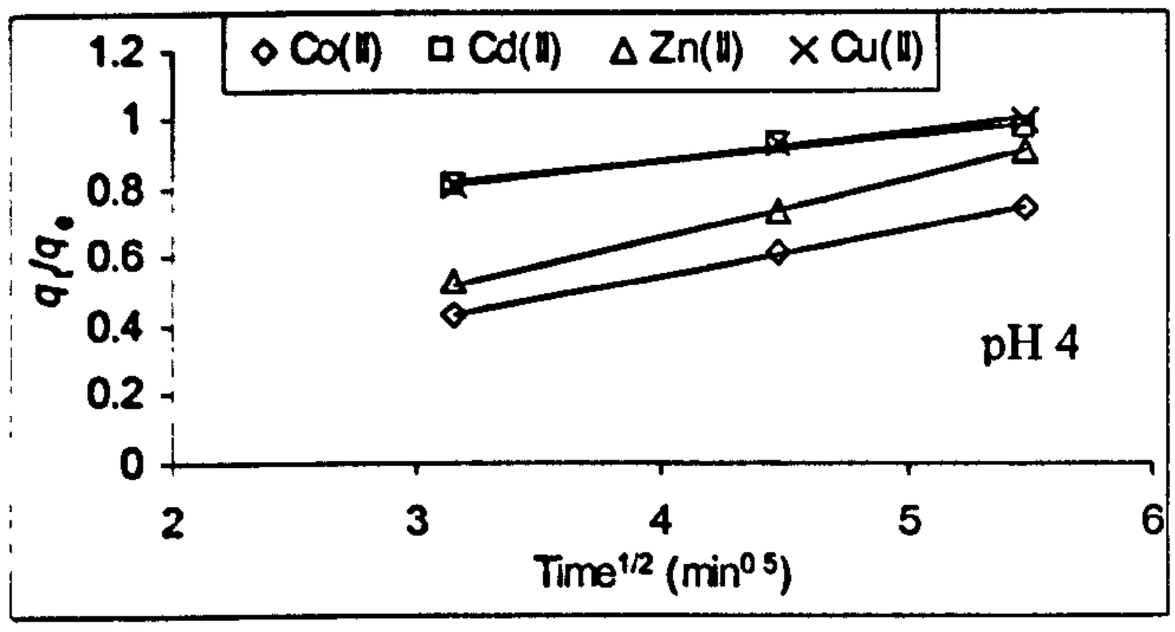

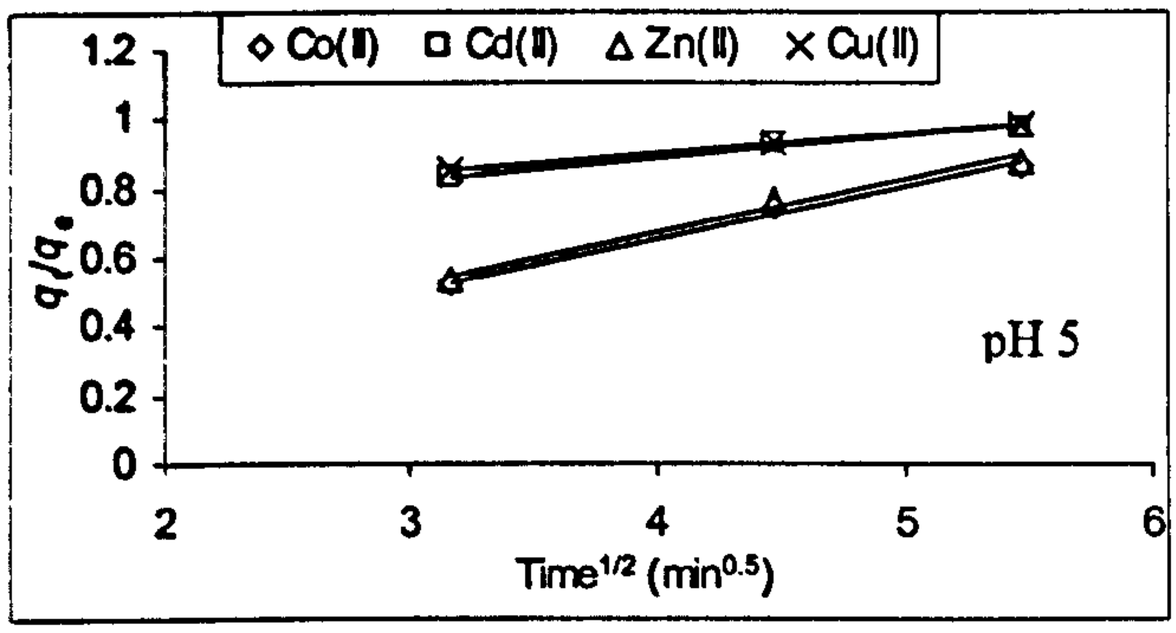

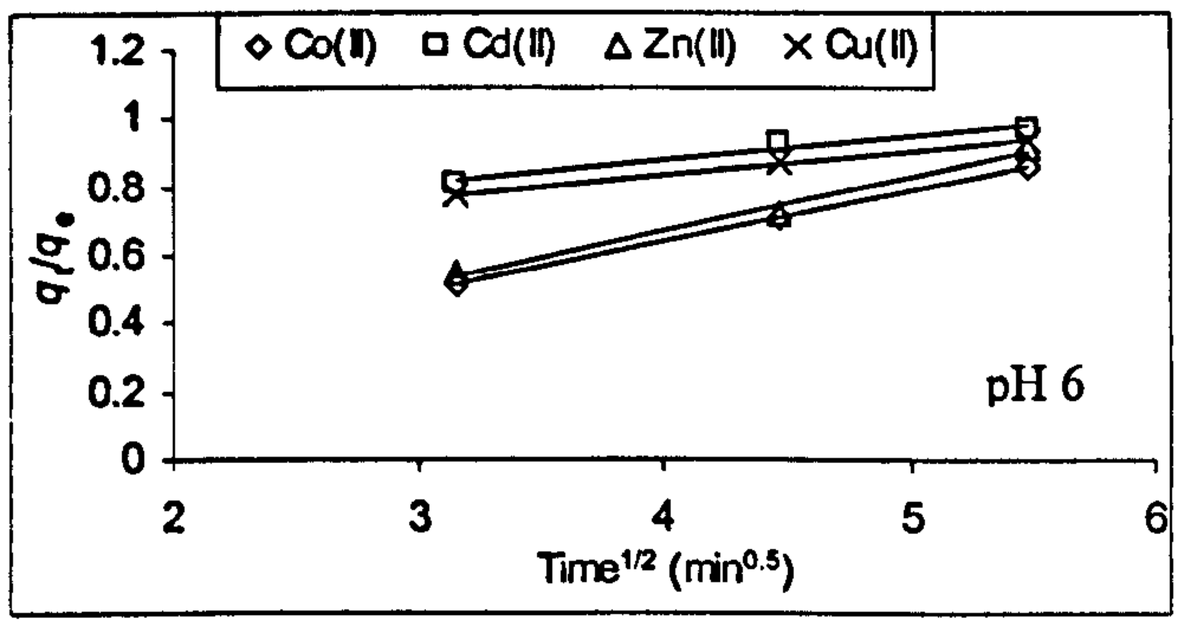

Figure 10.6: Plots of equation (18) at different initial pH values (25°C) for the determination of film diffusion coefficients, D_1, of M(II) with MF-DTPA.

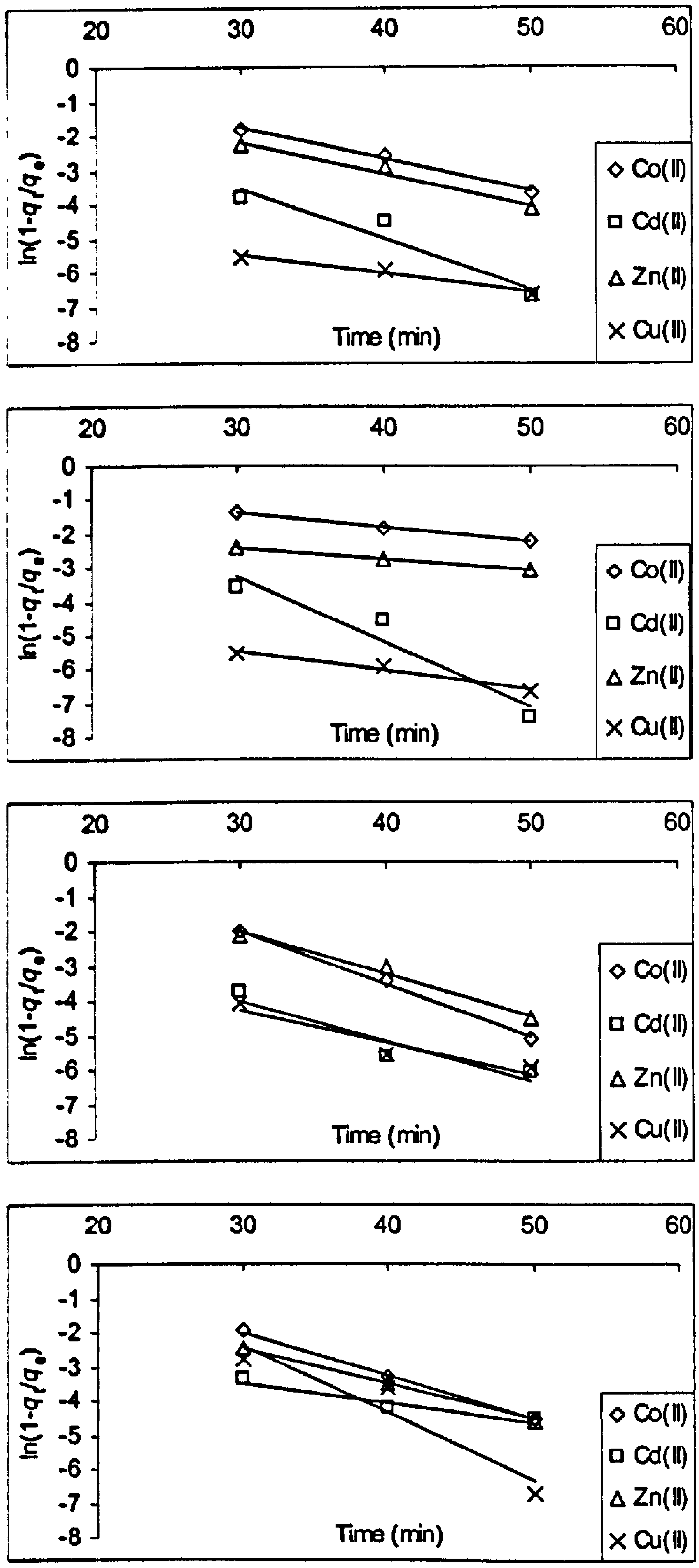

Figure 10.7: Plots of equation (19) at different initial pH values (25°C) for the determination of pore diffusion coefficients, D_2, of M(II) with MF-DTPA.

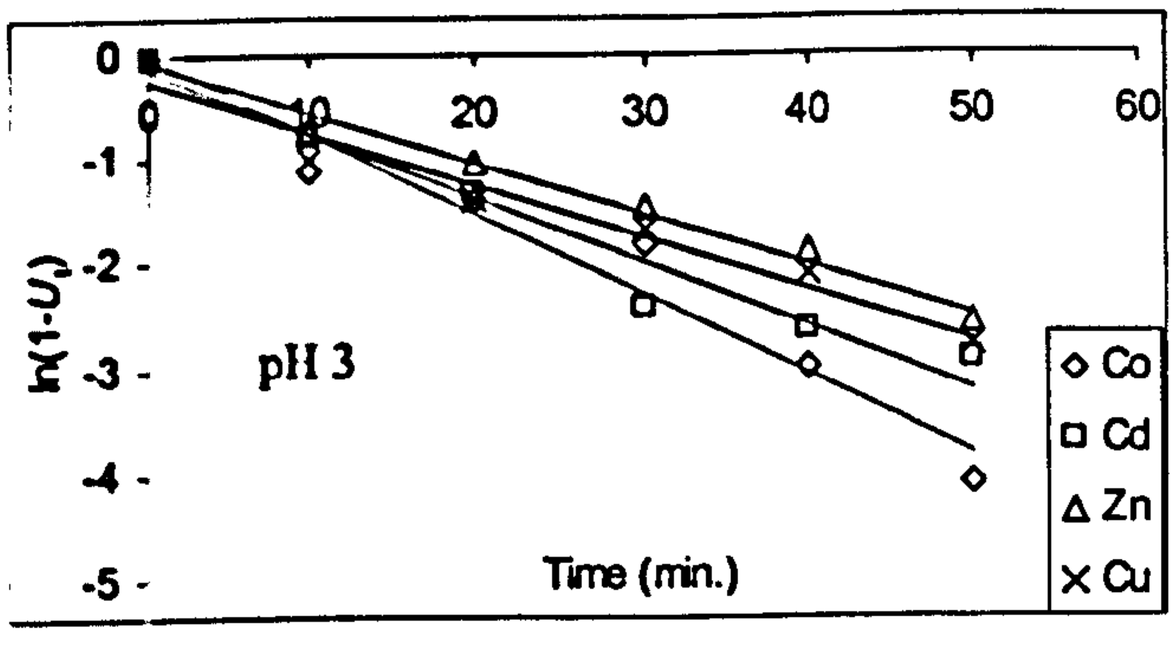

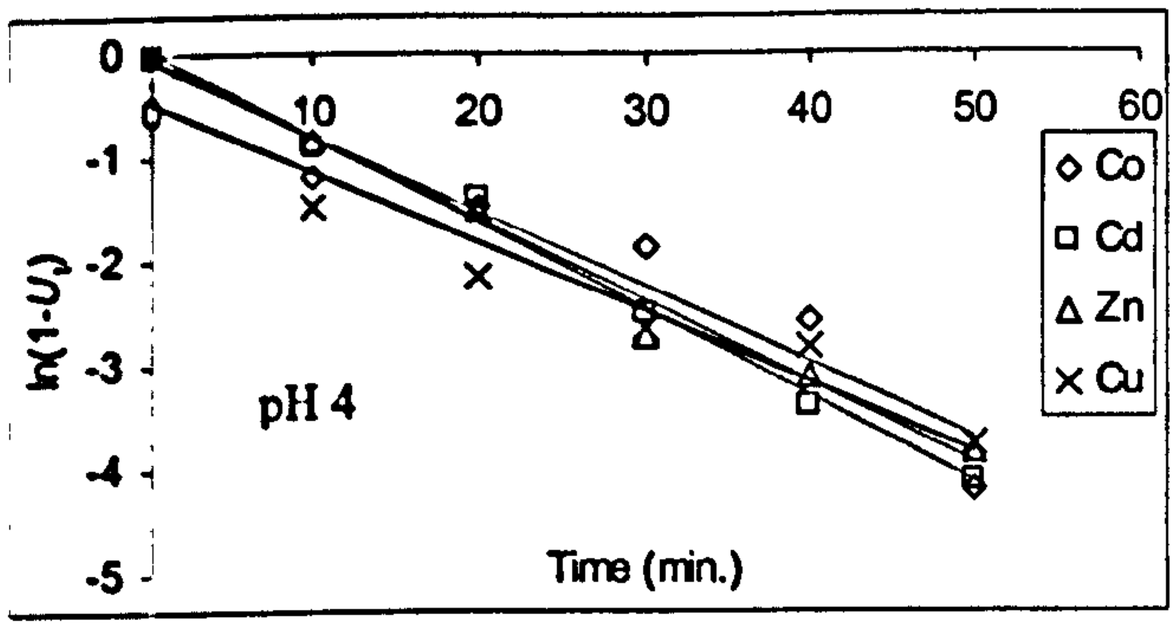

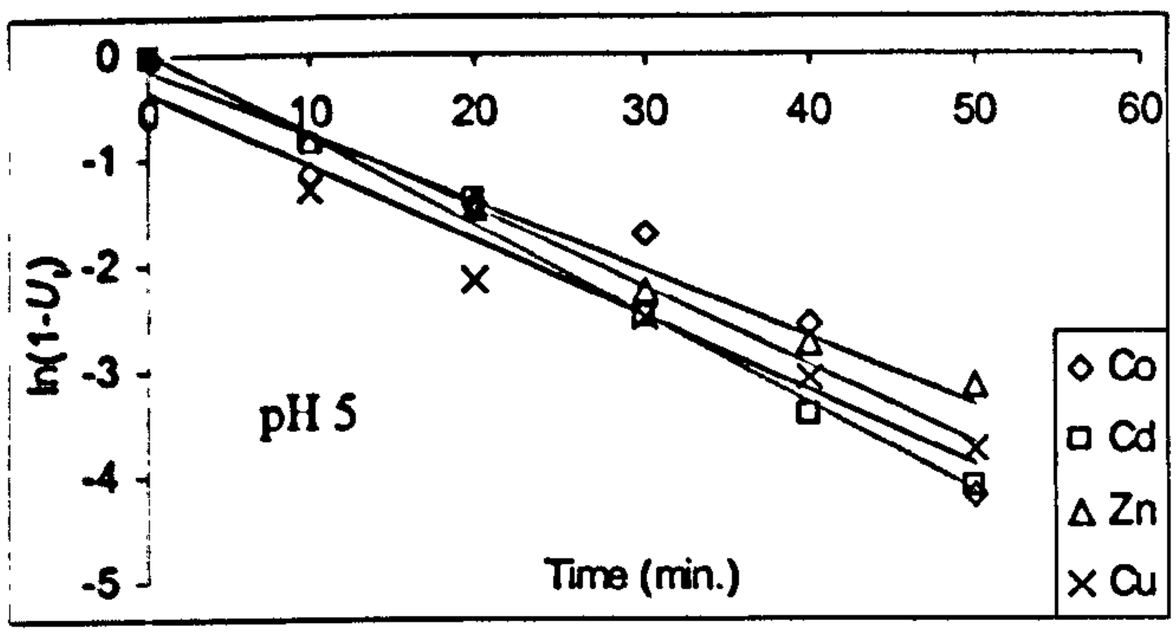

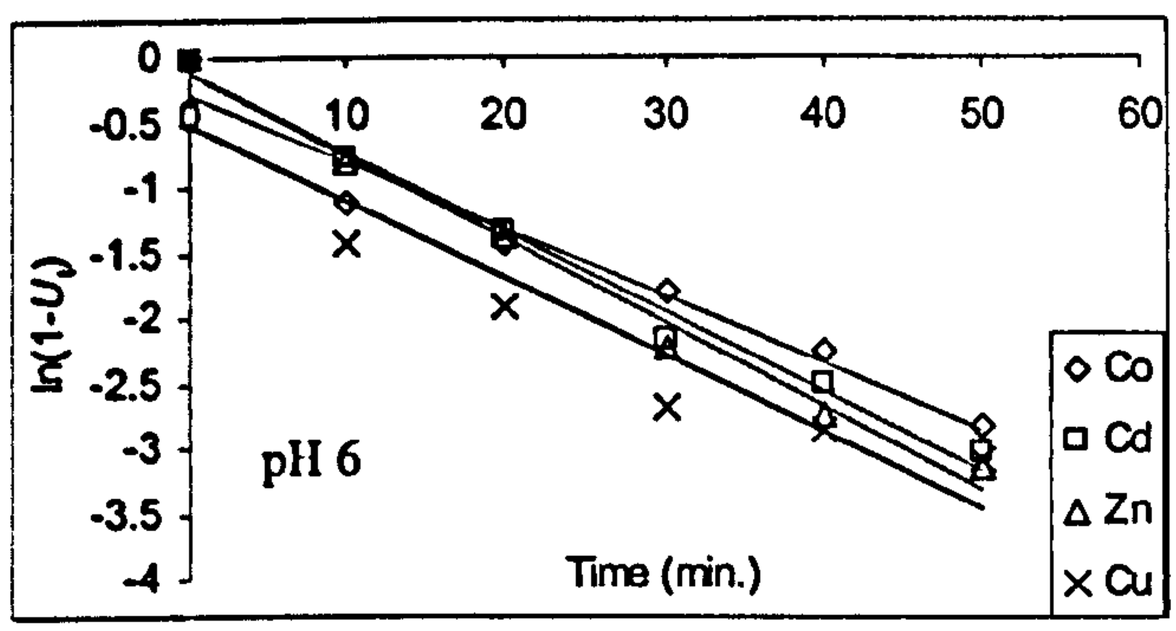

Figure 10.8: Reversible first-order plot of adsorption of Co(II), Cd(II), Zn(II) and Cu(II) on MF-CDTA at temperature 15°C for pH 3, 4, 5 and 6.

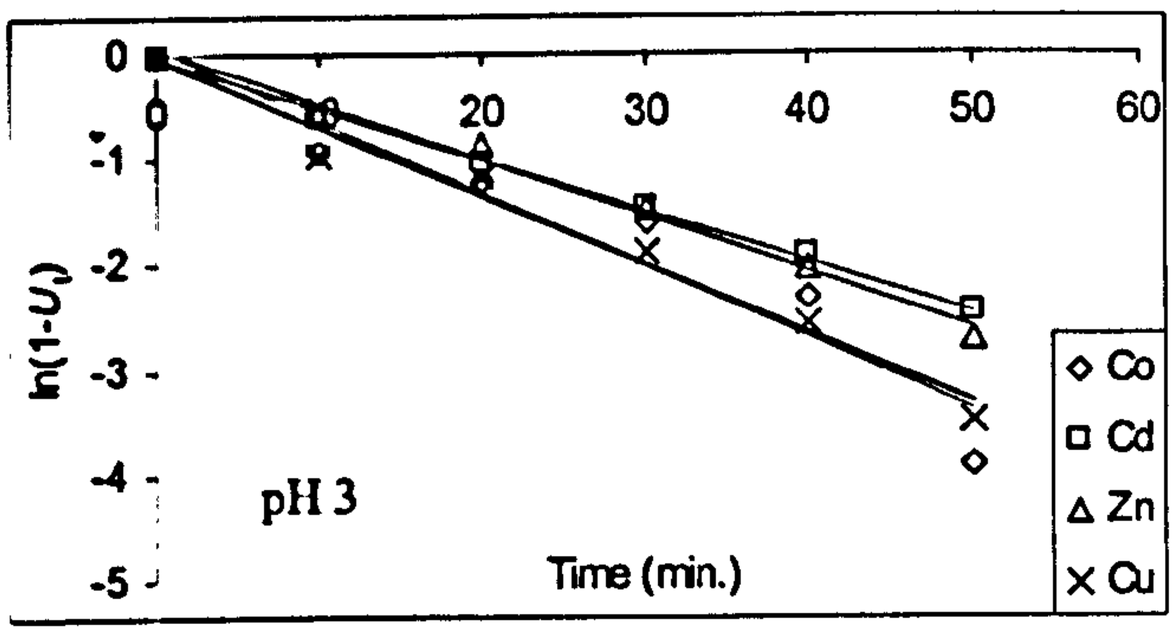

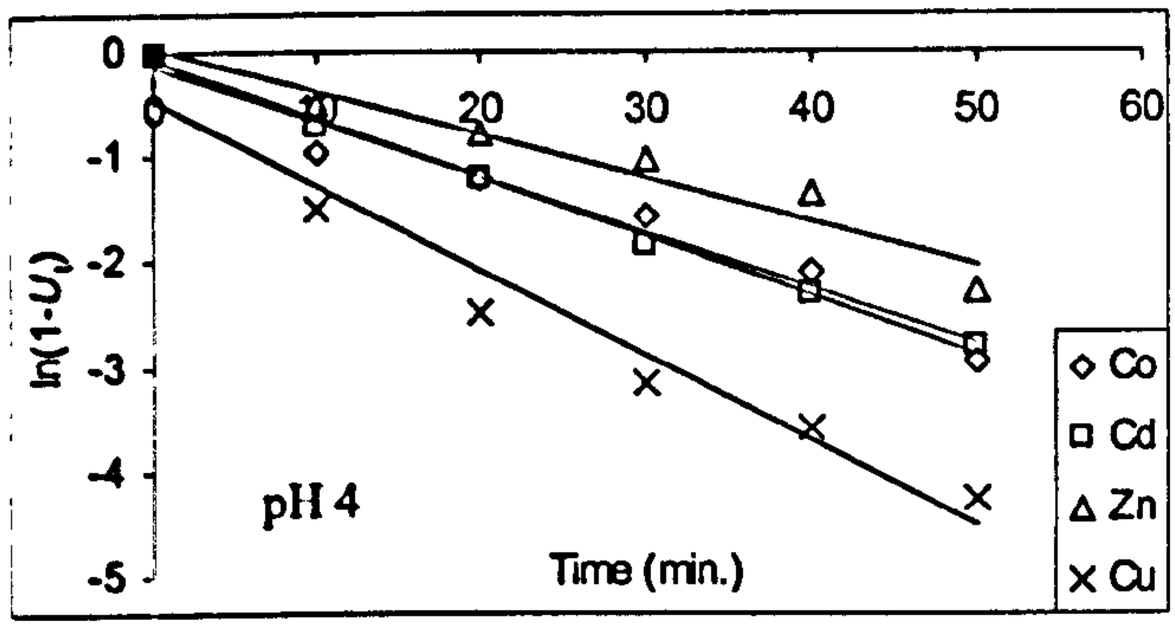

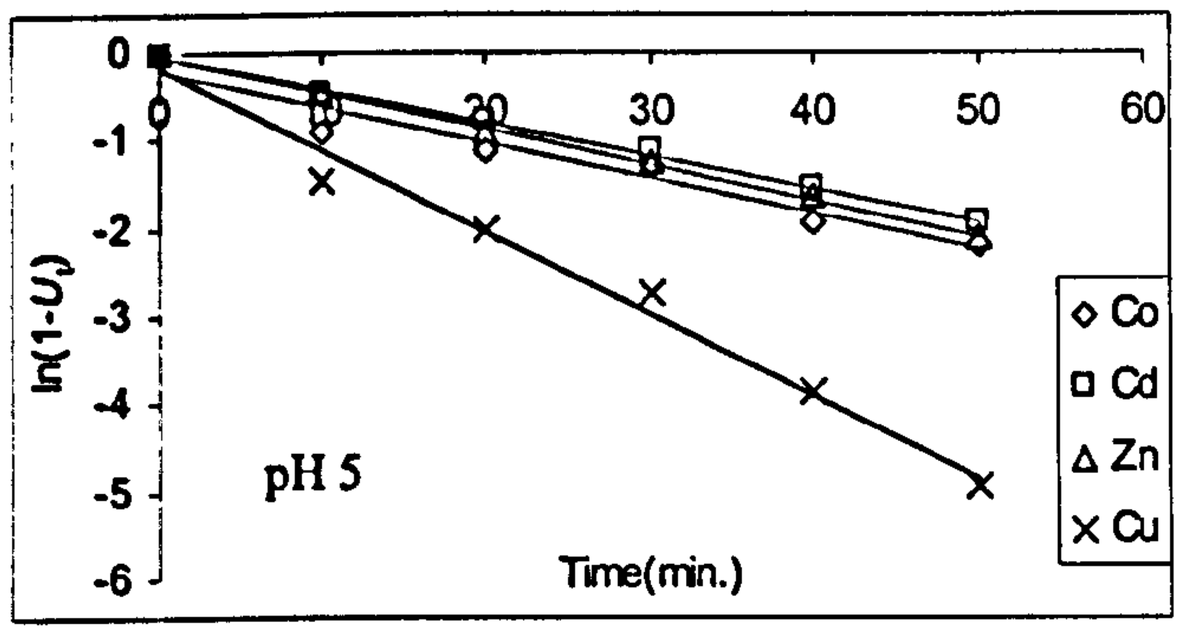

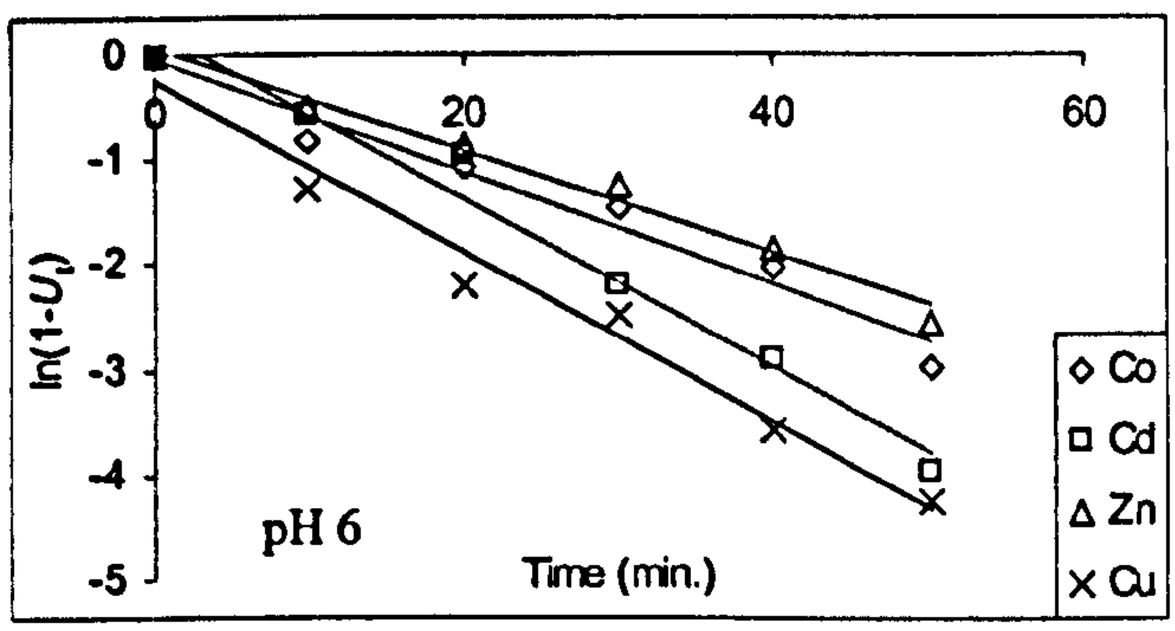

Figure 10.10: Reversible first-order plot of adsorption of Co(II), Cd(II), Zn(II) and Cu(II) on MF-CDTA at temperature 35°C for pH 3, 4, 5 and 6.

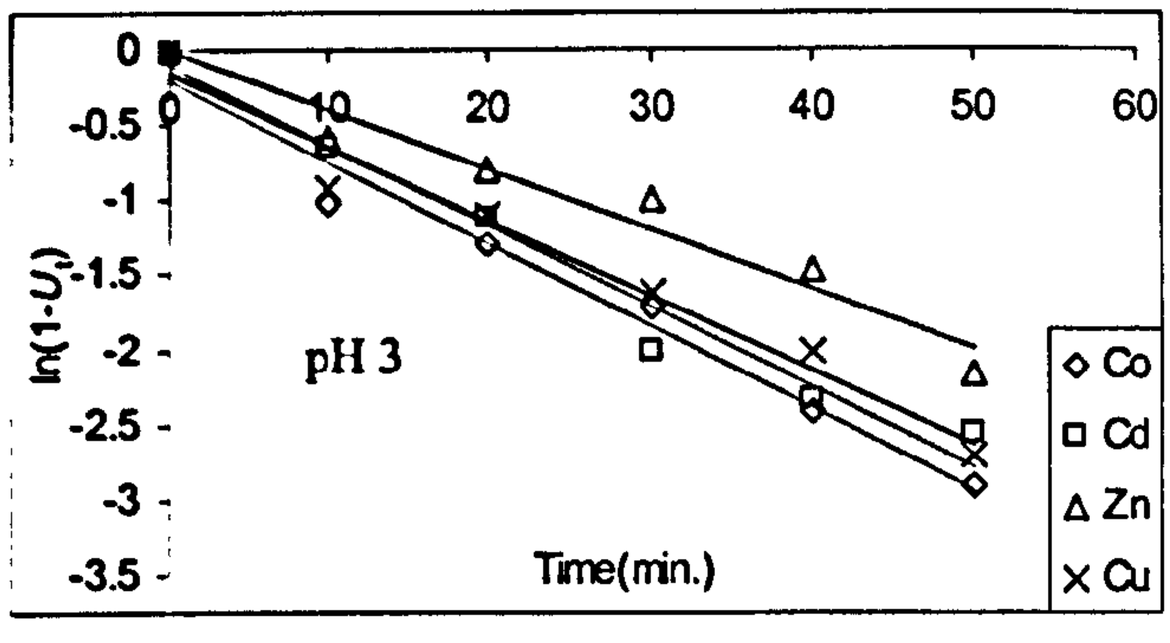

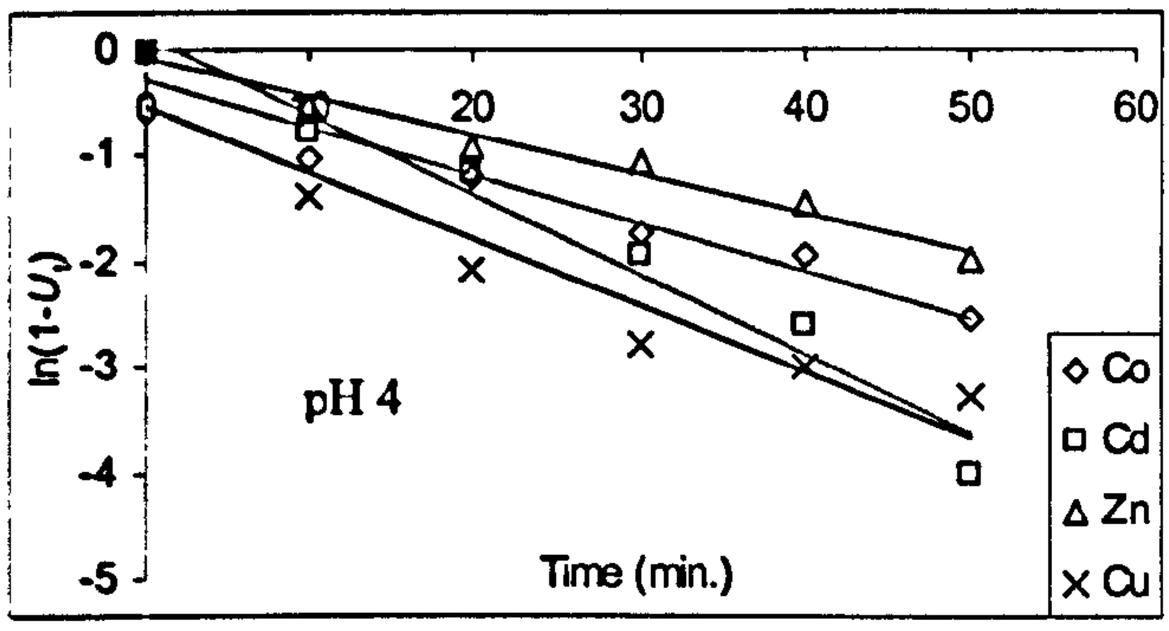

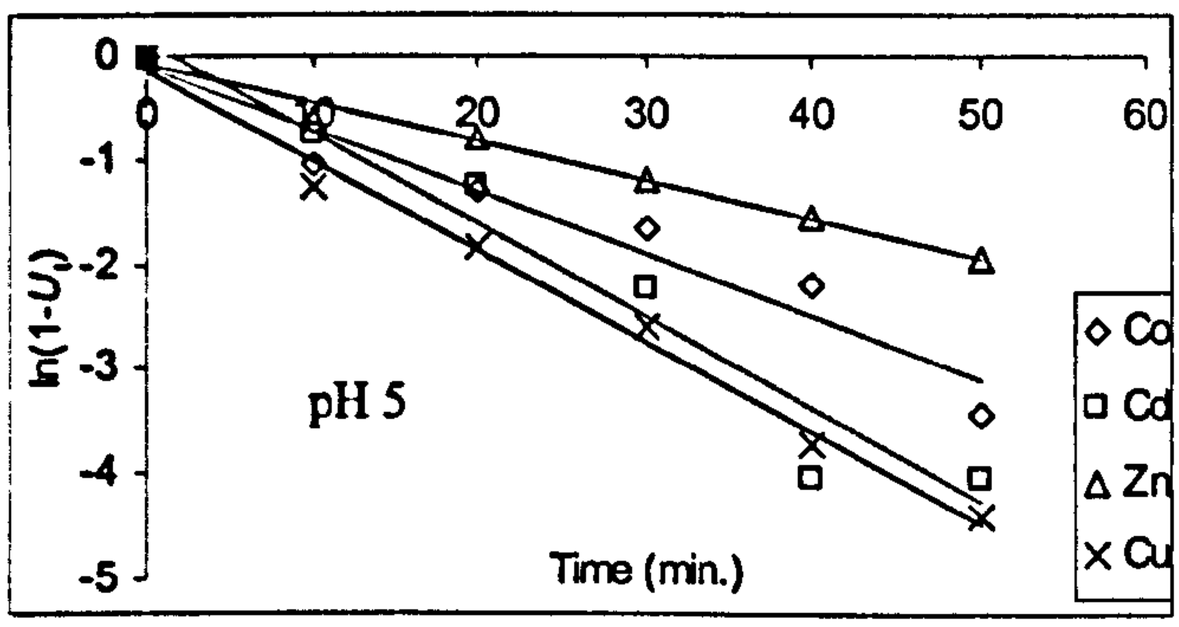

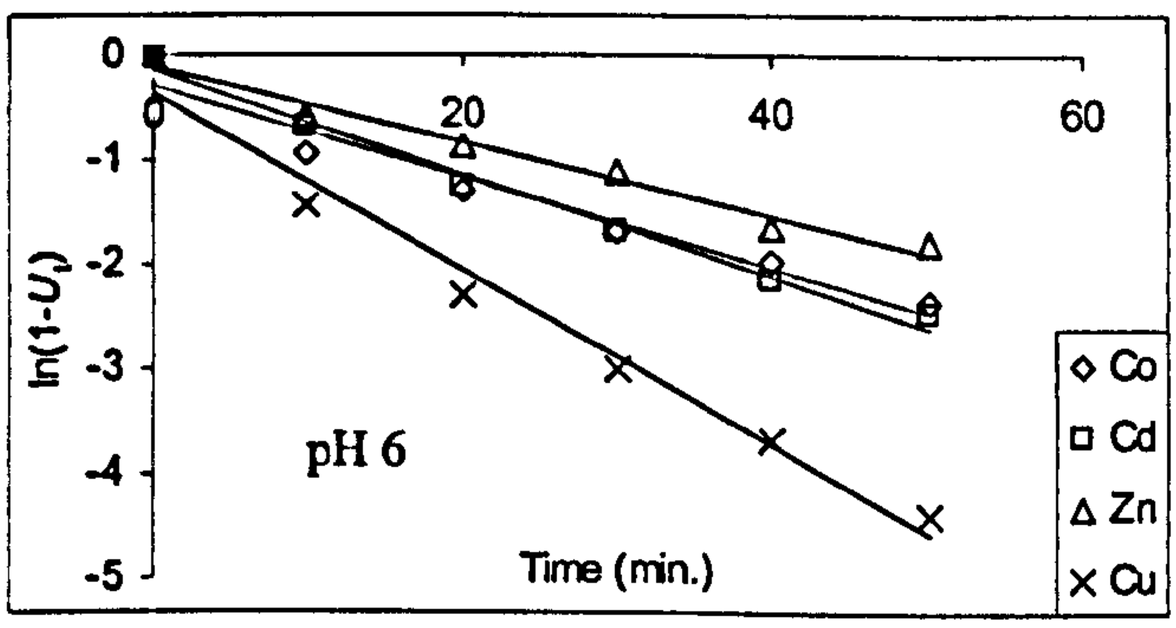

Figure 10.9: Reversible first-order plot of adsorption of Co(II), Cd(II), Zn(II) and Cu(II) on MF-CDTA at temperature 25°C for pH 3, 4, 5 and 6.

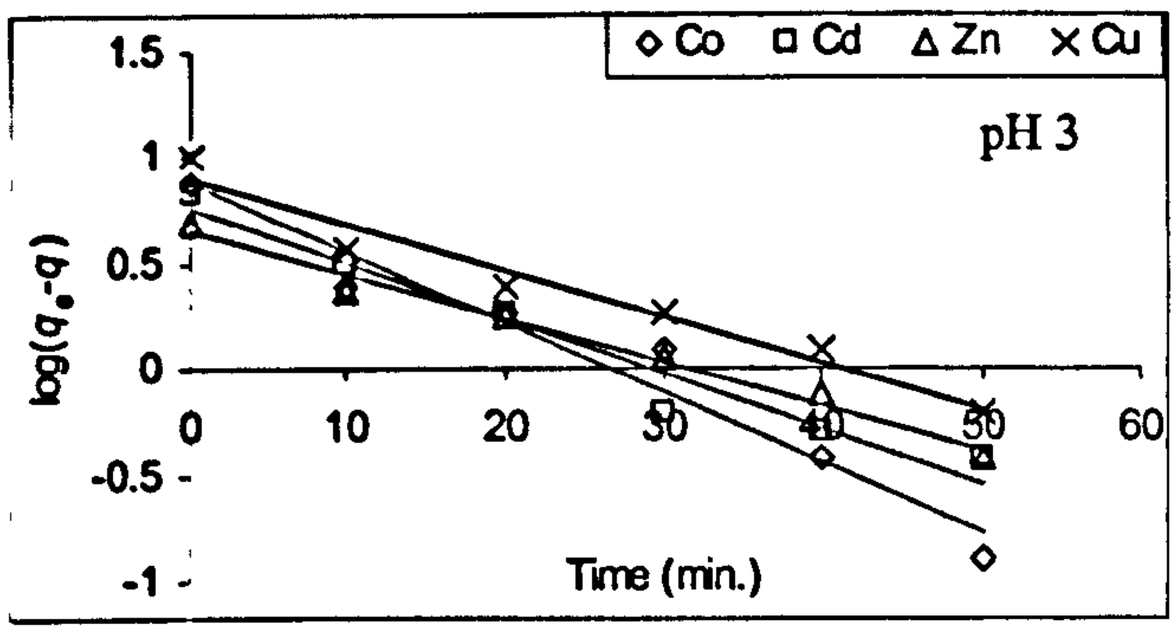

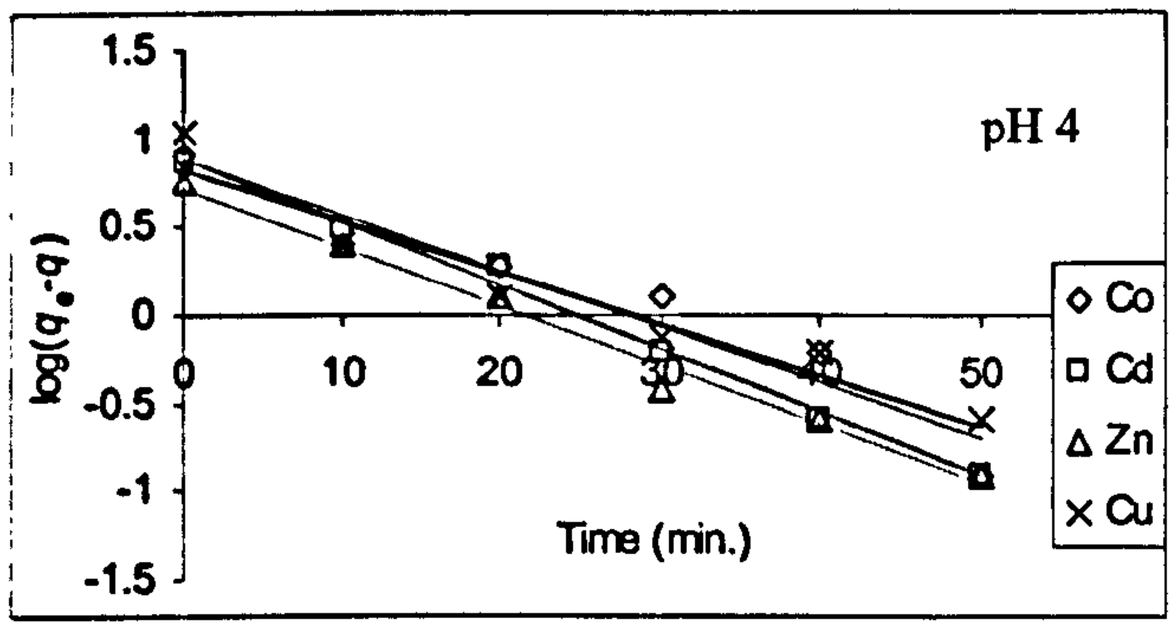

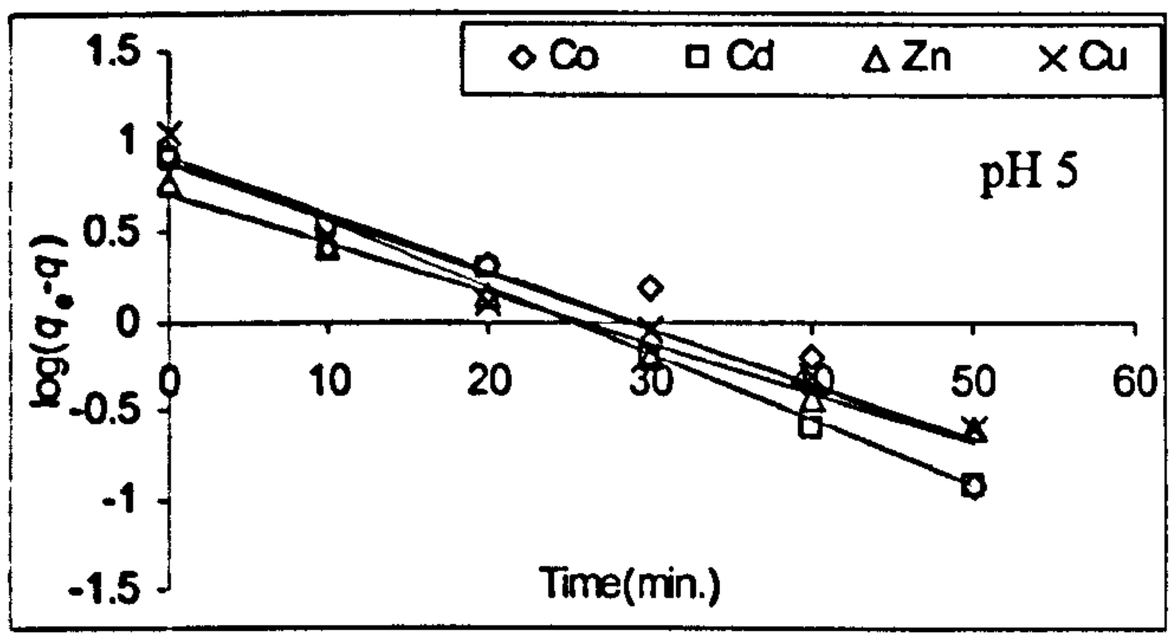

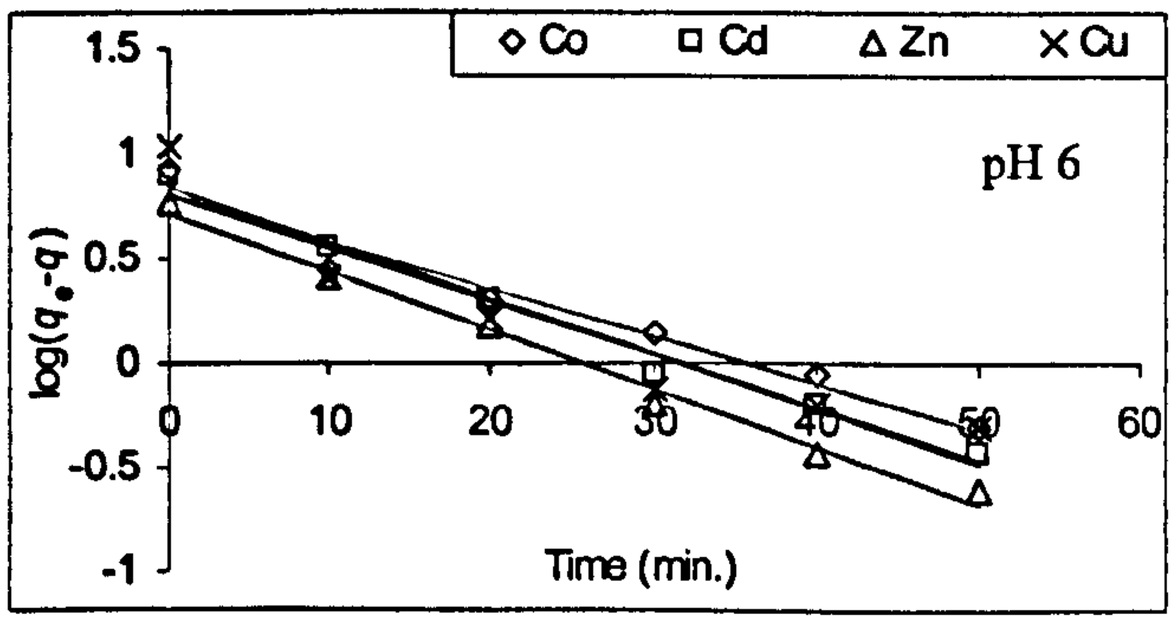

Figure 10.11: Pseudo first-order plot of adsorption of Co(II), Cd(II), Zn(II) and Cu(II) on MF-CDTA at temperature 15°C for pH 3, 4, 5 and 6.

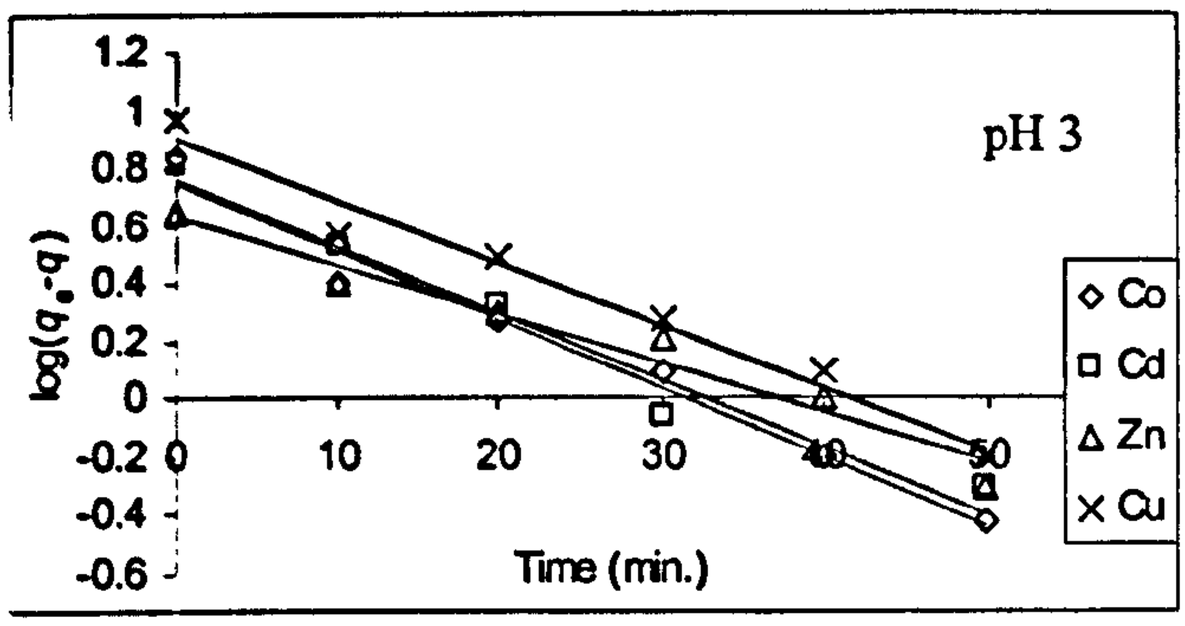

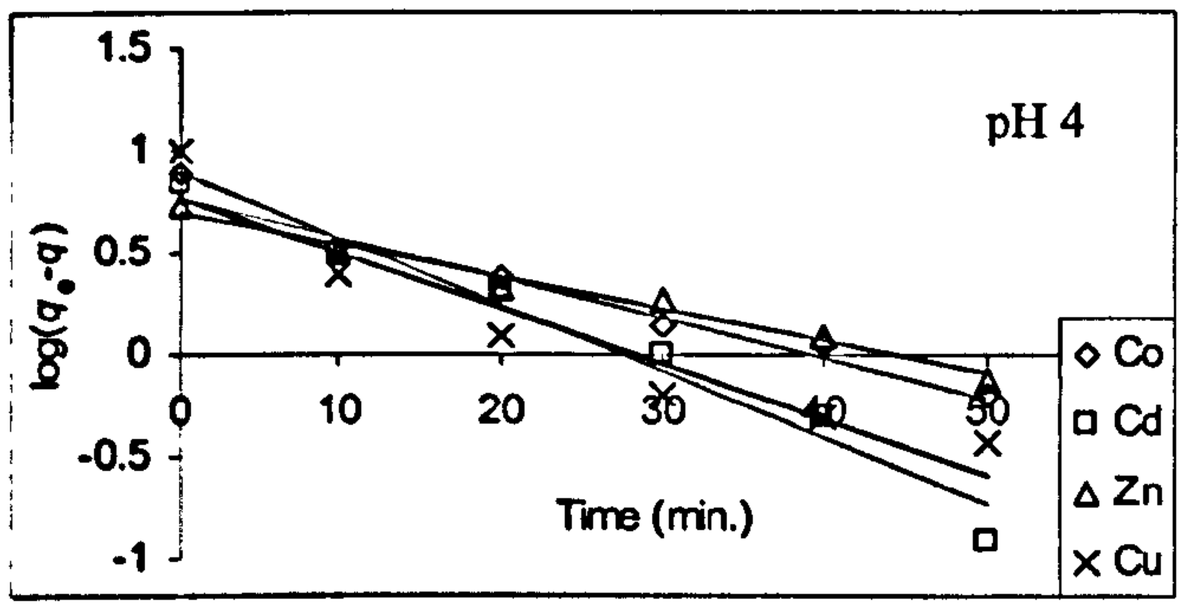

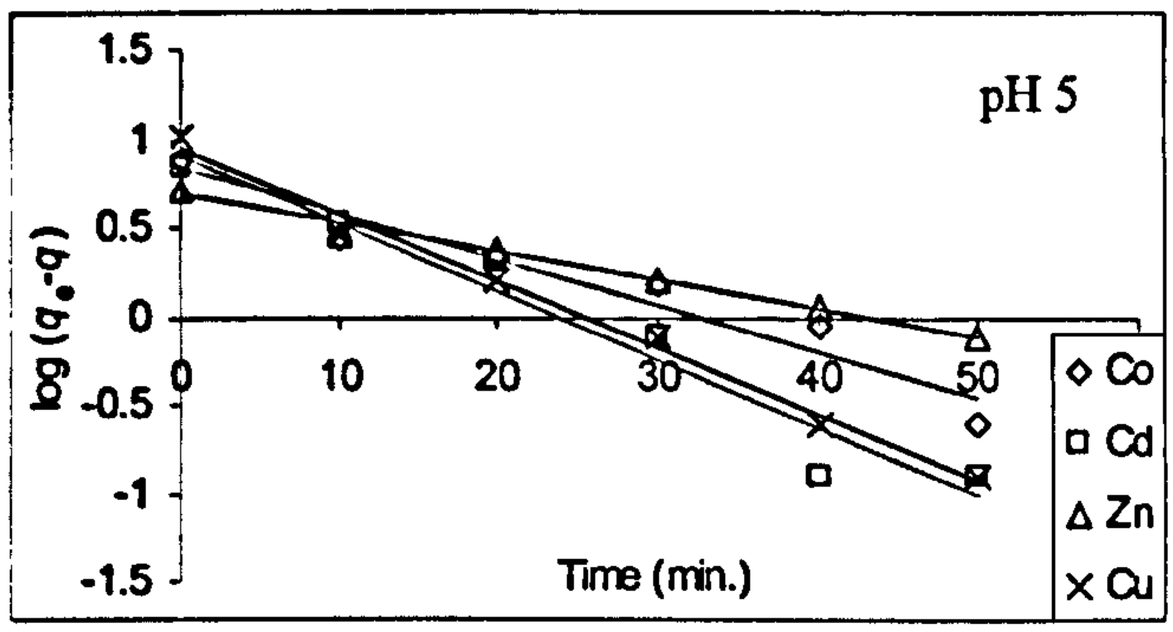

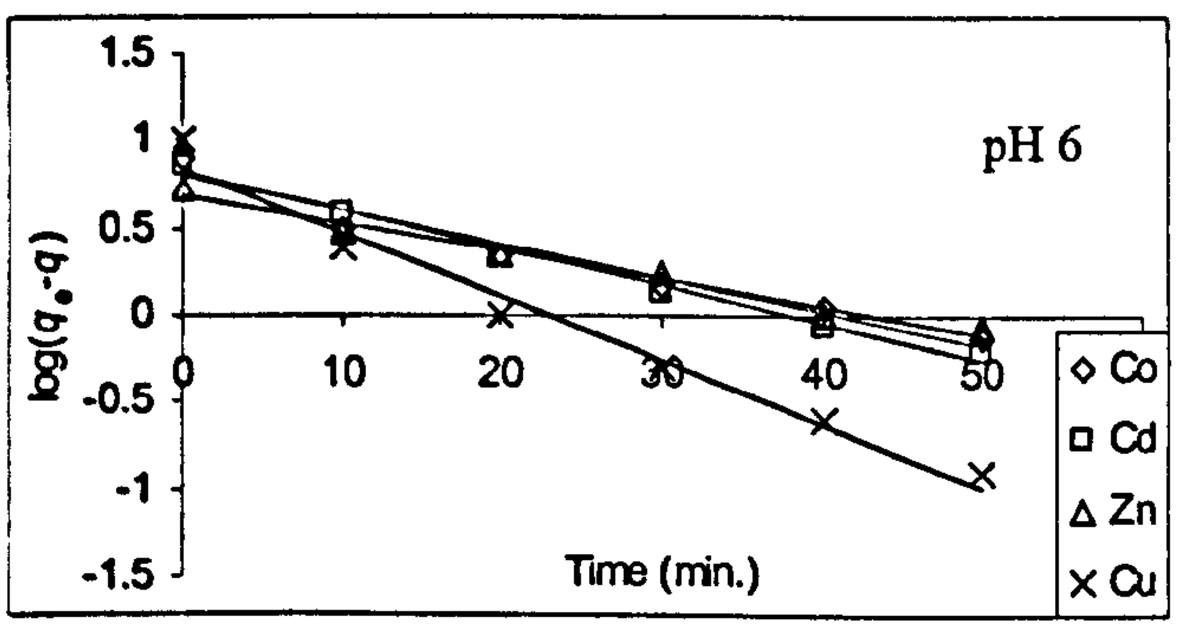

Figure 10.12: Pseudo first-order plot of adsorption of Co(II), Cd(II), Zn(II) and Cu(II) on MF-CDTA at temperature 25°C for pH 3, 4, 5 and 6.

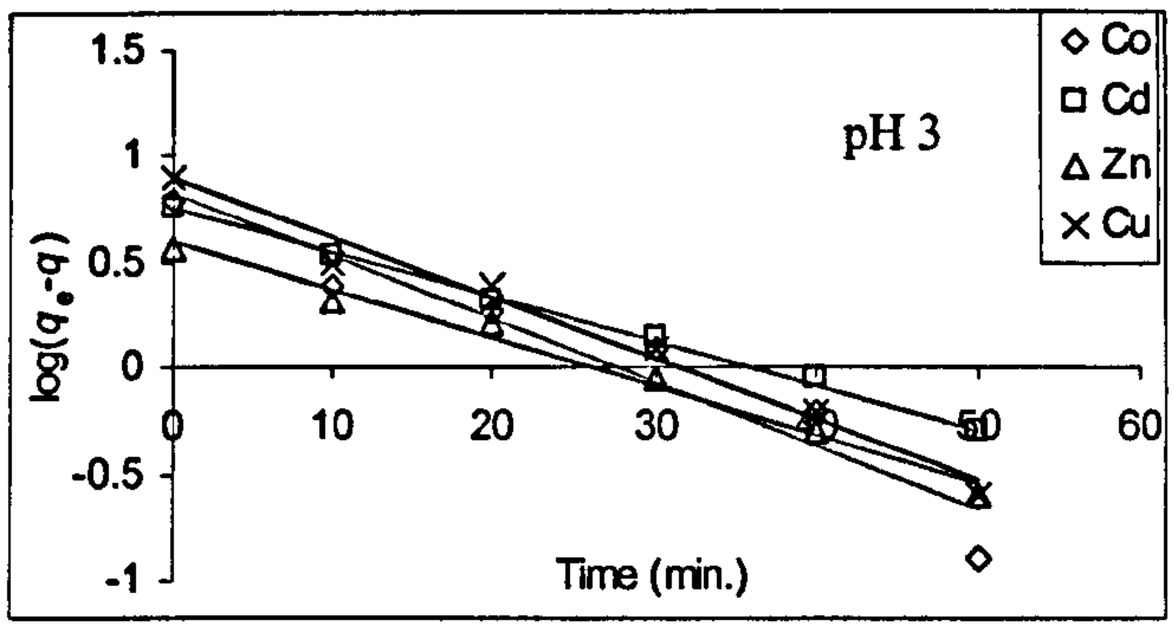

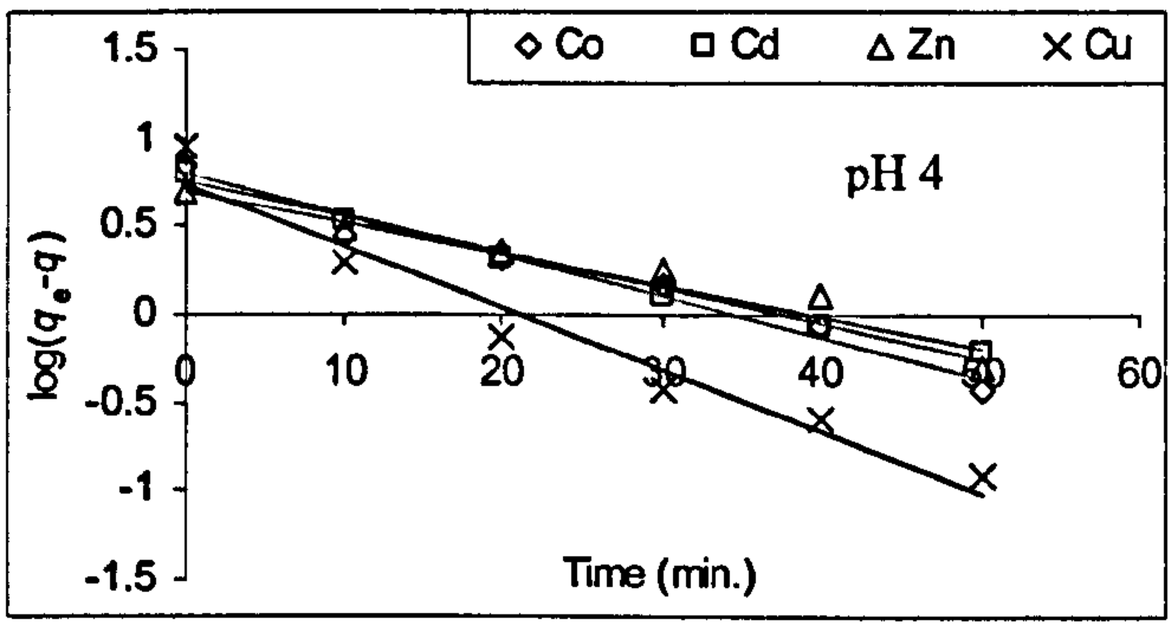

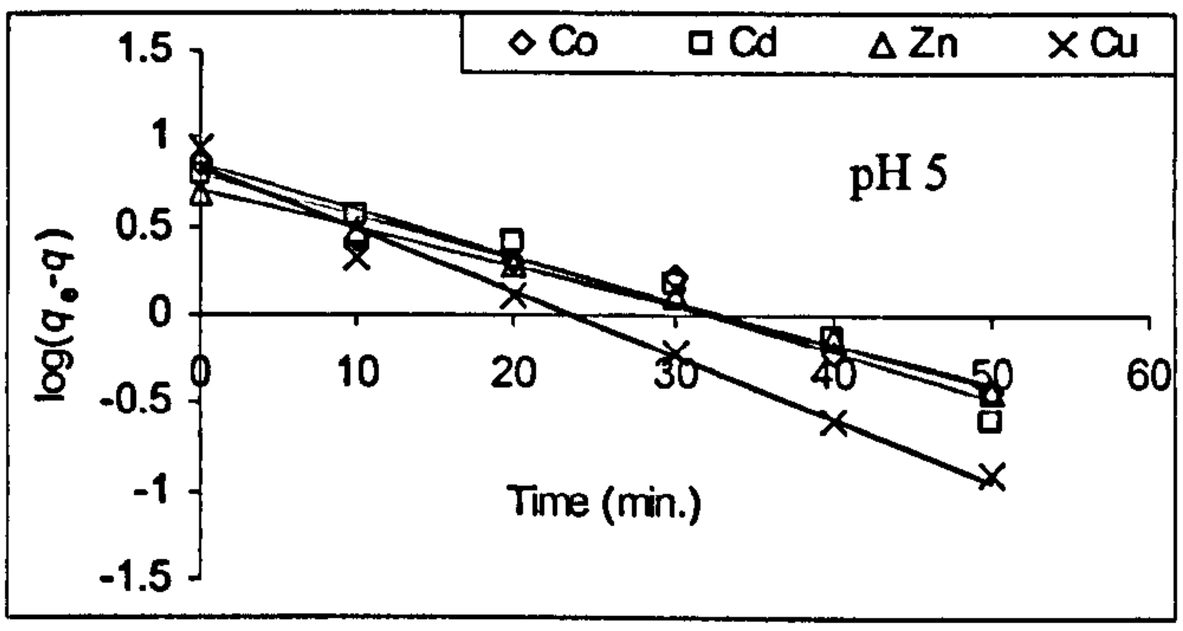

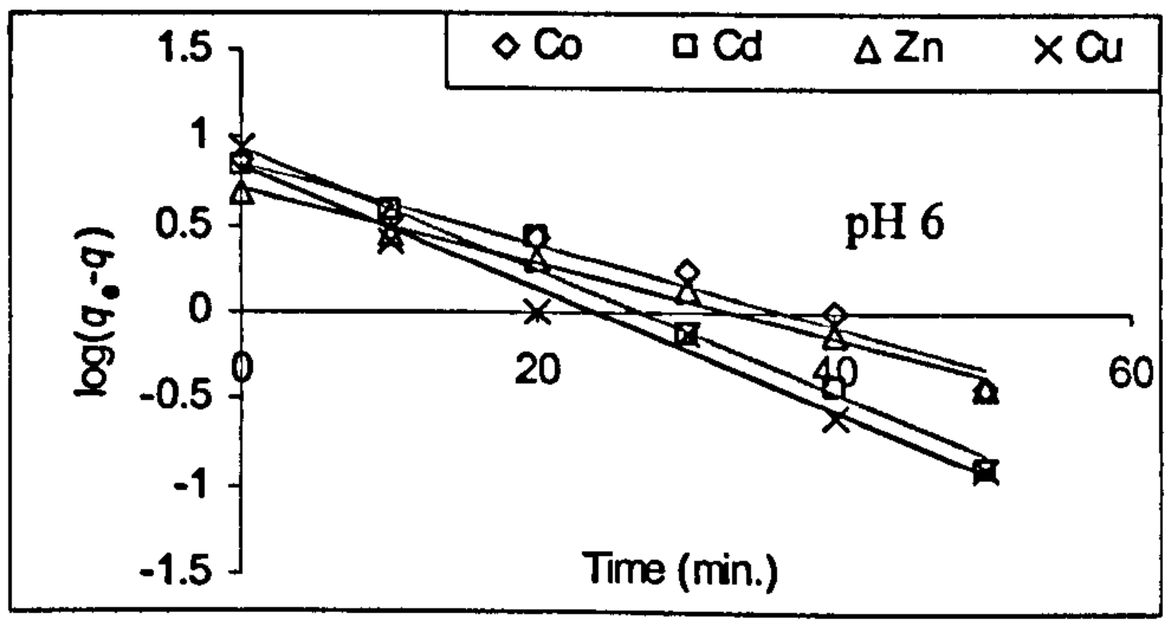

Figure 10.13: Pseudo first-order plot of adsorption of Co(II), Cd(II), Zn(II) and Cu(II) on MF-CDTA at temperature 35°C for pH 3, 4, 5 and 6.

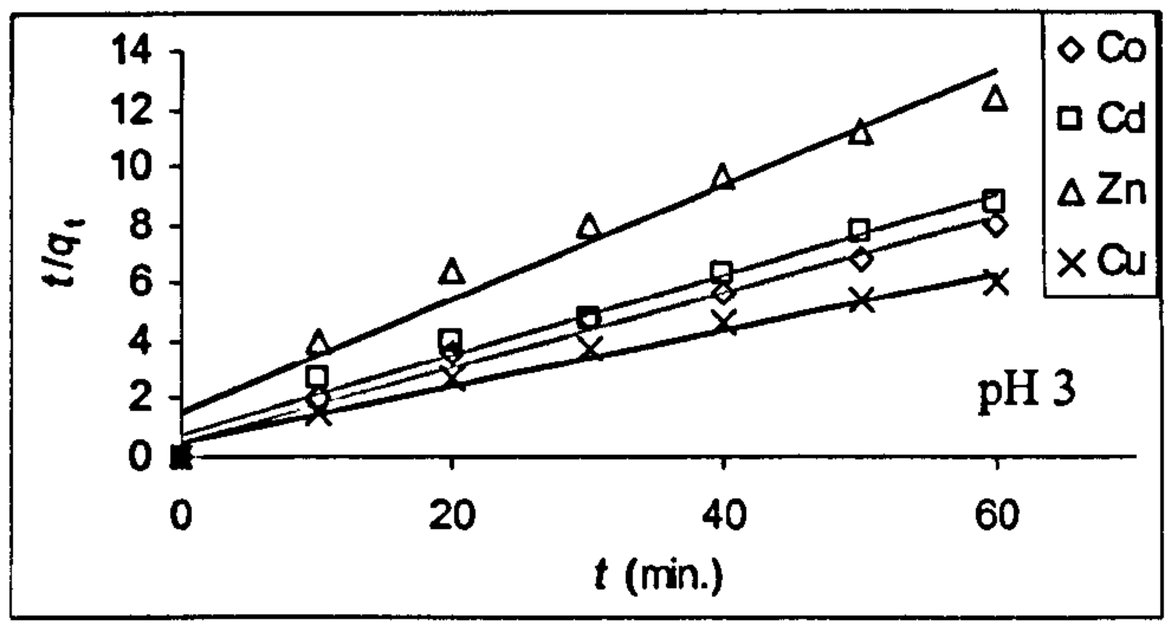

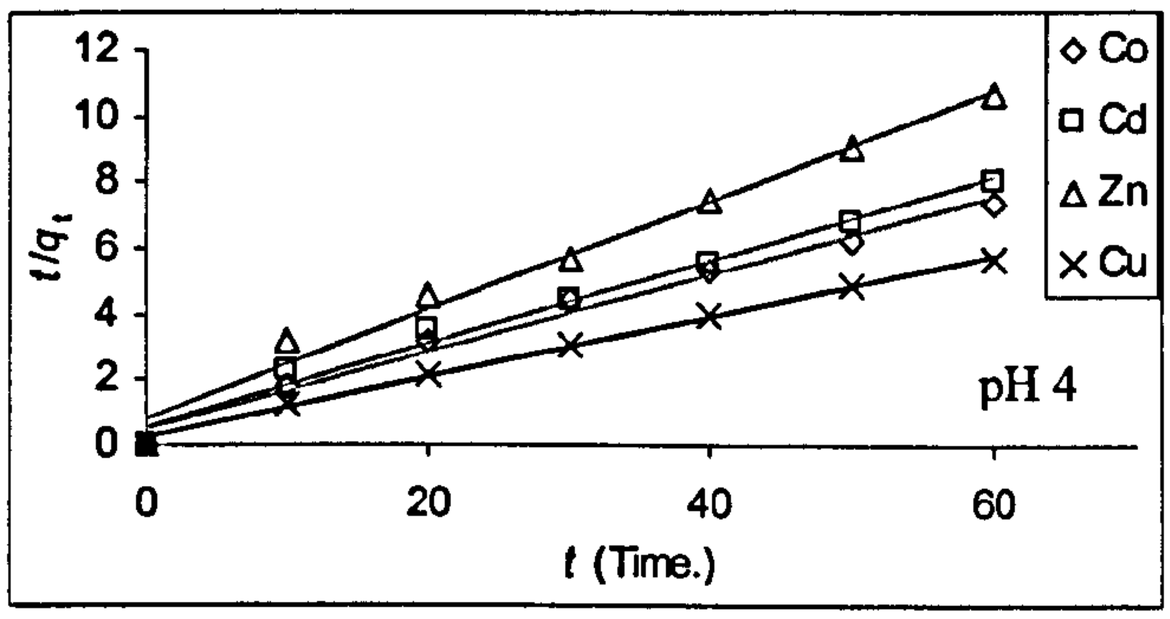

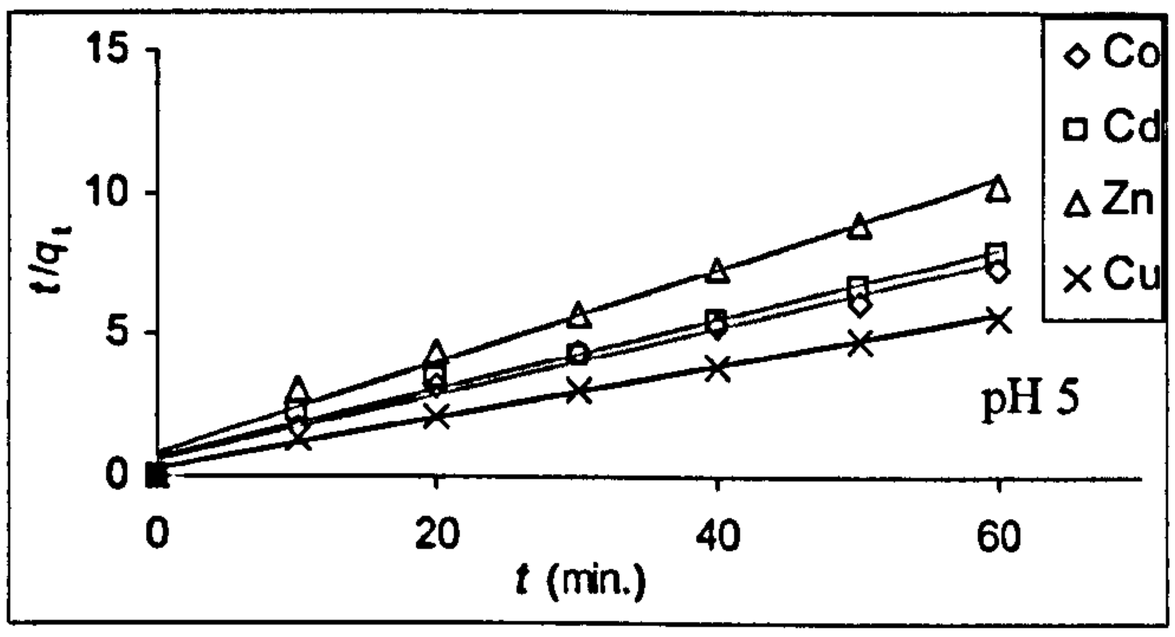

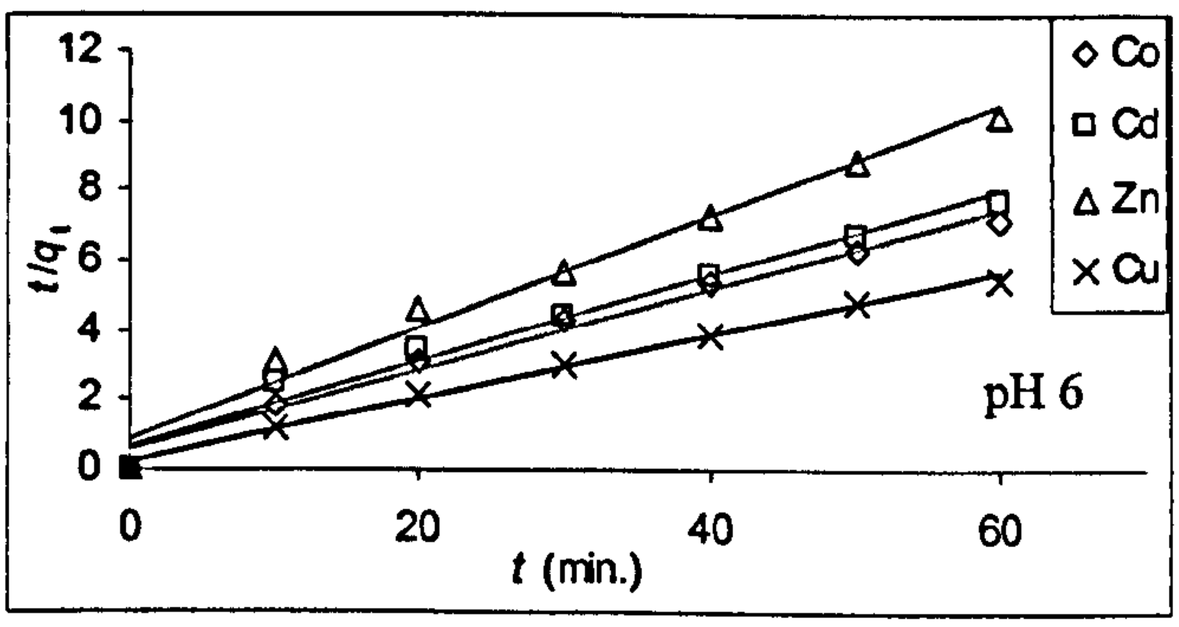

Figure 10.14: Pseudo second-order plot of adsorption of Co(II), Cd(II), Zn(II) and Cu(II) on MF-CDTA at temperature 15°C for pH 3, 4, 5 and 6.

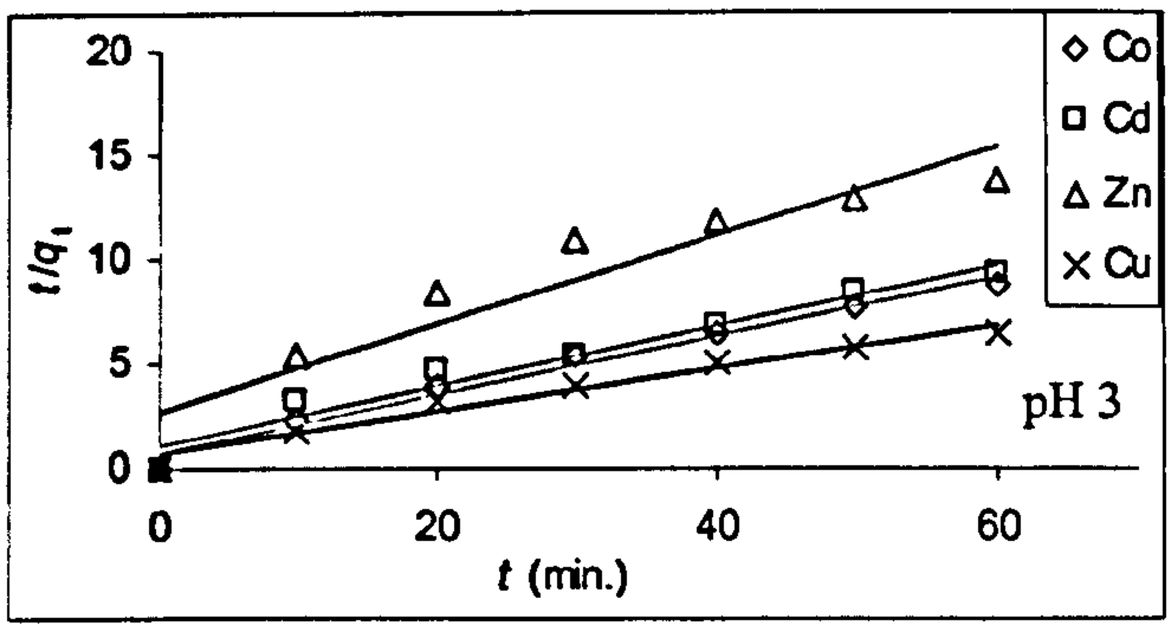

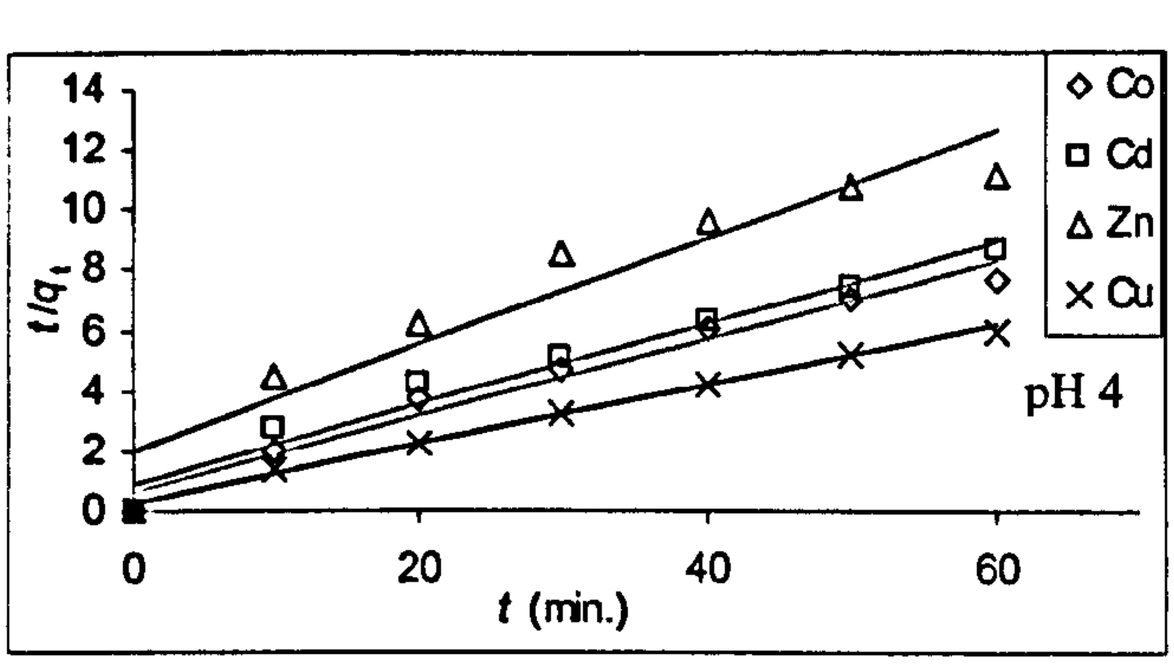

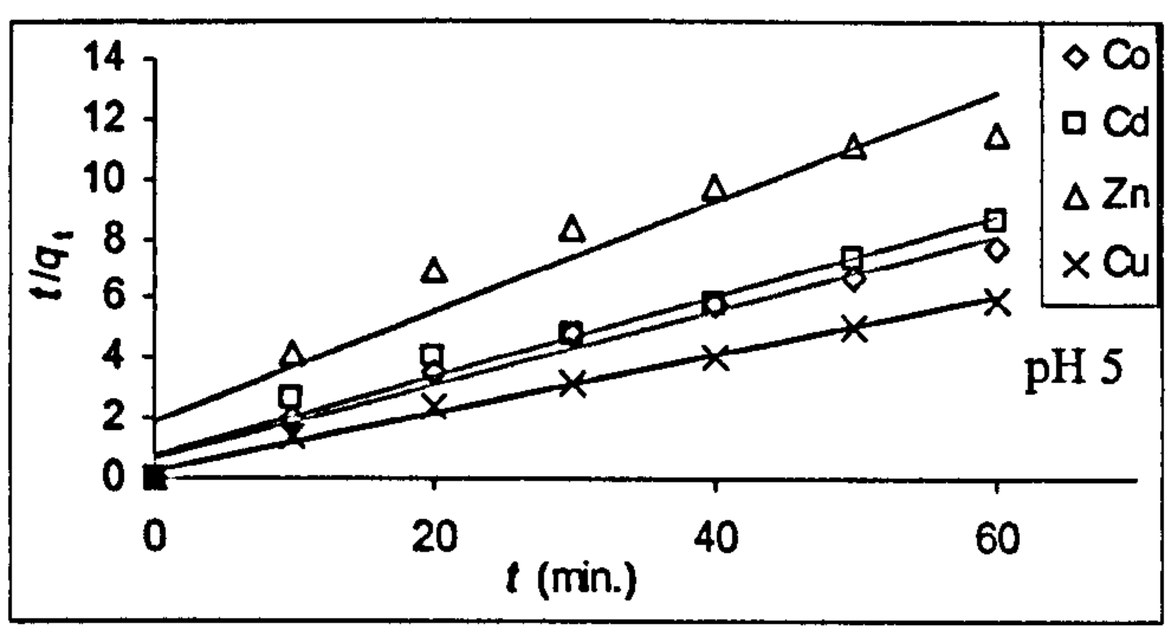

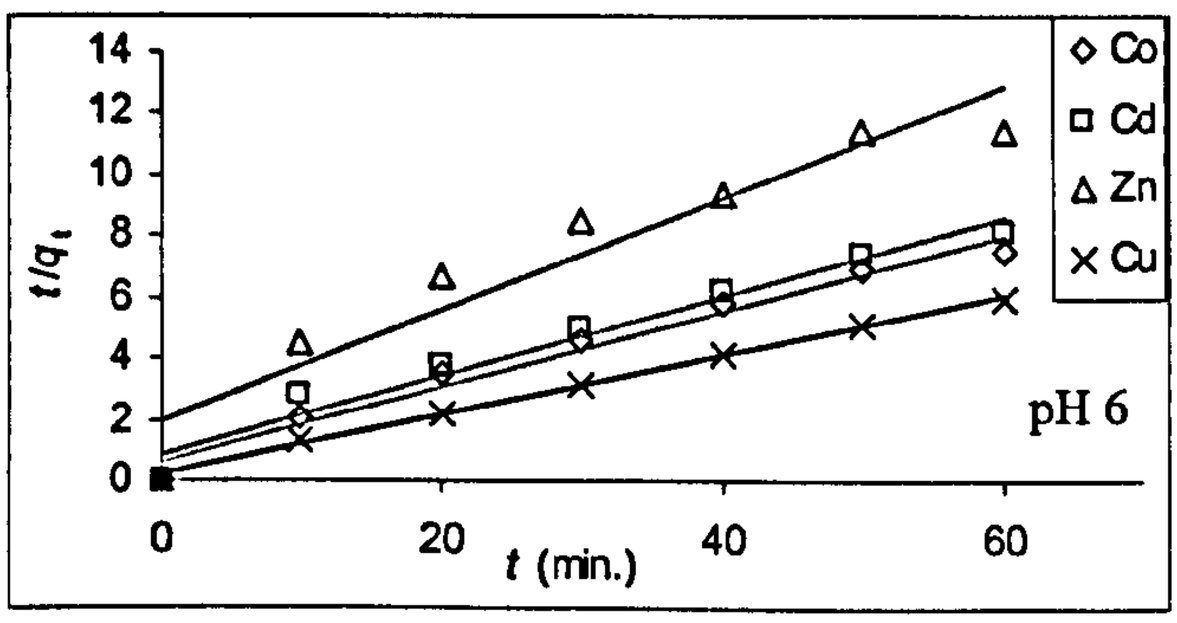

Figure 10.15: Pseudo second-order plot of adsorption of Co(II), Cd(II), Zn(II) and Cu(II) on MF-CDTA at temperature 25°C for pH 3, 4, 5 and 6.

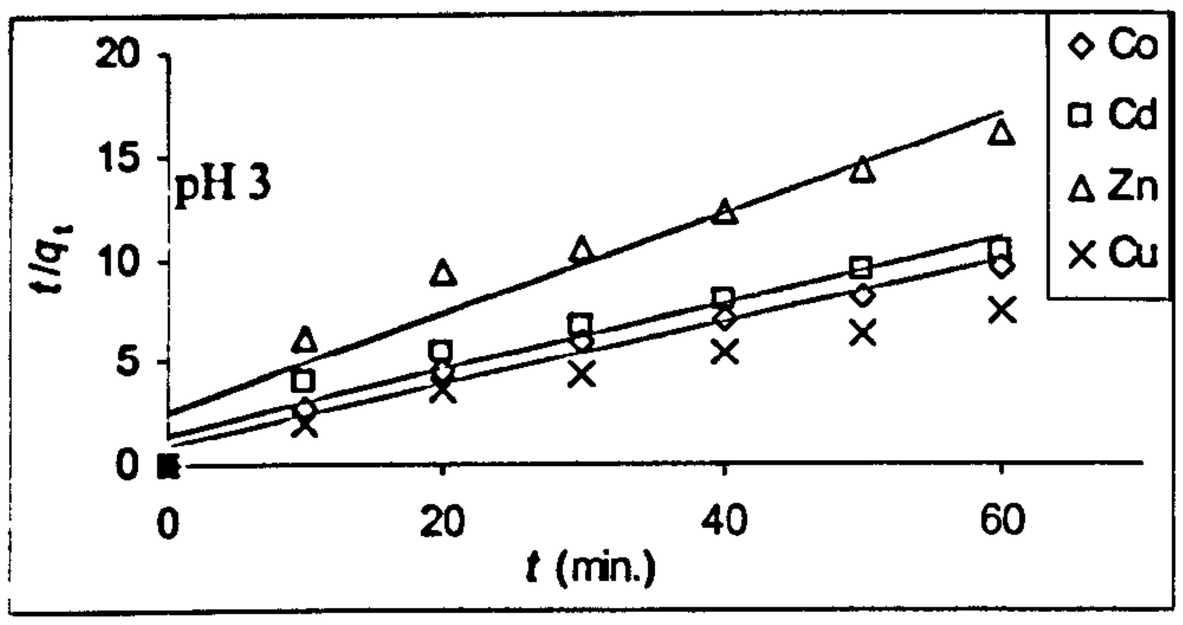

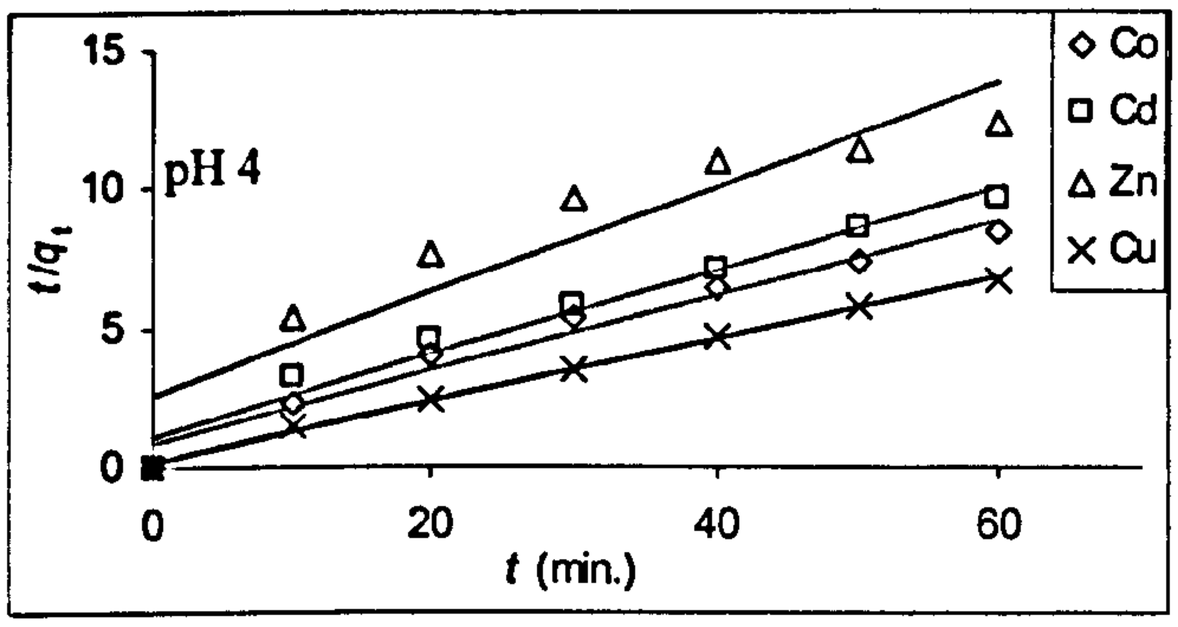

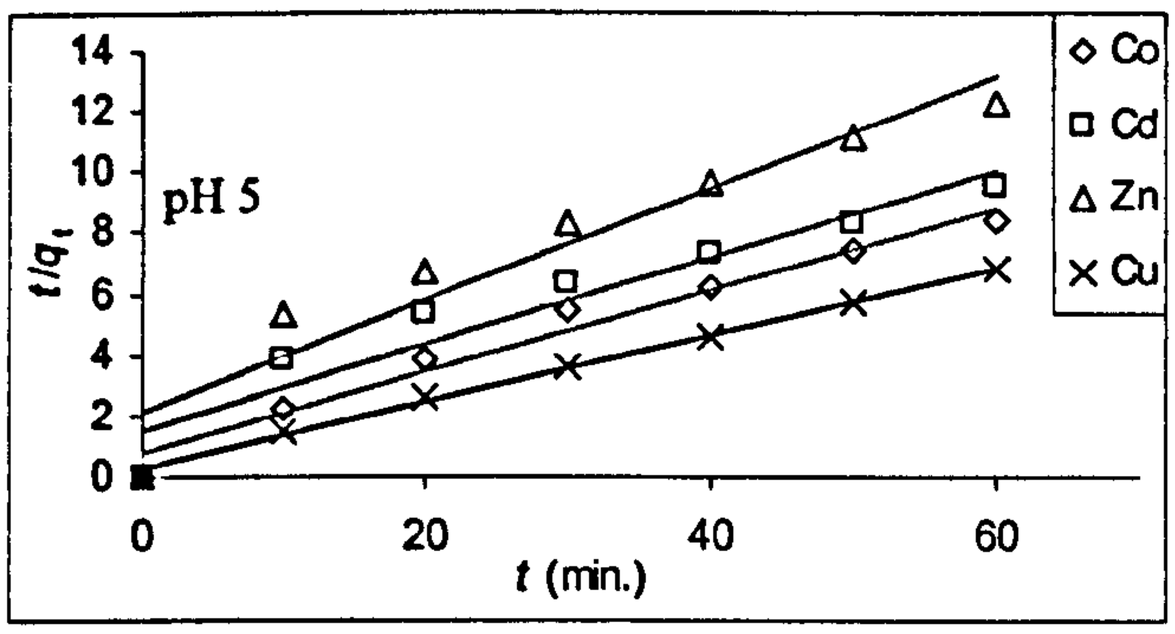

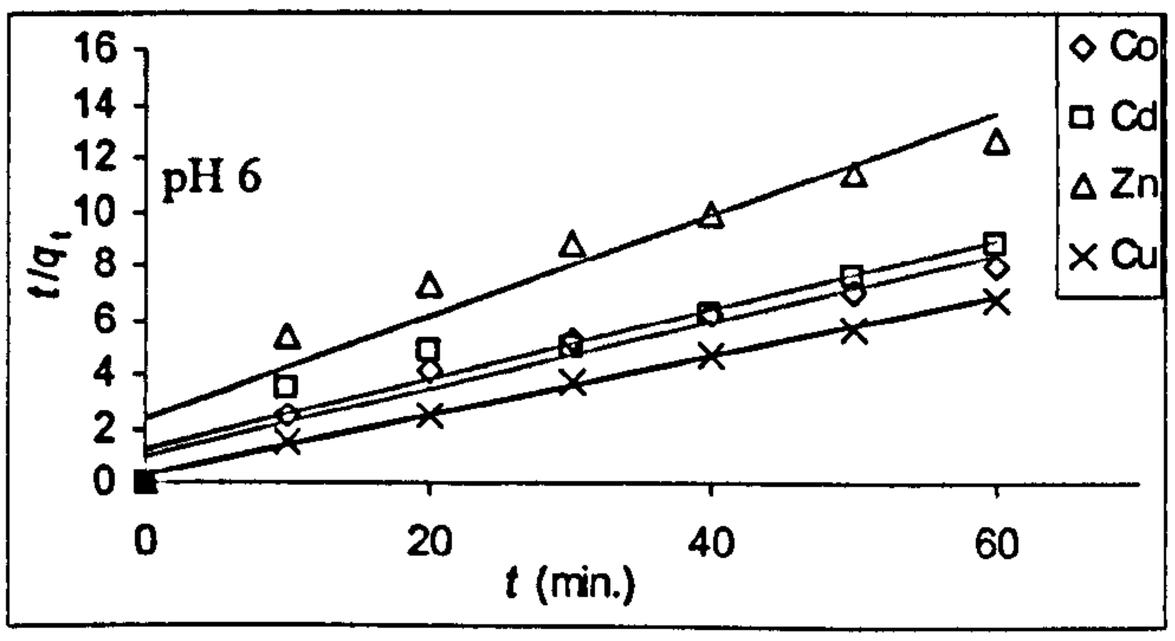

Figure 10.16: Pseudo second-order plot of adsorption of Co(II), Cd(II), Zn(II) and Cu(II) on MF-CDTA at temperature 35°C for pH 3, 4, 5 and 6.

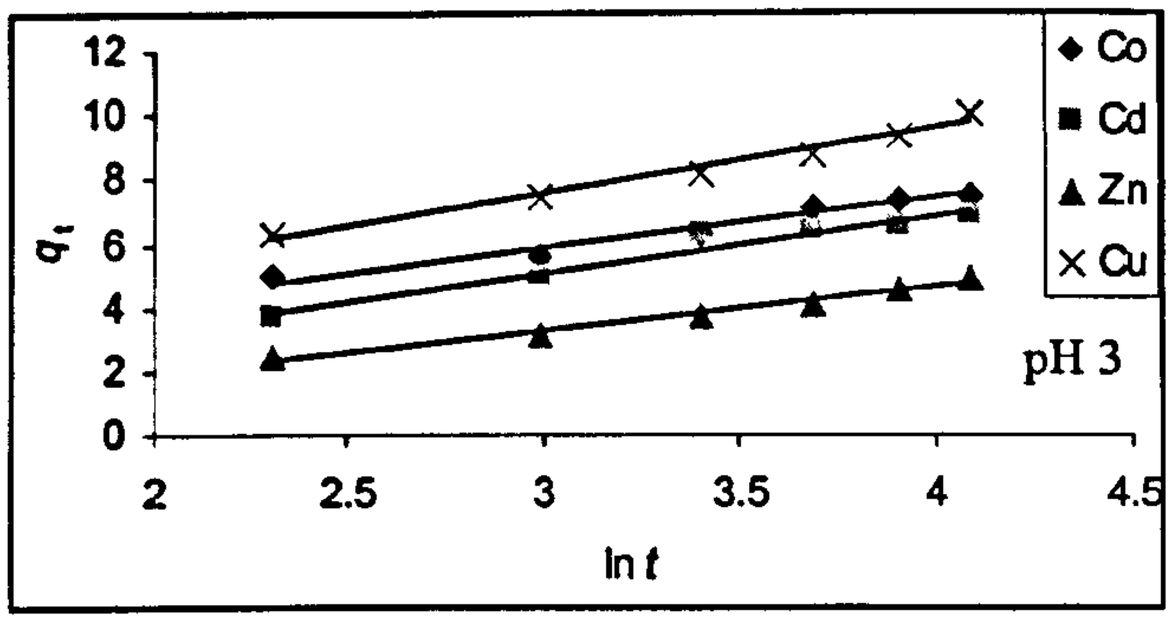

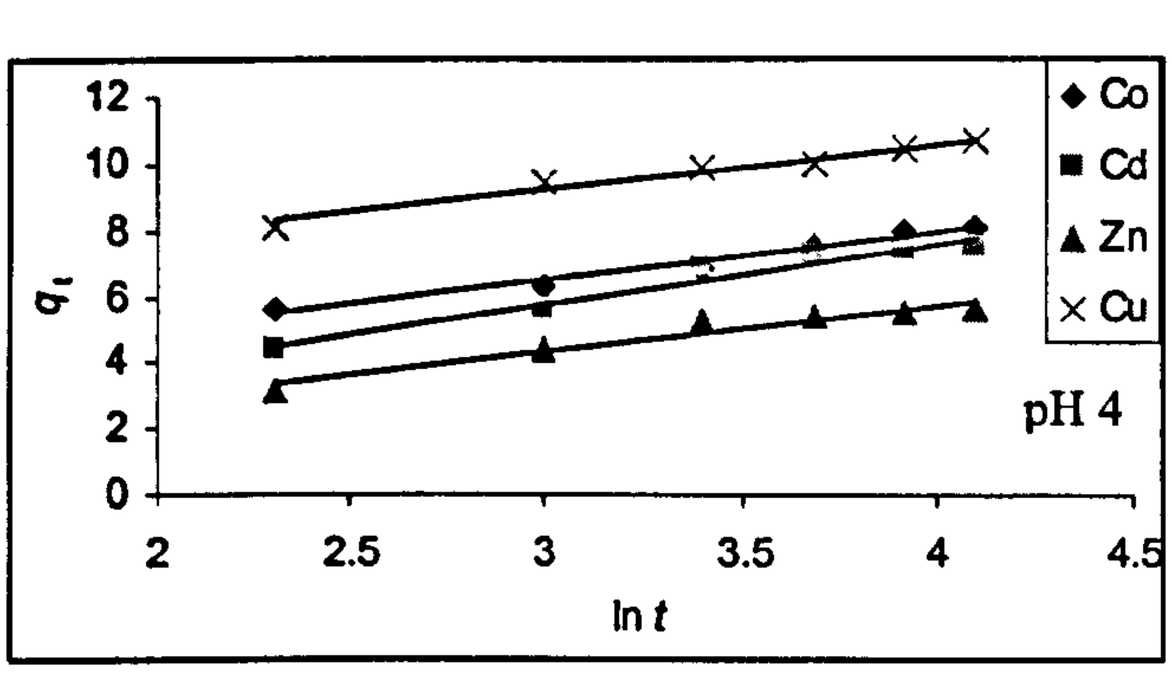

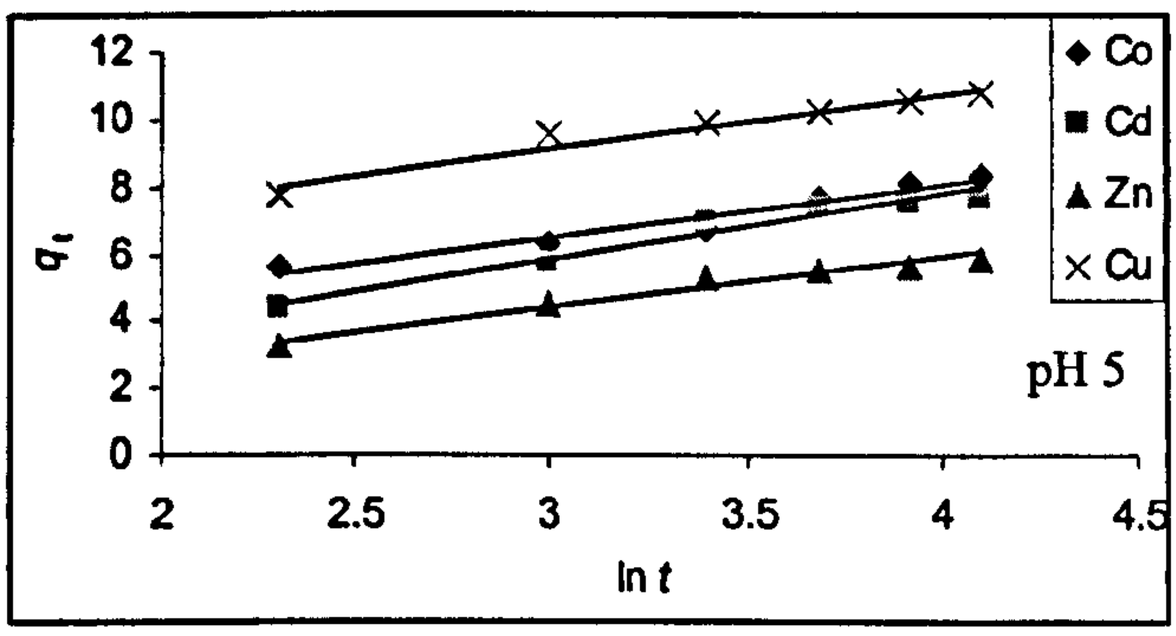

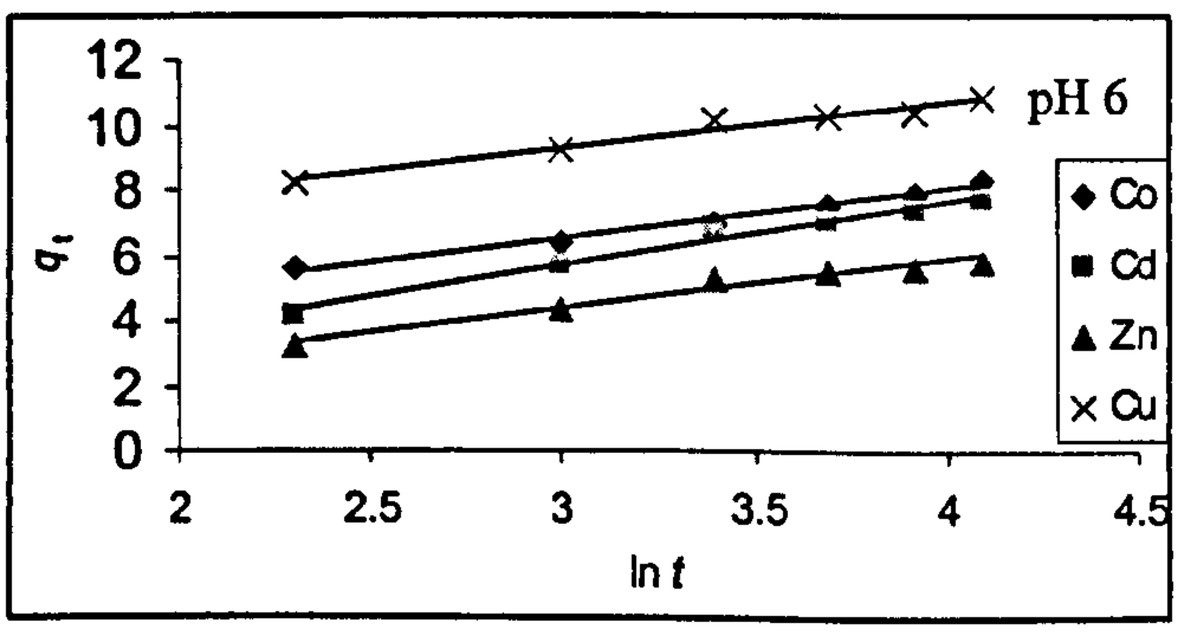

Figure 10.17: Elovich plot of adsorption of Co(II), Cd(II), Zn(II) and Cu(II) on MF-CDTA at temperature 15°C for pH 3, 4, 5 and 6.

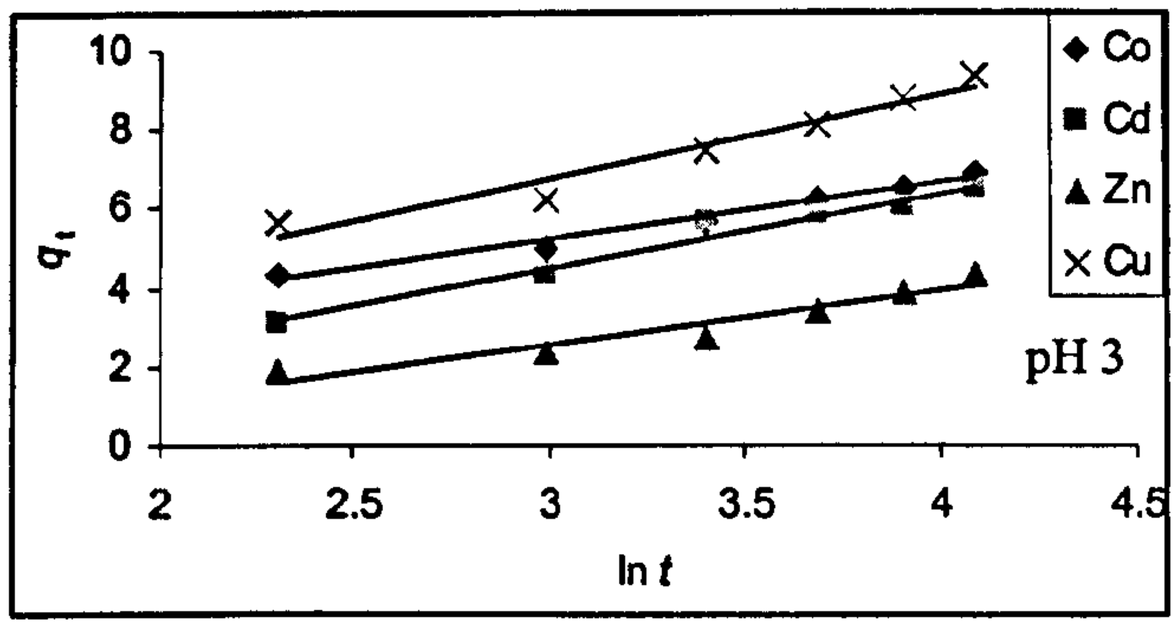

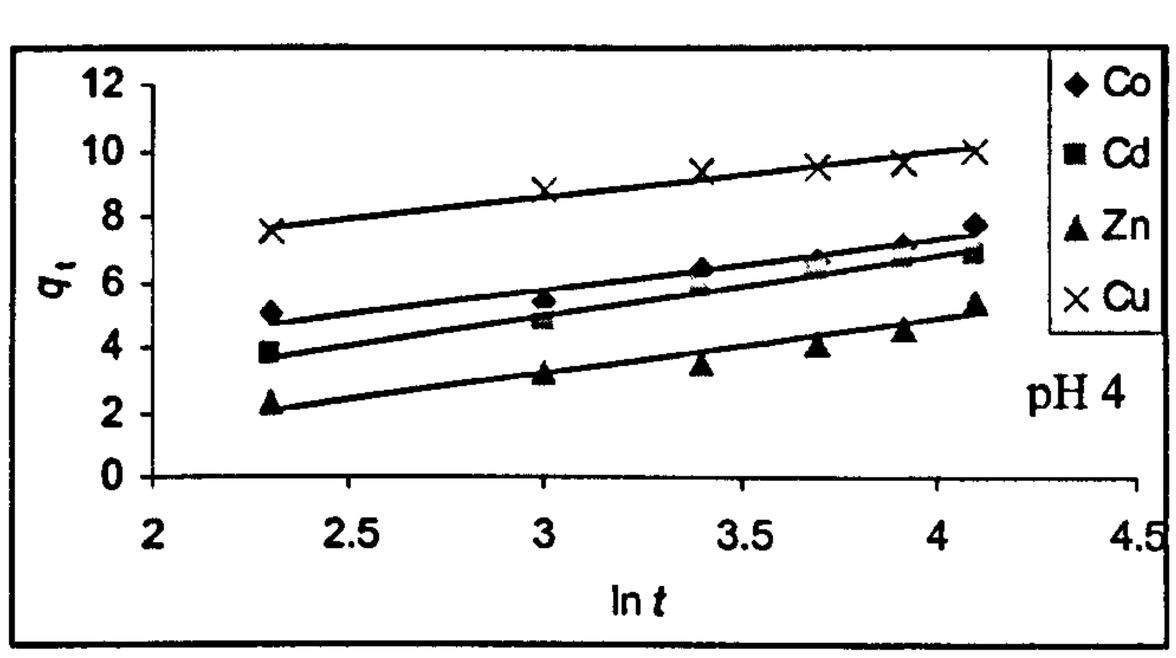

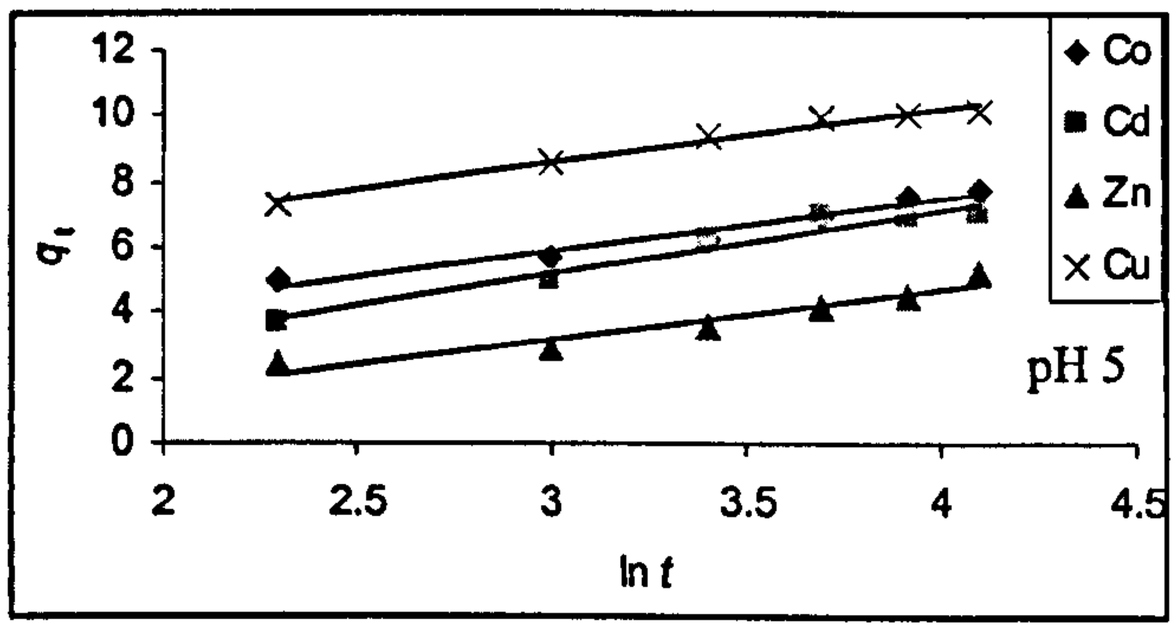

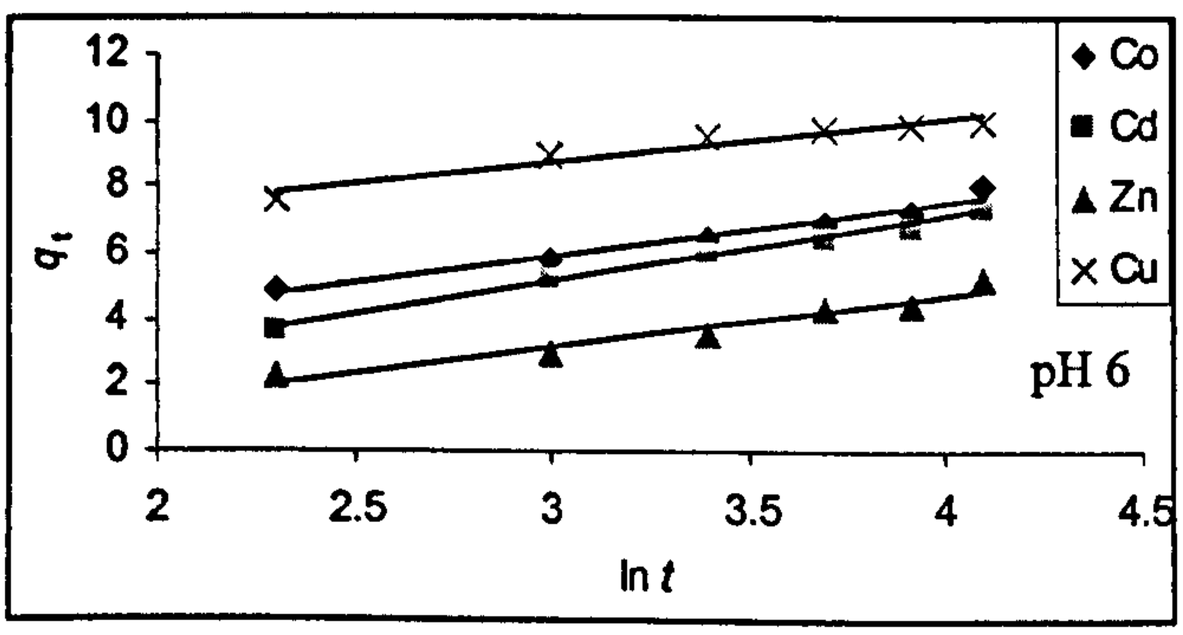

Figure 10.18: Elovich plot of adsorption of Co(II), Cd(II), Zn(II) and Cu(II) on MF-CDTA at temperature 25°C for pH 3, 4, 5 and 6.

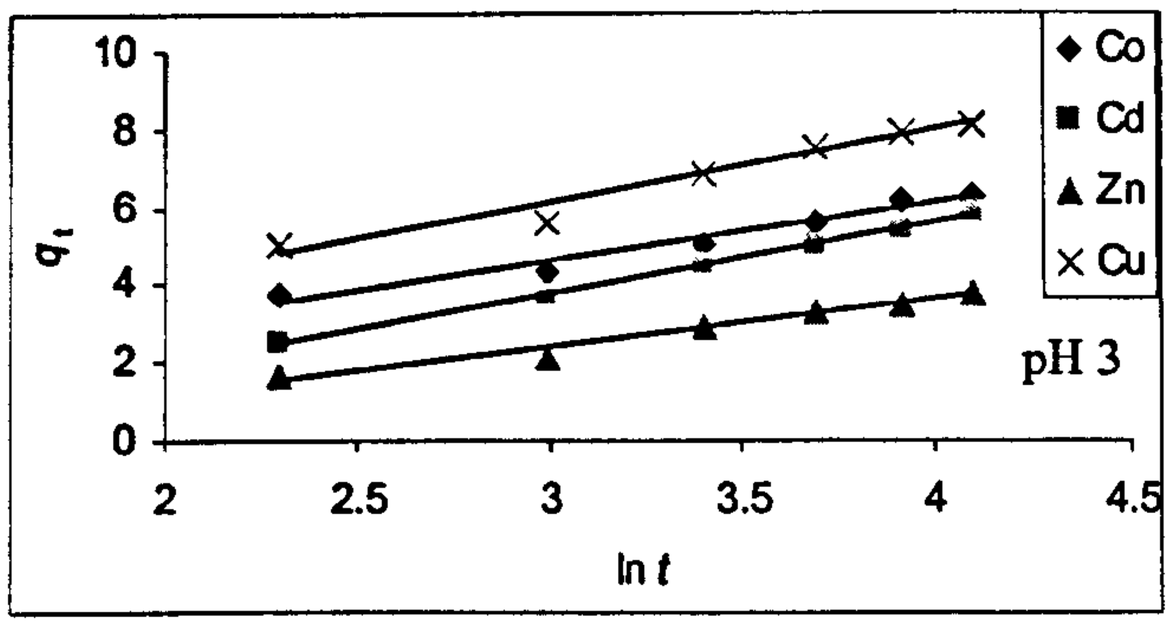

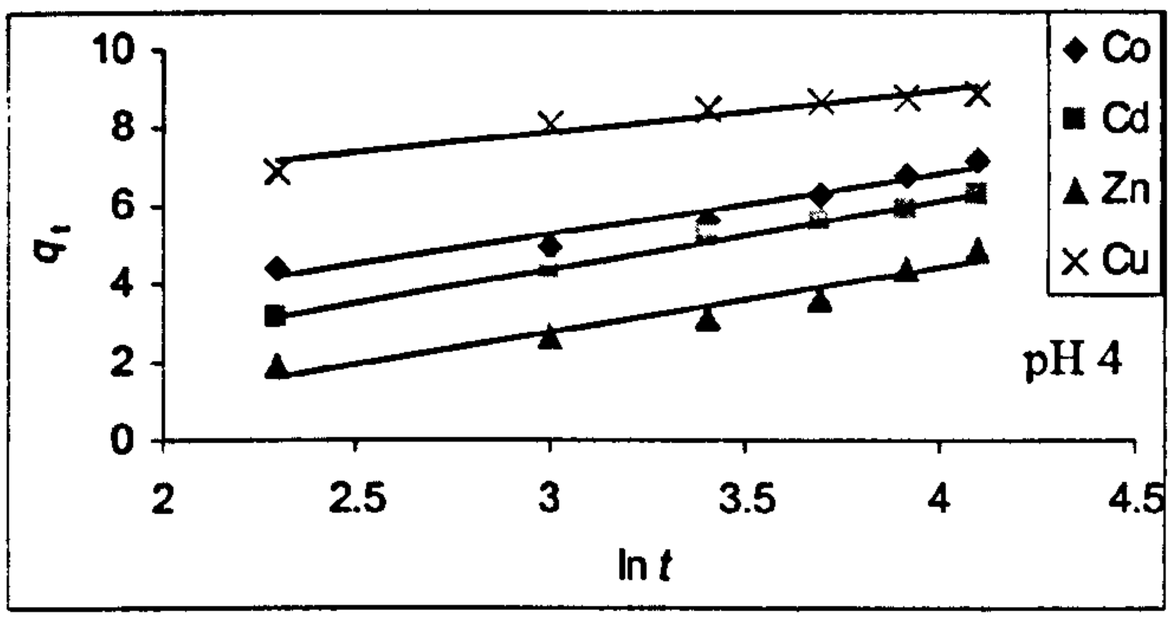

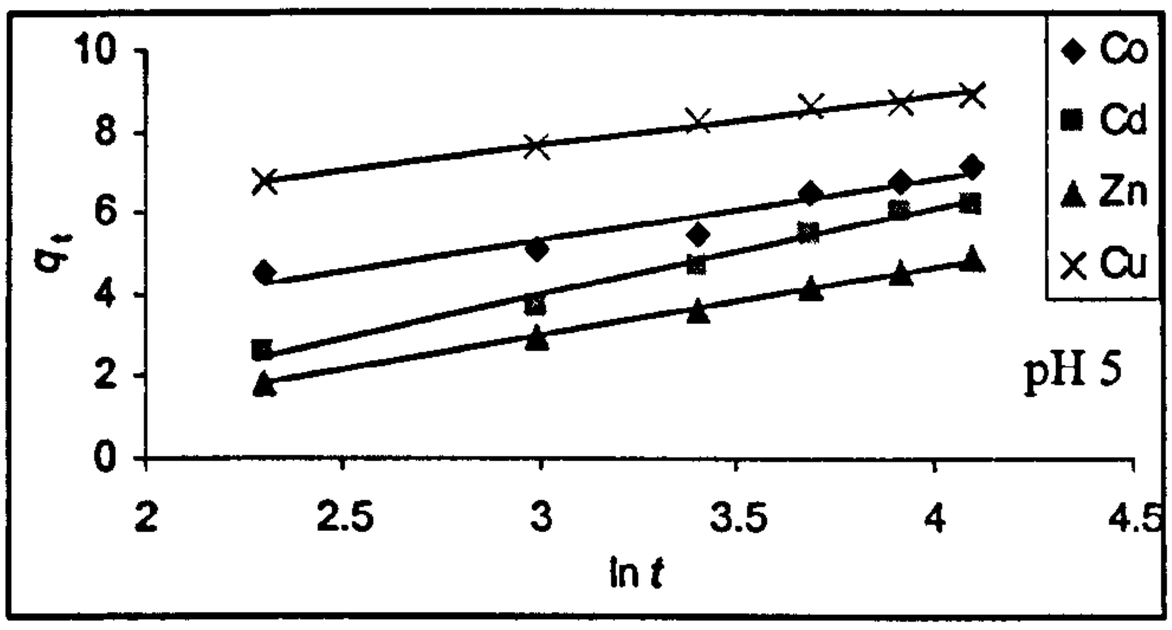

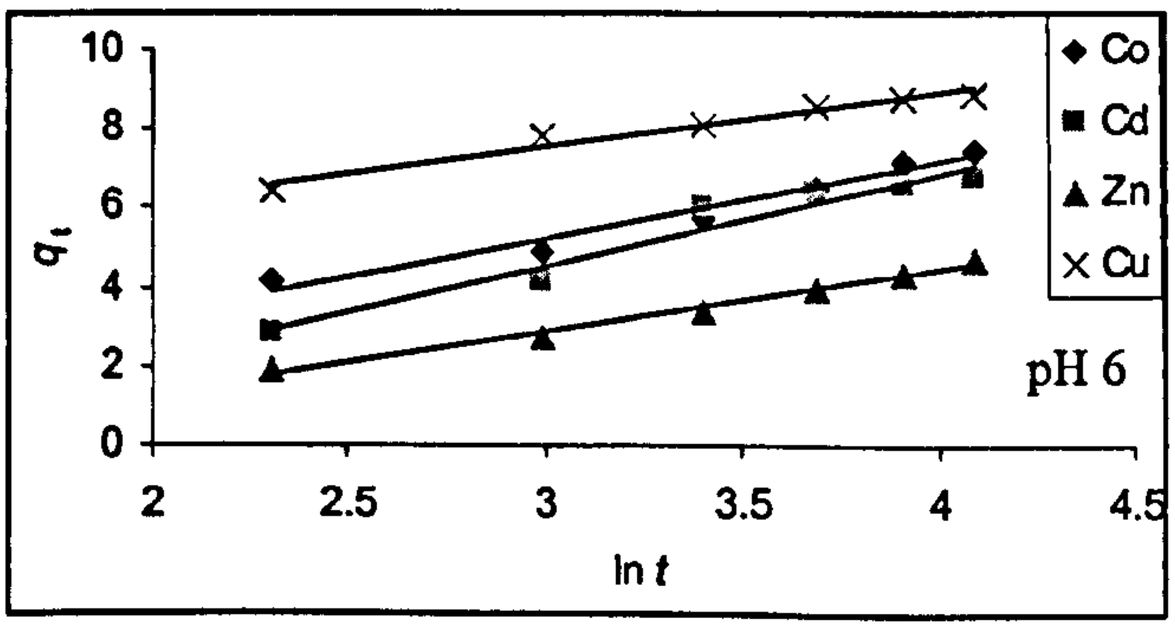

Figure 10.19: Elovich plot of adsorption of Co(II), Cd(II), Zn(II) and Cu(II) on MF-CDTA at temperature 35°C for pH 3, 4, 5 and 6.

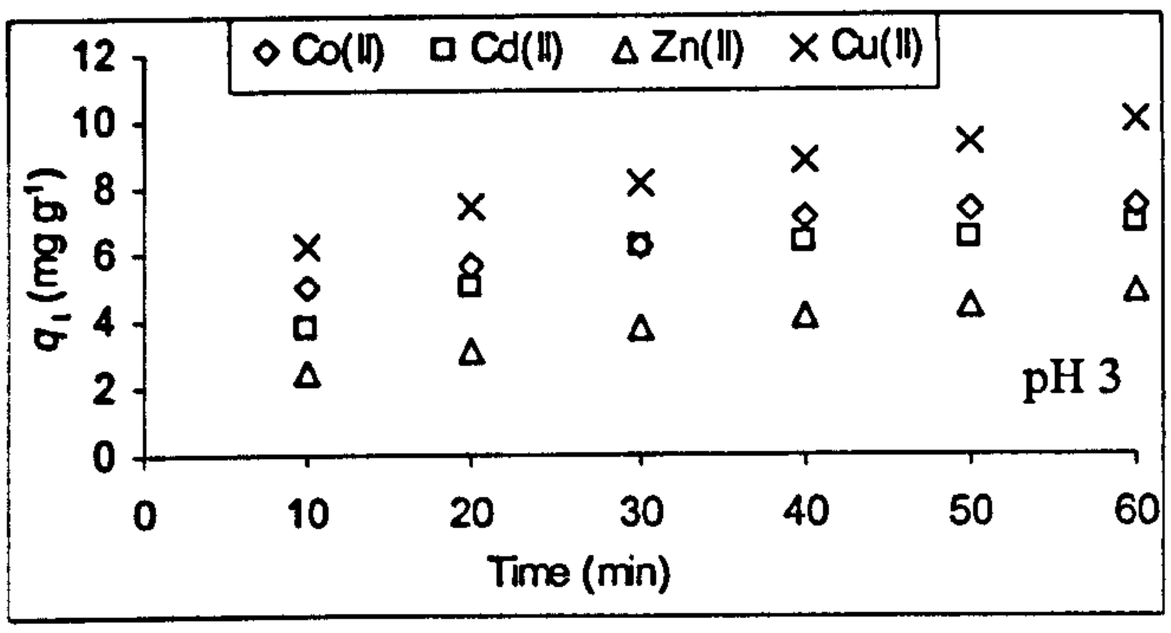

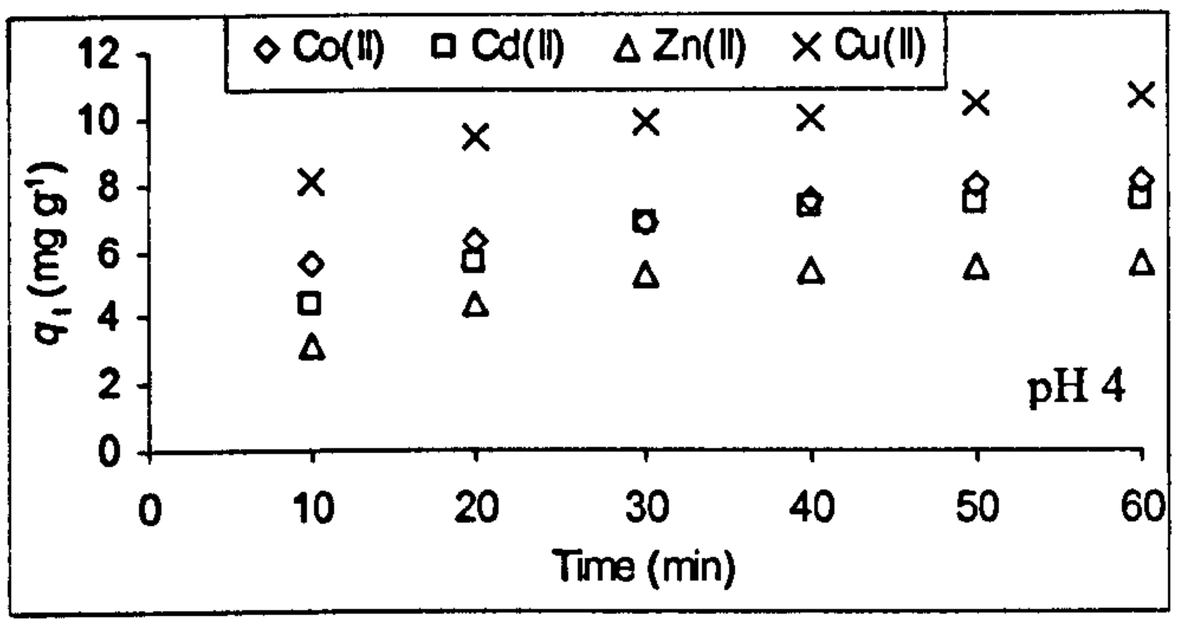

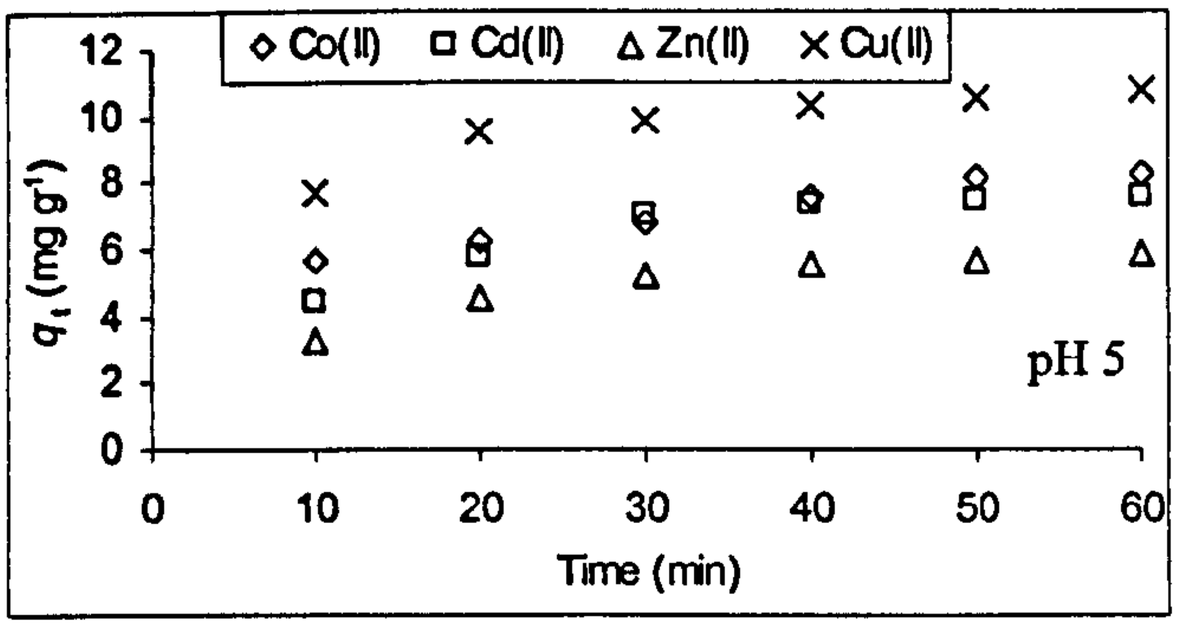

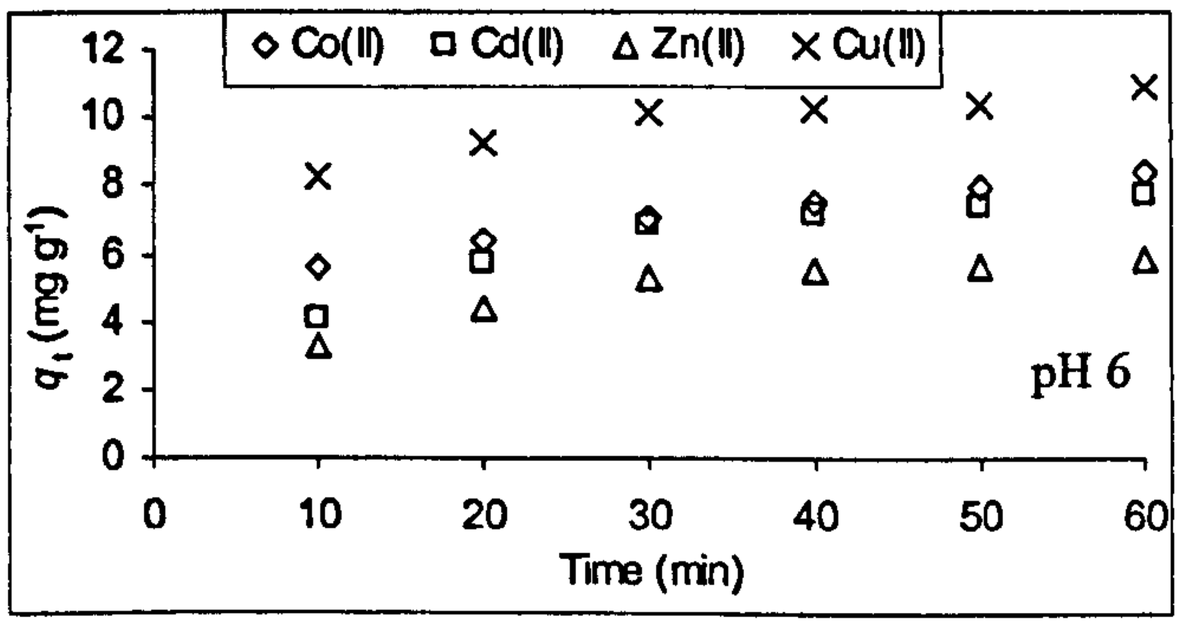

Figure 10.20: Increase of adsorbed amount of M(II) on MF-CDTA with time at different initial pH values (15°C).

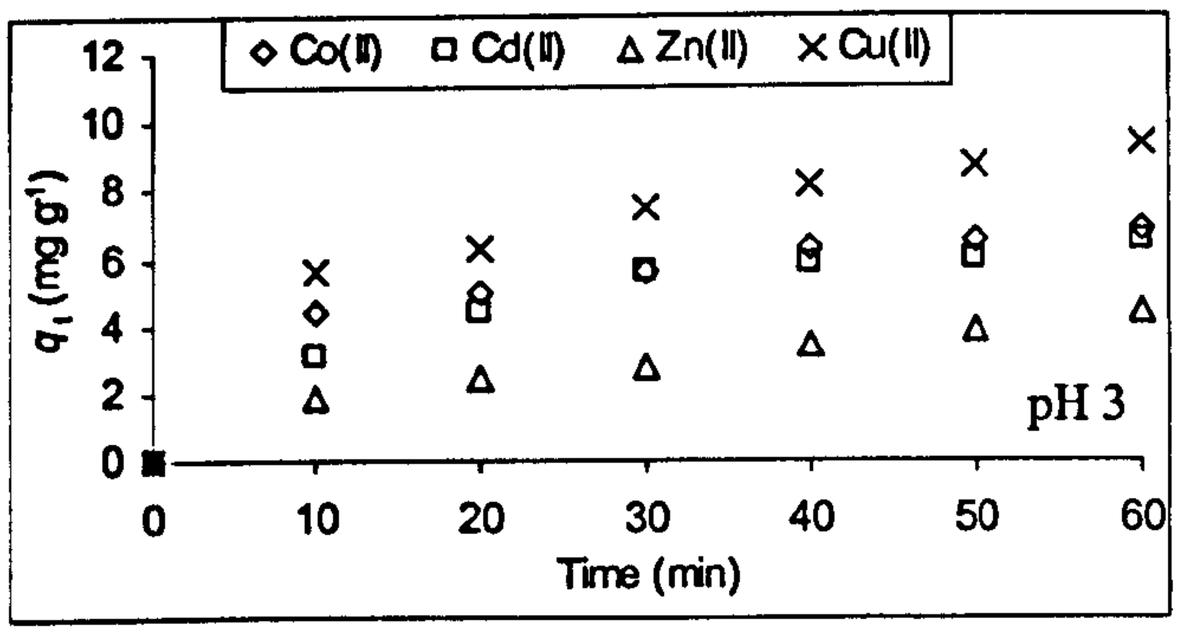

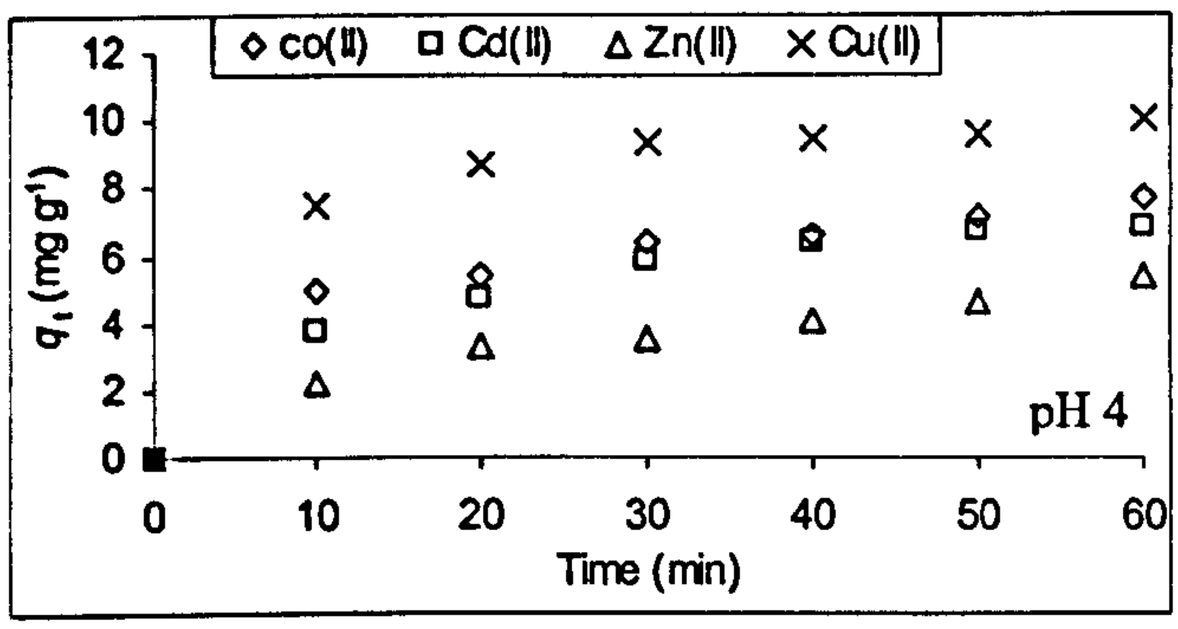

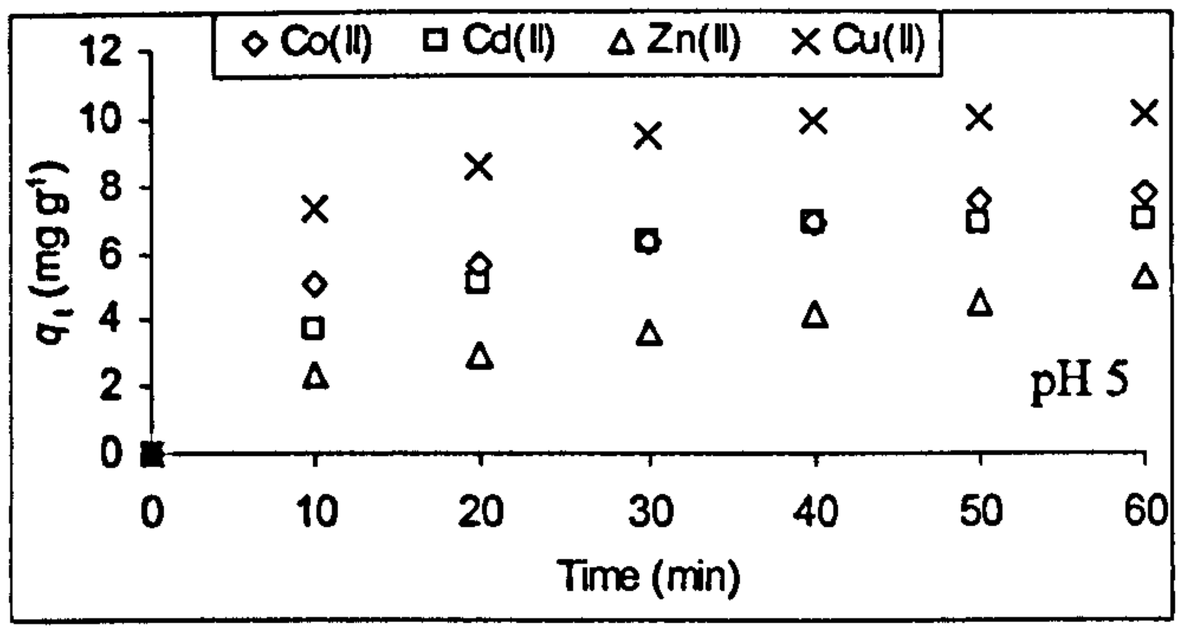

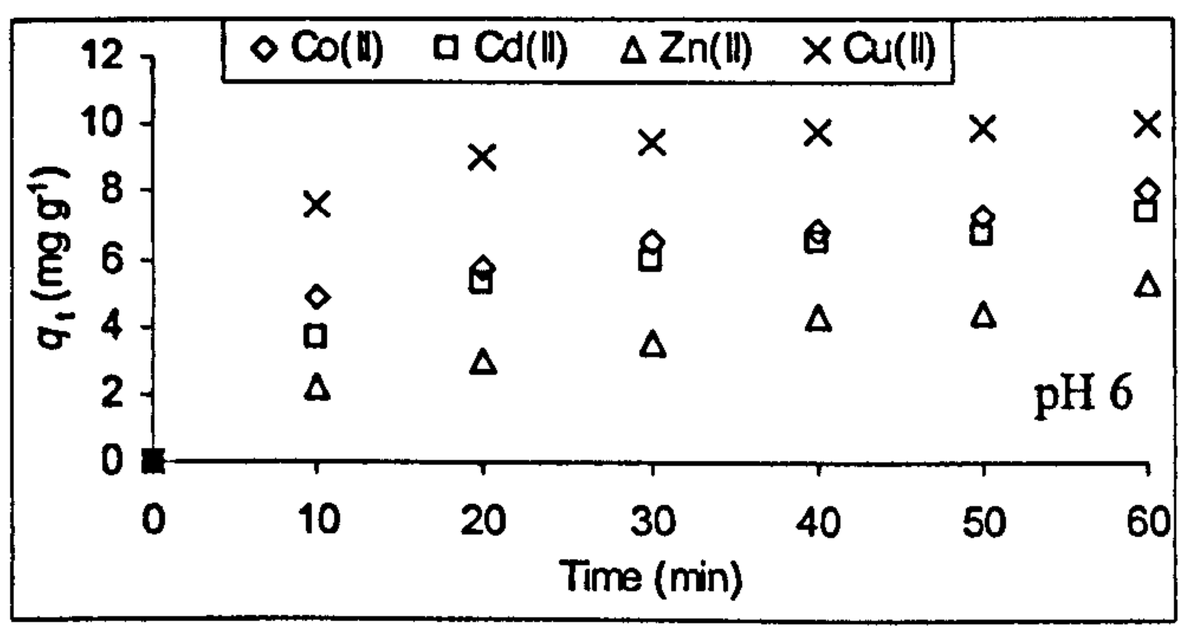

Figure 10.21: Increase of adsorbed amount of M(II) on MF-CDTA with time at different initial pH values (25°C).

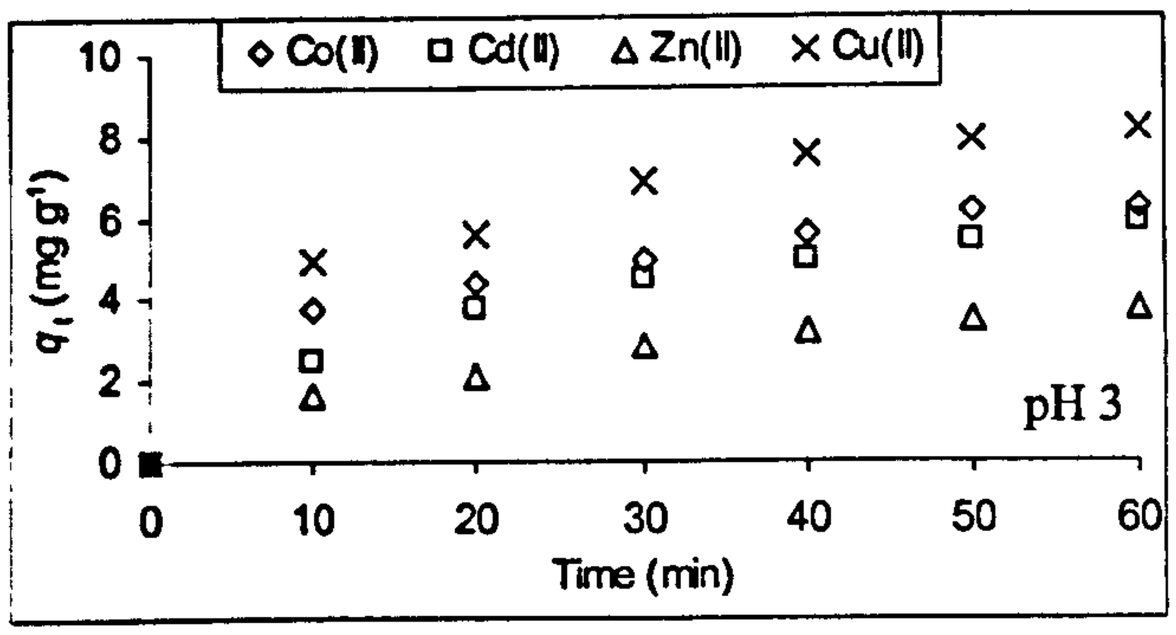

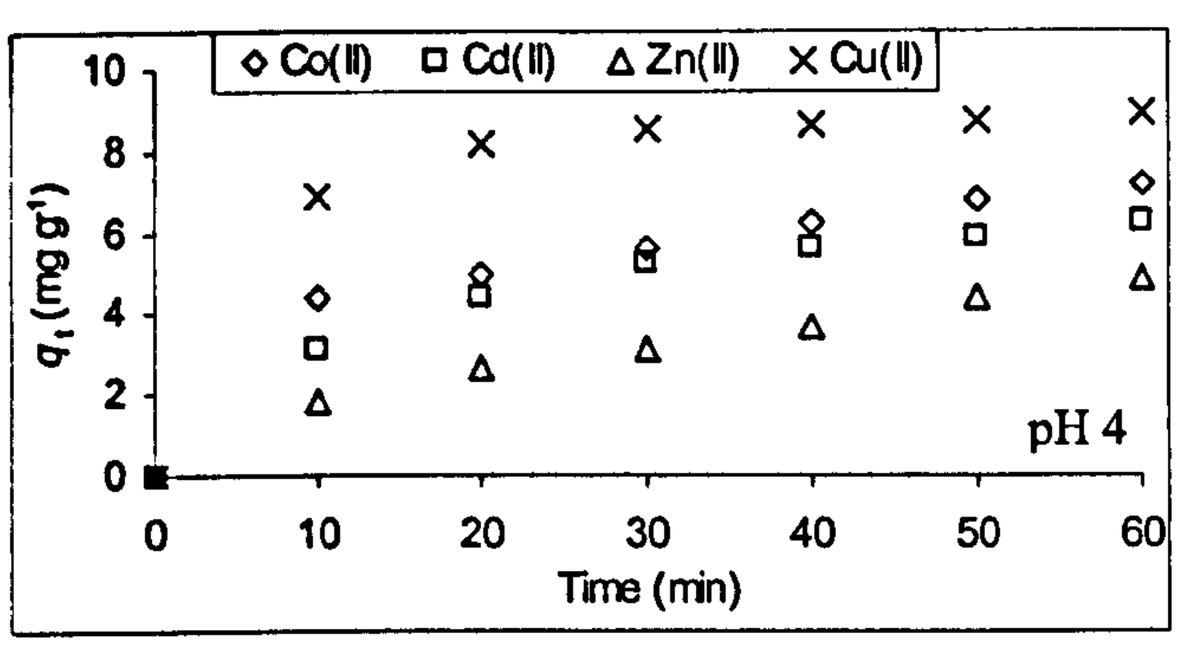

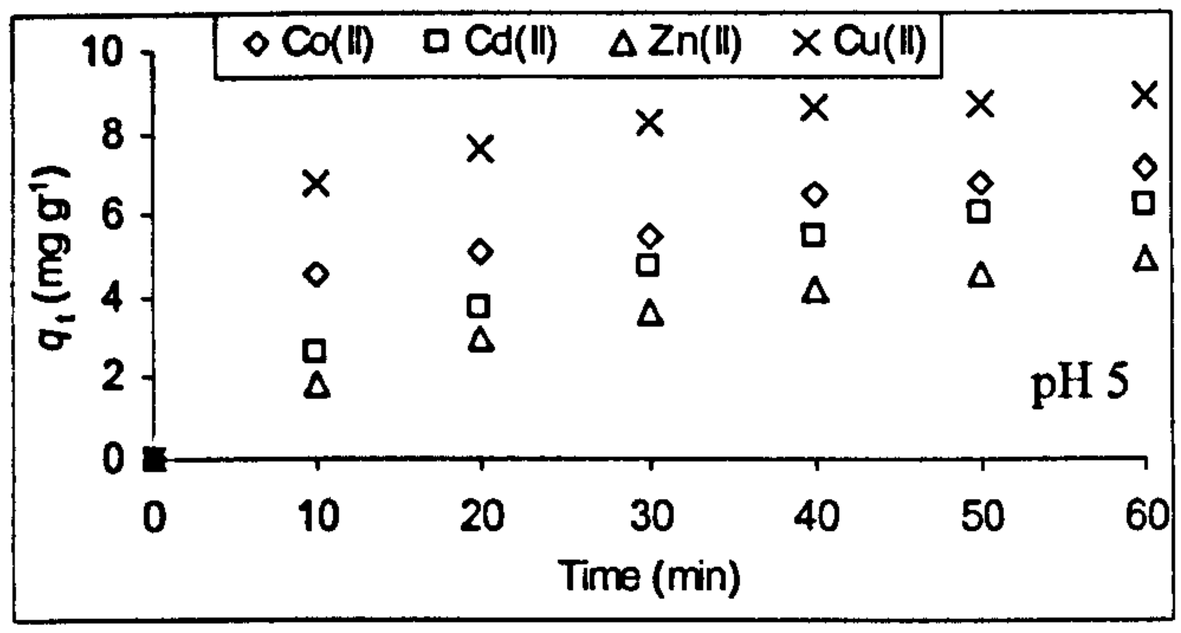

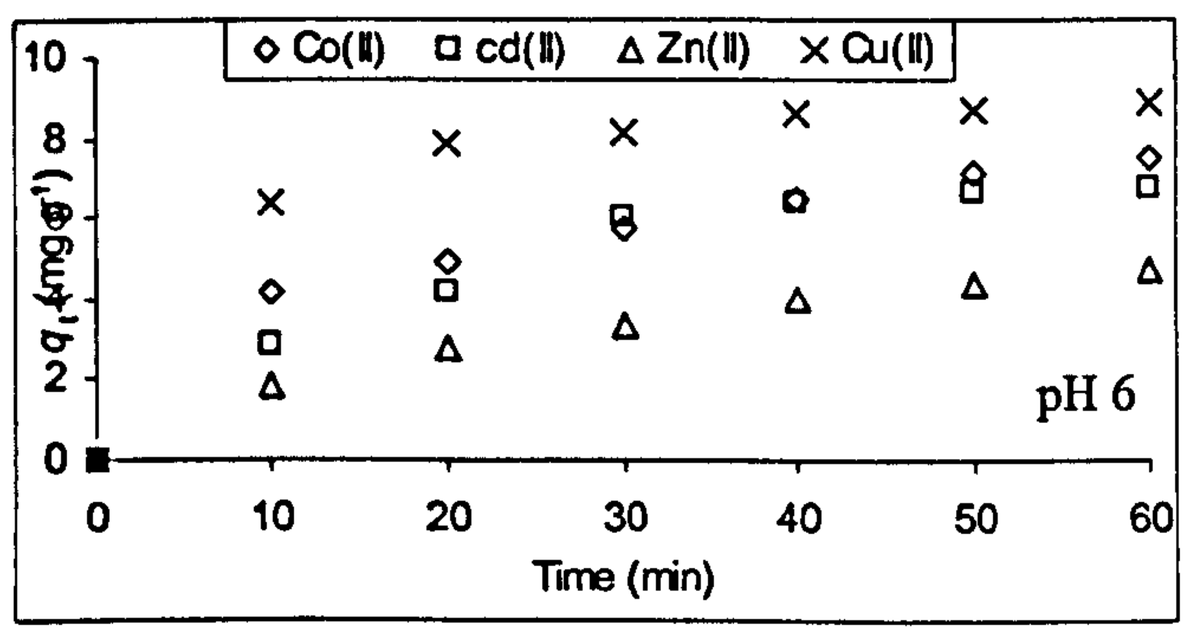

Figure 10.22: Increase of adsorbed amount of M(II) on MF-CDTA with time at different initial pH values (35°C).

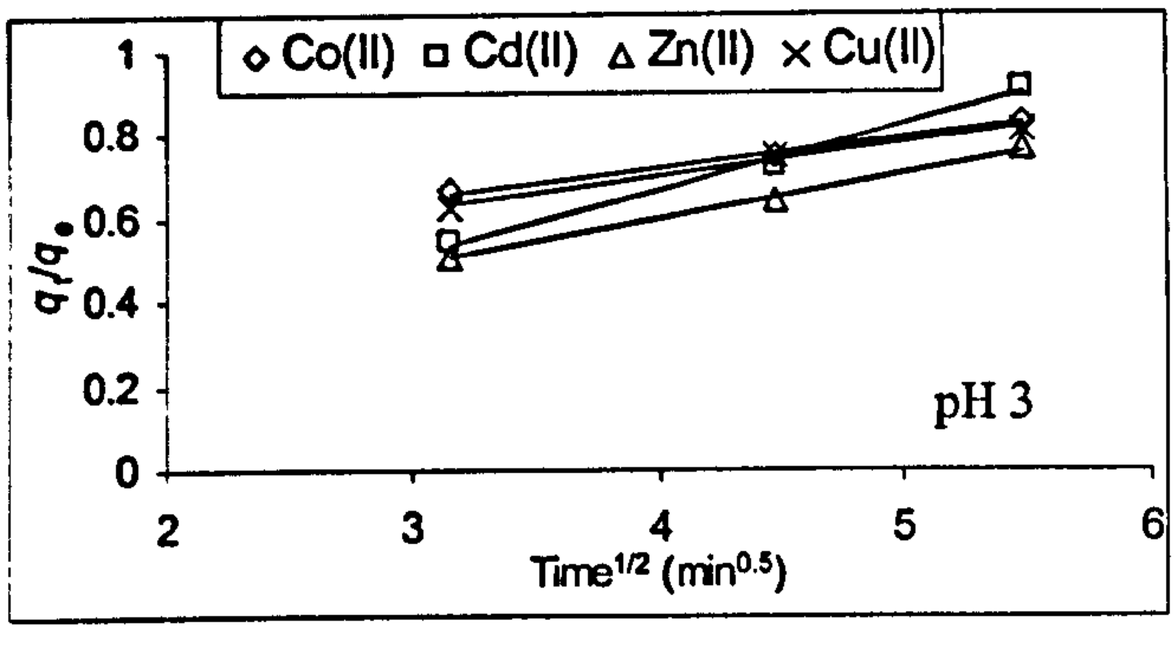

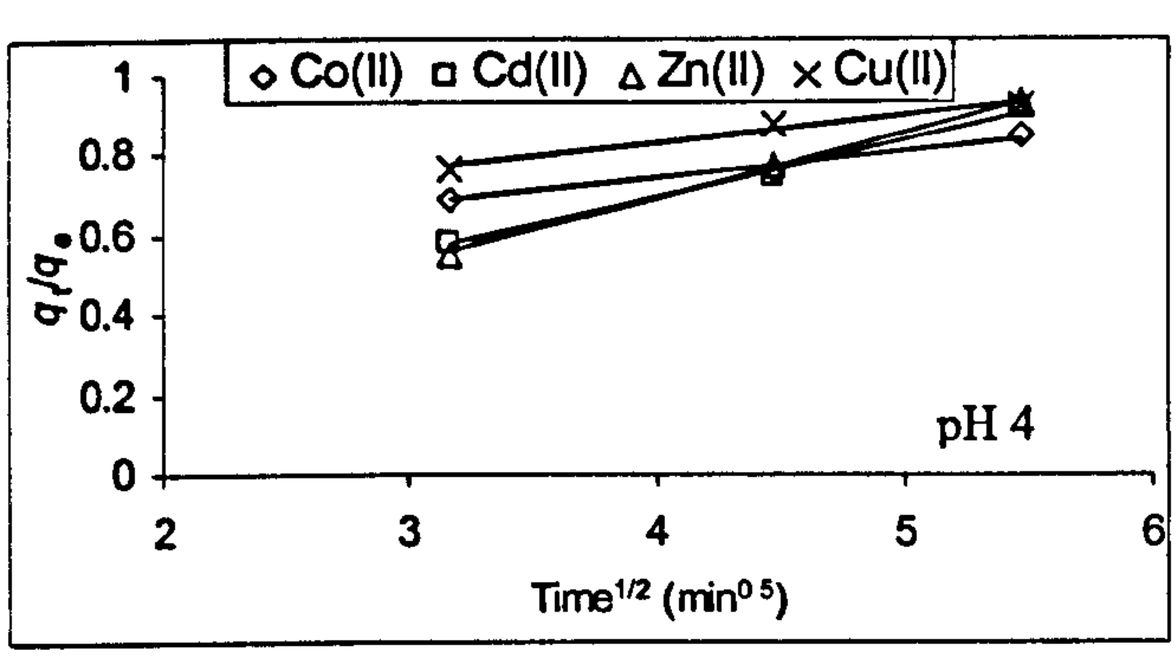

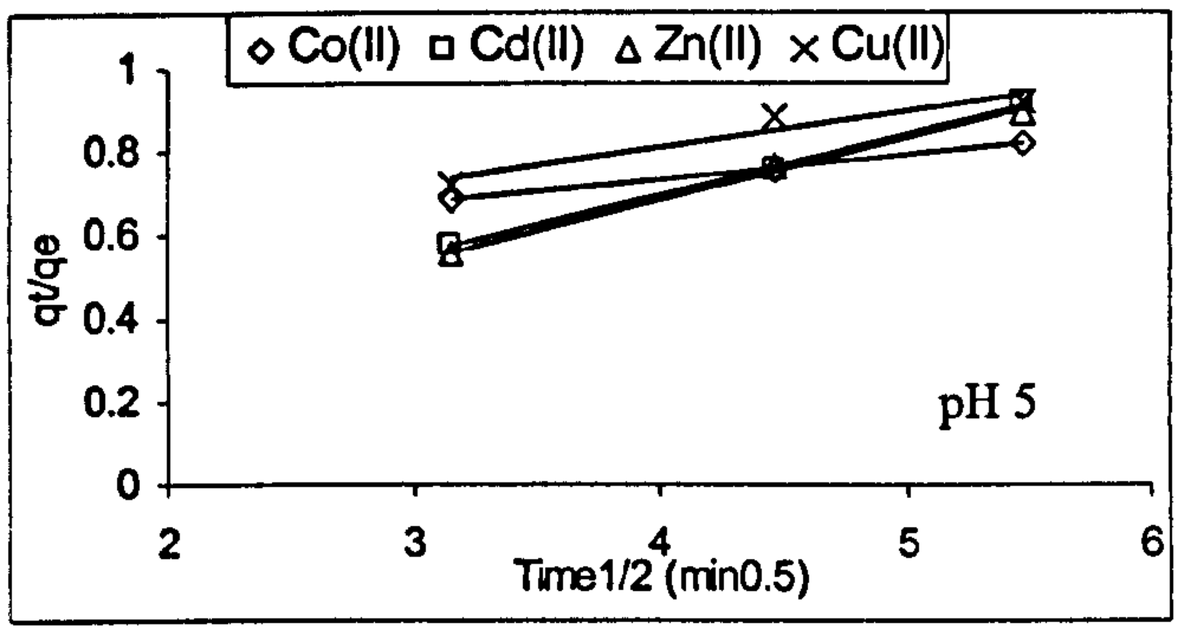

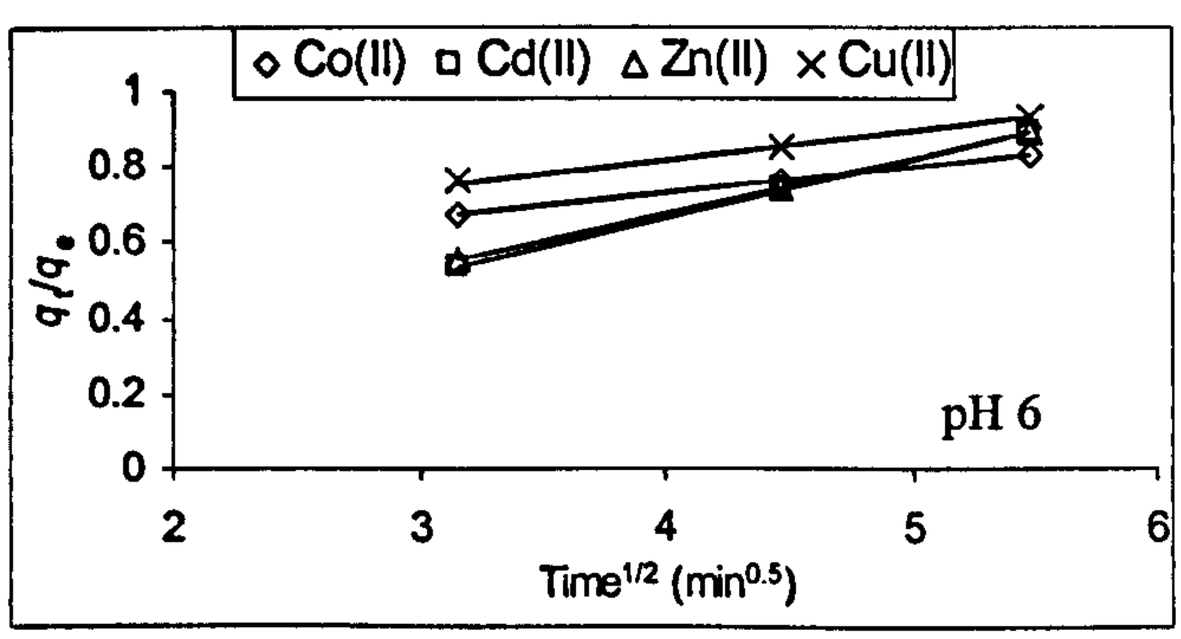

Figure 10.23: Plots of equation (18) at different initial pH values (15°C) for the determination of film diffusion coefficients (D_1) of M(II) with MF-CDTA.

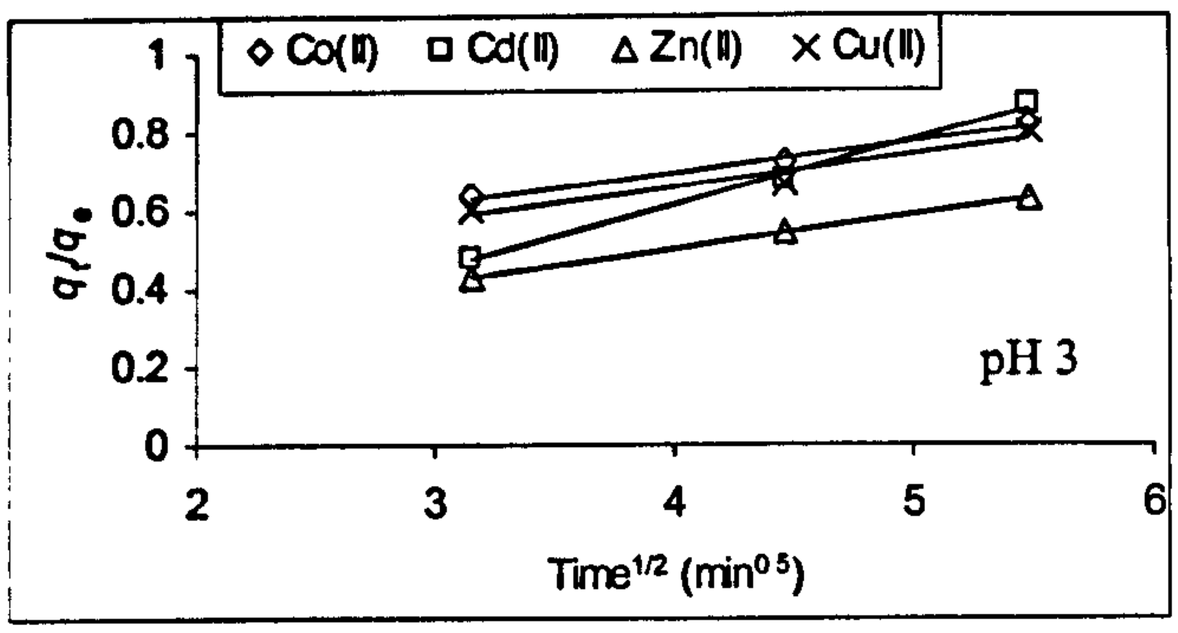

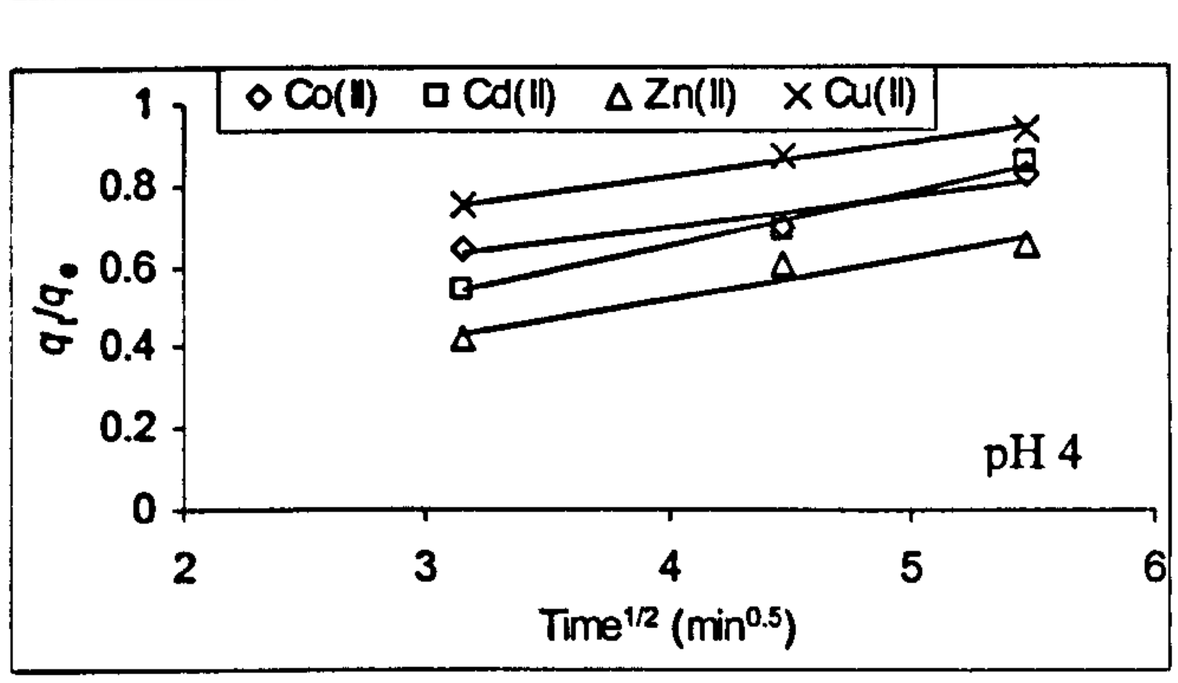

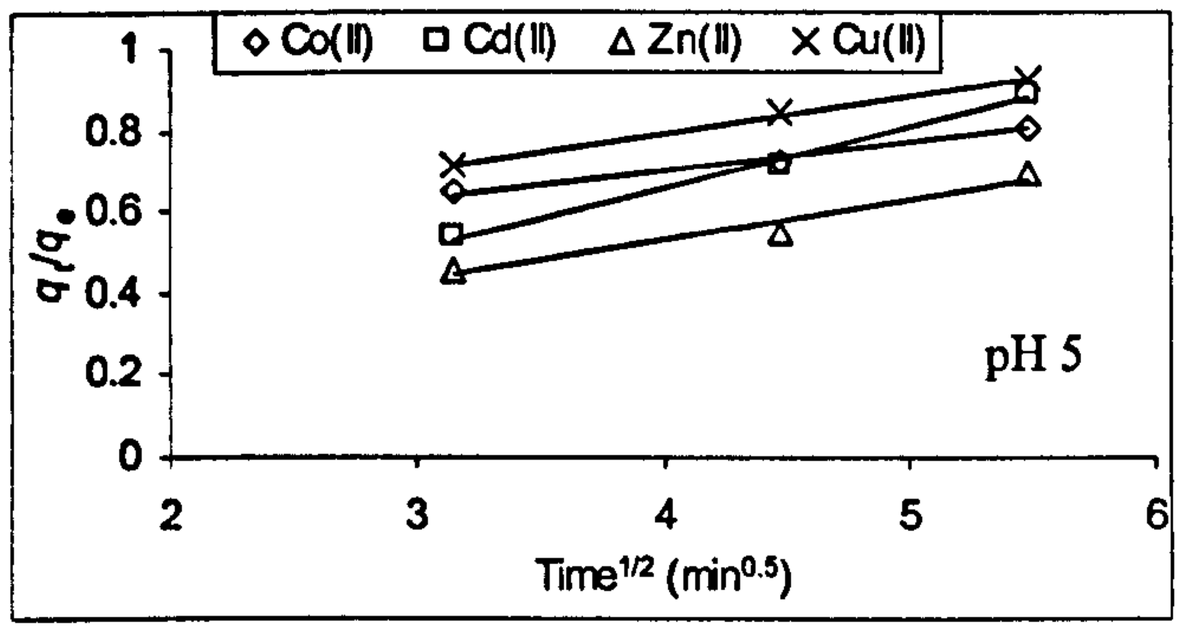

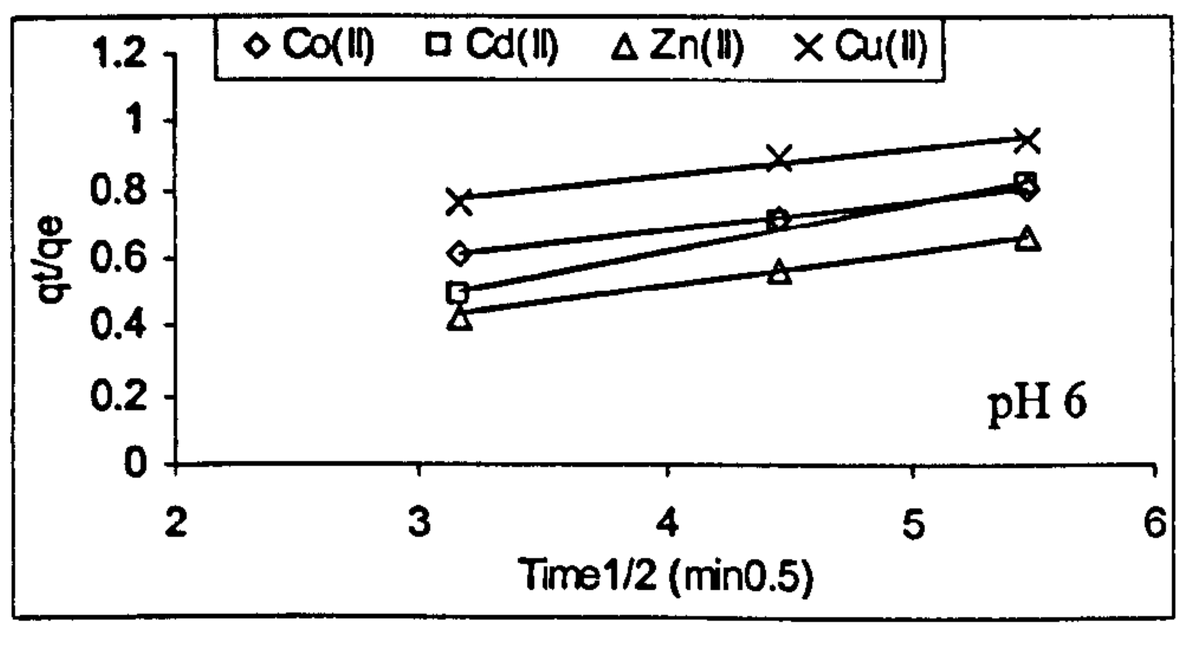

Figure 10.24: Plots of equation (18) at different initial pH values (25°C) for the determination of film diffusion coefficients (D_1) of M(II) with MF-CDTA.

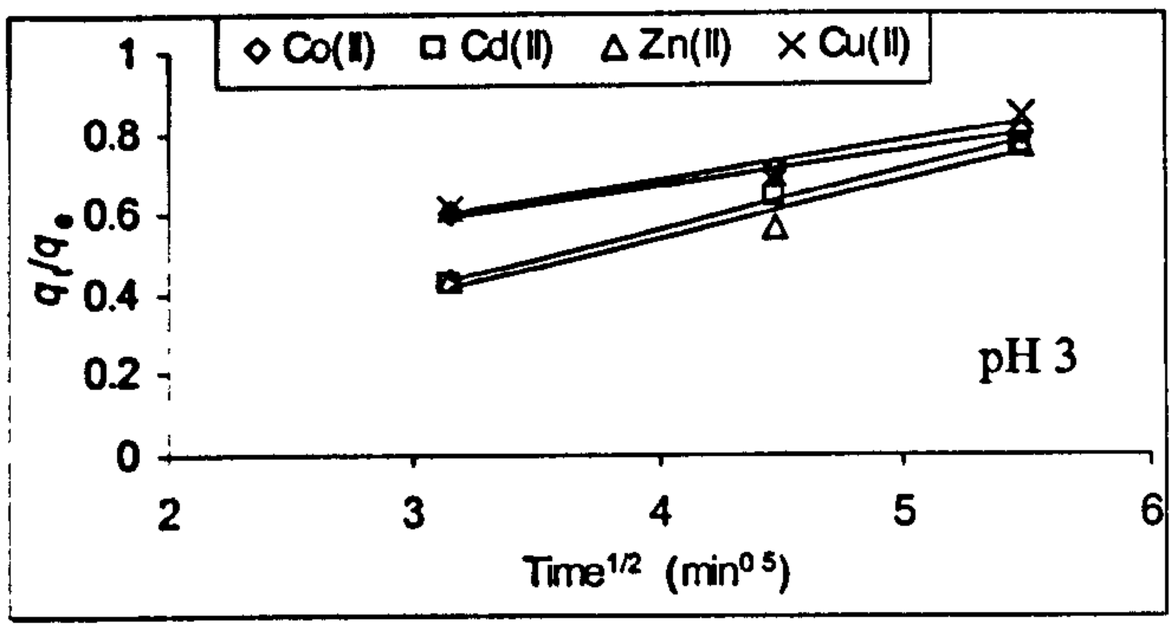

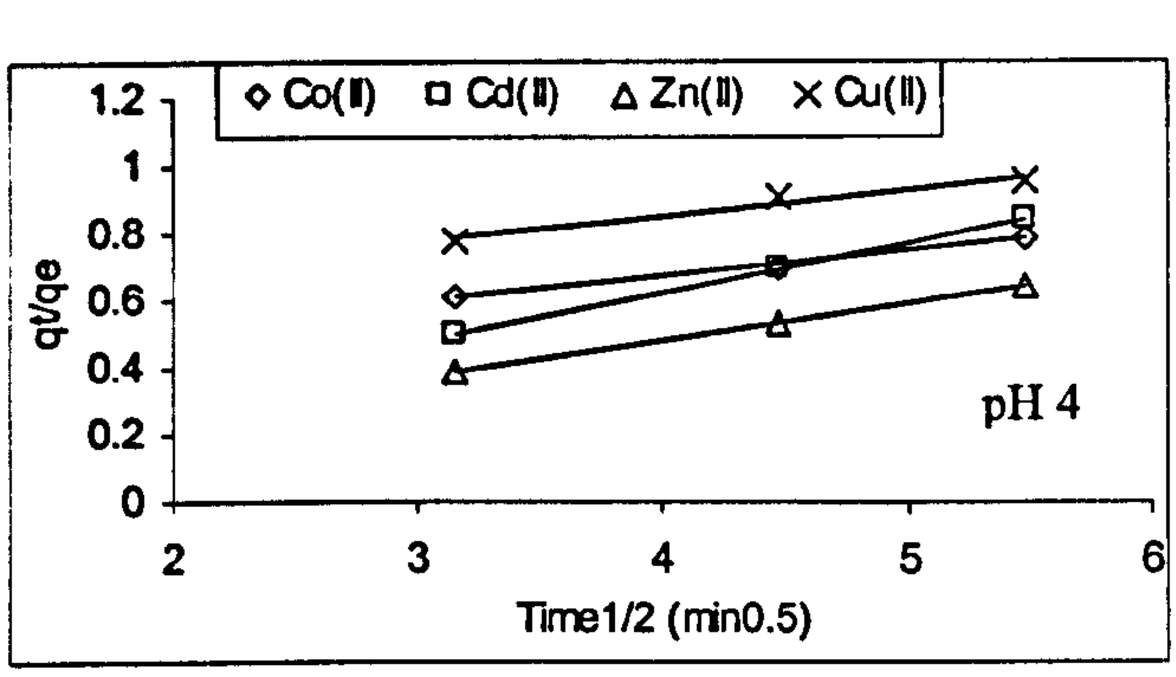

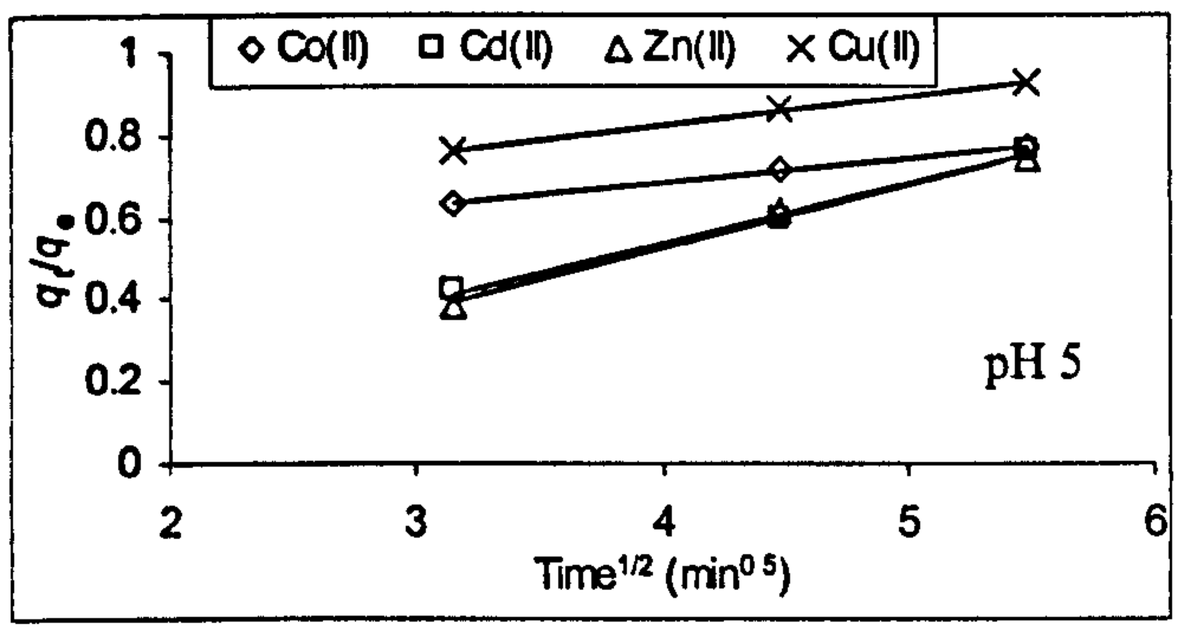

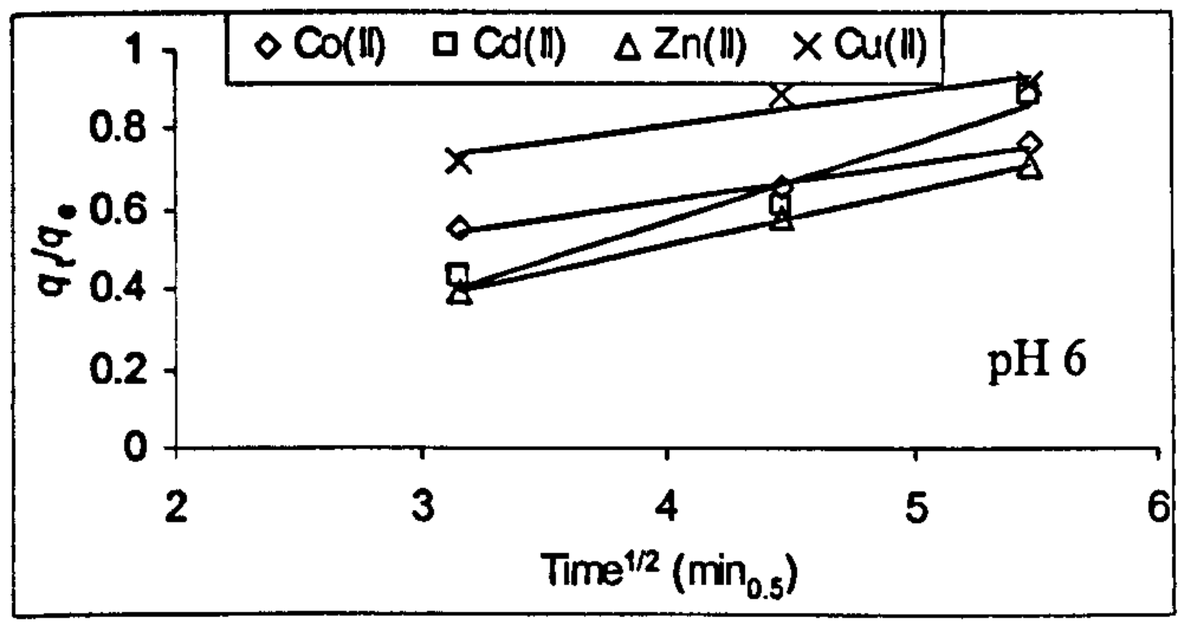

Figure 10.25: Plots of equation (18) at different initial pH values (35°C) for the determination of film diffusion coefficients (D_1) of M(II) with MF-CDTA.

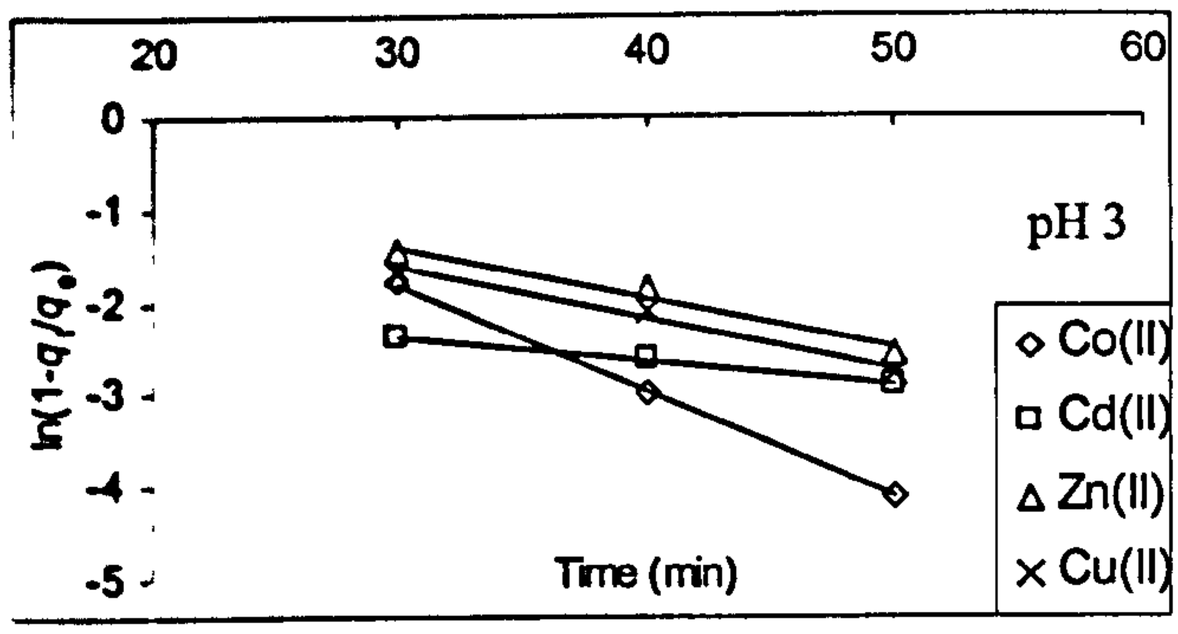

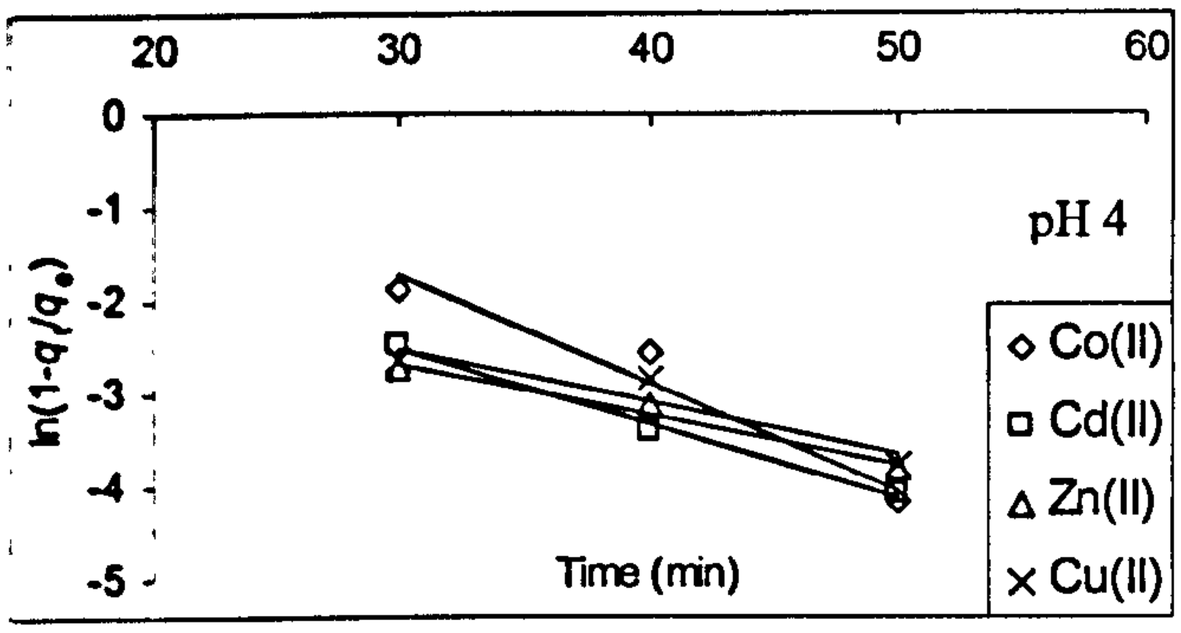

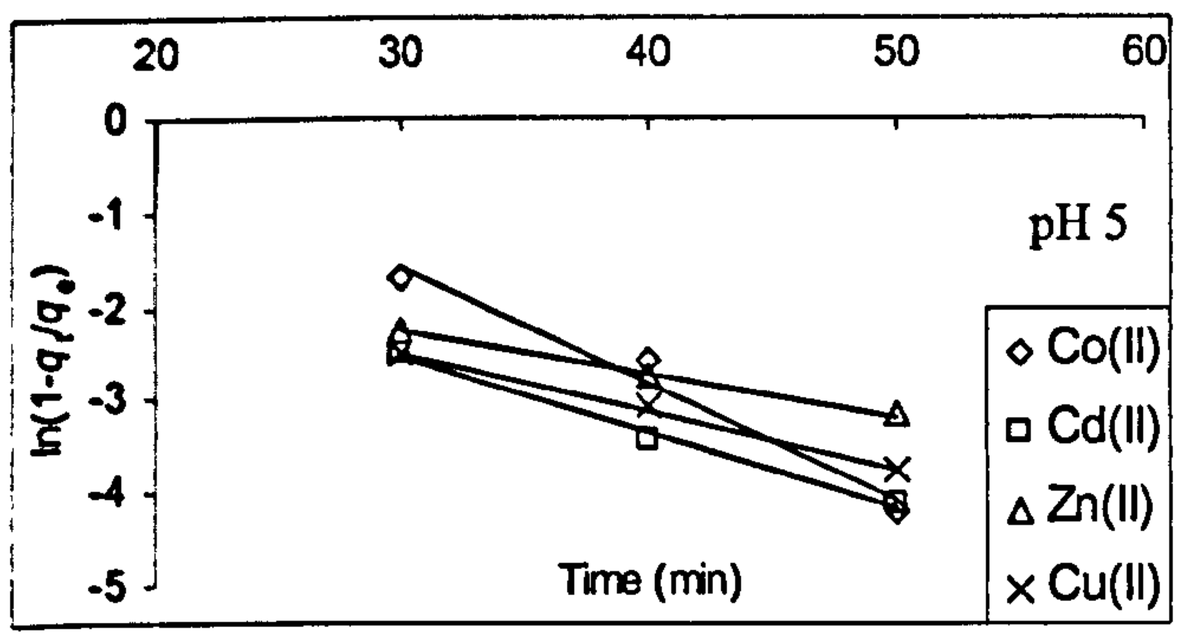

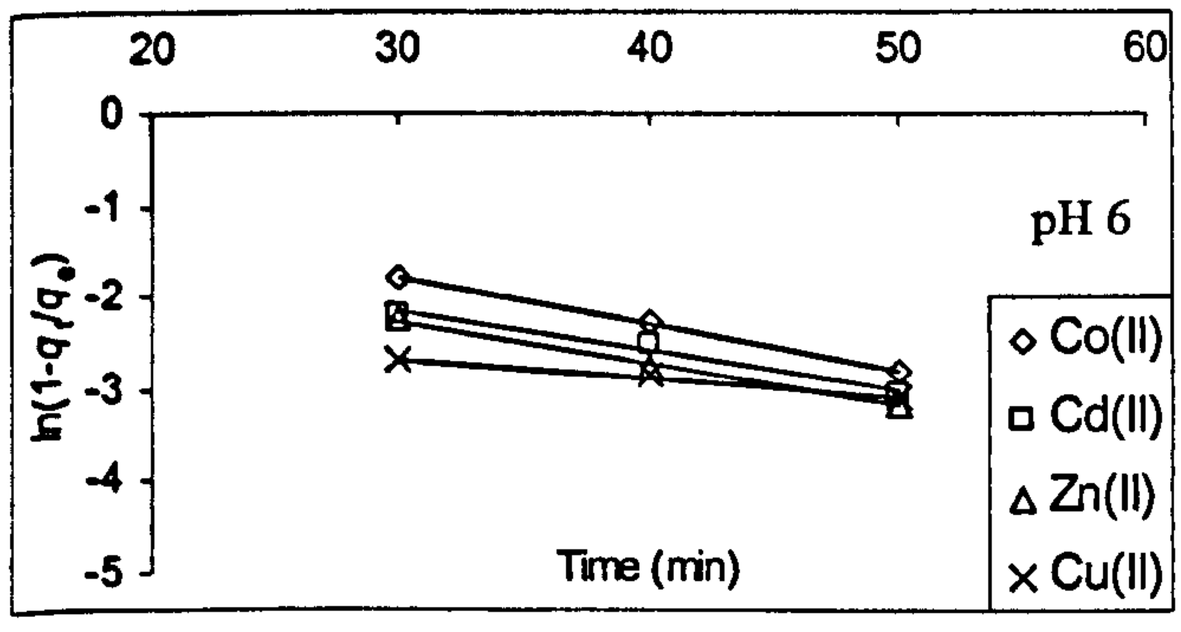

Figure 10.26: Plots of equation (19) at different initial pH values (15°C) for the determination of pore diffusion coefficients (D_2) of M(II) with MF-CDTA.

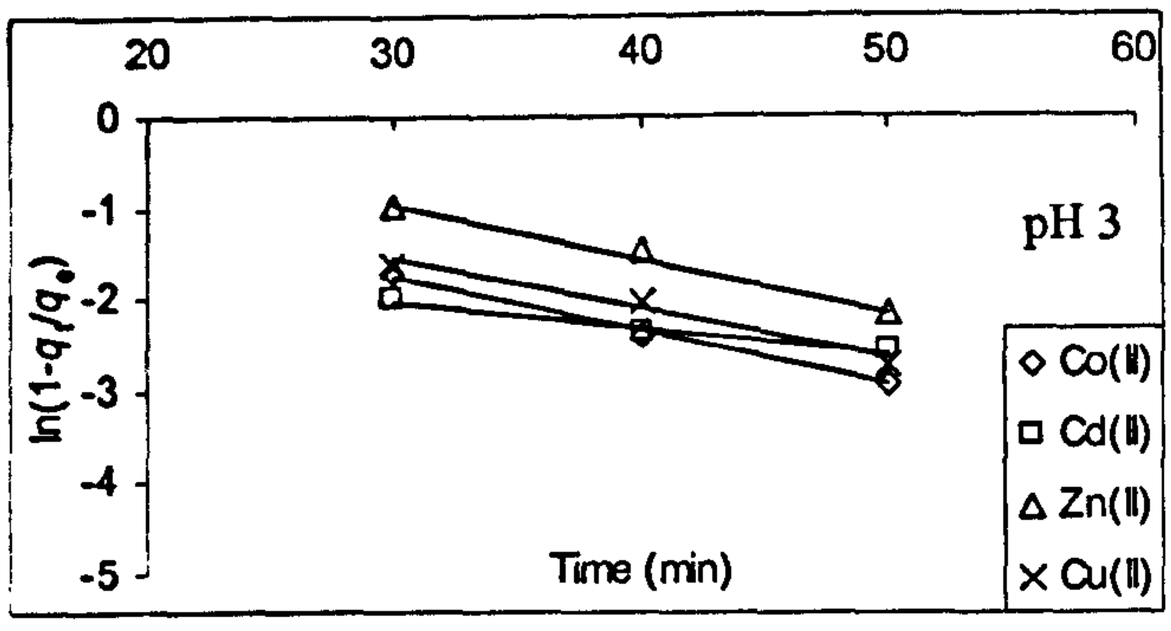

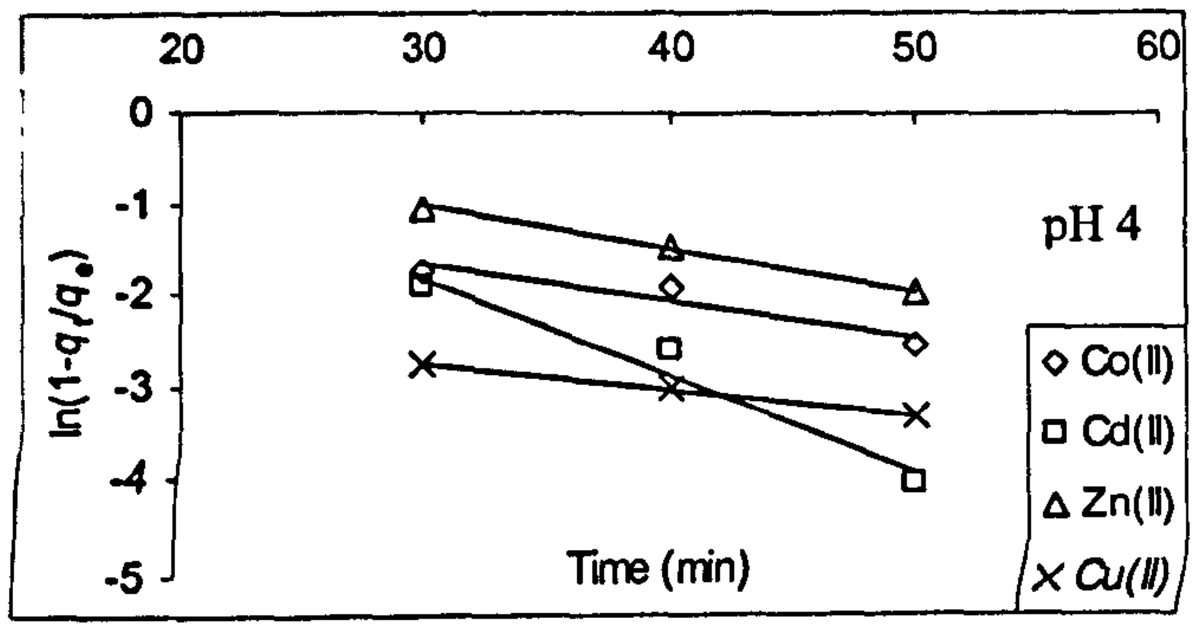

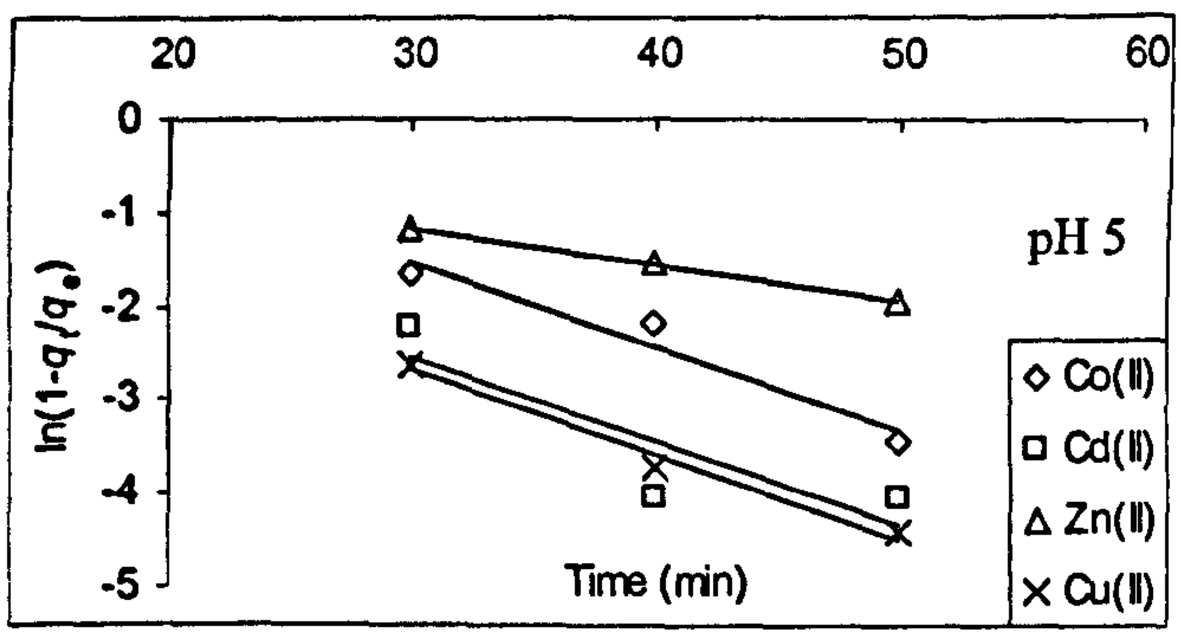

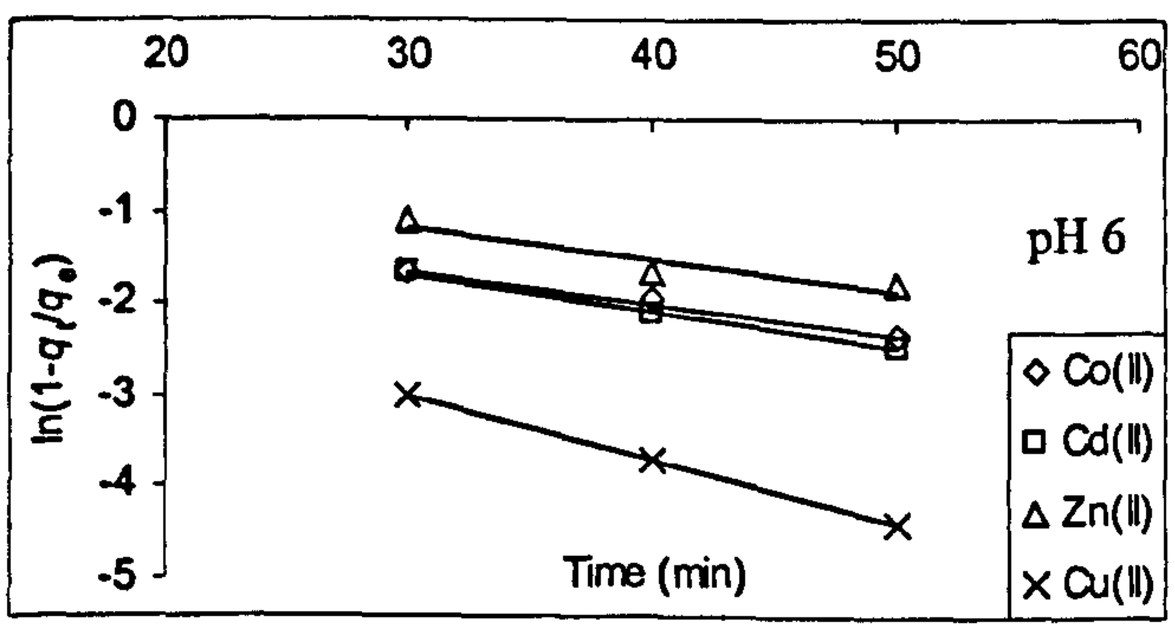

Figure 10.27: Plots of equation (19) at different initial pH values (25°C) for the determination of pore diffusion coefficients (D_2) of M(II) with MF-CDTA.

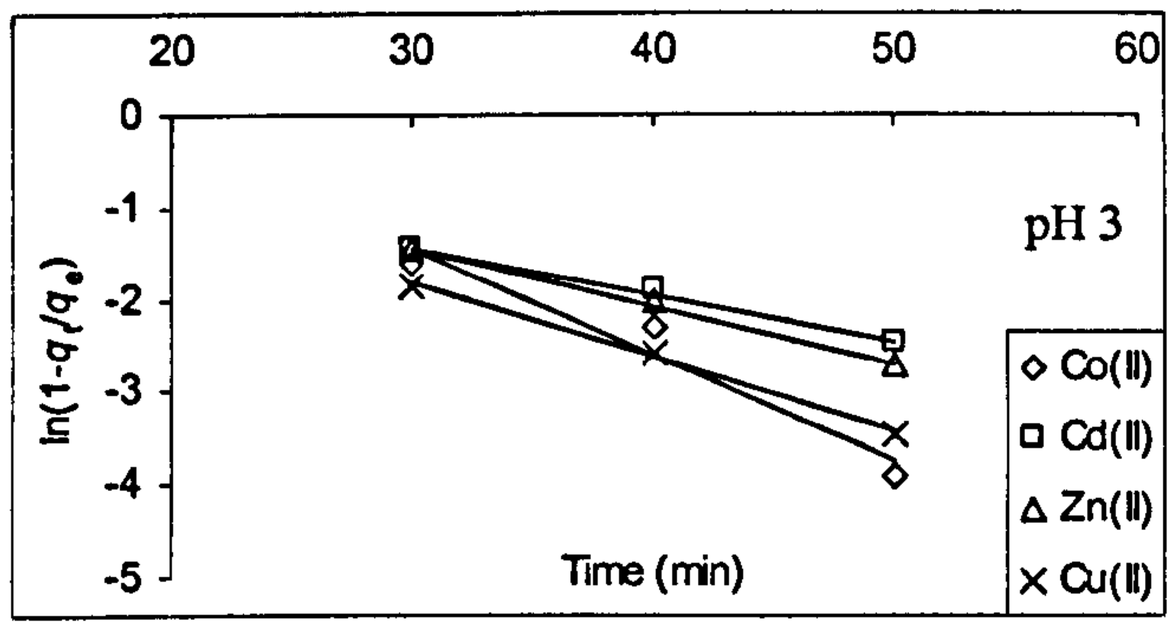

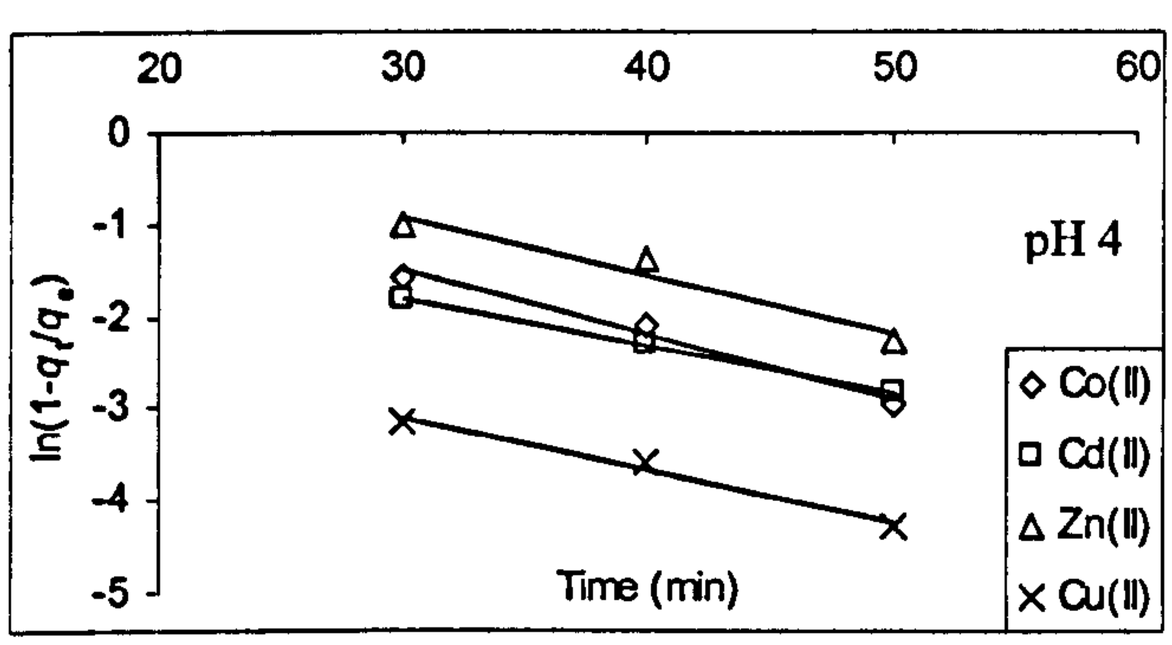

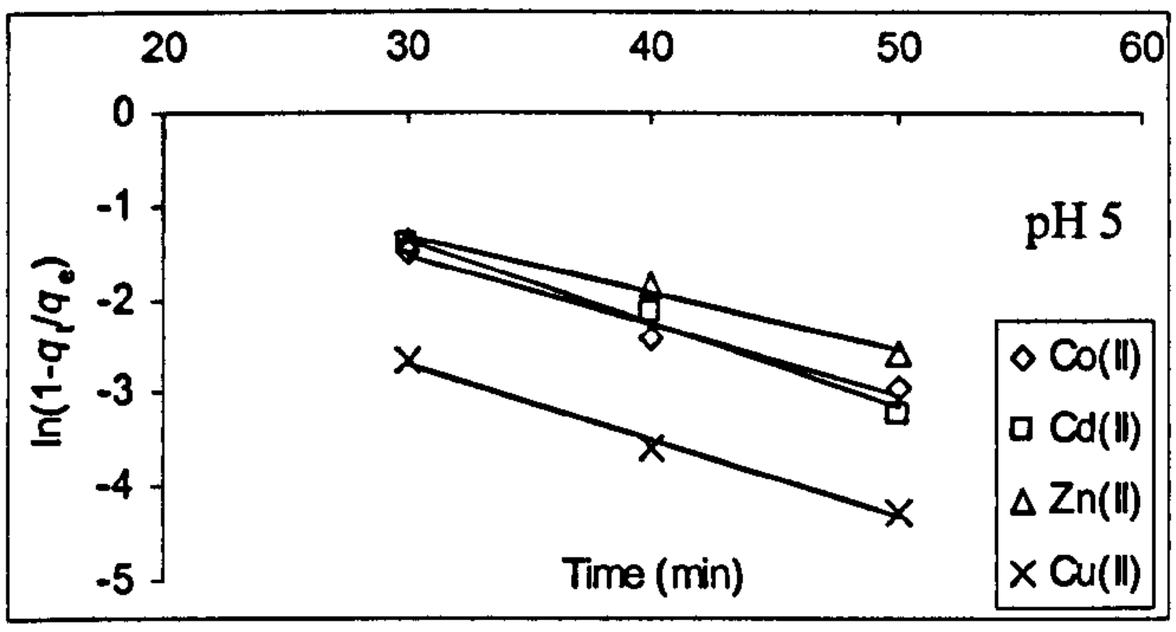

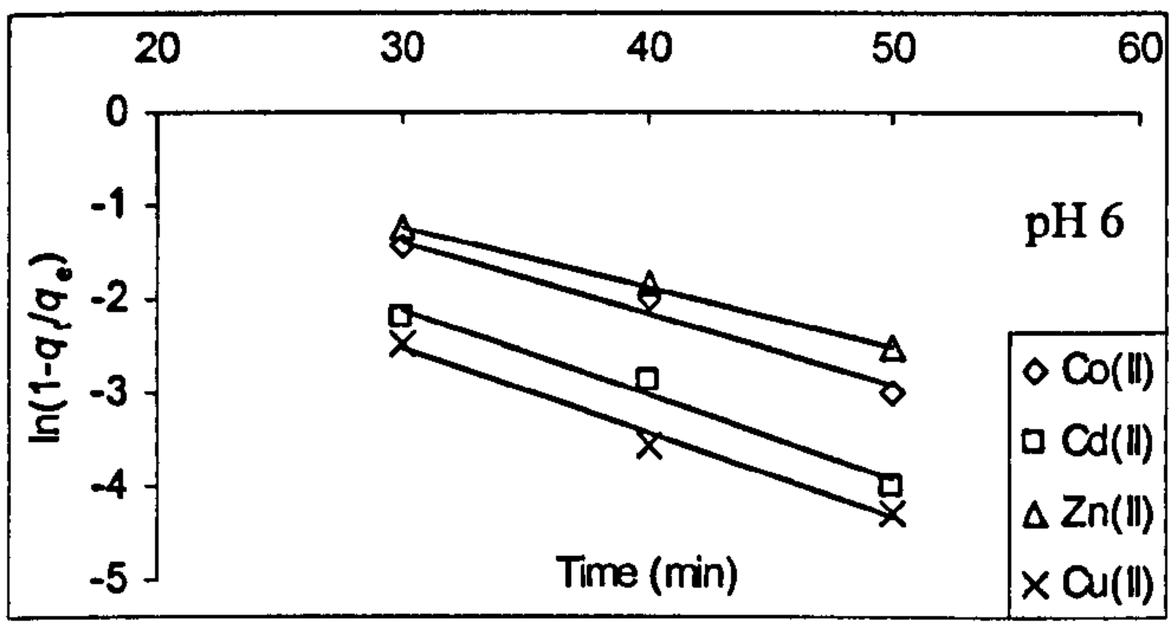

Figure 10.28: Plots of equation (19) at different initial pH values (35°C) for the determination of pore diffusion coefficients (D_2) of M(II) with MF-CDTA.

Appendix B: List of publications

[1] Ahmad Baraka, P.J. Hall, and M.J. Heslop, Melamine-formaldehyde-NTA chelating gel resin: Synthesis, characterization and application for copper(II) removal from synthetic wastewater, *Journal of Hazardous Materials* 140 (2006) 86–94.

[2] Ahmad Baraka, P.J.Hall, M.J.Heslop, Removal of copper(II) ions from aqueous effluent using melamine-formaldehyde-DTPA resin in a fixed-bed up-flow column, *3rd International conference on chemical & environmental engineering*, 16–18 May, 2006, Military technical college, Cairo, Egypt.

[3] P.J.Hall, M.J.Heslop & Ahmad Baraka, Selective adsorption of Cu(II) from synthetic wastewater using melamine-formaldehyde-NTA resin, *WIT Transactions on Ecology and the Environment*, Vol 95, 2006 WIT Press.

[4] Ahmad Baraka, P.J.Hall, M.J.Heslop Preparation and characterization of melamine-formaldehyde-DTPA chelating resin and its use as adsorbent for heavy metals removal from wastewater. Submitted (Mar 09, 2006) to the journal of *Reactive and Functional Polymers* (accepted).

References

[1] J.K. Walters and A. Wint, Industrial effluent treatment Vol.1 Water and solid *wastes, London Applied Science Publishers,* 1981.

[2] Walter Lorch, Handbook of water purification, Second edition, Halsted Press, Chichester, England, 1987.

[3] Jesse R. Conner, Chemical Fixcation and Solidification of Hazardous Wastes, VAN NOSTRAND REINHOLD, 1990.

[4] A. Ramesh, D.J. Lee, J.W.C. Wong, Thermodynamics parameters for adsorption equilibrium of heavy metals and dyes from wastewater with low-cost adsorbents, Journal of Colloid and Interface Science 291 (2005) 588–592.

[5] Colin Baird, Environmental chemistry, Second edition,W.H.Freeman and Company, New York, 1999.

[6] R. Donat, A. Akdogan, E. Erdem, H. Cetisli, Thermodynamics of Pb^{2+} and Ni^{2+} adsorption onto natural bentonite from aqueous solutions, Journal of Colloid and Interface Science 286 (2005) 43–52.

[7] K.S. Hui, C.Y.H. Chao, S.C. Kot, Removal of mixed heavy metals ions in wastewater by zeolites 4A and residual products from recycled coal fly ash, Journal of Hazardous Materials B127 (2005)89–101.

[8] Suneerat Ruangsomboona, Ladda Wongrat, Bioaccumulation of cadmium in an experimental aquatic food chain involving phytoplankton (*Chlorella vulgaris*), zooplankton (*Moina macrocopa*), and the predatory catfish *Clarias macrocephalus*×*C. gariepinus* Aquatic Toxicology 78 (2006) 15–20.

[9] A.M. El-Kamash, A.A. Zaki and M. Abed El Geleel, Modeling batch kinetics and thermodynamics of zinc and cadmium ions removal from waste solutions using synthetic zeolites A., Journal of Hazardous Materials B127 (2005) 211–220.

[10] Fatma Ekmekyapar, Ali Aslan, y. Kemal Bayhan, Avni Cakici, Biosorption of copper(II) by nonliving lichen biomass of *Cladonia rangiformis* hoffm, Journal of Hazardous Materials B137 (2006) 293–298.

[11] S. Rengaraj, Seung-Hyeon Moon, Kinetics of adsorption of Co(II) removal from water and wastewater by ion exchange resins, Water Research 36 (2002) 1783–1793.

[12] Tonni Agustiono Kurniawan, Gilbert Y.S. Chan, Wai-Hung Lo and Sandhya Babel, Chemical Engineering Journal 118 (2006) 83–98.

[13] Industrial wastewater and solid waste engineering edited by Vincent Cavaseno and the staff of Chemical Engineering. New York McGraw-Hill [for] Chemical Engineering c1980 {D628.54 IND}

[14] Martin T.K. Tsui, K.C. Cheung, Nora F.Y. Tam and M.H. Wong, A comparative study on metal sorption by brown seaweed, Chemosphere 65 (2006) 51–57.

[15] D. Max Roundhill, Extraction of metals from soils and waters, Kluwer Academic/Plenum Publishers, New York, 2001.

[16] Samuel D. Faust and Osman M. Aly, Adsorption processes for water treatment, Boston: Butterworth, c1987.

[17] Yuen-Hua Wang, Su-Hsia Lin, Ruey-Shin Juang, Removal of heavy metal ions from aqueous solutions using various low-cost adsorbents, Journal of Hazardous Materials B102 (2003) 291–302.

[18] Erhan Demirbas, Mehmet, Kobya, Elif Senturk, Tunacy Ozkan, Adsorption kinetics for the removal of chromium (VI) from aqueous solutions on the activated carbons prepared from agricultural wastes, Water SA Vol. 30 No. 4 October 2004.

[19] D. Max Roundhill, Extraction of metals from soils and waters, Kluwer Acadimic/Plenum Publishers, New York, 2001.

[20] N. F. Gray, Water Technology, An introduction for environmental scientists and engineers, 2nd ed., Oxford: Elsevier Butterworth-Heinemann, 2005.

[21] Douglas M. Ruthven, Editor, Encyclopaedia of Separation Technology, John Wiley & Sons, New York, 1997.

[22] Jesse R. Conner, Chemical Fixation and Solidification of Hazardous Wastes, Van Nostrand Reinhold, London EC4P 4EE, England, 1990.

[23] Tonni Agustiono Kurniawan, Gilbert Y.S. Chan, Wai-Hung Lo and Sandhya Babel, Physico–chemical treatment techniques for wastewater laden with heavy metals, Chemical Engineering Journal 118 (2006) 83–98.

[24] Vincent Cavaseno, industrial wastewater and solid waste engineering, McGraw-hill Pub.Co. 1980.

[25] W.J. Eilbeck and G. Mattock, Chemical processes in waste water treatment, Halsted Press, Chichester, England, 1987.

[26] Y. Fernández, E. Marañón, L. Castrillón and I. Vázquez, Removal of Cd and Zn from inorganic industrial waste leachate by ion exchange , Journal of Hazardous Materials B126 (2005) 169–175.

[27] S. Kocaoba and G. Akcin, Removal of chromium (III) and cadmium (II) from aqueous solutions, Desalination 180 (2005) 151–156.

[28] E. Erdem, N. Karapinar and R. Donat, The removal of heavy metal cations by natural zeolites , Journal of Colloid and Interface Science 280 (2004) 309–314.

[29] Hani Abu Qdais and Hassan Moussa, Removal of heavy metals from wastewater by membrane processes: a comparative study, Desalination 164 (2004) 105–110.

[30] Jan Rydberg, Claude Musikas, Gregory R. Choppin, Principles and practices of solvent extraction, New York, M. Dekker, 1992.

[31] K. Nazari, A. Ghadiri and H. Babaie, Elimination of cadmium from wet process phosphoric acid with Alamine 336, Minerals Engineering 18 (2005) 1233–1238.

[32] Walter J. Weber, JR, Physicochemical process for water quality control, Wiley-Interscience, USA, 1972.

[33] T. Mohammadi, A. Razmi and M. Sadrzadeh, Effect of operating parameters on Pb^{2+} separation from wastewater using electrodialysis, Desalination 167 (2004) 379–385.

[34] Mark D. Neville, Christopher P. Jones and Andrew D. Turner, The EIX process for radioactive waste treatment, Progress in Nuclear Energy, Vol. 32, No. 314, pp. 397–401, 1998.

[35] A.E. Elsherief, Removal of cadmium from simulated wastewaters by electrodeposition on spiral wound steel electrode, Electrochimica Acta 48 (2003) 2667–2673.

[36] Mykola Seredych, Teresa J. Bandosz, Removal of copper on composite sewage sludge/industrial sludge-based adsorbents: The role of surface chemistry, Journal of Colloid and Interface Science 302 (2006) 379–388.

[37] Ali Hakan Ören and Abidin Kaya, Factors affecting adsorption characteristics of Zn^{2+} on two natural zeolites, Journal of Hazardous Materials B131 (2006) 59–65.

[38] S.K. Pitcher, R.C.T. Slade, N.I. Ward, Heavy metal removal from motorway stormwater using zeolites, Science of the Total Environment 334– 335 (2004) 161–166.

[39] Sandhya Babel, Tonni Agustiono Kurniawan, Low-cost adsorbents for heavy metals uptake from contaminated water: a review, Journal of Hazardous Materials B97 (2003) 219–243.

[40] Mabel Vaca Mier, Raymundo López Callejas, Ronald Gehr, Blanca E. Jiménez Cisneros and Pedro J. J. Alvarez, Heavy metal removal with Mexican clinoptilolite: multi-component ionic exchange, Wat. Res. Vol. 35, No. 2, pp. 373–378, 2001.

[41] Myroslav Sprynskyy, Bogusław Buszewski, Artur P. Terzyk and Jacek Namieśnik, Study of the selection mechanism of heavy metal (Pb2+, Cu2+, Ni2+, and Cd2+) adsorption on clinoptilolite, Journal of Colloid and Interface Science 304 (2006) 21–28.

[42] S.K. Pitcher, R.C.T. Slade, N.I. Ward, Heavy metal removal from motorway stormwater using zeolites, Science of the Total Environment 334– 335 (2004) 161–166.

[43] Shaobin Wang and Hongwei Wu, Environmental-benign utilisation of fly ash as low-cost adsorbents, Journal of Hazardous Materials B136 (2006) 482–501.

[44] Heechan Cho, Dalyoung Oh and Kwanho Kim, A study on removal characteristics of heavy metals from aqueous solution by fly ash, Journal of Hazardous Materials B127 (2005) 187–195.

[45] M. Erol, S. Küçükbayrak, A. Ersoy-Meriçboyu and T. Ulubaş, Removal of Cu^{2+} and Pb^{2+} in aqueous solutions by fly ash, Energy Conversion and Management 46 (2005) 1319–1331.

[46] J.H. Potgieter, S.S. Potgieter-Vermaak and P.D. Kalibantonga, Heavy metals removal from solution by palygorskite clay, Minerals Engineering 19 (2006) 463–470.

[47] Ömer Yavuz, Yalçin Altunkaynak and Fuat Güzel, Removal of copper, nickel, cobalt and manganese from aqueous solution by kaolinite, Water Research 37 (2003) 948–952.

[48] Barry Crittenden and W John Thomas, Adsorption technology and design, butterworth-heinemann, 1998.

[49] Sergei I. Lyubchik, Andrei I. Lyubchik, Olga L. Galushko, Lilia P. Tikhonova, Joaquim Vital, Isabel M. Fonseca and Svetlana B. Lyubchik, Kinetics and thermodynamics of the Cr(III) adsorption on the activated carbon from co-mingled wastes, Colloids and Surfaces A: Physicochem. Eng. Aspects 242 (2004) 151–158.

[50] A. M. Youssef, Th. El-Nabarawy and S. E. Samra, Sorption properties of chemically-activated carbons: 1. Sorption of cadmium(II) ions , Colloids and Surfaces A: Physicochem. Eng. Aspects 235 (2004) 153–163.

[51] Dinesh Mohan and Kunwar P. Singh, Single- and multi-component adsorption of cadmium and zinc using activated carbon derived from bagasse—an agricultural, Water Research 36 (2002) 2304–2318.

[52] K. Kadirvelu, K. Thamaraiselvi and C. Namasivayam, Removal of heavy metals from industrial wastewaters by adsorption onto activated carbon prepared from an agricultural solid, Bioresource Technology 76 (2001) 63–65.

[53] M. Kobya, E. Demirbas, E. Senturk and M. Ince, Adsorption of heavy metal ions from aqueous solutions by activated carbon prepared from apricot stone, Bioresource Technology 96 (2005) 1518–1521.

[54] Ajay Kumar Meena, G.K. Mishra, P.K. Rai, Chitra Rajagopal and P.N. Nagar, Removal of heavy metal ions from aqueous solutions using carbon aerogel as an adsorbent , Journal of Hazardous Materials B122 (2005) 161–170.

[55] Renmin Gong a,b, Yi Ding c, Huijun Liu a, Qiuyi Chen b, Zhili Liu b, Lead biosorption and desorption by intact and pretreated *spirulina maxima* biomass, Chemosphere 58 (2005) 125–130.

[56] S. Senthilkumaar, S. Bharathi, D. Nithyanandhi, V. Subburam, Biosorption of toxic heavy metals from aqueous solutions, Bioresource Technology 75 (2000) 163–165.

[57] Núria Fiol, Isabel Villaescusa, María Martínez, Núria Miralles, Jordi Poch and Joan Serarols, Sorption of Pb(II), Ni(II), Cu(II) and Cd(II) from aqueous solution by olive stone, Separation and Purification Technology 50 (2006) 132–140.

[58] Gabriela Huamán Pino, Luciana Maria Souza de Mesquita, Mauricio Leonardo Torem and Gustavo Adolfo Saavedra Pinto, Biosorption of cadmium by green coconut shell, Minerals Engineering 19 (2006) 380–387.

[59] Asma Saeed, M. Waheed Akhter and Muhammed Iqbal, Removal and recovery of heavy metals from aqueous solution using papaya wood as a new, Separation and Purification Technology 45 (2005) 25–31.

[60] Runping Han, Jinghua Zhang , Weihua Zou, Huijun Xiao, Jie Shi, Hongmin Liu, Biosorption of copper(II) and lead(II) from aqueous solution by chaff in a fixed-bed column, Journal of Hazardous Materials B133 (2006) 262–268.

[61] V.K. Gupta, Arshi Rastogi a, V.K. Saini a, Neeraj Jain, Biosorption of copper(II) from aqueous solutions by *Spirogyra* species, Journal of Colloid and Interface Science 296 (2006) 59–63.

[62] S.R. Shukla, Roshan S. Pai, Amit D. Shendarkar, Adsorption of Ni(II), Zn(II) and Fe(II) on modified coir fibres, Separation and Purification Technology 47 (2006) 141–147.

[63] Prasert Pavasant, Ronbanchob Apiratikul, Vimonrat Sungkhum, Prateep Suthiparinyanont, Suraphong Wattanachira and Taha F. Marhaba, Biosorption of Cu^{2+}, Cd^{2+}, Pb^{2+}, and Zn^{2+} using dried marine green macroalga Caulerpa lentillifera, Bioresource Technology 97 (2006) 2321–2329

[64] María Martínez, Núria Miralles, Soraya Hidalgo, Núria Fiol, Isabel Villaescusa and Jordi Poch, Removal of lead(II) and cadmium(II) from aqueous solutions using grape stalk waste, Journal of Hazardous Materials B133 (2006) 203–211.

[65] Upendra Kumar and Manas Bandyopadhyay, Sorption of cadmium from aqueous solution using pretreated rice, Bioresource Technology 97 (2006) 104–109.

[66] S. Çay, A. Uyanık and A. Özasık, Single and binary component adsorption of copper(II) and cadmium(II) from aqueous solutions using tea-industry waste, Separation and Purification Technology 38 (2004) 273–280.

[67] Gülşad Uslu, Mehtap Tanyol, Equilibrium and thermodynamic parameters of single and binary mixture biosorption of lead (II) and copper (II) ions onto *Pseudomonas putida*: Effect of temperature, Journal of Hazardous Materials B135 (2006) 87–93.

[68] John A. Dean, Chemical separation methods, Van Nostrand Reinhold Company, 1969.

[69] J.D. Seader, Ernest J. Henley, Separation process principles, New York : Wiley, c1998.

[70] Claudia V. Diniz, Virginia S.T. Ciminelli and Fiona M. Doyle, The use of the chelating resin Dowex M-4195 in the adsorption of selected heavy metal ions from manganese solutions, Hydrometallurgy 78 (2005) 147–155.

[71] Prasun K. Roy, Ashok S. Rawat and Pramod K. Rai, Synthesis, characterisation and evaluation of polydithiocarbamate resin supported on macroreticular styrene–divinylbenzene copolymer for the removal of trace and heavy metal, Talanta 59 (2003) 239–246.

[72] Bahire Filiz Senkal and Niyazi Biçak, Glycidyl methacrylate based polymer resins with diethylene triamine tetra acetic acid functions for efficient removal of Ca(II) and Mg(II), Reactive & Functional Polymers 49 (2001) 151–157.

[73] Stella Lacour, Jean-Claude Bollinger, Bernard Serpaud, Pierre Chantron and Richard Arcos, Removal of heavy metals in industrial wastewaters by ion-exchanger grafted textiles, Analytica Chimica Acta 428 (2001) 121–132.

[74] Kais A. K. Ebraheem and Suhaila T. Hamdi, Synthesis and properties of a copper selective chelating resin containing a salicylaldoxime group, Reactive & Functional Polymers 34 (1997) 5–10.

[75] E. Korngold, S. Belfer and C. Urtizberea, Removal of heavy metals from tap water by a cation exchanger, Desalination 104 (1996) 197–201.

[76] Chuh-Yean Chen, Chen-Li Chiang and Po-Chen Huang, Adsorptions of heavy metal ions by a magnetic chelating resin containing hydroxy and iminodiacetate groups, Separation and Purification Technology 50 (2006) 15–21.

[77] Ramazan Coşkun, Cengiz Soykan and Mehmet Saçak, Removal of some heavy metal ions from aqueous solution by adsorption using poly(ethylene terephthalate)-g-itaconic acid/acrylamide fiber, Reactive and Functional Polymers 66 (2005) 599–609.

[78] Adil Denizil Bora Garipcan, Abdülkerim Karabakan and Hülya Senöz, Synthesis and characterization of poly(hydroxyethyl methacrylate-N-methacryloyl-(L)-glutamic acid) copolymer beads for removal of lead ions, Materials Science and Engineering C 25 (2005) 448–454.

[79] H.A. Essawy and H.S. Ibrahim, Synthesis and characterization of poly(vinylpyrrolidone-co-methylacrylate) hydrogel for removal and recovery of heavy metal ions from wastewater, Reactive and Functional Polymers 61 (2004) 421–432.

[80] Ali Kara, Lokman Uzun, Necati Besirli and Adil Denizli, Poly(ethylene glycol dimethacrylate-*n*-vinyl imidazole) beads for heavy metal removal, Journal of Hazardous Materials 106B (2004) 93–99.

[81] B.S. Grag, R.K. Sharma, N. Bhojak, S. Mittal, Chelating resins and their applications in the analysis of trace metal ions, Microchemical Journal 61 (1999) 94–114.

[82] Asif Ali Khan , M. Mezbaul Alam, Synthesis, characterization and analytical applications of a new and novel 'organic–inorganic' composite material as a cation exchanger and Cd(II) ion-selective membrane electrode: polyaniline Sn(IV) tungstoarsenate, Reactive & Functional Polymers 55 (2003) 277–290.

[83] Takeshi Gotoh, Keiei Matsushima, Ken-Ichi Kikuchi, Preparation of alginate–chitosan hybrid gel beads and adsorption of divalent metal ions, Chemosphere 55 (2004) 135–140.

[84] G.C. Steenkamp, K. Keizer, H.W.J.P. Neomagus and H.M. Krieg, Copper(II) removal from polluted water with alumina/chitosan composite membranes, Journal of Membrane Science 197 (2002) 147–156.

[85] Wael S. El-Sayed, Ashraf F. El-Baz and A.M. Othman, Applied Surface International Biodeterioration & Biodegradation 57 (2006) 75–81.

[86] Sung-Woo Hwang, Sang-Hoon Hyun, Journal of Non-Crystalline Solids 347 (2004) 238–245.

[87] R. W. Pekala, J. C. Farmer, C. T. Alviso, T. D. Tran, S. T. Mayer, J. M. Miller and B. Dunn, Carbon aerogels for electrochemical applications, Journal of Non-Crystalline Solids 225 (1998) 74–80.

[88] R. W. Pekala, C. T. Alviso, X. Lu, J. Gross and J. Fricke, Journal of Non-Crystalline Solids 188 (1995) 226–234.

[89] Rui Zhang, Wen Li, Kaixi Li, Chunxiang Lu, Liang Zhan and Licheng Ling, Microporous and Mesoporous Materials 72 (2004) 167–173.

[90] R. Zhang, W. Li, X. Liang, G. Wu, Y. Lü, L. Zhan, C. Lu, L. Ling, Effect of hydrophobic group in polymer matrix on porosity of organic and carbon aerogels from sol–gel polymerization of phenolic resole and methylolated melamine, Microporous and Mesoporous Materials 62 (2003) 17–27.

[91] Anna Deryło-Marczewska, Jacek Goworek, Ryszard Kusak, Wojciech Zgrajka, Applied Surface Science 195 (2002) 117–125.

[92] Katsutoshi Inoue, Kazuharu Yoshizuka and Keisuke Ohto, Adsorptive separation of some metal ions by complexing agent types of chemically modified chitosan, Analytica Chimica Acta 388 (1999) 209–218.

[93] Beat Meyer, Urea-Formaldehyde resins, Addison-Wesley publishing Company Inc., 1979.

[94] Ahmad Baraka, P.J. Hall, and M.J. Heslop, Melamine-formaldehyde-NTA chelating gel resin: Synthesis, characterization and application for copper(II) removal from synthetic wastewater, Journal of Hazardous Materials 140 (2007) 86–94.

[95] A. Brookes, C. P. Vale, Resins from urea, melamine and related materials, F. H. Castle & Co., LTD., 1954.

[96] E.Minopoulou, E.Dessipri, G.D.Chryssikos, V.Gionis, A.Paipetis, C.Panayiotou, Int. J. Adhes. Adhes, 23 (2003) 473.

[97] Xuefei Sun, and Zhikuan Chai, J. Chromatogr. A 943 (2002) 209.

[98] Rodrigo C. Baltieri, Lúcia H. Innocentini-Mei, Wirla M. S. C. Tamashiro, Leila Peres, Edison Bittencourt, Eur. Polym. J. 38 (2002) 57.

[99] K. Mequanint, R.Sanderson, Polymer 44 (2003) 2631.

[100] T. W. Graham Solomons, Organic Chemistry, sixth edition, John Wiley & Sons, INC., 1996.

[101] Eram Sharmin, L.Imo, S.M.Ashraf, Sherif Ahmad, Prog. Org. Coat. 50 (2004) 47.

[102] Sema Demirci Çekiç , Hayati Filik and Resat Apak, Use of an o-aminobenzoic acid-functionalized XAD-4 copolymer resin for the separation and preconcentration of heavy metal(II) ions, Analytica Chimica Acta 505 (2004) 15–24.

[103] Motoi Machida, Masami Aikawa, Hideki Tatsumoto, Prediction of simultaneous adsorption of Cu(II) and Pb(II) onto activated carbon by conventional Langmiur type equations, Journal of Hazardous Materials B120 (2005) 271–275.

[104] J.D. Lee, Concise Inorganic Chemistry, Fourth Edition, Chapman & Hall Ltd, 1991.

[105] W. Andrzej Trochimczuk, New ion-exchange/coordination resins with carboxylate and phosphate functional groups, European Polymer Journal 35 (1999) 1457–1464.

[106] Motoyuki Suzuki, Adsorption Engineering, New York, Elsevier, 1990.

[107] James W. Robinson, Eileen M. Skelly Frame, George M. Frame II, Undergraduate instrumental analysis, 6th ed, New York : M. Dekker, c2005.

[108] edited by Galen Wood Ewing, Analytical instrumentation handbook, New York: M. Dekker, c1997.

[109] Nuri Ünlü and Mustafa Ersoz, Adsorption characteristics of heavy metal ions onto a low cost biopolymeric sorbent from aqueous solutions, Journal of Hazardous Materials B136 (2006) 272–280.

[110] V.Vadivelan, K.Vasanth Kumar, Equilibrium, kinetics, mechanism and process design for the sorption of methlene blue onto rice husk, Journal of Colloid and Interface Science 286 (2005) 90–100.

[111] Y.S. Ho and G. McKay, Pseudo-second order model for sorption processes, Process Biochemistry 34 (1999) 451–465.

[112] K.K. Singh, R. Rastogi and S.H. Hasan, Removal of Cr(VI) from wastewater using rice bran, Journal of Colloid and Interface Science 290 (2005) 61–68.

[113] K. Vasanth Kumar, S. Sivanesan and V. Ramamurthi, Adsorption of malachite green onto Pithophora sp., a fresh water algae: Equilibrium and kinetic modelling, Process Biochemistry 40 (2005) 2865–2872.

[114] C.W. Cheung, J.F. Porter and G. McKay, Sorption kinetics for the removal of copper and zinc from effluents using bone, Separation and Purification Technology 19 (2000) 55–64.

[115]Susmita Sen Gupta and Krishna G. Bhattacharyya, Adsorption of Ni(II) on clays, Journal of Colloid and Interface Science 295 (2006) 21–32.

[116]Fethiye Gode, Erol Pehlivan, Removal of chromium(III) from aqueous solutions using Lewatit S 100:The effect of pH, time, metal concentration and temperature, Journal of Hazardous Materials B136 (2006) 330–337.

[117]Y.S. Ho and G. Mckay, The sorption of lead(II) ions on peat, Water Research Vol. 33, No. 2, pp. 578–584, 1999.

[118]Lagergren S., Zur theorie der sogenannten adsorption gelöster stoffe, Kungliga Svenska Vetenskapsakademiens, Handlingar 24(4), (1898) 1–39.

[119]Y. S. Ho and G. McKay, The kinetics of sorption of divalent metal ions onto sphagnum moss peat, Water Research, Volume 34, Issue 3, 15 February 2000, Pages 735–742.

[120]M.J.D. Low, Chem. Rev., 60 (1960) p. 267.

[121]A.B. Pérez-Marín, V. Meseguer Zapata, J.F. Ortuño, M. Aguilar, J. Sáez and M. Lloréns, Removal of cadmium from aqueous solutions by adsorption onto orange waste, Journal of Hazardous Materials B139 (2007) 122–131.

[122]Krishna G Bhattacharyya and Arunima Sharma, Adsorption of Pb(II) from aqueous solution by Azadirachta indica (Neem) leaf powder, Journal of Hazardous Materials B113 (2004) 97–109.

[123]Y.S. HO and G. McKay, Sorption of copper(II) from aqueous solution by peat, Water, Air, and Soil Pollution 158 (2004) 77–97.

[124]J. Guzman, I. Saucedo, J. Revilla, R. Navarro and E. Guibal, Copper sorption by chitosan in the presence of citrate ions: influence of metal speciation on sorption mechanism and uptake capacities, International Journal of Biological Macromolecules 33 (2003) 57–65.

[125]Mehmet Doğan, Mahir Alkan, Özkan Demirbaş, Yasemin Özdemir and Cengiz Özmetin, Adsorption kinetics of maxilon blue GRL onto sepiolite from aqueous solutions, Chemical Engineering Journal 124 (2006) 89–101.

[126]G. Kantipuly, S. Katragadda, A. Chow and H. D. Gesser, Chelating polymers and related supports for separation and preconcentration of trace metals, Talanta 37 (5) (1990) 491–517.

[127]Adnan Özcan, A. Safa Özcan, Sibel Tunali, Tamer Akar and Ismail Kiran, Determination of the equilibrium, kinetic and thermodynamic parameters of adsorption of copper(II) ions onto seeds of *Capsicum annuum.* Journal of Hazardous Materials B124 (2005) 200–208.

[128]T. Karthikeyan, S. Rajgopal, Lima Rose Miranda, Chromium(VI) adsorption from aqueous solution By *Hevea Brasilinesis* sawdust activated carbon, Journal of Hazardous Materials B124 (2005) 192–199.

[129]J. Crank, The Mathematics of Diffusion, 2nd ed., Clarendon, Oxford. 1975.

[130]B.F. Noeline, D.M. Manohar, T.S. Anirudhan, Kinetic and equilibrium modelling of lead(II) sorption from water and wastewater by polymerized banana stem in a batch reactor, Separation and Purification Technology 45 (2005) 131–140.

[131]Freundlich H., Colloid and capillary chemistry. Methuen and Co., London (1926).

[132]Freundlich H., Trans. Farad. Soc., 28 (1932) p. 195 .

[133]Tien, Chi, Adsorption calculations and modeling, Boston: Butterworth-Heinemann, c1994.

[134]Langmuir, I. J. Amer. Chem. Soc., 37 (1915) p. 1139.

[134]Langmuir, I. J. Amer. Chem. Soc., 40 (1915) p. 1361.

[136]K. Kadirvelu, C. Namasivayam, Activated carbon from coconut coirpith as metal adsorbent: adsorption of Cd(II) from aqueous solution, Advances in Environmental Research 7 (2003) 471–478.

[137]Jong Hun Choi, Shin Dong Kim, Yoon Jung Kwon, Wha Jung Kim, Adsorption behaviors of ETS-10 and its variant, ETAS-10 on the removal of heavy metals, Cu^{2+}, Co^{2+}, Mn^{2+}, and Zn^{2+} from a waste water, Microporous and Mesoporous Materials 96 (2006) 157–167.

[138]Ahmad Baraka, P.J.Hall, M.J.Heslop, Removal of copper(II) ions from aqueous effluent using melamine-formaldehyde-DTPA resin in a fixed-bed up-flow column, 3rd International conference on chemical & environmental engineering, 16–18 May, 2006, Military technical college, Cairo, Egypt.

[139]Emine Malkoc, Yasar Nuhoglu, Removal of Ni(II) ions from aqueous solutions using waste of tea factory: Adsorption on a fixed-bed column, Journal of Hazardous Materials B135 (2006) 328–336.

[140]Emine Malkoc, Yasar Nuhoglu, Fixed bed studies for the sorption of chromium(VI) onto tea factorywaste, Chemical Engineering Science 61 (2006) 4363–4372.

[141]H.C. Thomas, Heterogeneous ion exchange in a flowing system, J. Am. Chem. Soc., 66 (1944) 1664–1666.

[142]G.S. Bohart and E.Q. Adams, J.Amer. Chem. Soc., 42 (1920) 523–544.

[143]Asok Adak, Manas Bandyopadhyay, Anjali Pal, Fixed bed column study for the removal of crystal violet (C. I. Basic Violet 3) dye from aquatic environment by surfactant-modified alumina, Dyes and Pigments 69 (2006) 245–251.

[144]Hutchins RA. Am J Chem Eng 1973; 80:133–8.

[145]V. Christian Taty-Costodes, Henri Fauduet, Catherine Porte, Yuh-Shan Ho, Removal of lead (II) ions from synthetic and real effluents using immobilized *Pinus sylvestris* sawdust: Adsorption on a fixed-bed column, Journal of Hazardous Materials B123 (2005) 135–144.

[146]B.G. Prakash Kumar, Lima Rose Miranda, M. Velan, Adsorption of Bismark Brown dye on activated carbons prepared from rubberwood sawdust (*Hevea brasiliensis*) using different activation methods, Journal of Hazardous Materials B126 (2005) 63–70.

[147]Mehmet Erdem, Arzu Özverdi, Lead adsorption from aqueous solution onto siderite, Separation and Purification Technology 42 (2005) 259–264.

[148]Rıdvan Say, Ebru Birlik, Arzu Ersöz, Filiz Yılmaz, Tevfik Gedikbey and Adil Denizli, Preconcentration of copper on ion-selective imprinted polymer microbeads, Analytica Chimica Acta 480 (2003) 251–258.

[149]I.G. Shibi and T.S. Anirudhan, Adsorption of Co(II) by a carboxylate-functionalized polyacrylamide grafted lignocellulosics, Chemosphere 58 (2005) 1117–1126.

[150]M. Lehmann, A.I. Zouboulis, K.A. Matis, Modelling the sorption of metals from aqueous solutions on goethitr fixed-beds, Environmental Pollution 113 (2001) 121–128.

[151]M. A. Maheswari, and M. S. Subramanian, Extraction chromatographic method for the separation of actinides and lanthanides using EDHBA grafted AXAD-16 polymer, Talanta 65 (2005) 735–742.

[152]Rita Sundari, Musa Ahmad, Lee Yook Heng, Development of an optical fiber reflectance sensor for copper (II) detection based on immobilised salicylic acid, Sensors and Actuators B113 (2006) 201–206.

[153]L. Addour, D. Belhocine, N. Boudries, Y. Comeau, A Pauss, N. Mameri, Zinc uptake by *Streptomyces rimosus* biomass using a packed-bed column, Journal of Chemical Technology and Biotechnology, 74: 1089–1095 (1999).

[154]Duong D. Do, Adsorption Analysis: Equilibria and Kinetics, Vol. 2, Imperial College Press London, 1998.

[155] Selvaraj Rengaraj, Younghun Kim, Cheol Kyun Joo, and Jongheop Yi, J. Colloid Interface Sci. 273 (2004) 14.

[156] J. Goworek, A. Deryło-Marczewska, W. Stefaniak, W. Zgrajka, R. Kusak, Absorption/adsorption properties of porous phenolic-formaldehyde and melamine-formaldehyde polymers, Materials Chemistry and Physics 77 (2002) 276–280.

[157] Baojiao Gao, Fuqiang An, Kangkai Liu, Studies on chelation adsorption of noval composite material polyethyleneimine/silica gel for heavy-metal ions, Applied Surface Science 253 (2006) 1946–1952.

[158] Shengling Sun, Aiqin Wang, Adsorption properties of carboxymethyl-chitosan and cross-linked carboxymethyl-chitosan resin with Cu(II) as template, Separation and Purification Technology 49 (2006) 197–204.

[159] D. Prabhakaran, M.S. Subramanian, Enhanced metal extraction behaviour using dual mechanism bifunctional polymer: an effective metal chelagoten, Talanta 61 (2003) 431–437.

[160] Sadhan Pramanik, Pulak K. Dhara, Pabitra Chattopadhyay, A chelating resin containing bis(2-benzimidazolylmethyl)amine: synthesis and metal-ion uptake properties suitable for analytical application, Talanta 63 (2004) 485–490.

[161] Prashant Srivastava, Balwant Singh and Michael Angove, Competitive adsorption behaviour of heavy metals on kaolinite, Journal of Colloid and Interface, 290 (2005) 28–38.

[162] Chunhua Xiong, Caiping Yao, Yongjiang Wang, Sorption behaviour and mechanism of ytterbium(III) on imino-diacetic acid resin, Hydrometallurgy 82 (2006) 190–194.

[163] M.V. Sivaiah, K.A. Venkatesan, R.M. Krishna, P. Sasidhar, G.S. Murthy, Ion Exchange properties of strontium on in situ precipitated polyantimonic acid in amberlite XAD-7, Separation and Purification Technology 44 (2005) 1–9.

[164] G. Anderegg, Thermodynamics of complex formation with multi-dentate ligands, Inorganica Chimica Acta 40 (1980) 44.

[165] Ibrahim Shehatta, M.N.H. Moussa and M.A. Hafez, Thermodynamics of complexation of some transition metal ions by salicylaldehyde carbohydrazone pyridinium chloride and diacetyl carbohydrazone pyridine, Thermochimica Acta 219 (1993) 121–133.

[166] Andrea Melchior, Silvia Peressini, Roberto Portanova, Claudio Sangregorio, Claudio Tavagnacco and Marilena Tolazzi, Cobalt(II) and cadmium(II) chelates with nitrogen donors and O_2 bonding to Co(II) derivatives, Inorganica Chimica Acta 357 (2004) 3473–3482.

[167] Lotfi Khezami, Richard Capart, Removal of chromium(VI) from aqueous solution by activated carbons: Kinetics and equilibrium studies, Journal of Hazardous Materials B123 (2005) 223–231.

[168] Sudaporn Tangkawanit, Kunwadee Rangsriwatananon, Alan Dyer, Ion exchange of Cu^{2+}, Ni^{2+}, Pb^{2+} and Zn^{2+} in analcime (ANA) synthesized from Thai perlite, Microporous and Mesoporous Materials 79 (2005) 171–175.

[169] Arunima Sharma, Krishna G. Bhattacharyya, *Azadirachta indica* (Neem) leaf powder as a biosorbent for removal of Cd(II) from aqueous medium, Journal of Hazardous materials B125 (2005) 102–112.

[170] Nuri Ünlü and Mustafa Ersoz, Removal of heavy metal ions by using dithicarbamated-sporopollenin, Separation and Purification Technology 52 (2007) 461–469.

[171] Asem A. Atia, Ahmed M. Donia, Ahmed M. Yousif, Synthetic of amine and thio chelating resins and study of their interaction with zinc(II), cadmium(II) and mercury(II) ions in their aqueous solutions, Reactive & Functional Polymers 56 (2003) 75–82.

[172] Arthur E. Martell and Robert M. Smith, Critical stability constants, Vol. 1: Amino acids, Plenum Press, New York, 1974.

[173] Margot A. Llosa Tanco, David A. Pacheco Tanaka, Veronica C. Flores, Takako Nagase, Toshishige M. Suzuki, Preparation of porous chelating resin containing linear polymer ligand and the adsorption characteristics for harmful metal ions, Reactive & Functional Polymers 53 (2002) 91–101.

[174] Fethiye Gode, Erol Pehlivan, Sorption of Cr(III) onto chelating b-DAEG-sporopollenin and CEP- sporopollenin resins, Bioresources Technology 98 (2007) 904–911.

[175] Riaz Qadeer, Adsorption of erbium ions on activated charcoal from aqueous solutions, Colloids and Surfaces A: Physicochem. Eng. Aspects 254 (2005) 17–21.

[176] Birnur Akkaya, Lokman Uzun, Fedra Candan, Adil Denizil, *N*-methacryloyl-(L)-histidine methyl ester carrying porous magnetic beads for metal chelate adsorption of cytochrome *c*, Materials Science and Engineering C 27 (2006) 180–187.

[177] Saeid Azizian, Kinetic models of sorption: a theoretical analysis, Journal of Colloid and Interface Science 276 (2004) 47–52.

[178] L.D. Michelson, P.G. Gideon, E.G. Pace, L.H. Kutal, Removal of soluble mercury from wastewater by complexing technique, Bull. No. 74, US, Department of Industry, Office of Water Research and Technology, 1975.

[179] Adamson, Arthur W., Physical chemistry of surfaces, 6th ed., New York: Wiley, c1997.

[180] P.J.Hall, M.J.Heslop & Ahmad Baraka, Selective adsorption of Cu(II) from synthetic wastewater using melamine-formaldehyde-NTA resin, WIT Transactions on Ecology and the Environment, Vol 95, 2006 WIT Press.

[181] Tuğba Tüğsüz, Mehmet Doğan and Fatma Sevin, A theoretical study on the location of Ni^{2+}, Cu^{2+}, Cr^{2+}, Cd^{2+} and Pb^{2+} in zeolite Y, Journal of Molecular Structure: Theochem., 728 (2005) 103–109.

[182] Karin Cristiane Justi, Valfredo T. Fávere, Mauro C.M. Laranjeira, Ademir Neves, Rosely A. Peralta, Kinetics and equilibrium adsorption of Cu(II), Cd(II), and Ni(II) ions by chitosan functionalized with 2[-bis-(pyridylmethyl)aminomethyl]-4-methyl-6-formylphenol, Lournal of Colloid and Interface Science 291 (2005) 369–374.

[183] Tony Sarvinder Singh, K.K. Pant, Experimental and modelling studies on fixed bed adsorption of As(III) ions from aqueous solution, Separation and Purification Technology 48 (2006) 288–296.

[184] K. Vijayaraghavan , J. Jegan , K. Palanivelu , M. Velan, Biosorption of copper, cobalt and nickel by marine green alga Ulva reticulata in a packed column,Chemosphere 60 (2005) 419–426.

[185] K. Vijayaraghavan, J. Jegan, K. Palanivelu, M. Velan, Removal of nickel(II) ions from aqueous solution using crab shell particles in a packed bed up-flow column, Journal of Hazardous Materials B113 (2004) 223–230

[186] K. Vijayaraghavan, D. Prabu, Potential of *Sargassum wightii* biomass for copper(II) removal from aqueous solutions: Application of different mathematical models to batch and continuous biosorption data, Journal of Hazardous Materials B137 (2006) 558–564

[187] P. Lodeiro, R. Herrero, M.E. Sastre de Vicente, The use of protonated *Sargassum muticum* as biosorbent for cadmium removal in a fixed-bed column, Journal of Hazardous Materials B137 (2006) 244–253.

[188] K.Vijayaraghavan, J. Jegan, K. Palanivelu, M. Velan, Removal of nickel(II) ions from aqueous solution using crab shell particles in a packed bed up-flow column, Journal of Hazardous Masterials B113 (2004) 223–230.

[189] Danny C. K. Ko, Jhon F. Porter, Godon Mckay, Optimised correlation for the fixed-bed adsorption of metal ions on bone char, Chemical Engineering Science 55 (2000) 5819–5829.

[190] Cheng-Chien Wnag, Chun-Chin Wang, Adsorption characteristics of metal complexes by chelated copolymers with amino group, Reactive Functional Polymers 66 (2006) 343–356.

[191] Z. Matejka, Z. Zitkova, The sorption of heavy-metal cations from EDTA complexes on acrylamide resins having oligo(ethyleneamine) moieties, Reactive & Functional Polymers 35 (1997) 81–88.